AD NUMBER

AD480429

LIMITATION CHANGES

TO:

Approved for public release; distribution is unlimited. Document partially illegible.

FROM:

Distribution authorized to U.S. Gov't. agencies and their contractors; Critical Technology; DEC 1965. Other requests shall be referred to Air Force Technical Application Center, Vela Seismological Center, Washington, DC 20333. Document partially illegible. This document contains export-controlled technical data.

AUTHORITY

usaf ltr 25 jan 1972

AFTAC Project VT/4053

ARRAY RESEARCH

Milo M. Backus, Project Scientist
FL 7-5411 Ext. 319

Richard G. Baldwin, Program Manager
FL 7 5411 Ext 441

TEXAS INSTRUMENTS INCORPORATED
Science Services Division
P.O. Box 5621
Dallas, Texas 75222

Contract No. AF 33(657)-12747
Date of Contract: 13 November 1963
Contract Expiration Date: 20 January 1967

SEMIANNUAL TECHNICAL REPORT NO. 4
Covering the Period
15 May 1965 to 15 November 1965

Prepared for

AIR FORCE TECHNICAL APPLICATIONS CENTER
VELA SEISMOLOGICAL CENTER
Washington, D.C. 20333

ARPA Order No. 104-60
Project Code No. 8100

15 December 1965

AFTAC Project VT/4053

ARRAY RESEARCH

Milo M. Backus, Project Scientist
FL 7-5411 Ext. 319

Richard G. Baldwin, Program Manager
FL 7 5411 Ext 441

TEXAS INSTRUMENTS INCORPORATED
Science Services Division
P.O. Box 5 .1
Dallas, Texas /5222

Contract No. AF 33(657)-12747
Date of Contract: 13 November 1963
Contract Expiration Date: 20 January 1967

SEMIANNUAL TECHNICAL REPORT NO. 4
Covering the Period
15 May 1965 to 15 November 1965

Prepared for

AIR FORCE TECHNICAL APPLICATIONS CENTER
VELA SEISMOLOGICAL CENTER
Washington, D.C. 20333

ARPA Order No. 104-60
Project Code No. 8100

15 December 1965

ARRAY RESEARCH

SEMIANNUAL TECHNICAL REPORT NO. 4

AFTAC Project VT/4053

Contract AF 33(657)-12747

Principal Authors of this Report are:

Section I	Milo M. Backus Richard G. Baldwin
Section II	Robert Roden
Section III	Robert Roden
Section IV	Frank Binder
Section V	Frank Binder
Section VI	Aaron Booker
Section VII	Jim Edwards Steve Benno
Section VIII	Jim Edwards Paul Lintz
Section IX	George Baker John Hoffman
Section X	Milo Backus George Baker
Section XI	George Baker Frank Eubanks

TABLE OF CONTENTS

TABLE OF CONTENTS (CONTD)

TABLE OF CONTENTS (CONTD)

LIST OF ILLUSTRATIONS

LIST OF ILLUSTRATIONS (CONTD)

LIST OF ILLUSTRATIONS (CONTD)

LIST OF ILLUSTRATIONS (CONTD)

LIST OF ILLUSTRATIONS (CONTD)

LIST OF TABLES

SECTION I

SUMMARY

A. INTRODUCTION

Project VT/4053 is directed toward continued development of array processing technology for nuclear surveillance and exploitation of the superior data available from arrays for analysis of distant P-waves.

Work during the period covered by this report has included:

- Processing of vertical array data for the purposes of evaluating MCF systems and decomposing the ambient noise field into constituent modes
- Theoretical investigation of the use of horizontal seismometers in combination with vertical seismometers for extraction of signals
- Processing of CPO teleseisms for the purposes of investigating crustal reverberation deconvolution, determining depth of focus, studying CPO crustal structure, and investigating propagation mechanisms
- Further study of CPO partial array with particular emphasis on the problems associated with seismometer inequalization
- A study of non-directional array processing at TFO utilizing the large cross array.
- A study of seismic signal detection as a separate problem from the problem of signal extraction
- A study of the ability of the Montana LASA to separate nuclear blast signals from natural earthquakes, and a study of an operational LASA signal processing system
- Collection and preparation of seismic data to be used in future experimental work
- Development of an automated mapping program which makes it practical to present the world in wavenumber space relative to a particular station
- Investigation of the predictability of seismic noise in the shallow-buried UBO array
- A study into the extraction of teleseismic signals from cultural noise at UBO

B. PROCESSING OF VERTICAL ARRAY DATA

Section II of this report presents results obtained from processing vertical array data. Those results considered most pertinent to the nuclear-detection problem are presented very briefly in the following paragraphs.

Analysis of vertical array data has lent support to the hypothesis that high-velocity body-wave noise is a significant fraction of the ambient noise at quiet sites in the frequency range from 0.5 cps to 1.2 cps. An example is the modal analysis of ambient noise at UBO, illustrated in Figure I-1. The vertical array analysis at UBO has also answered the question as to whether the high-velocity noise might originate at the surface in the vicinity of the array. At UBO, that 20 percent of the ambient noise power at 1.0 cps which was observed on wavenumber analysis of the surface array to be high-velocity noise, has now been identified on the vertical array as body waves originating below the vertical array. Further analysis at UBO and a granite well have supported the hypothesis that the body-wave noise component is relatively uniform from one site to the next.

This hypothesis explains the poor signal-to-noise improvement obtained in this frequency range at very quiet sites by limited aperture surface arrays and by deeply buried seismometers (down boreholes). It also limits the steady state performance of vertical arrays at the UBO and granite well sites to a few db in this frequency range. Such systems must be considered to be limited to reduction of trapped-mode noise bursts at very quiet sites in this frequency range. Performance for such noise bursts should be related to the theoretical analyses which have been previously published. Evaluation of vertical array performance in this sense has not been completed.

In the frequency range below 0.3 cps, most evidence supports the hypothesis that Rayleigh-wave noise is dominant. Although the vertical arrays examined have limited aperture for this very low frequency noise, theoretical studies suggested a possible moderate performance at very low frequencies. Steady state noise reduction of 5 to 6 db has been observed at the very low frequencies at the granite well site. However, this could be due to instrument gain problems and requires further examination.

Analysis suggests (Figure I-1) that above 1.0 to 1.2 cps the dominant noise, even at quiet sites, is dominantly trapped-mode noise or noise which is not sufficiently correlated at the experimental spacings to be identifiable. In the 1.5 cps to 3.0 cps band, gains of $\sqrt{N}$ or better have been obtained at quiet sites such as TFO and UBO and at noisy sites such as CPO, with small aperture surface arrays of N elements. In this frequency range, it is reasonable to expect good signal-to-noise improvement from vertical arrays with the limitations suggested by previous theoretical work. Improvements of the order of 10 db have been found at UBO in this frequency range.

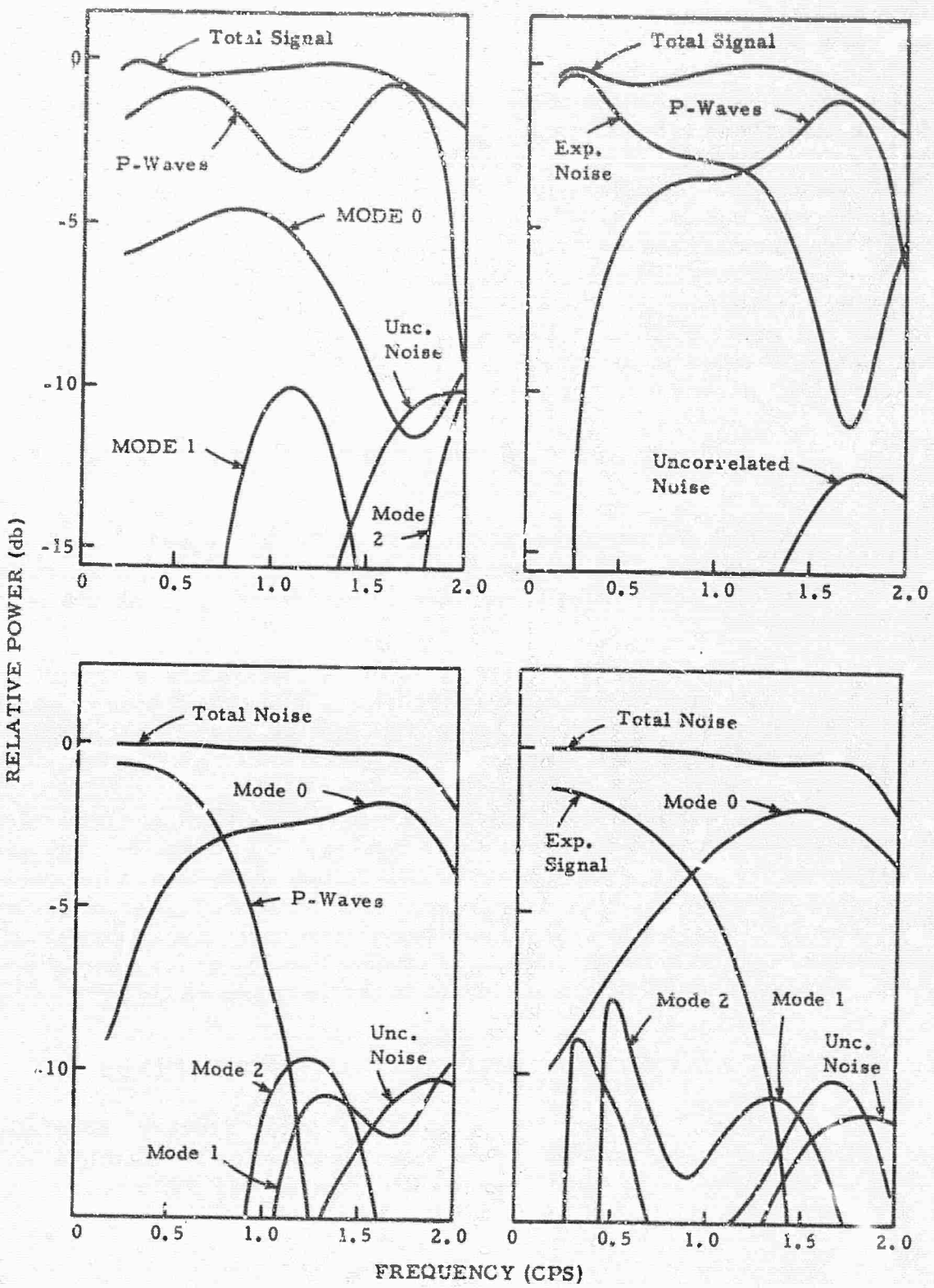

Figure I-1. Estimated Power of Constituent Modes in UBO Signal and Noise Fields

Significant lesser gains have been observed at the granite well, although data analyzed to date has probably been contaminated by tape noise in the high-frequency range.

In evaluation of vertical arrays in the frequency range below 0.5 cps and above 1.5 cps, results to date have been less than conclusive because of difficulties in the specification of the signal model. Use of "measured signal" models is limited to the frequency band where good teleseism signal-to-noise ratios have been obtained on individual seismometers, which thus far have not extended to the low and high frequencies of interest. Theoretical models are harassed by uncertainties in the relative gains of the different seismometers. The best approach would appear to be the use of a theoretical signal model with limited gain slop , using the best available estimate of relative signal gain. This approach has not yet been adequately tested at any of the vertical array sites.

The major potential value of vertical arrays in VELA UNIFORM is twofold:

(1) Reduction of noise in the 0.5 to 1.5 cps range to body wave noise. At quiet sites, this imporvement will be small on an average basis. However, noise "bursts" or intermittent "local" noise should be reduced.

(2) The most significant potential gain lies in the frequency band above 1.5 cps. It may turn out that smaller spacings than those employed so far may be required for maximum vertical array performance in this high frequency range.

The principal direction of the continuing vertical array work is in the evaluation of performance above 1.5 cps. If performance significantly better than the observed 10 db at UBO can be achieved at quiet sites, a possibly attractive system may be a moderate depth vertical array for high-frequency performance that is combined with some horizontally-displaced, near-surface radial seismometers to handle the low-frequency microseism peak. The latter possibility is discussed in the following section.

C. SYSTEMS OF HORIZONTAL AND VERTICAL SEISMOMETERS

Special Report No. 7 entitled "Array Research Theoretical Capability of Systems of Horizontal Seismometers for Predicting a Vertical Component in Ambient Trapped Mode Noise" was published 9 November 1965. A discussion of that report follows.

1. Multicomponent Seismometers

Mathematical formulae were derived for the noise-rejection properties of a 2-component seismometer, consisting of 1 vertical-component and 1 horizontal-component instrument at the same point. For most applications, this system may be considered equivalent to a 3-component seismometer. It is possible to design a processing system wherein different filters are applied to the outputs of 2 horizontals and the noise estimate is obtained by summing the filter outputs.

Some general conclusions were stated regarding the usefulness of a single horizontal-component instrument for eliminating noise from the output of a vertical instrument at the same location. It appeared that such effects as system noise, gain fluctuations and Love waves would not generally present serious problems, although in some cases they may very well do so. The most important consideration is usually the properties of the noise to be eliminated. If significant noise rejection is to be achieved, then some rather stringent conditions must be satisfied. Even when there is only a single-noise mode present, it is essential that the azimuths of the noise sources be confined within a range somewhat less than 180° and that the horizontal be oriented near the center of this range. This requirement follows from the obvious fact that a filter which cancels out noise traveling in a given direction must also amplify noise traveling in the opposite direction. In practice, this requirement may be partially met in major microseismic "storms."

If more than one noise mode is important, large differences in the horizontal-to-vertical transfer functions, k(t), cannot be permitted. A two-mode situation was presented in which no noise rejection is possible because one mode is characterized by a progade particle motion and the other is associated with retrograde motion.

With a 3-component seismometer at point location, it is theoretically possible to determine both the direction of propagation and the shape of the particle orbit for an observed Rayleigh wave. However, the sense of propagation and the sense of the orbital motion cannot be found unless a spatial separation is introduced into the system. For this reason it is concluded that ordinary 3-component systems offer little promise for most applications and that attention must be directed toward arrays of horizontal- and vertical-component seismometers.

2. Multicomponent Arrays

Theoretical results obtained in this study indicated that arrays of horizontal-component seismometers should prove to be useful tools for the removal of trapped-mode noise from the outputs of vertical-component instruments. A necessary condition is that the horizontals must be spatially separated from the vertical. In the case of a single-noise mode, arrays with a single ring of horizontal seismometers should perform best when the array diameter is approximately one-half wavelength. Signal enhancement systems employing only vertical instruments require, in general, array diameters of at least one wavelength. Thus, multicomponent arrays should offer meaningful advantages in terms of land and telemetry requirements.

It is unlikely that difficulties presented by system noise, uncorrelated seismic noise and Love waves should be any more serious than they are in the case of vertical-component arrays. The effect of additional noise modes on multicomponent array performance has not been studied yet. However, it is reasonable to assume that a multiplicity of modes may be dealt with by the application of multichannel filter techniques to the outputs of multiple rings of horizontals. It has been shown that an array consisting of a number of rings of verticals can be useful in the presence of a similar number of noise modes, and there is no known reason for assuming that this usefulness might be a property peculiar to vertical-component arrays.

The results derived theoretically for multicomponent seismometer arrays are quite conducive to optimism. It was shown that, if the array dimensions are suitable ($r/\lambda \sim 0.25$), the theoretical prediction error is less than 0.01, the Love wave response function is less than 0.01 and the Rayleigh wave response function is approximately 0.7. Thus, it is theoretically possible to predict (and hence remove) more than 99 percent of the Rayleigh noise on the vertical component in the frequency range in which the wavelength is appropriate. The low value of the Love wave response function implies that very little extraneous noise power should be introduced into the system output as a result of Love waves appearing in the outputs of the horizontal instruments. The high value of the Rayleigh wave response function implies that the filter responses need not be unduly large and that uncorrelated noise from the horizontals will not be amplified to a serious degree. The finding that all three response functions take on desirable values in the same range of wavelength is both unexpected and fortuitous.

From the results of the theoretical investigations presented in this report, it is concluded that multicomponent seismometer arrays offer a great deal of promise for signal enhancement applications. Experimental investigations of such systems is underway using data from TFO. It is recommended that experimental investigations of such systems be undertaken at a site where a large percentage of the ambient noise is trapped-mode noise.

D. ANALYSIS OF CPO TELESEISMS

Several large ensembles of CPO teleseisms have been analyzed for the purposes of:

- Investigating crustal reverberation deconvolution
- Determining depth of focus
- Studying CPO crustal structure
- Investigating propagation mechanisms
- Investigating teleseismic signal properties relevant to the nuclear detection problem

Some of these investigations have been discussed in Semi-annual Technical Reports 2 and 3. Some further discussion, particularly with regard to CPO crustal structure, is provided in Section III. A complete report on these studies will be provided in Special Report 14. Fairly good evidence of a significant shallow layering effect on teleseisms at CPO has been found. Compensation for this effect by deconvolution has given improvement in some senses and is probably not highly range-sensitive. The deeper reflectors, the Conrad and Mohorovicic, do not present a significant signal alteration problem in the short period range and have been only marginally identified thus far in teleseism autocorrelations. There is some question as to the adequacy of the existing ensemble statistics to unambiguously identify deep reflectors due, in part, to the range and azimuth dependence of the delay time for the deep reflectors. It is of interest that the crustal effects are clearly most evident on deep focus earthquakes as a result of the source simplicity of deep-focus events as compared with shallow events. It is not unlikely that, even in view of the capabilities of ensemble statistics, studies of station response and propagation path phenomena should be more fruitful when based on a small ensemble of deep-focus events rather than a large ensemble of shallow events.

E. FURTHER STUDY OF CPO PARTIAL ARRAYS

The seismometer equalization problem at CPO was considered and the results indicated that conclusions previously drawn, regarding the effectiveness of partial arrays at CPO, remain valid.

F. NONDIRECTIONAL CROSS ARRAY PROCESSING AT TFO

An MCF system designed to operate on the large cross array at TFO provided 3 db to 5 db greater S/N improvement than a simple summation at frequencies below about 1.0 cps. At 0.2 cps, the MCF system provided 8-db S/N improvement relative to a simple summation. Above about 1.0 cps, the MCF and summation provided about equal S/N improvement.

Results obtained are consistent with the hypothesis that trapped-mode noise at TFO is 3 to 4 db above body-wave noise in the 0.25 to 0.75 cps range and about 13 db above body-wave noise in the 0.15 to 0.25 cps range. It is interesting that the latter result is in semiquantitative agreement with the coherence analyses reported in Section VI of Semiannual Technical Report 3. The wavenumber response analysis is of interest in the general LASA subsystem problem. In the range of 0.15 to 0.25 cps, the array is clearly concentrating on a trapped-mode microseismic wavetrain coming from N 60° E at a velocity of 3 to 4 km/sec. In the 0.5 to 1.0 cps band, the 10-km array is primarily concentrating on a high-velocity body-wave component coming from the southeast at a velocity probably in excess of of 16 km/sec. Above 1.5 cps, the array provides $\sqrt{N}$ improvement or better, whether employed as a simple beam former or as an adaptive noise rejector.

G. DETECTION OF SEISMIC SIGNALS

Special Report No. 8 entitled "Array Research Preliminary Report, Matrix Multiply Detection Processing of Array Data" was published 13 October 1965. Assumptions, derivations of equations, and an illustration of the method of signal detection by probabilistic processing were presented.

Results of applying a probabilistic processor to actual signals are presented in Section VI of this report. This processor was designed using a theoretical model of signal and noise. Three events were processed and the results were compared with a detection scheme employing Wiener signal-extraction processing and the square and integrate process on the output trace. For one of the signals, an indication of superiority of the matrix-multiply technique over the Wiener technique was obtained.

It is planned to evaluate the matrix multiply detection technique using a processor designed from measured CPO noise correlations. It is also planned to compare the results with a comparable Wiener square and integrate process and with a technique known as Analysis of Variance.*

*Booker, Aaron, 1965: Analysis of variance as a method for seismic signal detection, SDL Rpt. No. 116, Contract AF 33(657)-12447, VT/2037, 25 Feb.

H. LASA PROCESSING, DATA COLLECTION, AUTOMATED MAPPING AND PREDICTABILITY OF NOISE FROM SHALLOW-BURIED ARRAYS

A study was completed to determine the effectiveness of LASA multichannel processing in separating teleseismic nuclear blast signals (originating in particular regions on the earth) from teleseismic earthquakes (originating in certain seismically active regions of the earth). Several different cases were investigated and the results are given in Section VII. A conceptual method of processing LASA data on-line was evolved and is presented in summary form in Section X.

Data collection programs in support of Dallas-based research efforts have been active and are summarized in Section IX.

An automated mapping system for presenting the world in wavenumber space is presented in Section XI.

The UBO studies dealing with spatial predictability of shallow-buried seismic noise and extraction of signals from cultural noise are incomplete.

REPORTS SUBMITTED OR PLANNED FOR ARRAY RESEARCH — VT/4053

Date	Title	Author(s)	Identification
12/31/63	Detailed Information Pertaining to Monthly Report 1, Project VT/4053	Backus	Spec. Rpt. 1
5/15/64	Semiannual Tech. Rpt. 1	Baker, Hoffmann, Backus, Burg Roden, Baldwin	S/A Tech. Rpt. 1
8/64	An Evaluation of Vertical Seismometer Array and Horizontal Array Performance Based Upon a Theoretical Model of Noise and Teleseismic Signal	Roden	
9/1/64	Multichannel Filter Systems for Tonto Forest Observatory	Baldwin	Spec. Rpt. 2
9/21/64	Multichannel Filter Systems for Tonto Forest Observatory	Baldwin, Backus	Spec. Rpt. 3
11/15/64	Semiannual Tech. Rpt. 3	Burg, Roden, Harley, Baldwin, Baker	S/A Tech. Rpt. 2
12/3/64	Basic Theory of Probabilistic Processing	Burg, Backus	Spec. Rpt. 4
12/15/64	A Reevaluation of Signal-to-Noise Improvement for Cumberland Plateau Observatory Using Local Noise	Baldwin, Backus	Spec. Rpt. 5
2/15/65	Horizontal and Vertical Arrays for Teleseismic Signal Enhancement: UBO Model Theoretical Results	Roden	Spec. Rpt. 6
6/3/65	Semiannual Technical Report 3	Backus, Roden, Rogers, Burg, Hoffman, Booker, Binder	S/A Tech. Rpt. 3
8/65	Vertical Array Experiments at Uinta Basin Seismological Observatory	Roden	

Date	Title	Author(s)	Identification
10/65	Some Theoretical Calculations of the Performance of a 6-Element Vertical Seismometer Array	Roden	
10/13/65	Preliminary Report Matrix-Multiply Detection Processing of Array Data	Booker	Spec. Rpt. 8
10/25/65	A Comparison of Weiner and Maximum Likelihood Multichannel Filtering	David Jackson	Summer Development Spec. Rpt.
11/9/65	Theoretical Capability of Systems of Horizontal Seismometers for Predicting a Vertical Component in Ambient Trapped-Mode Noise	Potter, Roden	Spec. Rpt. 7
1/66	A Study of Multichannel Filter Systems Incorporating Statistical Gain Fluctuation Designed for Cumberland Plateau Observatory	Binder	Spec. Rpt. 9
1/66	An Evaluation of the Properties of the TFO Cross Array Based on the Evaluation of a Multichannel Filter System Design Using the Entire Cross Array	Binder	Spec. Rpt. 10
1/66	Five Programs of Automated Mapping System	Baker, Eubanks	Spec. Rpt. 11
1/66	Array Research Data Collection (Acquisition)	Baker, Hoffmann	Spec. Rpt. 12
1/66	LASA Processing Requirements	Baker, Backus	Spec. Rpt. 13
2/66	Study of Teleseisms Recorded at Cumberland Plateau Observatory	Roden	Spec. Rpt. 14
3/66	Results of Matrix-Multiply Detection Processing of Array Data (Tentative Title)	Booker	Spec. Rpt. 15

SECTION II

NEW RESULTS FROM PROCESSING OF VERTICAL ARRAY DATA

A. RESULTS OF NOISE STUDY, FILTER DESIGN AND EVALUATION BASED ON PI2WY DATA

Deep-well seismic data which have been obtained from the granite well designated PI2WY are displayed in Figures II-1 and II-2. As indicated, noise recordings were made with a surface instrument and deep-well instruments at four different depths. Signal recordings were available for the surface instrument and for two depths. Each recording consists of simultaneous data from the surface and two depths in the well.

Start times (GMT) of the noise samples are indicated in Figure II-1. Noise samples 1, 2 and 3 were recorded between 7 a.m. and 11 a.m. (local time) while noise sample 4 was recorded near midnight (local time). Differences in noise power may indicate a difference between day and night levels, but also could result from a long-term effect since the recordings span an interval of 3-1/2 weeks. Sources of the teleseismic signals have been identified as follows:

- Signal 1. Fiji Islands Region; 17.0° S, 177.4°W; origin time, 01/36/45.4 GMT; C&GS focal depth, 386 km; magnitude, 5.5 to 6.0; distance, 85°.
- Signal 2. Aegean Sea; 39.4°N, 24.0°E; origin time, 17/57/53.7 GMT; C&GS focal depth, 18 km; magnitude 5.7 to 6.5; distance, 86°.

Records originally were digitized with 40-msec sample rate. After the application of a high-cut antialiasing filter (3-db down-point at 3.5 cps), the records were resampled at 120 msec for analysis. Power spectra of the surface instrument outputs (not corrected for instrument response) are shown in Figures II-3 and II-4. A strong low-frequency microseismic peak is evident in all four noise spectra, but does not appear at all in the signal spectra. Apparently, two distinct types of noise have been recorded. Low-frequency microseismic noise is observed in short (less than 10 sec) bursts which seem to arrive at random times (Figure II-1). This type of noise is extremely reproducible from one depth to another and its amplitude shows only slight depth dependence. The other type of noise may be observed between the low-frequency bursts and also before the signal onsets (Figure II-2). This noise has much more high-frequency energy and displays a clear amplitude decrease with depth, even at low frequencies. It appears that this second type of noise is relatively steady and never approaches the strength of the microseismic bursts.

Text cont'd page II-6

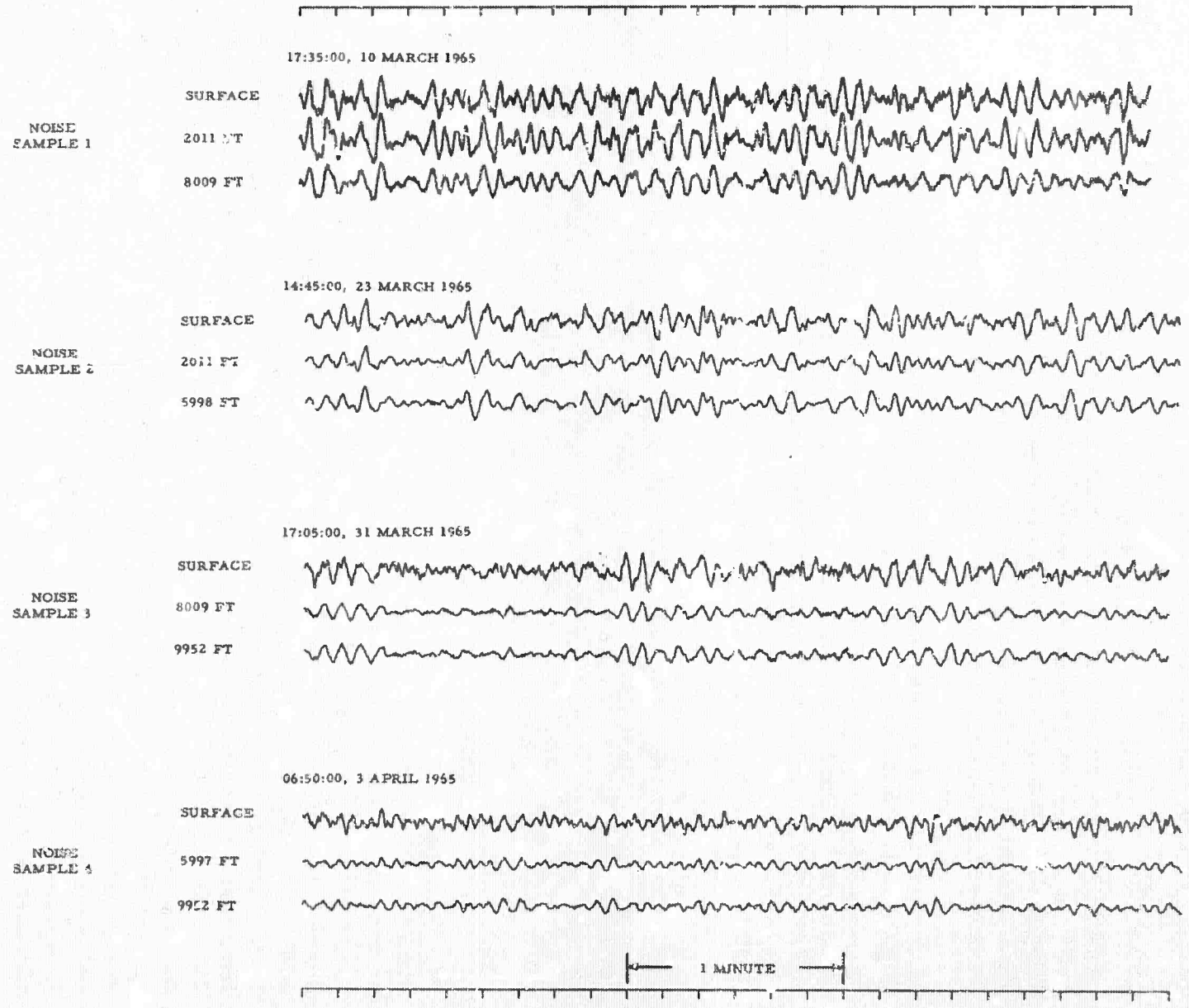

Figure II-1. Noise Samples Recorded in the Well PI2WY

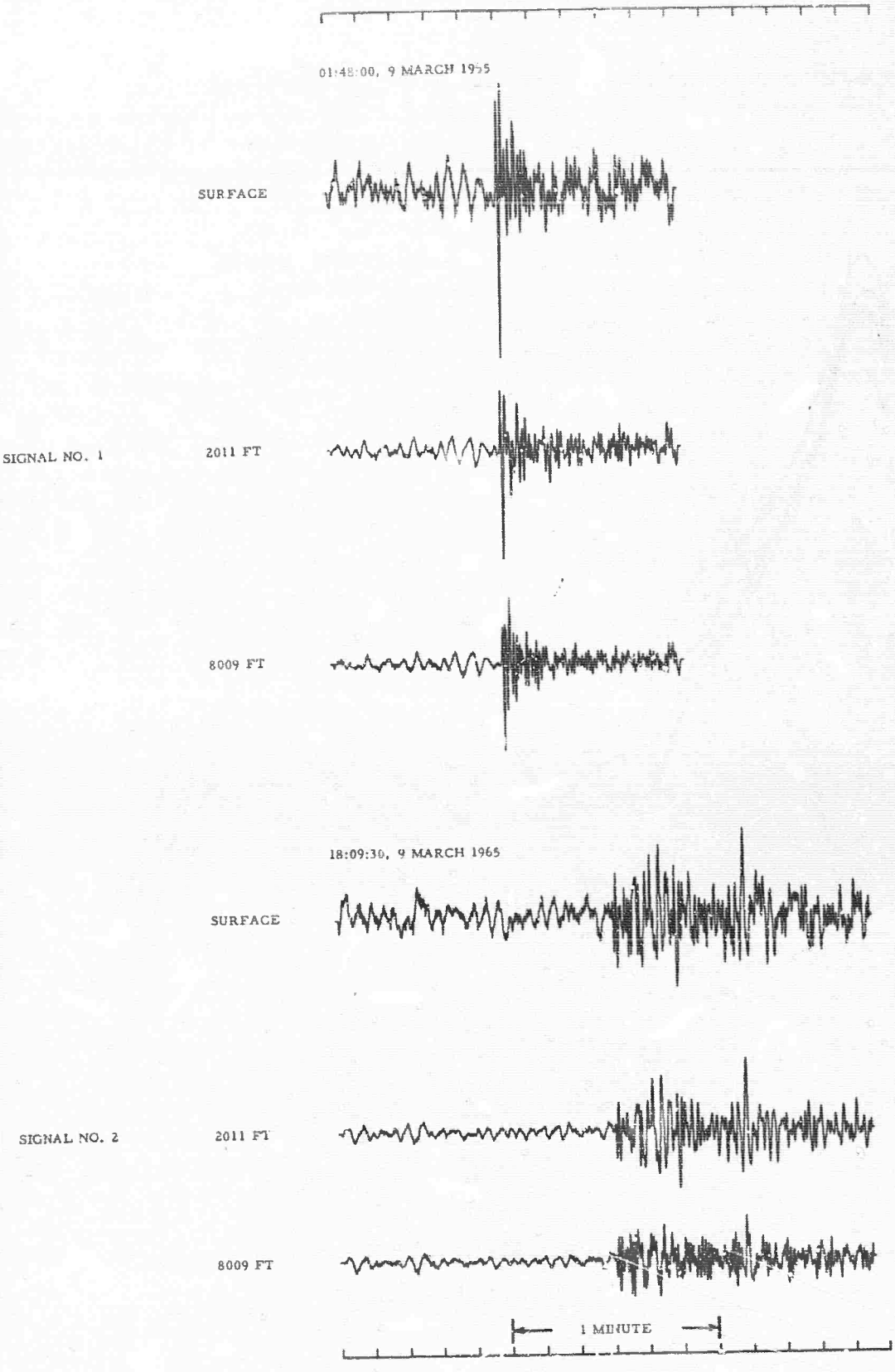

Figure II-2. Teleseismic Signals Recorded in the Well PI2WY

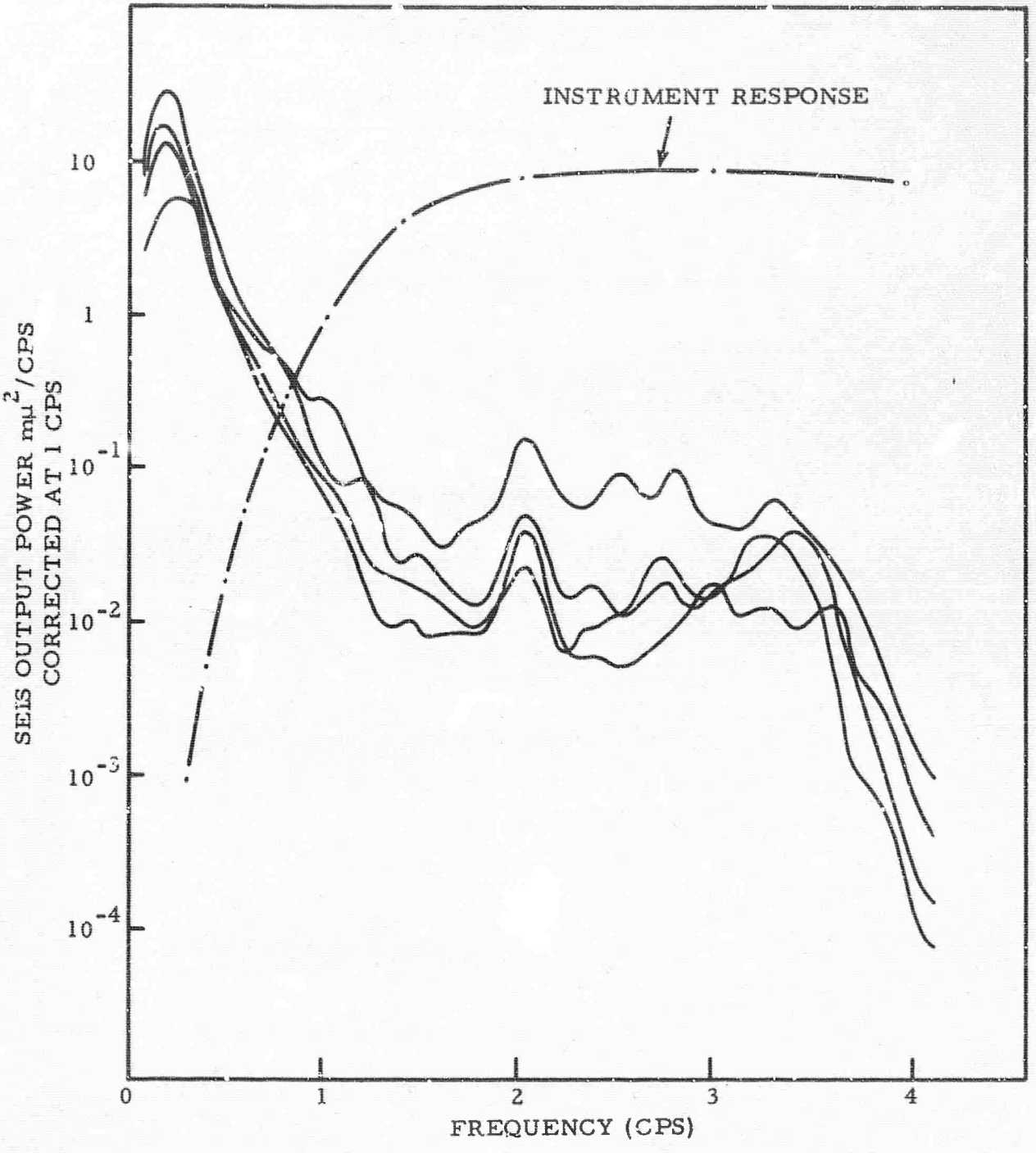

Figure II-3. Power Spectra Computed from Noise Samples Recorded by Surface Seismometer at PI2WY Well Site

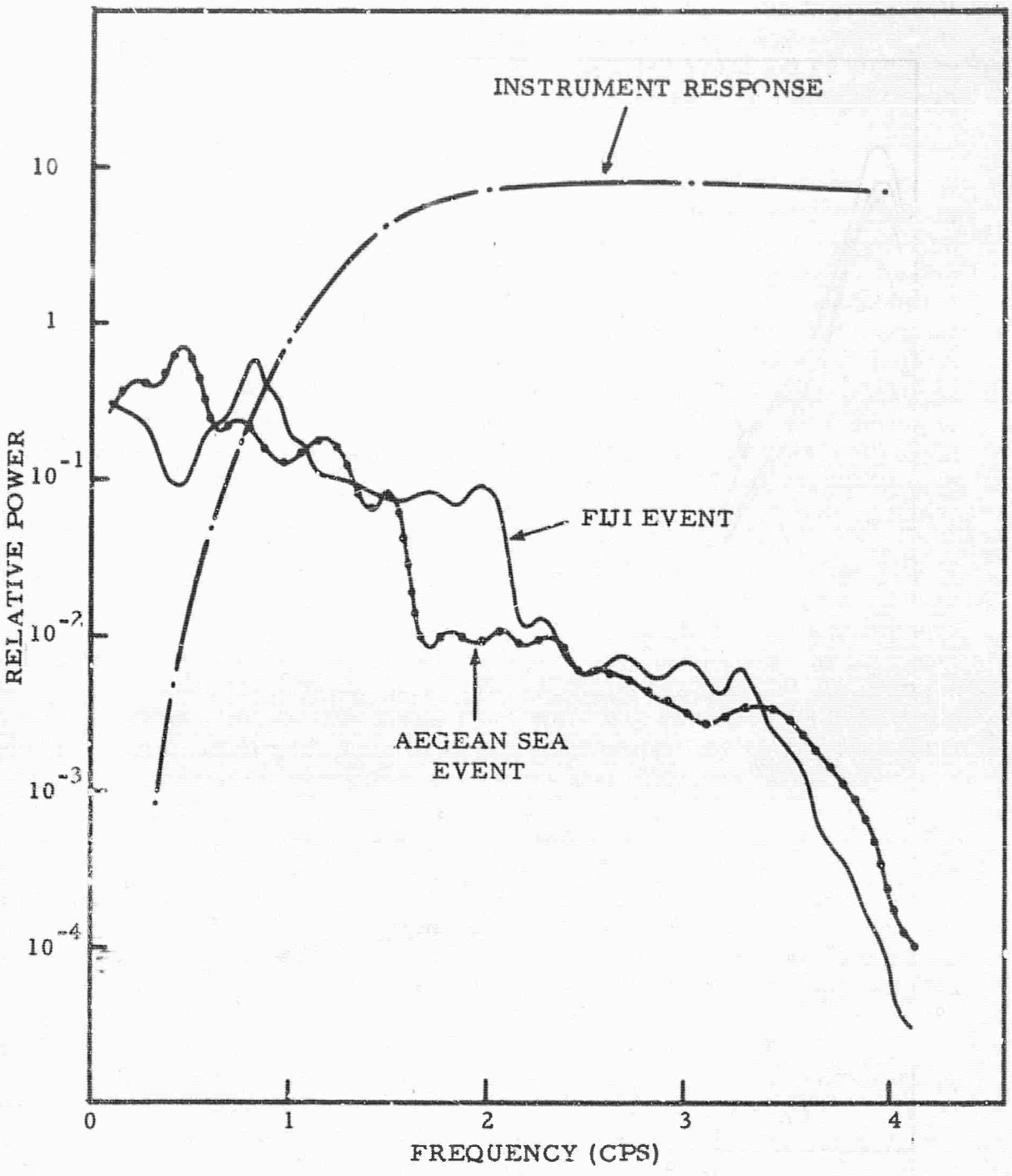

Figure II-4. Power Spectra Computed from Teleseisms Recorded by Surface Seismometer at PI2WY Well Site

The flattening of the noise spectra above 1.5 cps is an indication of system noise which could have been introduced either in the recording or digitization operations. Since system noise is dominant in the high-frequency range, vertical array evaluation is possible only for frequencies below 1.5 cps.

An important objective of this study was the evaluation of multichannel filter techniques applied to data from vertical arrays in wells such as PI2WY for the purpose of signal-to-noise ratio improvement. Such improvement can be significant only if the amplitudes of signal and noise depend upon depth in different predictable ways or if the noise is not coherent. Deep well-to-surface power spectral ratios computed from the available data are shown in Figure II-5. Below 1.5 cps, only minor differences between signal and noise behavior can be observed. Coherence functions computed for Noise Sample 1 (Figure II-6) indicate that the noise is predictable from channel to channel up to approximately 1.0 cps for the larger receiver separations (6000 ft, 8000 ft) and 1.5 cps for the smallest separation (2000 ft).

For multichannel filter design, two models were employed. In both cases, correlation functions computed from noise sample 1 were used as the noise model. The signal model for the first case (MCF-1) was obtained by averaging correlation functions of the two experimental signals. For the second case (MCF-2), a theoretical signal with white spectrum in the range of 0 to 3 cps was used. Before experimental correlations were computed, each record was whitened by applying to all three traces a deconvolution filter designed from the surface trace. Impulse responses of the two MCF sets are shown in Figures II-7 and II-8.

Results of applying the filters to noise sample 1 and signals 1 and 2 are shown in Figures II-9 and II-10. For each filter set, the output trace and the reject trace (difference between input trace 1 and output trace) are shown. For the high-frequency behavior of the systems to be seen more clearly, a low-cut filter (3-db down-point at 0.76 cps) has been applied to both the input and output traces (Figures II-11 and II-12).

Input and output power spectra of signal and noise are shown in Figure II-13. The only significant difference between the performances of the two systems is that MCF-2, designed on an assumption of zero-signal power above the frequency of 3 cps, rejected everything above that frequency. Signal-to-noise improvements of the two systems are given in Figure II-14.

Text cont'd page II-18

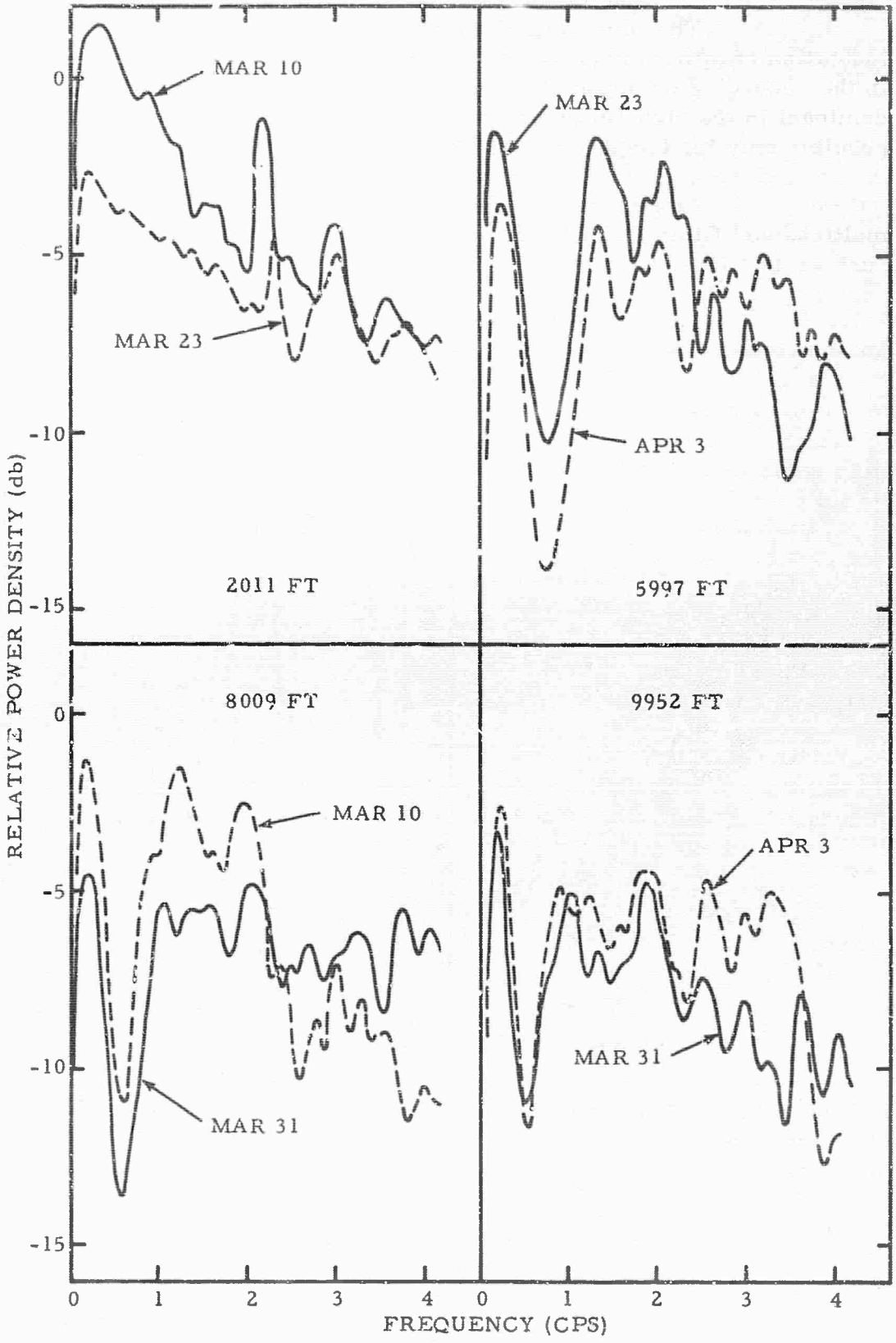

Figure II-5a. Deep-Well to Surface Spectral Ratio of Seismic Noise

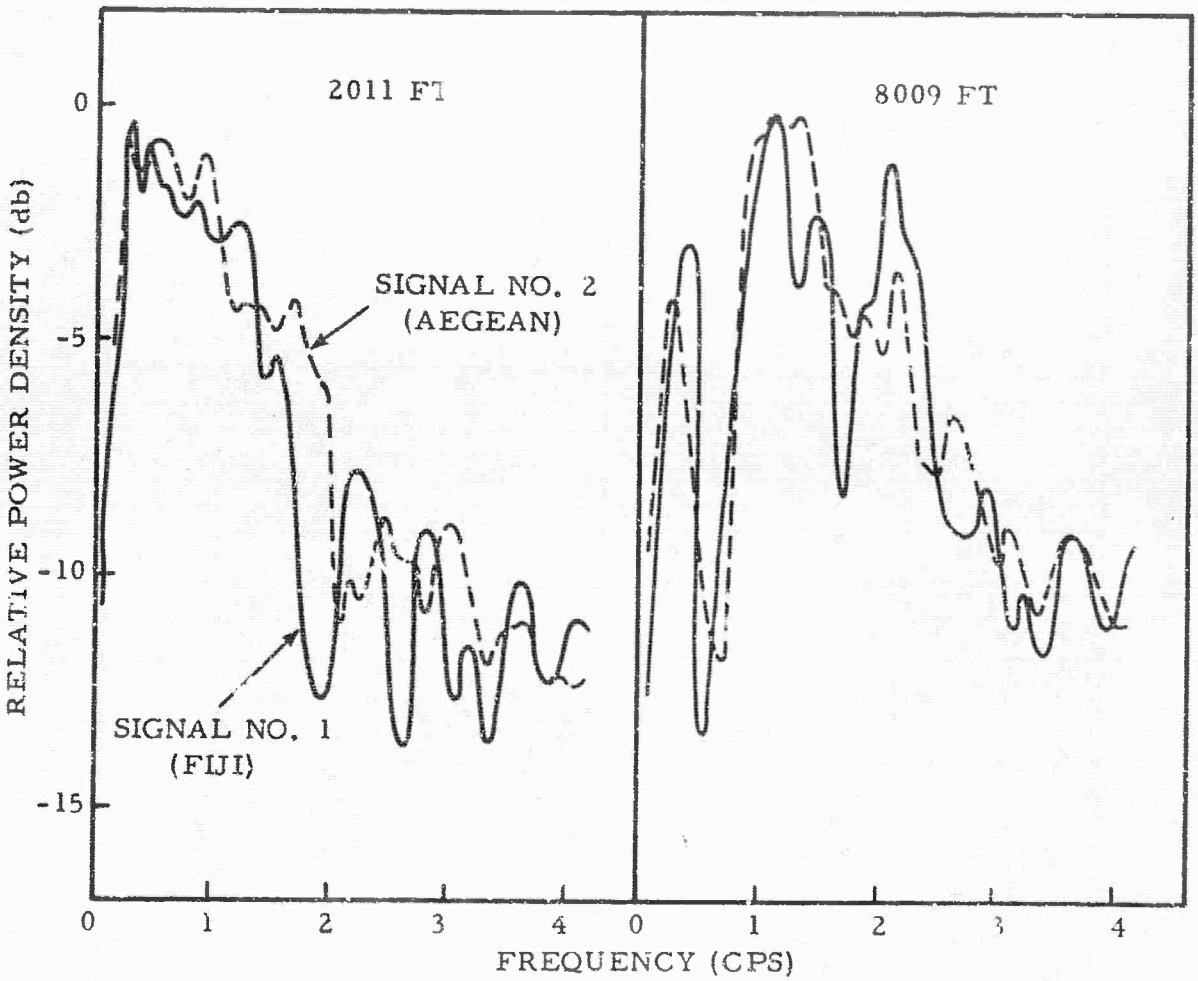

Figure II-5b. Deep-Well to Surface Spectral Ratios of Teleseismic Signals

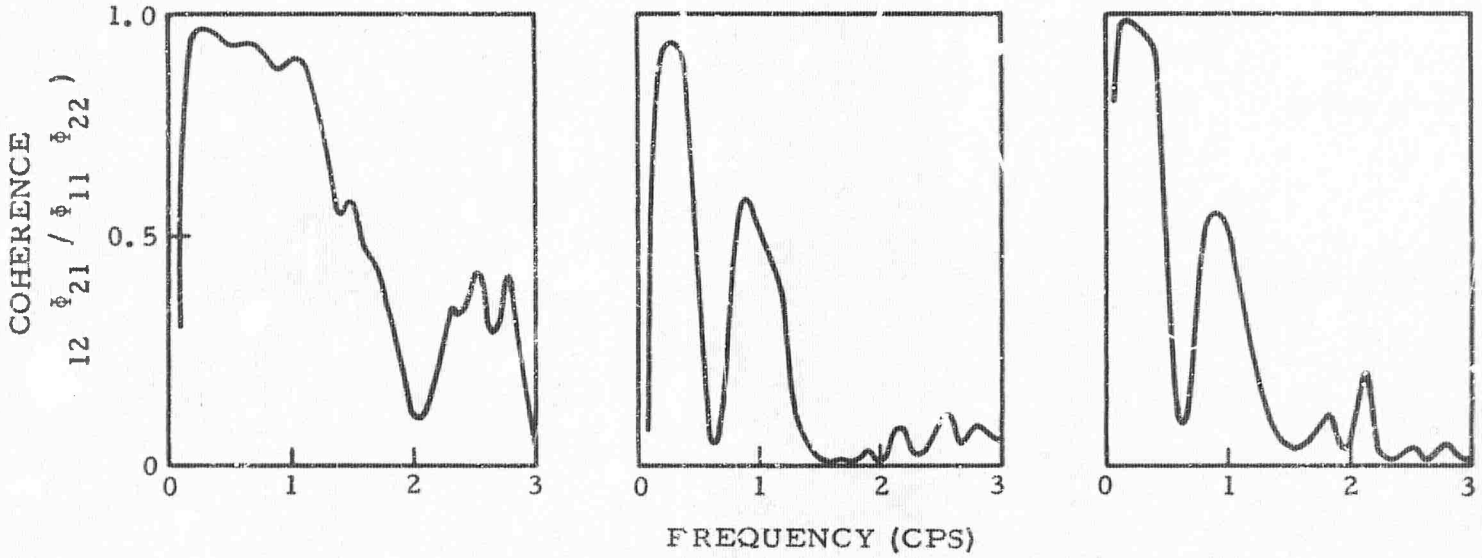

Figure II-6. Two-Channel Coherence Functions from PI2WY Noise Sample 1

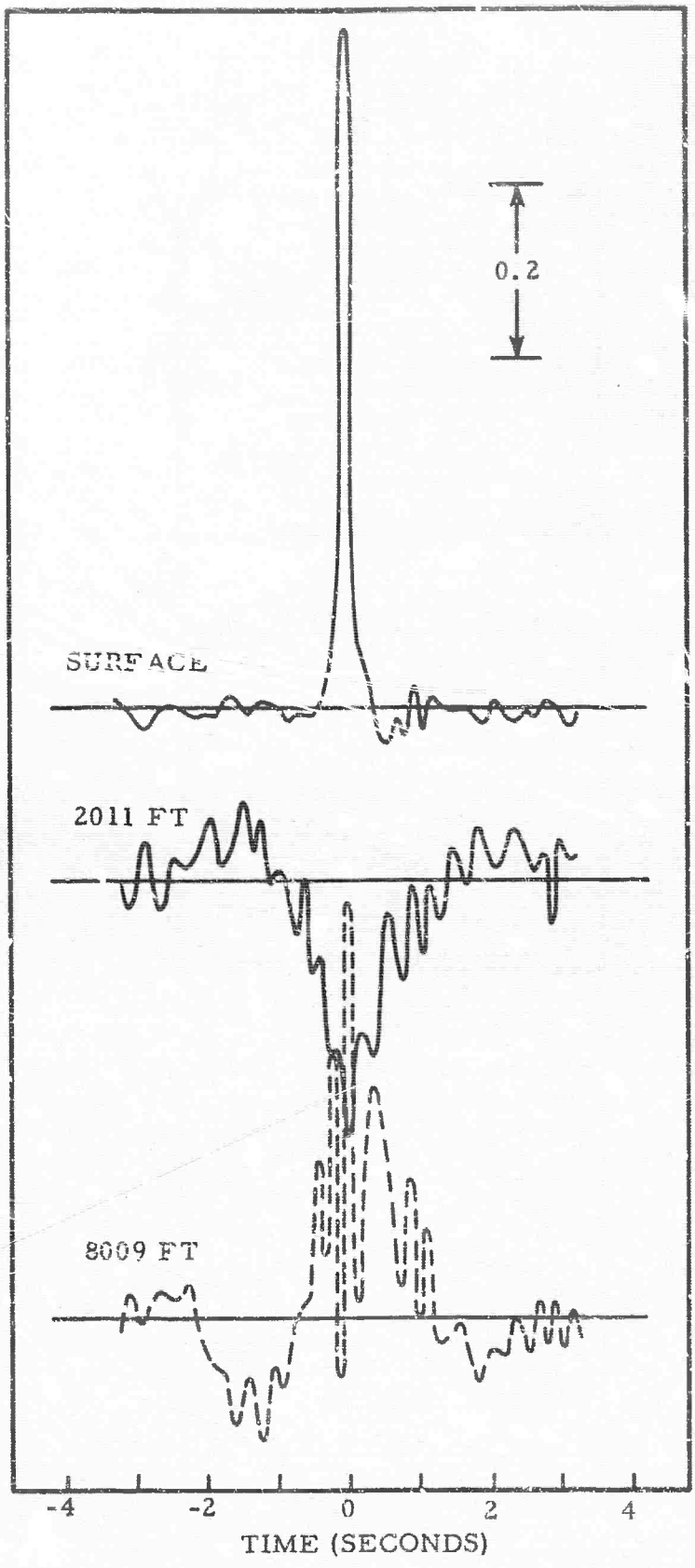

Figure II-7. Impulse Responses of Filter Set MCF-1

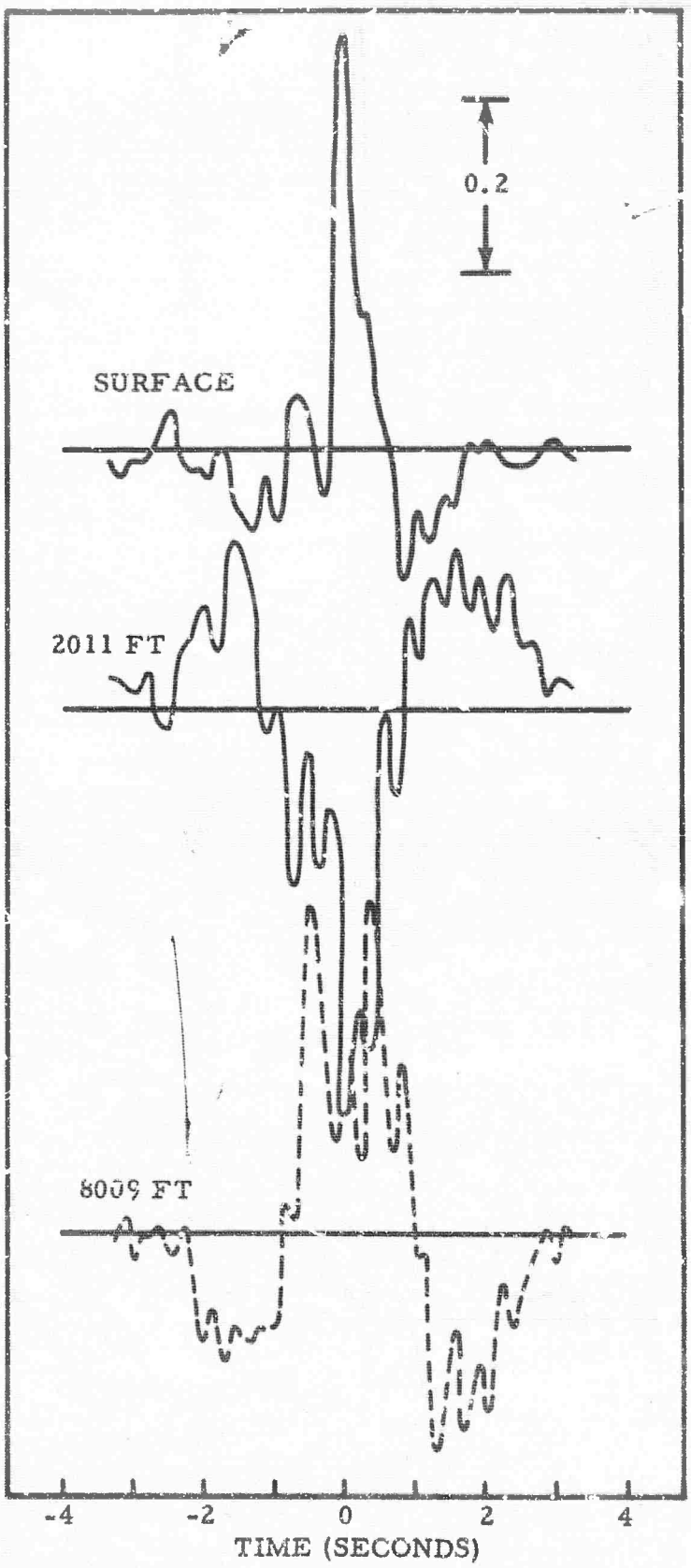

Figure II-8. Impulse Responses of Filter Set MCF-2

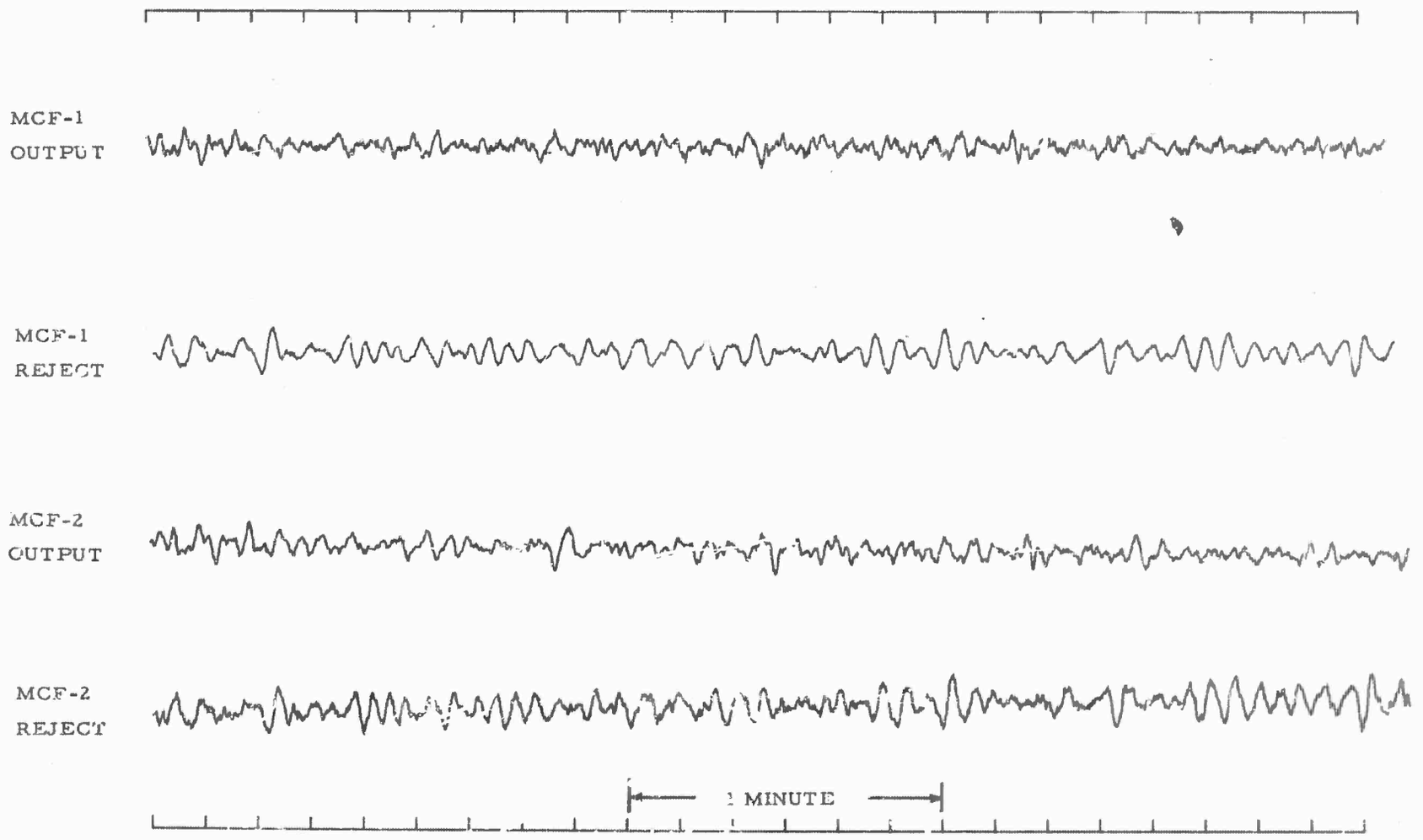

Figure II-9. Results of Processing Noise Sample 1

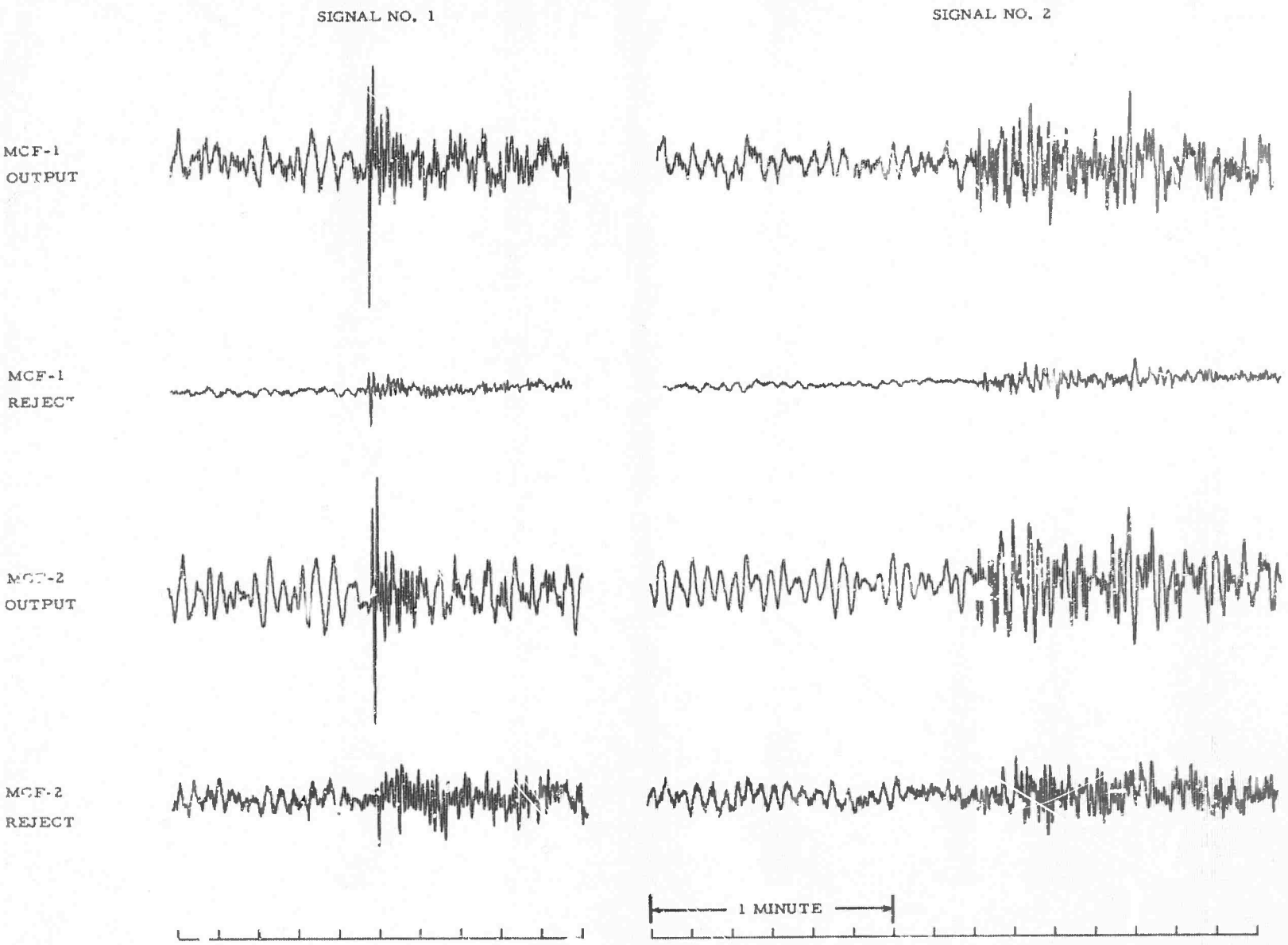

Figure II-10. Results of Processing Teleseismic Signals

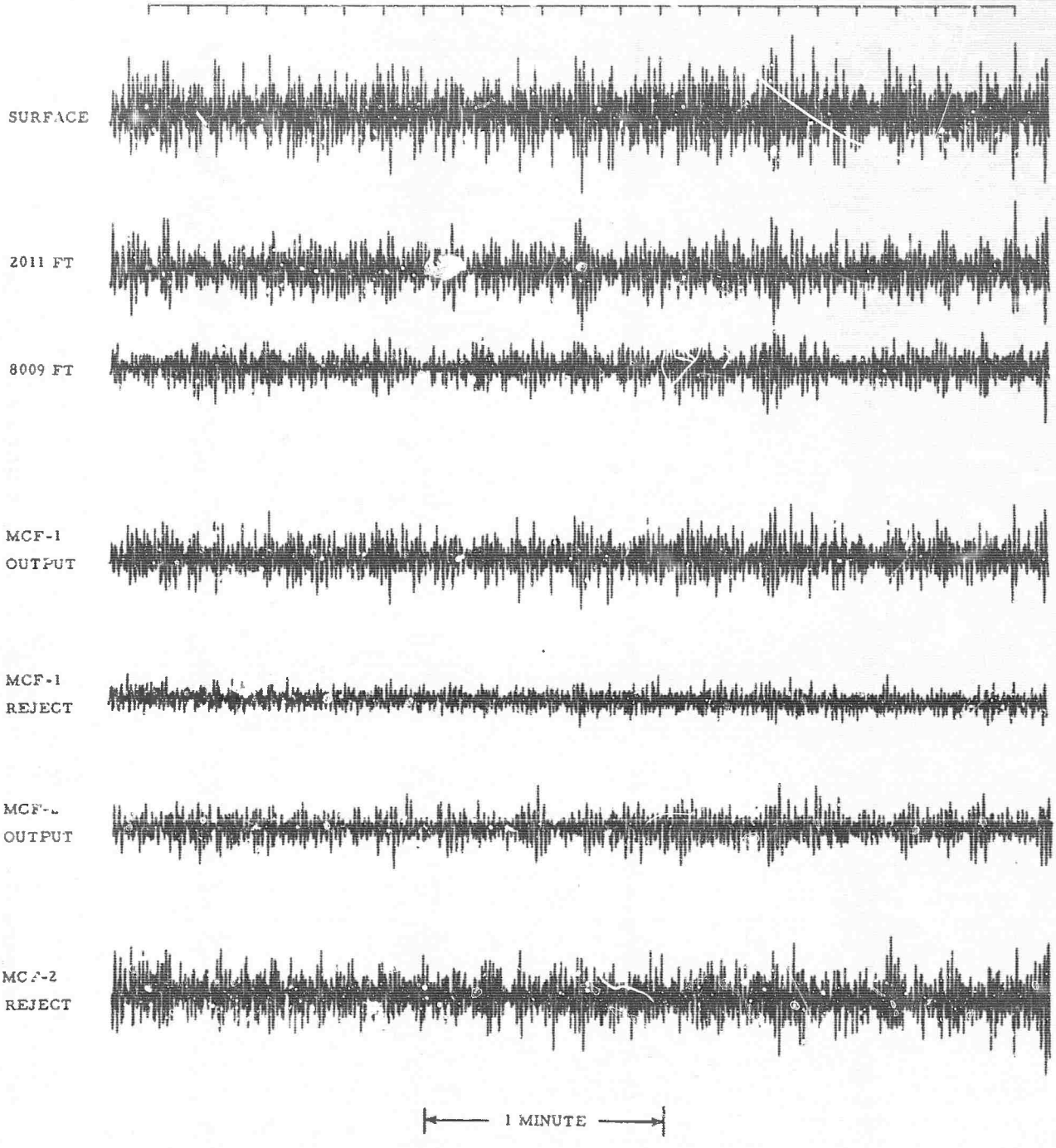

Figure II-11. Low-Cut Filtered Input and Output Records of Noise Sample 1

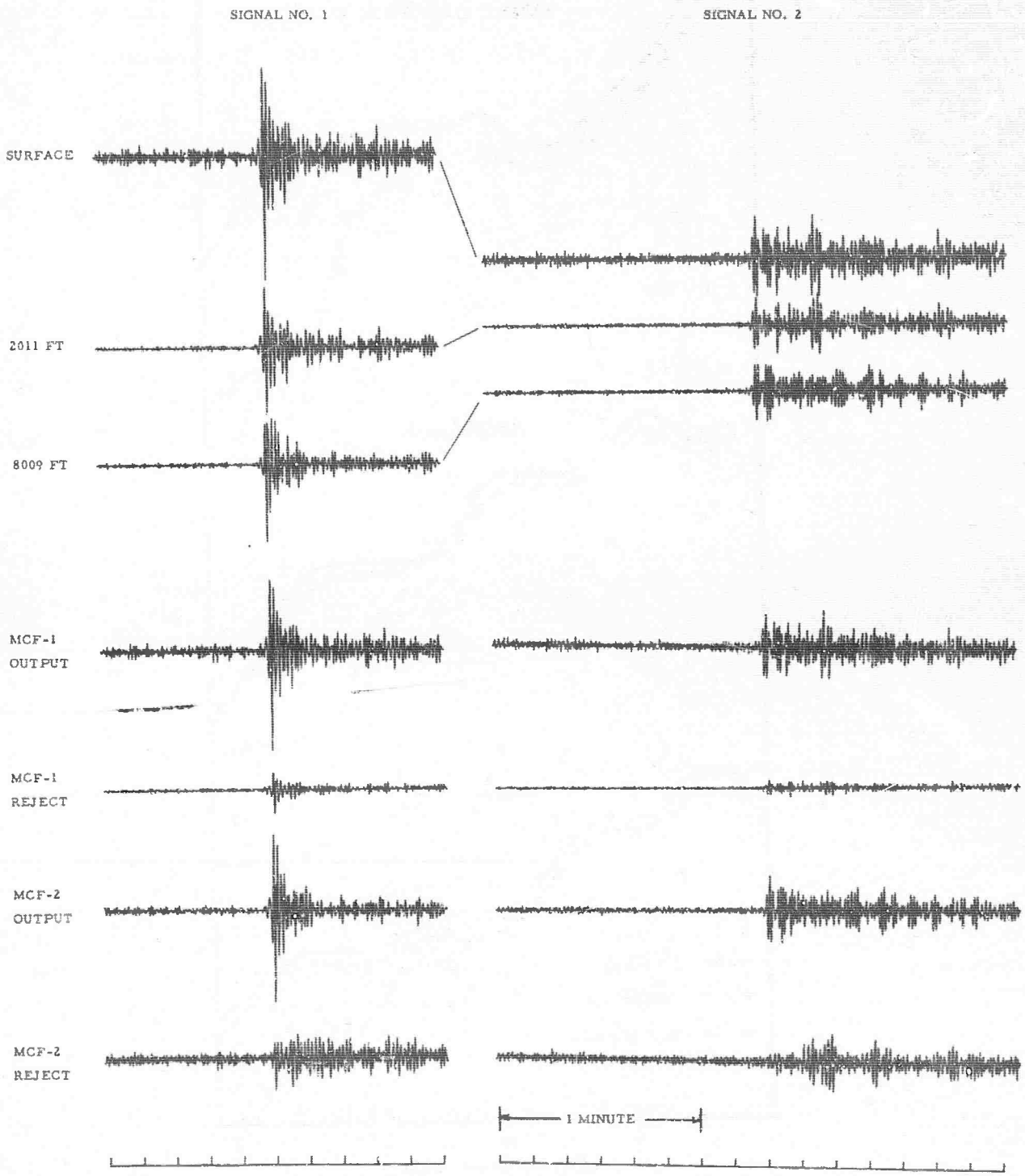

Figure II-12. Low-Cut Filtered Input and Output Records of Teleseismic Signals

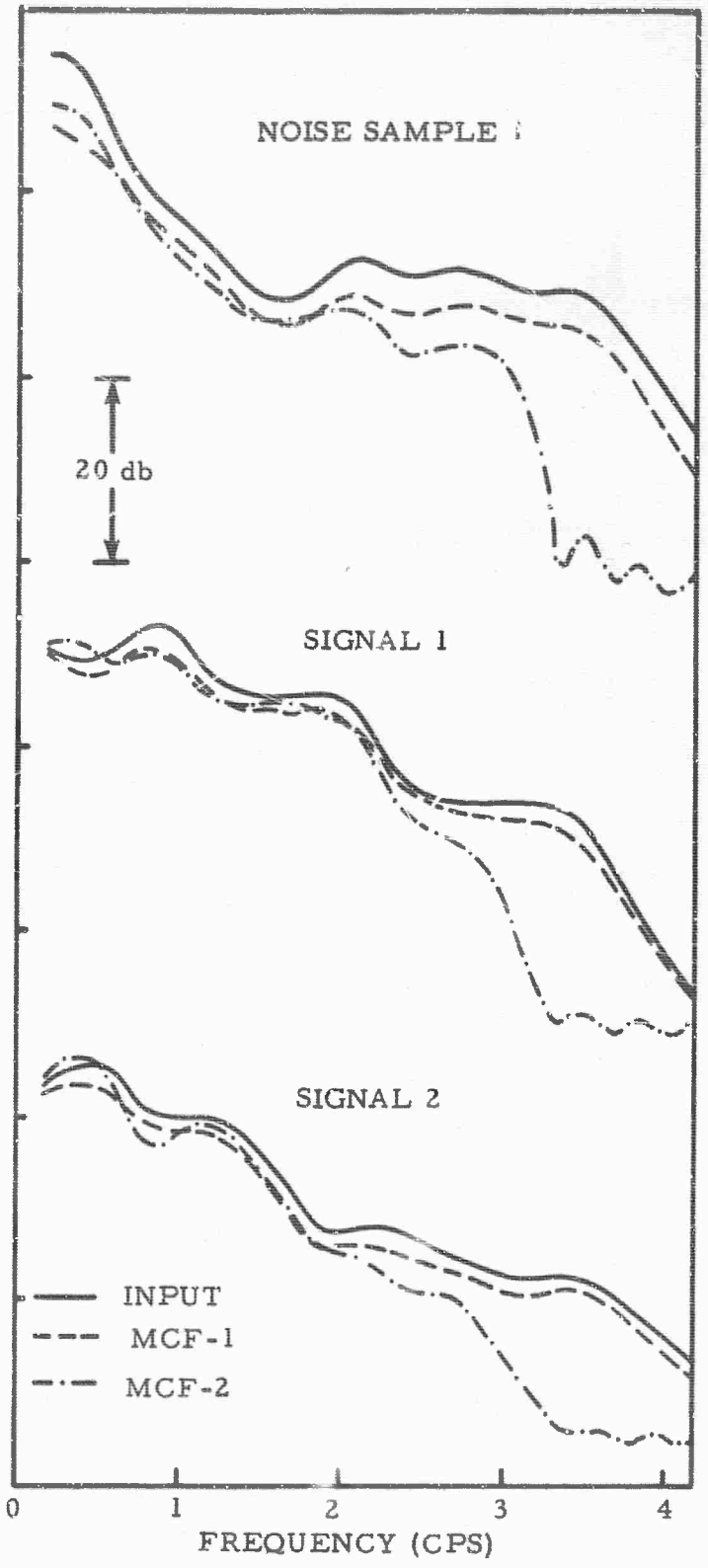

Figure II-13. Input and MCF Output Power Spectra of Noise and Signal

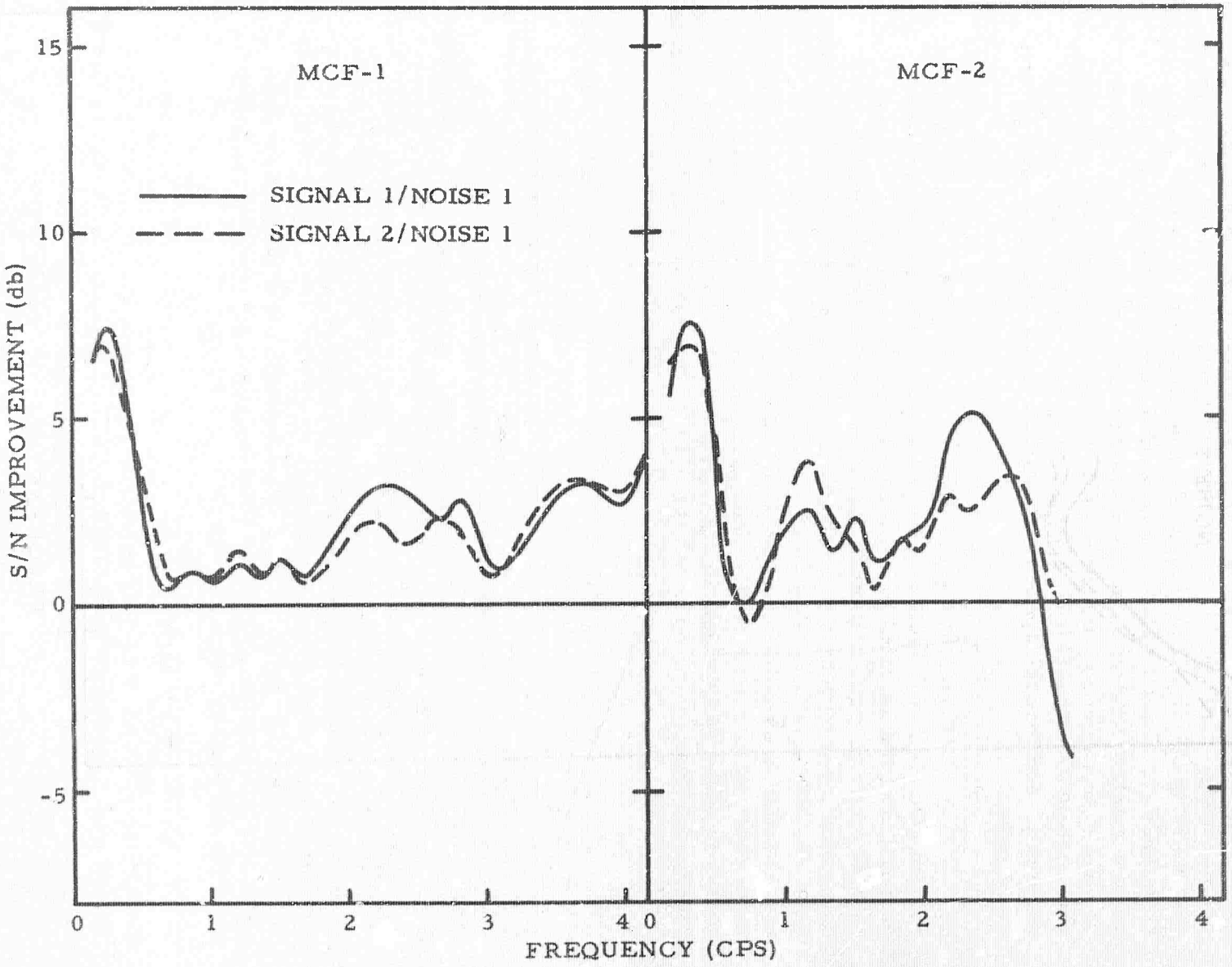

Figure II-14. S/N Improvements Computed for the Two MCF Systems

At low frequencies (< 0.5 cps) both systems achieved about 7 to 8 db signal-to-noise improvement. Since it is unlikely that there could have been significant signal energy at such low frequencies, this result implies that noise in Noise Sample 1 was rejected more effectively than noise in the signal records. Such behavior could be expected from MCF-1, designed from experimental signal statistics, if there were a marked difference in the character of the noise. The failure of MCF-2 to reject low-frequency noise in the signal records suggests that channel-to-channel gain compensation may not have been applied correctly, and that the apparent changes in noise character may be artificial ones.

At intermediate frequencies ($0.5 < f < 1.2$ cps), neither system achieved any significant improvement. This failure and the properties of the spectral ratios and coherences computed for Noise Sample 1 can be explained most easily by assuming that the ambient noise is composed mainly of P-waves in the intermediate frequency range. Since the subsurface at the well site may, for practical purposes, be represented by an infinite homogeneous half space, the only kind of surface wave which should exist is the fundamental-mode Rayleigh wave. The observed peaks and troughs in the experimental spectral ratios and coherences agree very well with those found theoretically and experimentally for P-waves, but should not be produced at all by Rayleigh-wave noise.

As was mentioned above, information in the high-frequency range (> 1.2 cps) has been destroyed by system noise. The lack of coherence observed for this noise indicates that it was probably introduced in the analog-to-digital conversion. Noise due to digitization round-off should be between 30 and 40 db lower than the observed system noise level. It is therefore concluded that the explanation lies in inaccuracies in the analog tape transports. Since performance in the intermediate-frequency band is apparently limited by the P-wave noise level, it is clear that the higher frequencies deserve more attention than they have received in the past. Useful information, however, cannot be obtained with the system used to collect the data described here. The additional dynamic range afforded by digital field recording is sufficient for this purpose. Alternatively, low-cut filtering of the data before recording could be used to ease dynamic range requirements.

In summary, the results obtained for the PI2WY are inconclusive. It appears that useful vertical array performance must be limited to the frequency range ($f > 1.2$ cps) but it is impossible to estimate how much, if any, signal-to-noise improvement can be expected there.

Table II-1

CATALOG OF SELECTED UBO VERTICAL ARRAY RECORDINGS

Record Identification	Record No.	Date	Start Time (GMT)	Description
Noise Sample 1	45	Oct. 5	134010	Quiet Noise
Noise Sample 2	46	5	135410	Intense Noise
Noise Sample 3	47	5	135810	Quiet Noise
Noise Sample 4	50	5	142210	Intermediate-Level Noise
Noise Sample 5	52	5	144410	Intense Noise
Noise Sample 6	53	5	144810	Intense Noise
Local Event 1	501	3	220110	Unidentified Local or Near-Regional Event
Local Event 2	506	5	001410	Unidentified Local or Near-Regional Event
Local Event 3	512	6	002010	Unidentified Local or Near-Regional Event
Signal 1	407	5	002210	Yukon Earthquake
Signal 2	423	5	100330	Mid-Indian Rise Earthquake
Signal 3	403	4	041550	Oregon Offshore Earthquake
Signal 4	406	5	001110	Mexico Earthquake
Signal 5	412	5	081910	Rat Island Earthquake
Signal 6	420	5	035100	Chile Offshore Earthquake

B. MULTICHANNEL FILTERING OF VERTICAL ARRAY DATA FROM GRAPEVINE AND UBO

During 1965, deep-well digital recording programs have been carried out at Grapevine, Texas, and the Uinta Basin Observatory (UBO). It is hoped that these data will prove to be much more useful for vertical array evaluation than were any data reported to date, since for the first time, six deep seismometers were operated simultaneously in the wells. Instruments employed at Grapevine were a 3-component seismometer at the surface and six deep seismometers at 3500, 4500, 5500, 6500, 7500, and 8500 ft. Depths of the six downhole seismometers at UBO were 3900, 4900, 5900, 6900, 7900, and 8900 ft. In addition, the following were recorded at UBO: 1 vertical-component surface instrument, 10 vertical-component shallow-buried seismometers, 2 horizontal-component surface instruments, outputs of 10 delay-line multichannel filters operating on-line at UBO.

Samples edited from the Grapevine recordings have been described in Semiannual Technical Report 3 under Contract AF 33(657) - 12747. Eighty-seven samples were edited from the first available set of UBO records including 23 teleseisms, 10 local events and 48 noise samples. From this set, the 15 records listed in Table II-1 were selected for use in filter design and evaluation.

At this time, approximately six MCF systems have been designed from and applied to each set of data. Results have not been examined yet in detail and will not be discussed in this report, except for the following observation. Preliminary study of some UBO results appears to confirm previously reported conclusions that the seismic noise at UBO is dominantly P-waves between 0.5 and 1.0 cps. Estimated signal-to-noise improvements for two of the best (to date) experimental UBO MCF systems are about 5 db below 0.66 cps, less than 2 db between 0.66 and 1.66 cps and almost 10 db above 1.66 cps. These figures probably are not representative of the best performance which could be obtained with proper MCF design, but seem to be reliable indicators of the frequencies at which effective signal enhancement can be achieved at UBO.

C. DECOMPOSITION OF UBO AMBIENT-NOISE FIELD INTO CONSTITUENT MODES *

From September through October 1964, 3-channel vertical array recordings were made at UBO. Data collection was described in Semiannual Technical Report 2 and results of filter design and evaluation

*Results described in this paragraph have been presented in "Vertical Array Experiments at Uinta Basin Seismological Observatory", paper presented at 35th annual meeting Society of Exploration Geophysicists, Dallas, Texas, Nov. 24, 1965.

were reported in Semiannual Technical Report 3, both under Contract AF 33(657)-12747. Since observed MCF performance was much worse than had been predicted previously on a theoretical basis,* it was deemed worthwhile to investigate the nature of the ambient noise at UBO.

By averaging values computed from 67 recordings, average sets of signal and noise autocorrelation and crosscorrelation functions were synthesized for a hypothetical 6-element vertical array with receivers at depths of 200, 900, 2900, 4900, 6900, and 8900 ft. For the same array, theoretical sets of correlation functions have been computed for P-waves (vertically incident) and surface waves. These are displayed in Figure II-15, each set being arranged in the sequence φ_{11}, φ_{12}, . . . , φ_{16}, φ_{22}, . . . , φ_{26}, φ_{33}, . . . φ_{66} where the subscripts refer to seismometers in the order of increasing depth.** The theoretical models represented in Figure II-15 are the following:

(1) Vertically incident P-waves with white spectrum in the range of 0 to 2 cps.

(2) Fundamental-mode surface waves with white spectrum in the range of 0 to 2 cps

(3) First higher-mode surface waves with white spectrum in the range of 0.3 to 2 cps

(4) Second higher-mode surface waves with white spectrum in the range of 0.5 to 2 cps

(5) Uncorrelated white noise with equal power on all channels

Since the theoretical models were band-limited to the range of 0 to 2.0 cps, it was decided to limit the frequencies in the experimental correlation sets to the same range. The upper traces in Figures II-16 and II-17 are the band-limited experimental correlation sets for noise and signal. The aim of this study is to approximate the experimental noise correlation set by a summation of a group of correlation sets of known origin. The relative contributions of the various correlation sets to the best summation may be interpreted then as estimates of the relative contributions of the corresponding types of noise to the observed noise field.

---

* Texas Instruments, 1965, Array Research; horizontal and vertical arrays for teleseismic signal enhancement; UBO model theoretical results: Spec. Rpt. No. 6, AFTAC, Contract AF 33(657)-12747, 15 Feb.

** For purposes of computational economy, each set of correlation functions has been arranged in a form analogous to a seismic trace and, in this report, are displayed in that form.

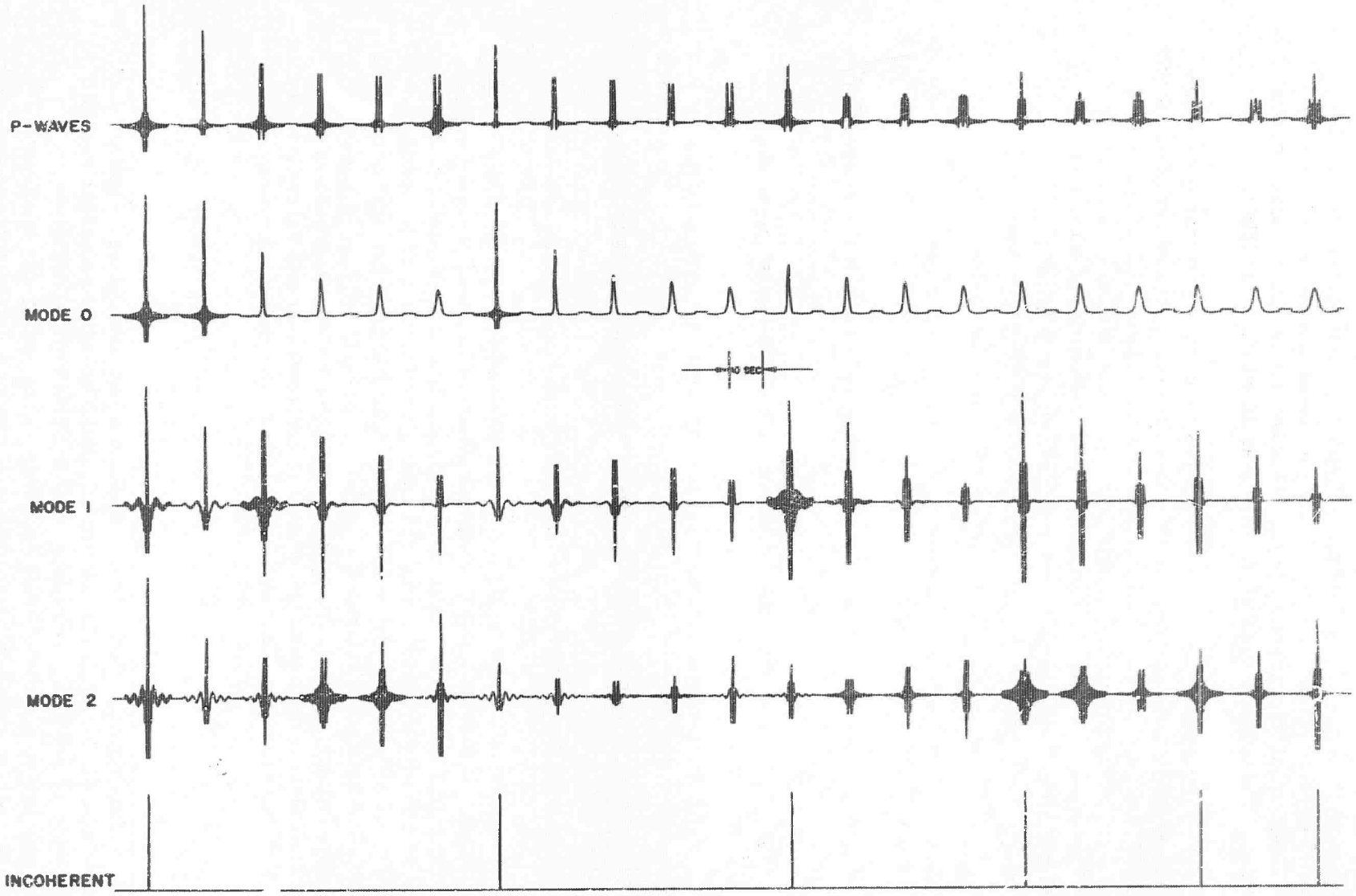

Figure II-15. Theoretical Correlation Sets for P-Waves, Surface Waves, and Incoherent Noise

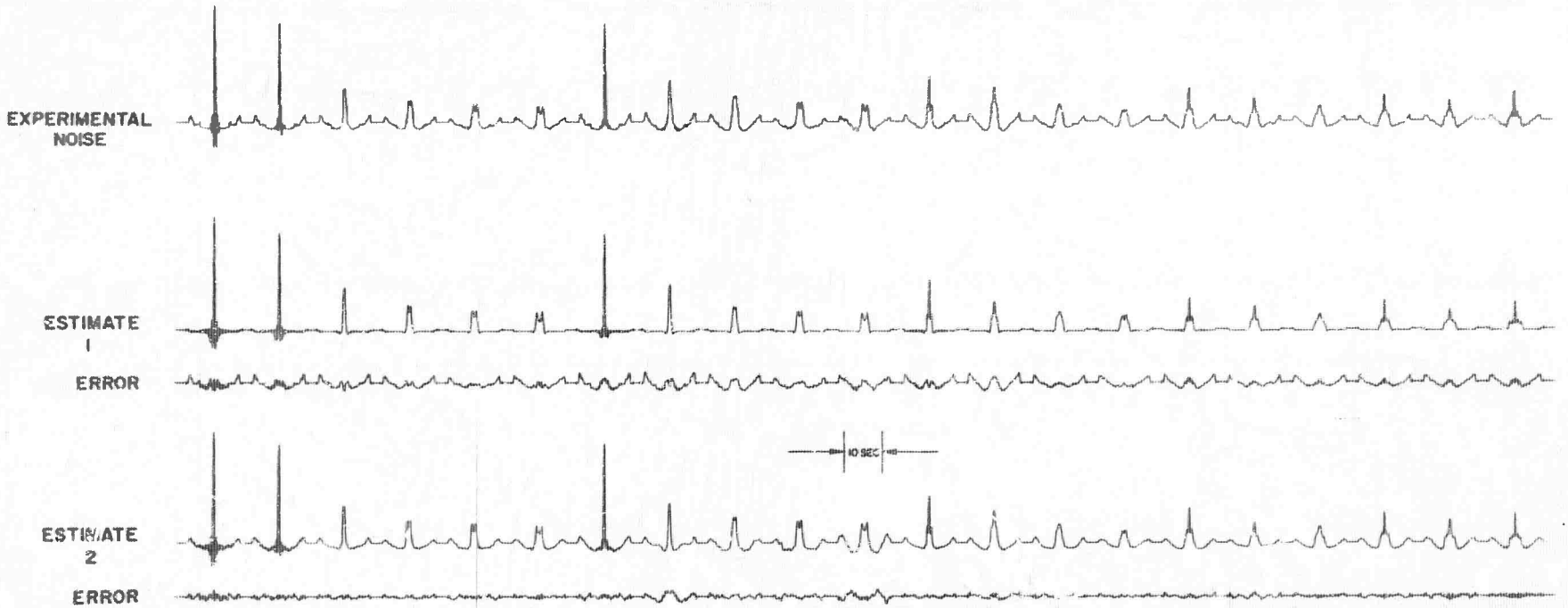

Figure II-16. Experimental Noise Correlation Set and the Optimum Estimates

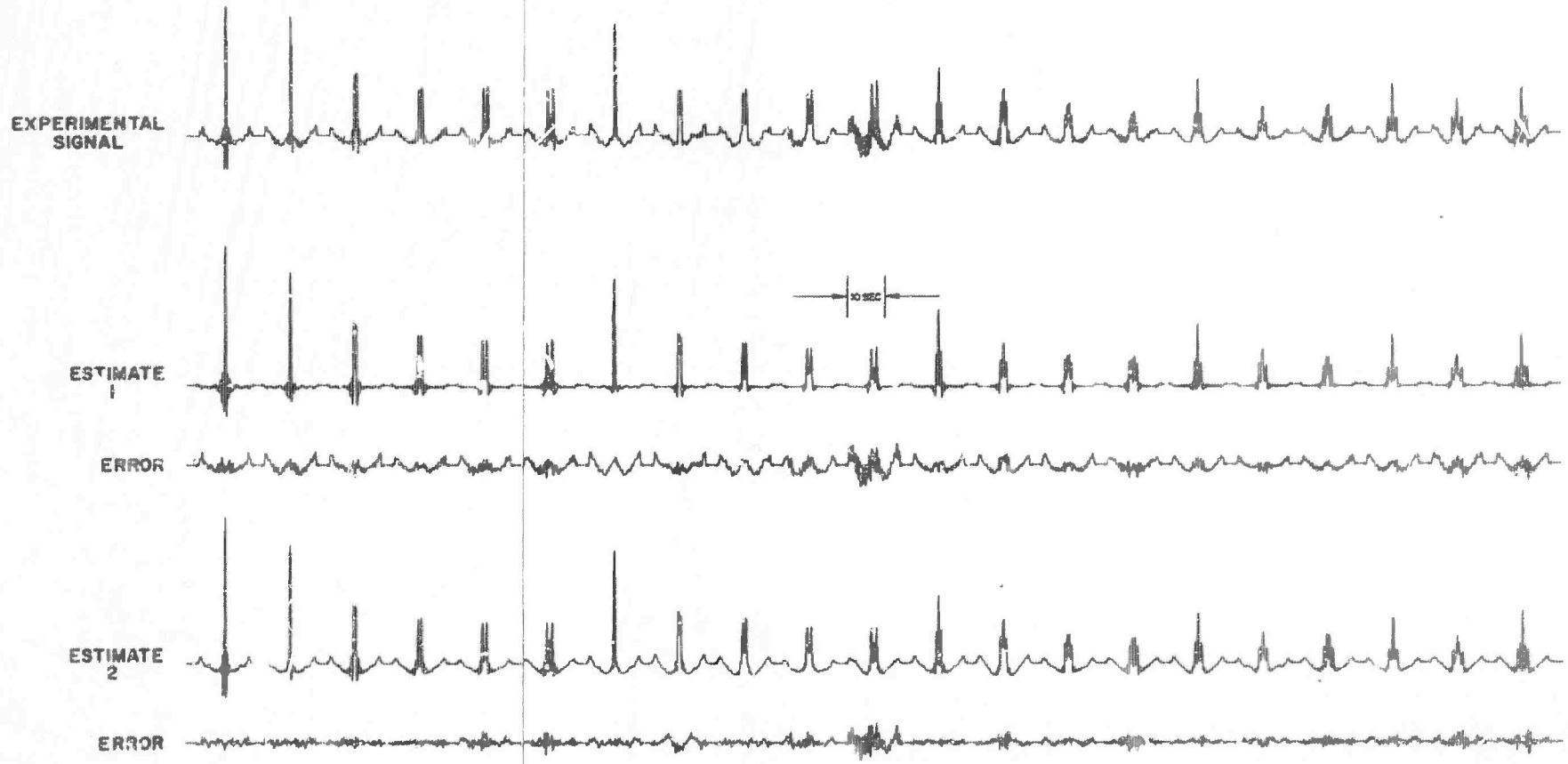

Figure II-17. Experimental Signal Correlation Set and the Optimum Estimates

The simplest means of analyzing the experimental noise field would be to compute the weighted sum of the theoretical correlation sets which provides the best fit to the experimental correlation set on a least-mean-square-error basis. This is somewhat undesirable since the estimated components would be constrained (unreasonably) to have the same spectra that were used in computing their correlation functions. In order to provide more freedom in the estimates, computations were run to obtain an optimum set of filters (one filter for each theoretical correlation set) which could be applied to the theoretical correlations.

The filters were optimized on the basis that a summation of the filtered correlation sets must be the best possible estimate of the experimental correlation set. Since the input correlations were derived initially from an assumption of white spectra, and since in the filtering operation their Fourier transforms are multiplied by the amplitude responses of the appropriate filters, then the power spectra associated with the filtered correlation sets must be identical in form to the filter amplitude responses. These responses are interpreted as the best estimates of the power spectra of the contributions of the corresponding constituents to the noise field.

A length of 21 points (1.44 sec) was chosen for the filters. The corresponding frequency resolution is 0.695 cps. If the filters were of infinite length, it would be possible to make independent fits to the experimental data at every frequency. This would be almost equivalent to the method used by A. J. Seriff in the analysis of deep-well data from Juno, Texas* (a "quiet" site similar to UBO in many respects). In that case, the decomposition was performed in the frequency domain. At each of four frequencies, optimum weighting functions were determined to estimate observed power ratios and coherences of seismic noise from theoretical power ratios and coherences computed for P-waves and surface waves. These weights were interpreted as estimates of the power densities of the modes at the corresponding frequencies. When short optimum filters are designed in the time domain, the solutions are forced to be smooth functions of frequency. Statistical significance is gained at the expense of frequency resolution.

The above discussion has been concerned with the approximation of the experimental noise correlation set by the group of five theoretical correlation sets (Noise Estimate 1). The best estimate obtained in this way is shown by the second trace in Figure II-16. The third trace contains the error set — the difference between the correlations being decomposed and the best estimate. In addition, three other decompositions were performed:

*Shell Development Company, 1965, Seismic noise in deep boreholes: Semiannual Tech. Rpt. No. 3, Contract AF 19(628)-2785.

- Noise Estimate 2 — as above, but with the theoretical P-wave correlation set replaced by the experimental signal set
- Signal Estimate 1 — approximation of the experimental signal correlation set by a combination of the five theoretical sets
- Signal Estimate 2 — approximation of the experimental signal correlation set by a combination of the theoretical sets for P-waves and incoherent noise and the experimental noise correlation set

The optimum summation traces and the associated error traces are shown in Figures II-16 and II-17. The estimated power spectra (i.e., the optimum filter responses) are plotted in Figure II-18.

The results indicate that P-waves form a major part of the UBC ambient-noise field below 1 cps and that the fundamental Rayleigh mode is much more important at the surface than any of the higher-order modes. This finding is in general agreement with the results obtained for Juno, Texas, from which it was estimated that P-waves and surface waves were of approximately equal strength at 0.25 and 0.50 cps and that P-wave power was about -5 db relative to surface-wave power at 1 cps. Further support for the hypothesis of the existence of strong P-wave noise at Juno was provided by the observation of noise bursts with velocities greater than 8 km/sec. The UBO 1-cps wavenumber spectra (Semiannual Technical Report 3, Contract AF 33(657)-12747 indicate that about 20 percent of the ambient noise is P-waves and that the only other important contributor is the fundamental mode. Unfortunately, the UBO array is not sufficiently large to permit useful resolution in wavenumber space at frequencies very much lower than 1 cps.

In both signal and noise predictions, it was found that the residual error was less for Estimate 2 (obtained from a mixture of experimental and theoretical correlation sets) than for Estimate 1 (obtained from theoretical sets alone). This difference is most pronounced at low frequencies, especially below 0.25 cps; thus, the low-frequency parts of the two experimental sets resemble each other much more closely than any of the theoretical models. Since low-frequency S/N is very poor in the signals recorded at UBC, it is reasonable that "signal" statistics and "noise" statistics should appear similar. Lack of agreement with theoretical values probably is due to the failure to correct for seismometer responses at frequencies other than 1 cps. When the process was forced to choose among theoretical models, the results indicated high P-wave-to-surface-wave power ratios at low frequencies in both cases. In spite of disagreements between theoretical and experimental statistics, the process was able to make a clear choice in favor of P-wave noise.

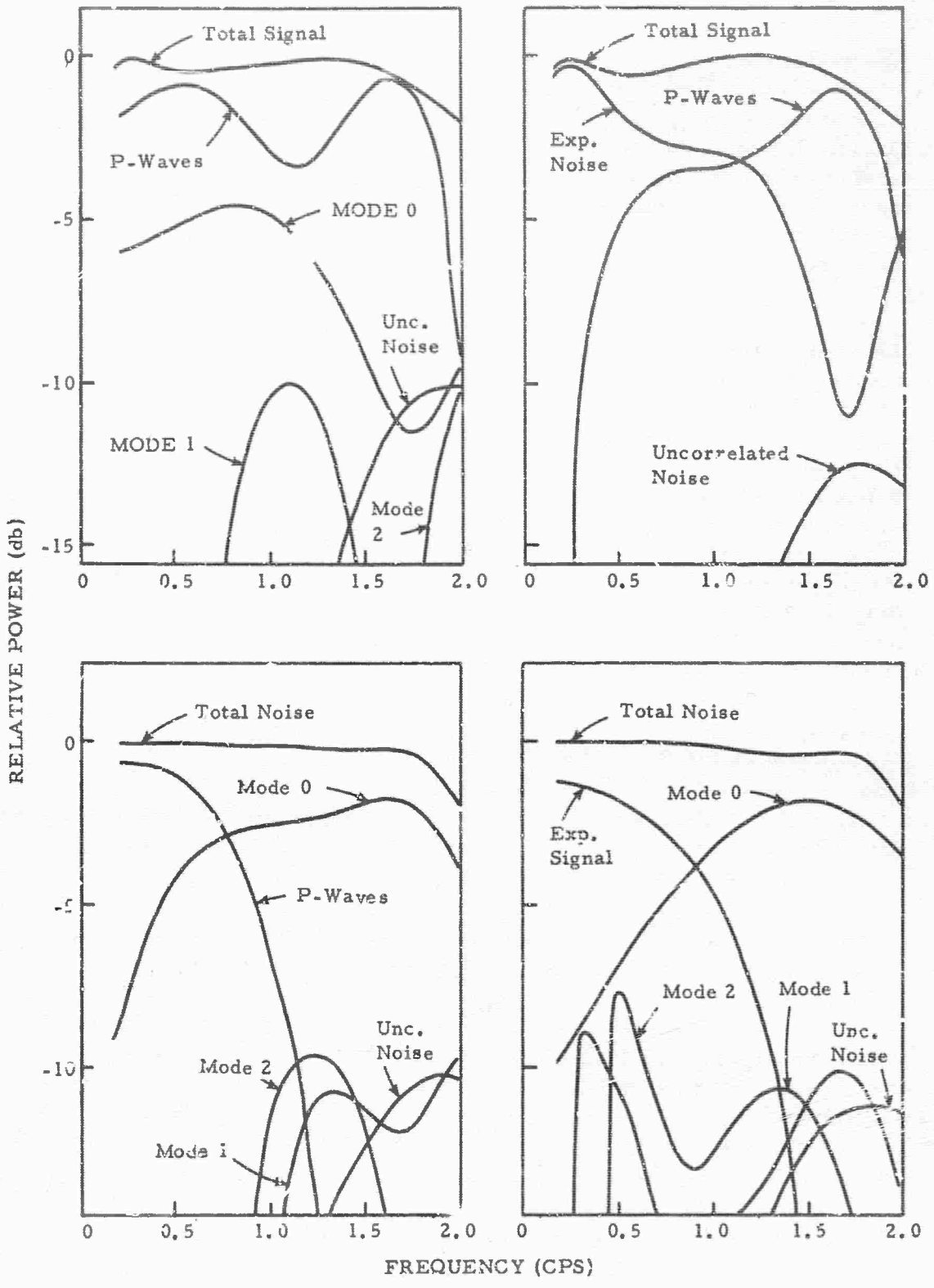

Figure II-18. Estimated Power of Constituent Modes in UBO Signal and Noise Fields

D. INVESTIGATIONS OF AMBIENT P-WAVE NOISE

Results obtained from a number of recording sites indicate the existence of a P-wave constituent in the ambient seismic noise. It has been suggested that the P-wave noise is caused by a steady background of P-waves emerging from the mantle with uniform power on a worldwide scale. It would follow that the only spatial variations observed at the surface should be those which are due to differences in crustal transmission characteristics. Such differences would not be expected to produce variations in observed power of more than a factor of two (assuming good coupling of sensors to solid unweathered rock).

Multichannel filter systems employed in conjunction with 3-km (approximately) arrays at "noisy" sites, such as Wichita Mountains and Cumberland Plateau, have been found to be very effective for wide-band ambient-noise rejection. At "quiet" sites, such as Uinta Basin and Tonto Forest, significant signal-to-noise improvement has not been obtained in the frequency range 0.5-1.2 cps. These findings are consistent with the hypothesis of a constant level of P-wave noise, since it appears that 0.5-1.2 cps noise outputs of processors applied to small (less than 5 km) arrays are restricted by a lower limit which is much more uniform than the input-noise power levels. If information below 1.2 cps is essential, then the only known method of penetrating this barrier is the use of large arrays such as the 200-km LASA array in Montana. With such an array, it should be possible to use processing systems tuned to pass only P-waves originating from specified regions of the globe. It is clear that P-wave noise must be a consideration of prime importance in the design and location choice of future array installations.

Figure II-19 shows ambient-noise power spectra obtained from five recording sites. It is believed that these curves should be related to P-wave noise level as follows:

- UBO: This spectrum was obtained by applying the computed fractional contribution of P-waves to the total noise power spectrum for a single noise sample and smoothing. This appears to be a reasonable estimate of P-wave noise power in the neighborhood of 1 cps, but probably is too high at lower frequencies because of the strong microseismic peak in the original data and the forced smoothness of the estimated P-wave fraction.
- TFO: This curve is the spectrum of a noise sample as recorded by a single seismometer. Since the 0.5-1.2 cps noise at TFO is assumed to be almost entirely P-waves, the plotted values should be only slightly higher than the P-wave spectrum in this range.

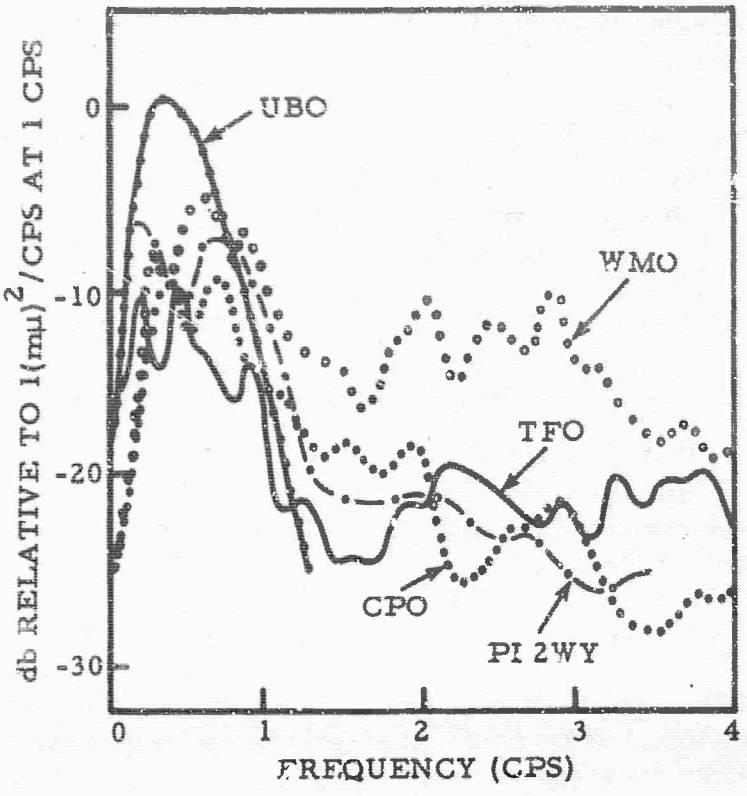

Figure II-19. Ambient Noise Spectra from Five Array Sites (Not Corrected for Frequency Response of J-M Seismometers)

- CPO: This spectrum was computed for a noise sample after it was passed through a signal enhancement filter (isotropic velocity filter). It is believed that the output noise is due mainly to P-waves below 1.0 cps and surface waves or uncorrelated noise above 1.0 cps.

- PI2WY: The curve represents the lower envelope of spectra computed for the six PI2WY records (paragraph A). If a constant P-wave noise level is assumed, then the total noise power always must be at least as great as that constant level. Therefore, the curve plotted must be an upper limit to the P-wave spectrum. The poor performance of MCF systems designed for this site implies that the P-wave spectrum is not more than 3 db below the limit in the 0.5-1.2 cps range.

- WMO: A simple summation of the outputs of the 10-seismometer array was obtained and a power spectrum was computed for a single noise sample. Surface-wave rejection was less effective here than in the case of the CPO processor and so this curve can only be interpreted as an upper bound on the possible P-wave noise spectrum.

If the low-frequency part of the UBO curve is discarded, then the agreement becomes very good. It should be noted that the P-wave noise power density reported by Seriff for Juno, Texas, is approximately -13 db relative to 1 $m\mu^2$/cps at 1 cps. This independent estimate is also in good agreement. The curves of Figure II-19 are not corrected for the J-M seismometer response. Application of this correction to an average P-wave spectrum deduced from those curves yields the absolute P-wave power spectrum in Figure II-20.

Experimental evidence supports the hypothesis of P-wave noise with a uniform (within a factor of 2) worldwide power level. An estimated figure of 0.05 $m\mu^2$/cps at 1 cps appears to be accurate to better than an order of magnitude. The only known method for enhancing desired P-wave signals in the presence of such a background of unwanted P-wave noise is to improve the wavenumber resolution of an array by increasing its size to hundreds of kilometers, if signal and noise both occupy the same frequency band. The shape of the estimated spectrum of P-wave noise implies that some advantage might be gained by a concentration of effort in the neighborhood of 2 cps instead of 1 cps. It is felt that vertical arrays and small-aperture horizontal arrays may well offer useful advantages at frequencies above 1.5 cps. Such advantages could probably be exploited more effectively by vertical arrays with smaller receiver spacings than have been used to date.

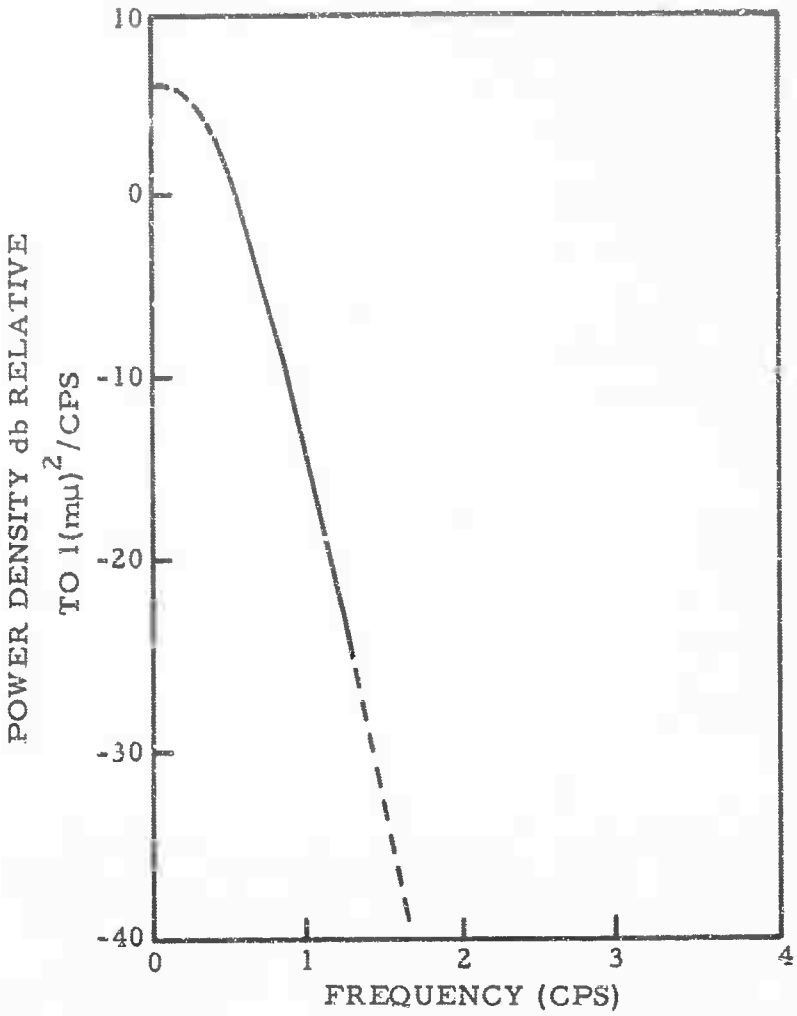

Figure II-20. Estimate of Absolute P-Wave Noise Power Spectrum (After Instrument Response Correction)

The spectrum presented in Figure II-20 is admittedly a very crude estimate. It is planned to attempt to refine the mode separation results for UBO and also to apply similar techniques to data from other vertical arrays. It should be possible to gain additional useful information from a study of ambient-noise wavenumber spectra which have been computed for a number of horizontal array installations.

SECTION III

STUDY OF TELESEISMS RECORDED AT CPO

A. INTRODUCTION

Three ensembles of teleseisms recorded by multiple array processor (MAP) systems at Cumberland Plateau Observatory (CPO) have been and are being studied. Almost all attention has been restricted to the records output by isotropic processors which were designed to reject low-velocity noise and preserve high-velocity signals with a minimal dependence on azimuth. These records contain relatively clean body-wave signals since both ambient noise and signal-generated noise (energy scattered into surface waves in the vicinity of the receiver) are attenuated by the processors.

Figure III-1 shows an example of the processor performance. For a representative event, power spectra were computed for an interval containing the signal and an interval preceeding the signal onset. Between 0.75 and 2 cps, a signal-to-noise improvement of about 10 to 15 db is observed for the processor relative to a single seismometer. Since the estimated signal spectra are actually spectra of signal plus noise, the improvement is, in fact, somewhat greater than it appears.

Objectives of the study are described in the following paragraphs. In some cases, only brief outlines of the results will be given, since more detailed accounts may be found in Semiannual Technical Reports 1, 2 and 3 under Contract AF 33(657)-12747.

B. CRUSTAL REVERBERATION DECONVOLUTION

An impulsive P-wave signal emerging from the mantle encounters a series of reflecting interfaces. The resulting reverberations of the signal have the effect of a frequency filter which converts the impulse into a wavelet of theoretically infinite duration. In practice, the time span of the wavelet is finite since the amplitude cannot remain above detection threshold. It would be desirable to design an inverse filter which would operate on the observed signal in such a way as to remove crustal effects by transforming the waveform back to an impulse.

As reported in the Semiannual Technical Reports 2 and 3, attempts have been made to apply dereverberation processing to the events of all three ensembles. Filter design was based upon signal auto-correlations computed from data samples containing the P-phase.

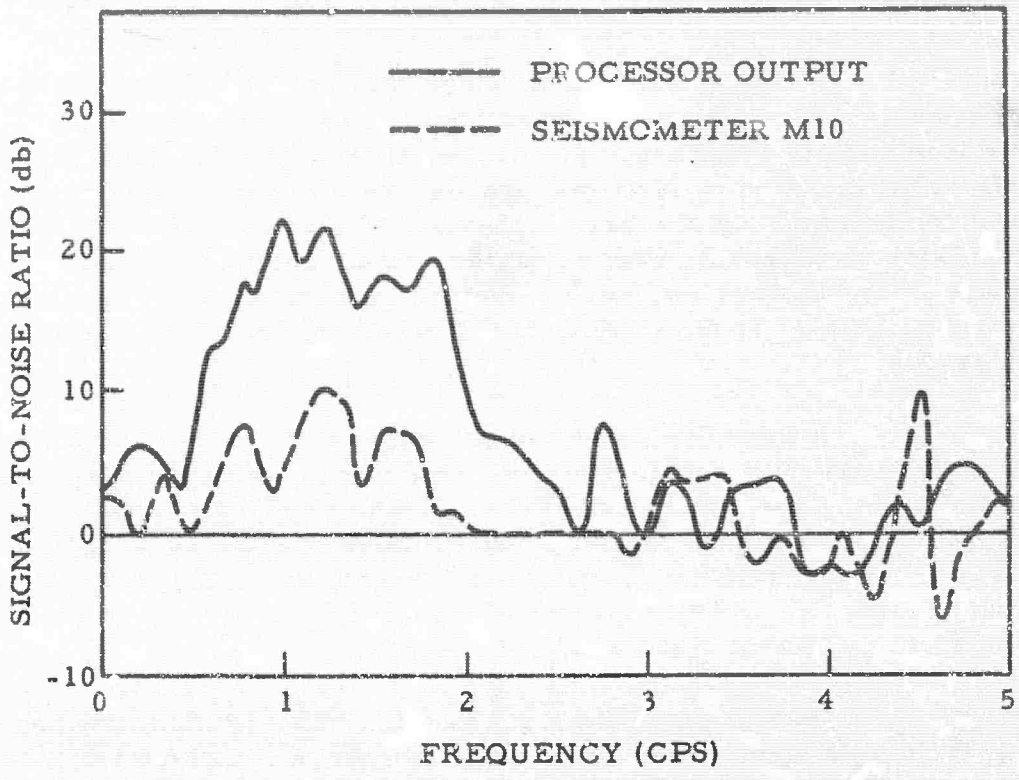

Figure III-1. S/N Ratios Computed for Center-Seismometer and Processor Output (Event 2-5)

These correlations depend on crustal effects to a much lesser degree than on incident signal spectra, which depend on both source spectra and mantle transmission effects (including anelastic absorption). Thus, the major effect of a deconvolution filter is to compensate for the incident signal spectrum which is assumed to be severely band-limited, but not to exhibit fine structure. However, if the filter is sufficiently long, the fine structure produced by crustal effects may also be compensated for.

Unless the span of the deconvolution filter is more than a few seconds, differences in emergence angle will not be important. For example, Figure III-2 shows that some fine structure (probably associated with Moho reflections) persisted even when power spectra for 60 teleseisms of world-wide origin were averaged. Thus, it is possible to design an "average" filter which will deconvolve an "average" teleseismic signal. It was shown in the case of Ensemble I that an ensemble average deconvolution filter was almost as effective for waveform contraction as filters designed individually for each event.

Although some crustal dereverberation may be achieved with deconvolution filters, it must be borne in mind that the filter response cannot be interpreted directly as the inverse of the crustal response since the most important effect is compensation for the incident signal spectrum. Since signal-to-noise ratio is generally poor wherever signal power is low, this compensation will tend, in general, to amplify noise more than signal. It is therefore advisable to apply band-limiting filters to the deconvolved data in order to reject noise in the frequency ranges where signal power is low. If these filters have smooth frequency responses, compensation for fine structure will have been achieved.

C. DEPTH OF FOCUS DETERMINATION

Focal depths of earthquakes are determined most often by least-mean-square fits to observed arrival times of P. An alternative method depends upon the difference in observed arrival times of P and pP. The pP - P method probably is more accurate, but requires that pP be observed and identified with certainty. The value of multichannel velocity filtering of seismometer array outputs has been demonstrated in that it has been possible sometimes to identify pP in the output trace of the CPO processor where it was not observable in single-seismometer records. However, in other cases, pP could not be seen even when its predicted arrival time was favorable for observation (i.e., when USC&GS estimated focal depth indicated pP should arrive after P has died out, but before end of the record).

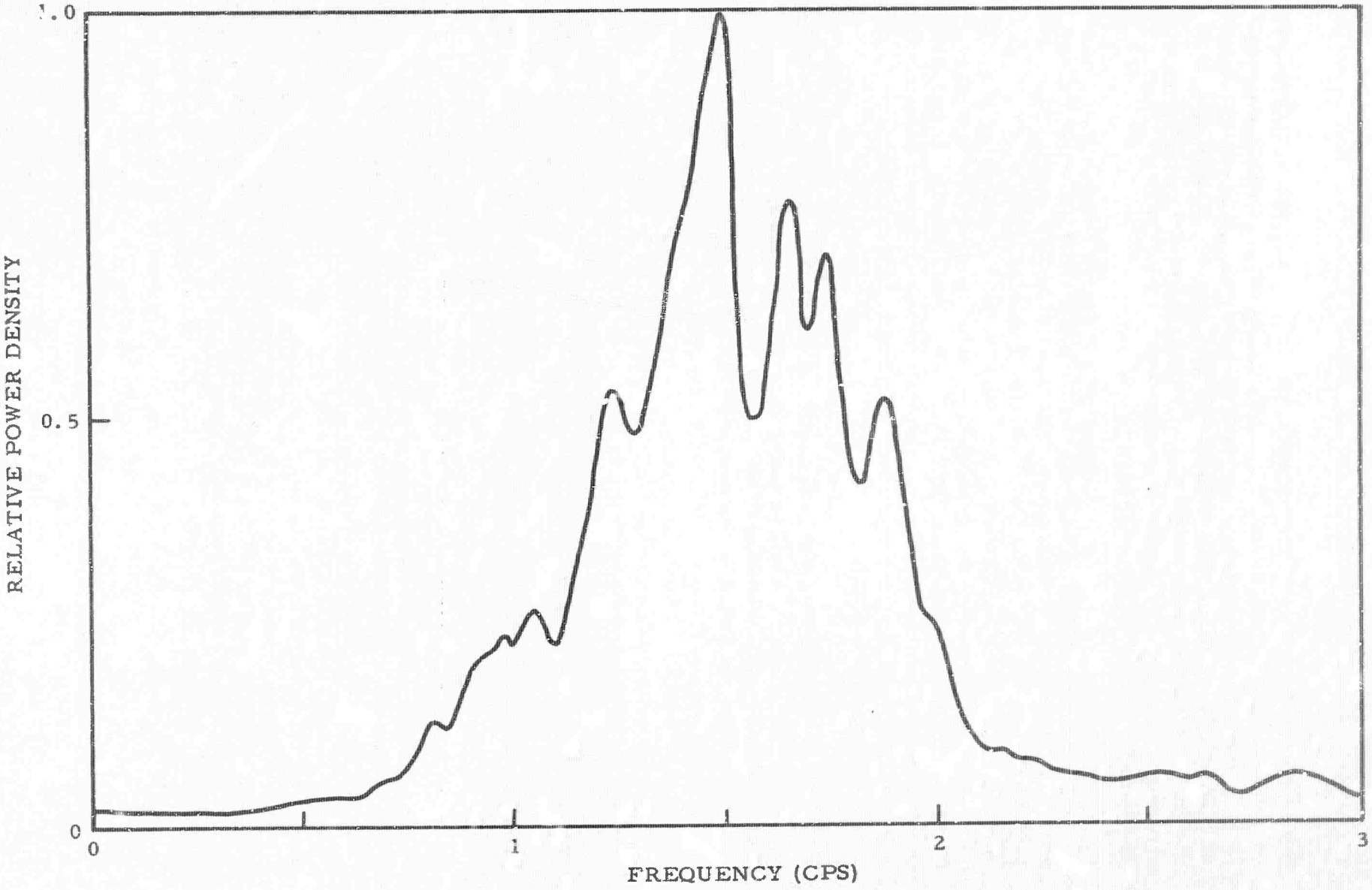

Figure III-2. Average Power Spectrum of 60 Ensemble II Teleseisms

It has been suggested that it might be possible to improve pP detectibility by deconvolving the processor output record or by computing autocorrelations for either the raw trace or the deconvolved trace. None of these techniques was found to offer improvements. This failure has been attributed to differences between the waveforms of P and pP from the same events.

It must be concluded that pP - P analysis is of limited value in focal depth estimation for earthquake/explosion discrimination. A well-documented pP phase offers excellent proof that focal depth was greater than a few kilometers. However, several deep-focus (USC&GS estimated depth >100 km) events did not produce observable pP arrivals. A possible explanation is asymmetry of the radiation pattern at the source. Regardless of the reasons for pP absence, it must be concluded that such absence cannot be accepted as evidence of near-surface origin.

D. STUDY OF CPO CRUSTAL STRUCTURE

Two important effects must be considered when deduction of crustal structure beneath CPO from analysis of teleseismic records is attempted. Since crustal response depends on signal angle of emergence, it is not meaningful to estimate a single average response function for the complete set of teleseisms. In the case of Ensemble I, 73 events from a small range of distances were available. By forming seven different subgroups and computing average autocorrelations (Semiannual Technical Report 3), it was possible to find "events" in the autocorrelation functions which could be interpreted as evidence of major reflecting horizons below CPO. In Figure III-3, it can be seen that such "events" no longer appear when ensembles of worldwide origin are averaged. The one coincidence indicated at 18-sec lag is probably not physically significant.

Also, observed spectra can be interpreted as crustal response functions only after they have been corrected for spectral content of the original signal incident at the base of the crust. Figure III-4 shows average autocorrelations of all Ensemble II and III events between 60° and 75°. Evidence of reflections has been smeared out beyond recognition, probably because of differences in signal spectra. Figure III-5 illustrates the great diversity observed in teleseisms from a small range of distances. Power spectra have been computed for 18 Ensemble II events between 20° and 30°. It can easily be demonstrated that these differences are associated with the signals, since noise power spectra (Figure III-6) computed for intervals just preceding each event show excellent time-stationarity. It is believed that observed differences in signals from nearly the same distance may be explained by near-source effects. It should be possible to average out these effects to some extent by the use of large numbers of teleseisms.

Text cont'd page III-10

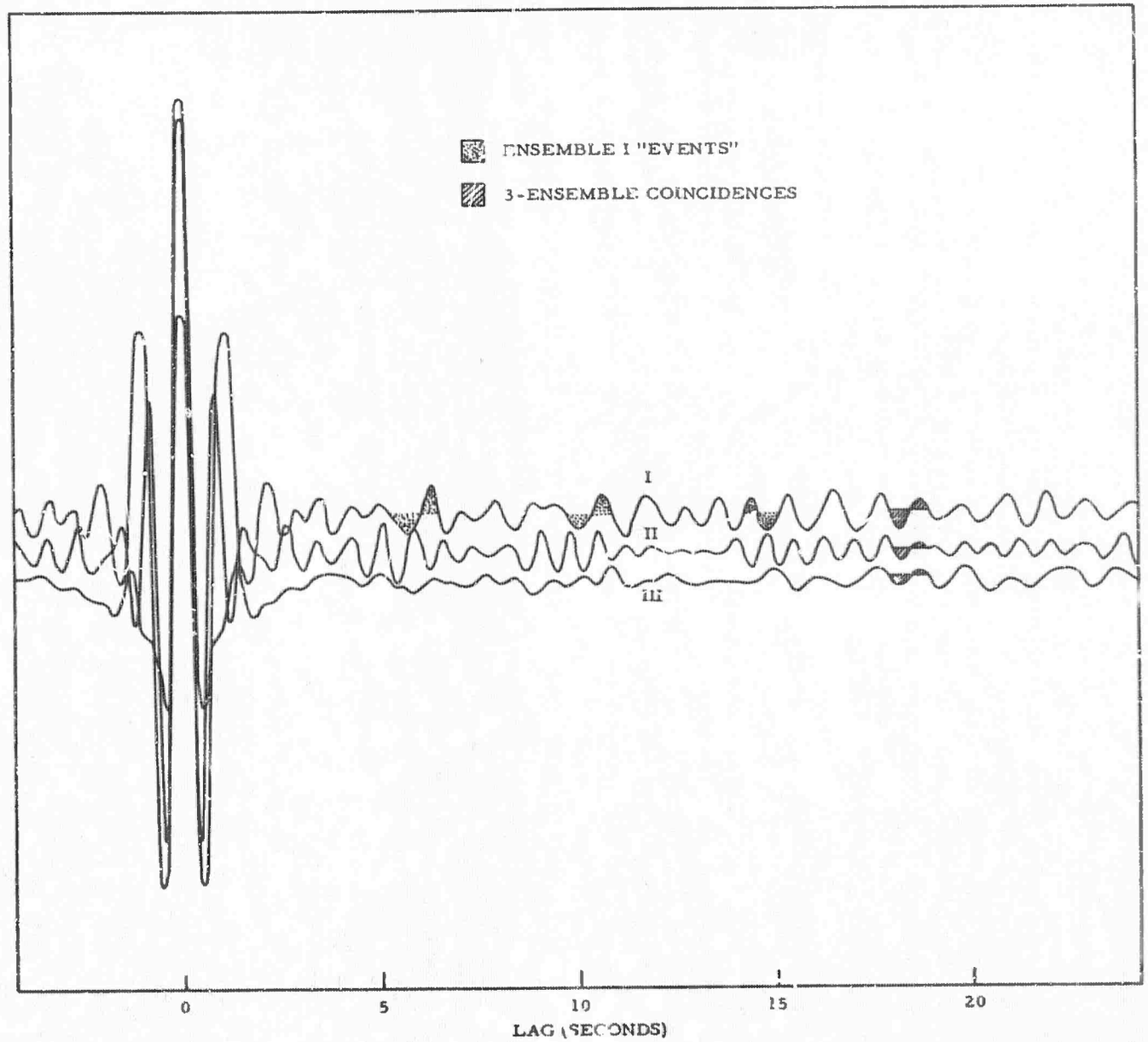

Figure III-3. Unnormalized Average Autocorrelation Functions from Ensembles I, II and III

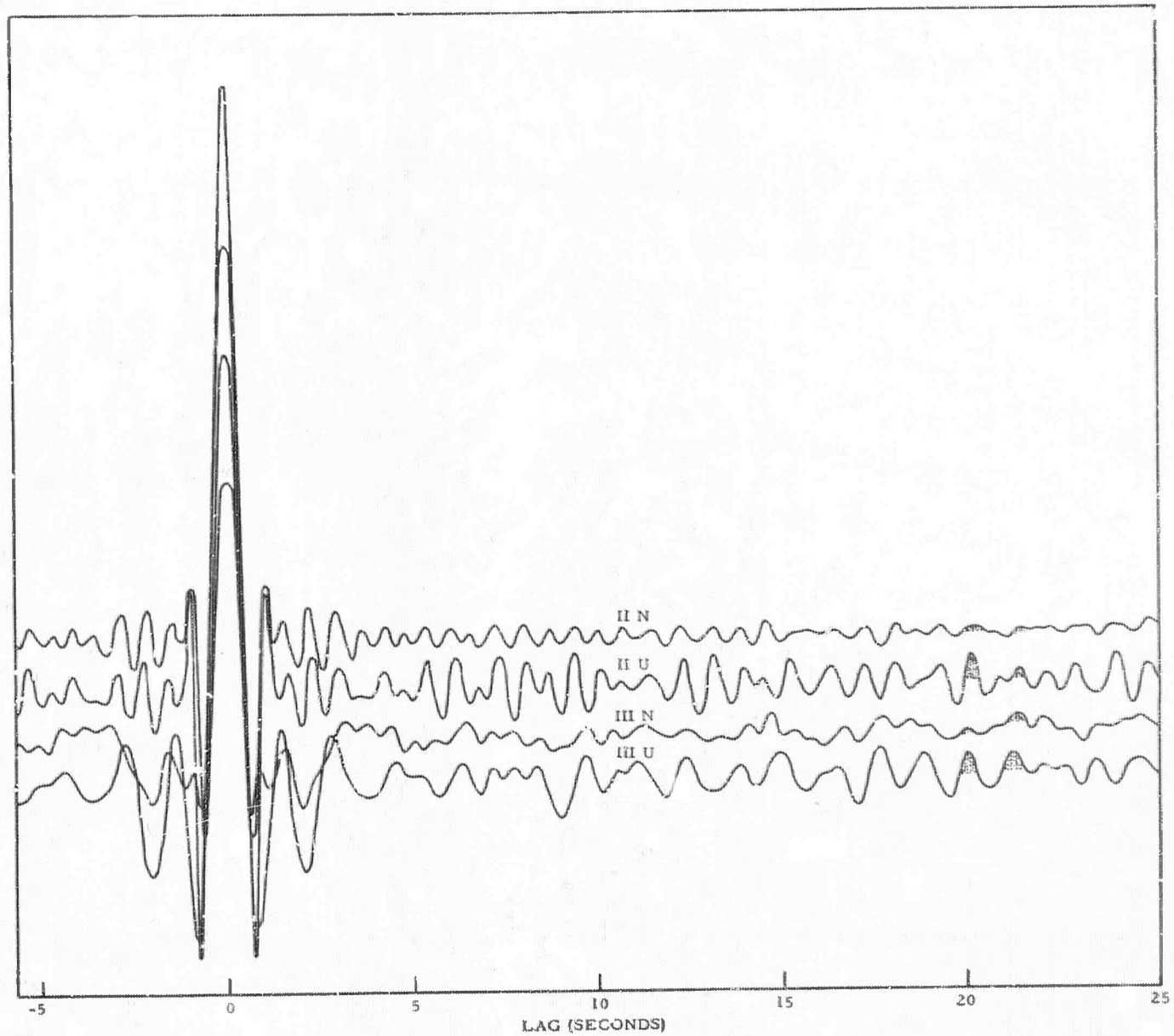

Figure III-4. Normalized (N) and Unnormalized (U) Average Autocorrelations of Ensemble II and III Teleseisms Between 60° and 75°

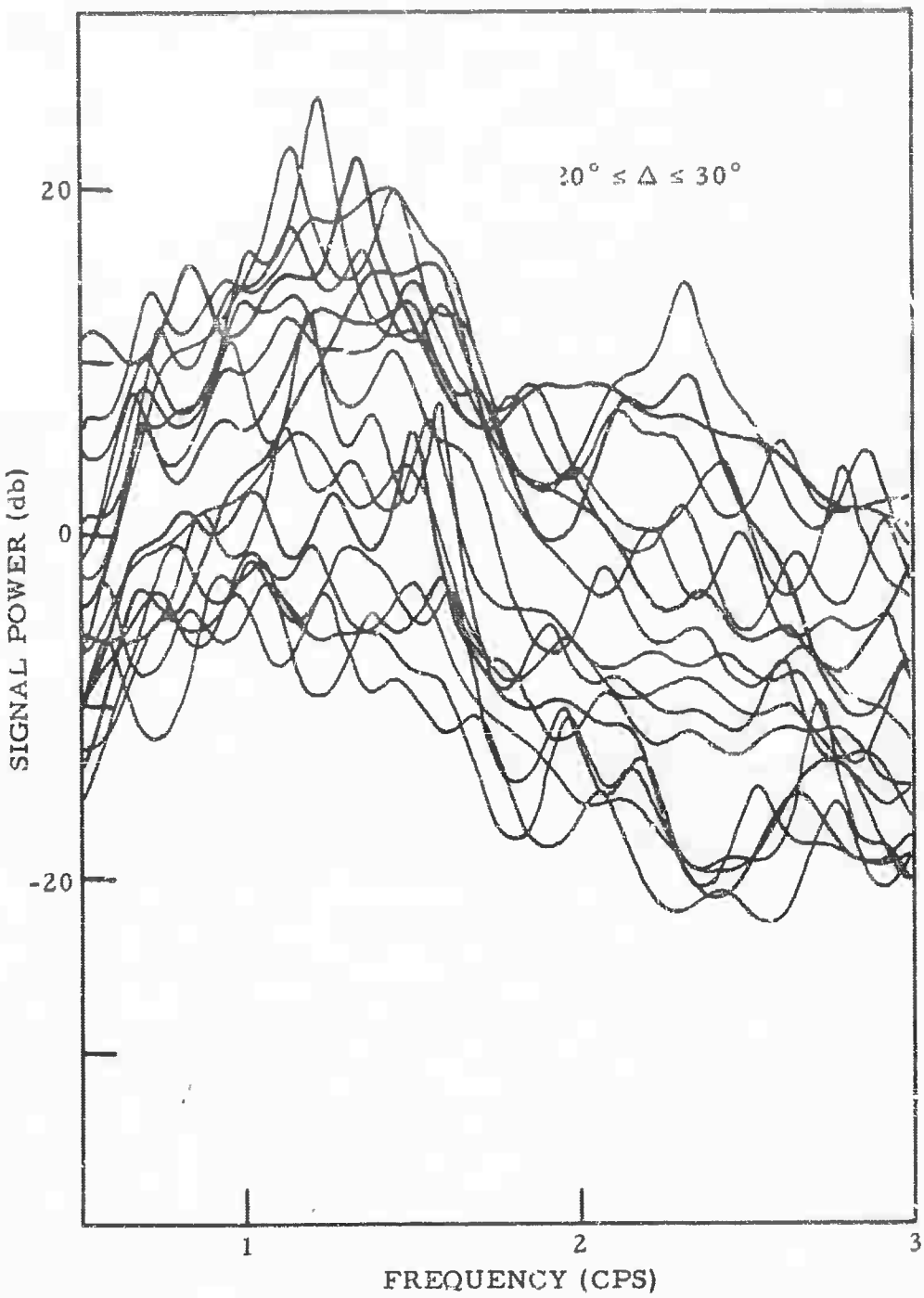

Figure III-5. Signal Power Spectra of 18 Ensemble II Events Between 20° and 30°

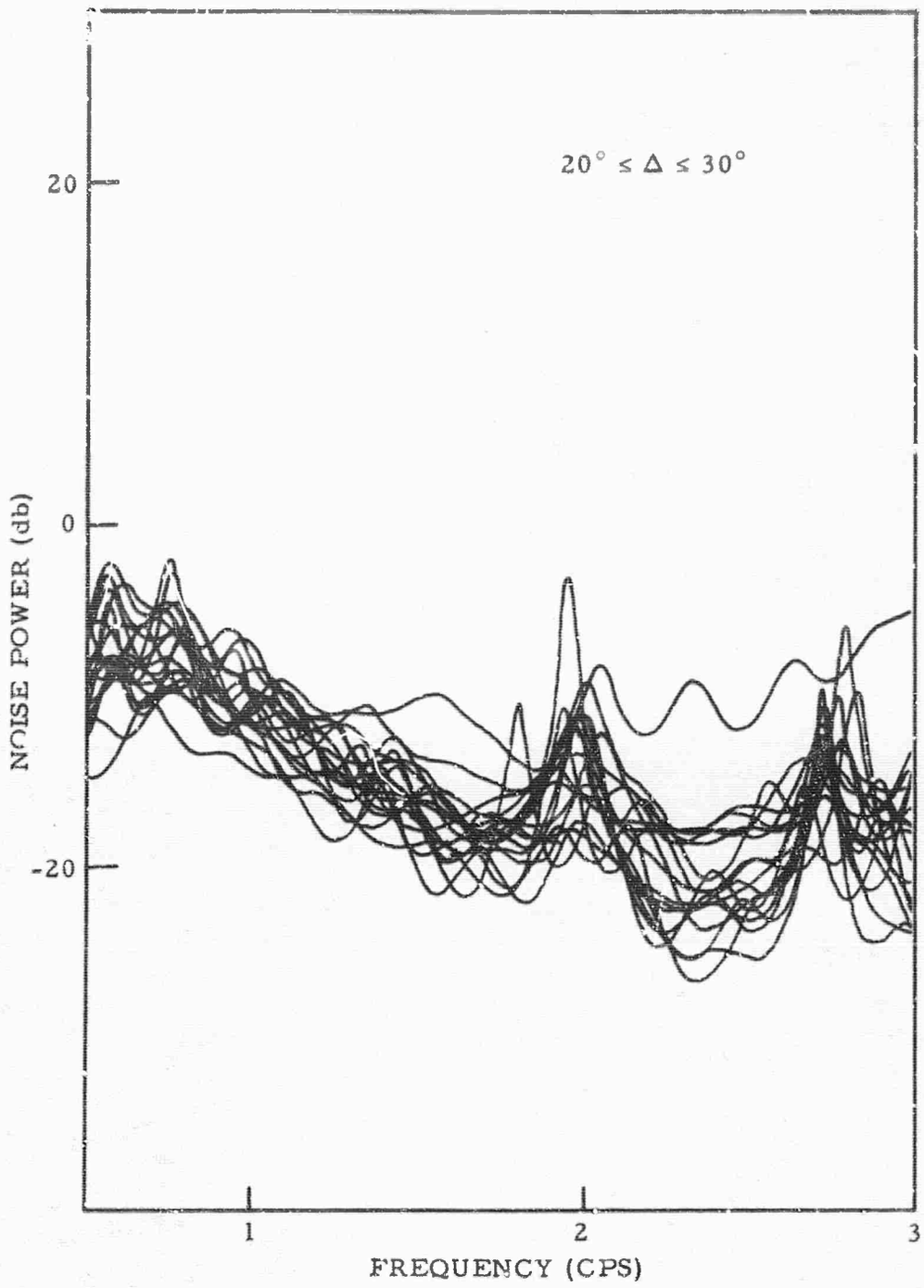

Figure III - 6. Noise Power Spectra Associated with 18 Ensemble II Events Between 20° and 30°

In Ensembles II and III, it is not possible to obtain such a concentration of foci. It appears that the most effective method of eliminating source effects might be to discard all shallow-focus events. As an example, power spectra for seven deep-focus events (II-21 and III-25 through III-30) are shown in Figure III-7; it has not been possible to find such striking resemblances in similar groups of shallow-focus events. In Figure III-8, autocorrelations of four teleseisms (III-27 through III-30) show four "events" which are reproducible throughout the set. A thorough study of the available data has failed unfortunately to turn up any other sets which display such similarities. The four earthquakes which contributed to Figure III-8 occurred at distances of 30.9°, 30.73°, 31.33°, and 31.01° with azimuths between 155.1° and 155.6° and focal depths between 140 and 176 km. This set was the only available set of deep-focus earthquakes from such a small area.

A major difficulty in interpreting the autocorrelations and power spectra in terms of crustal structure arises from the limited bandwidth of the signals being studied. Since most signals have useful bandwidths of about 1 cps, the finest resolution which can be obtained is about 1 sec of time or a few kilometers of depth. A suggested model for the structure under CPO is reproduced in Figure III-9.* Since the two-way travel time through the entire sedimentary section is only 1.05 sec for this model, it is impossible to learn anything about detailed structure in the sediments and very difficult to determine even their total thickness. Ideally, autocorrelation functions should exhibit peaks at time lags corresponding to the differences in arrival times of direct and reflected signals. The correlations in Figures III-3 and III-8 are computed from signals with phase velocities of 22.5 km/sec (Kurile Islands, 85°) and 12.6 km/sec (Colombia Venezuela, 31°). The difference in phase velocities should be reflected by shifts of the peaks in the autocorrelations.

Some events that are multiply reflected and are most likely to contain significant energy are illustrated in Figure III-10. The time lags of these events relative to the direct P-wave are given in Table III-1 for the crustal model of Figure III-9. Some features in the autocorrelations have been selected as evidence of reflected arrivals, but it is difficult to decide upon the proper lag times which should be assigned to such features. Ideally, a reflected arrival should give rise to a reproduction of the center part of the autocorrelation, symmetrical and centered at the lag time of the arrival. Therefore, it is preferable to seek center times rather than onset times of the "events." Since most of the "events" selected are unsymmetrical, center times are difficult to estimate. The added complication of limited

*Foreman, J., 1964, Some theoretical calculations on a model of the crust under the Cumberland Plateau Observatory: Texas Instruments (Unpublished).

Text cont'd page III-15

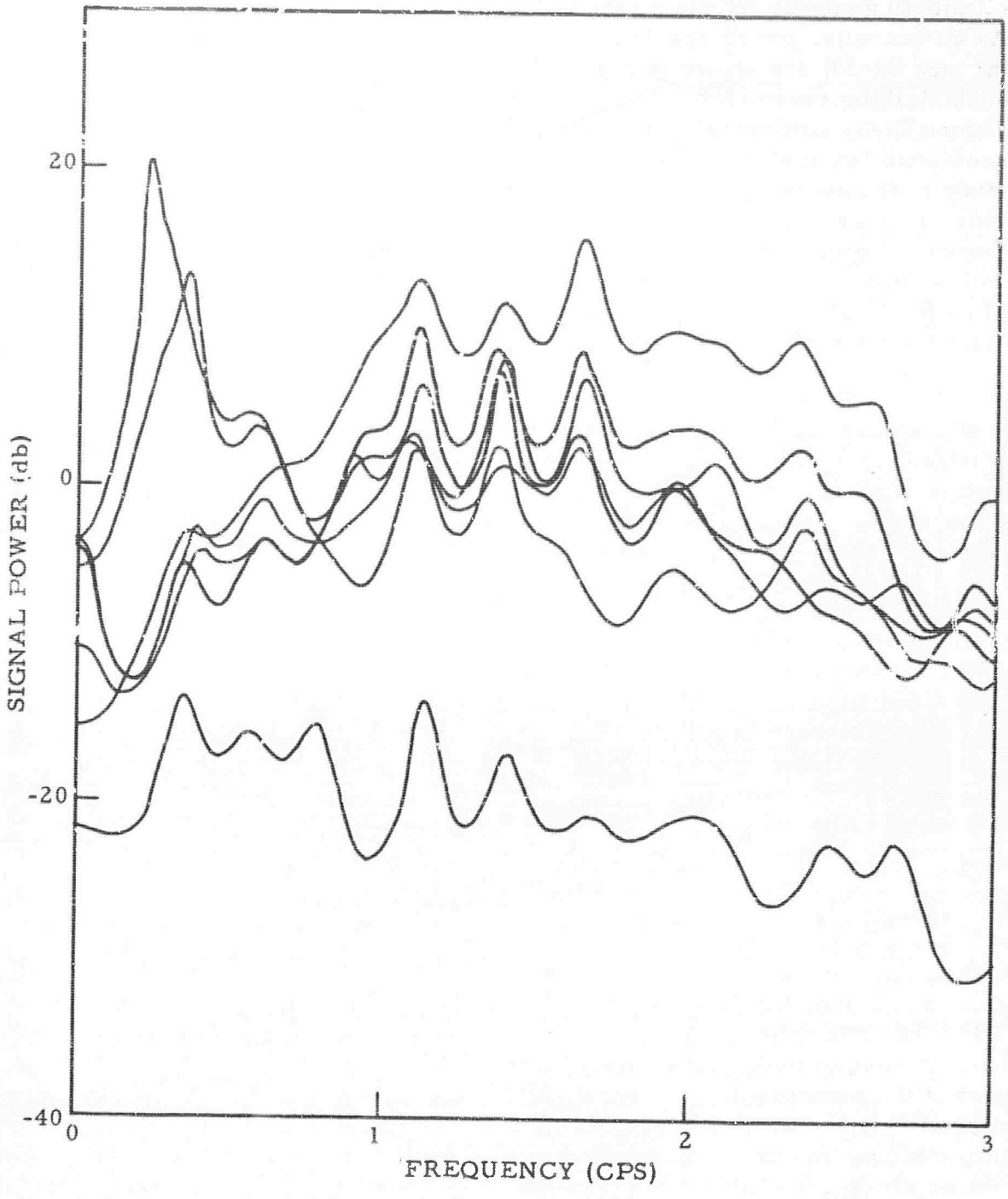

Figure III-7. Signal Power Spectra of 7 Deep-Focus Events Between 30° and 31.3°

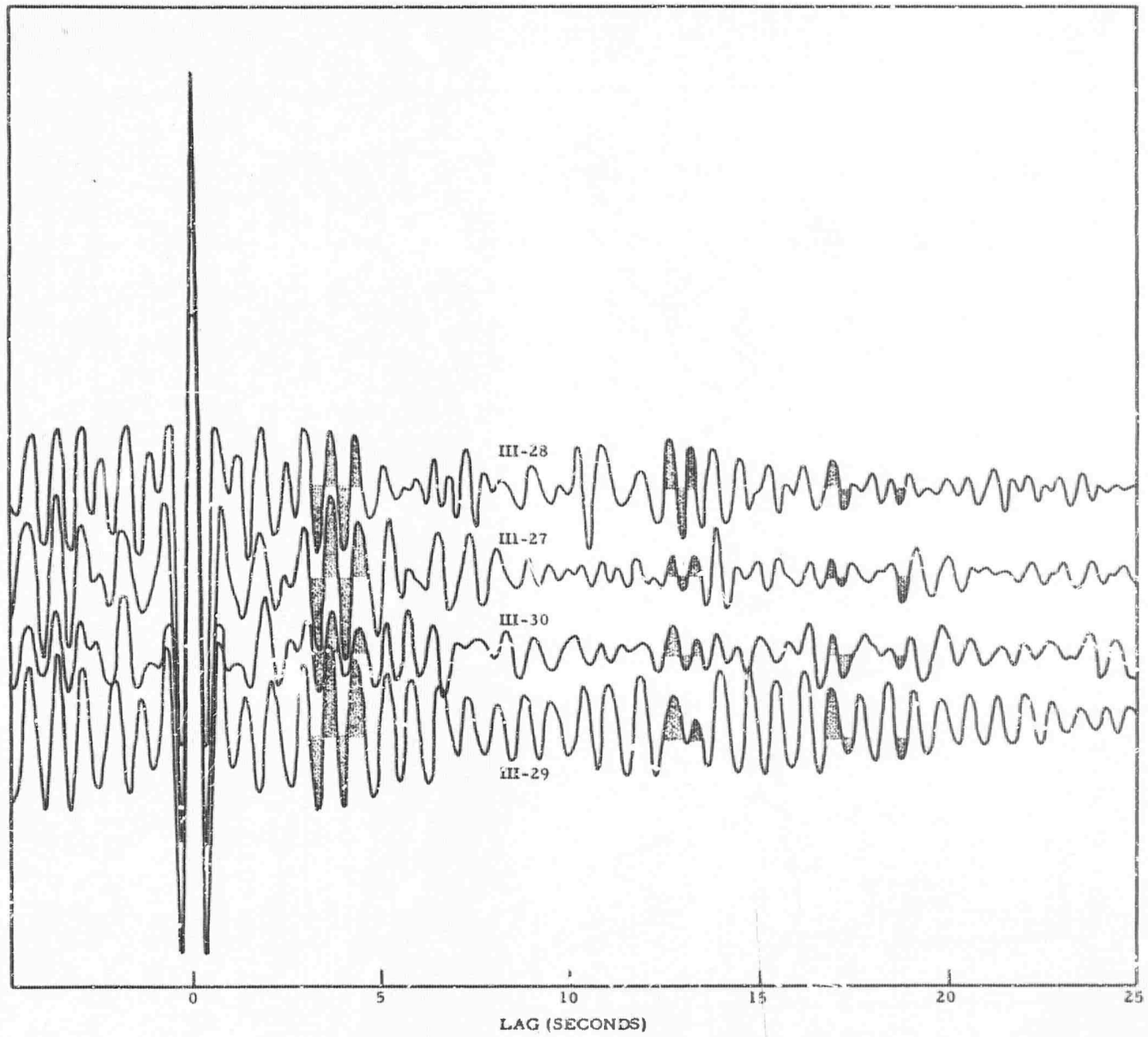

Figure III-8. Autocorrelations of 4 Teleseismic Signals from Earthquakes Near the Colombia–Venezuela Border

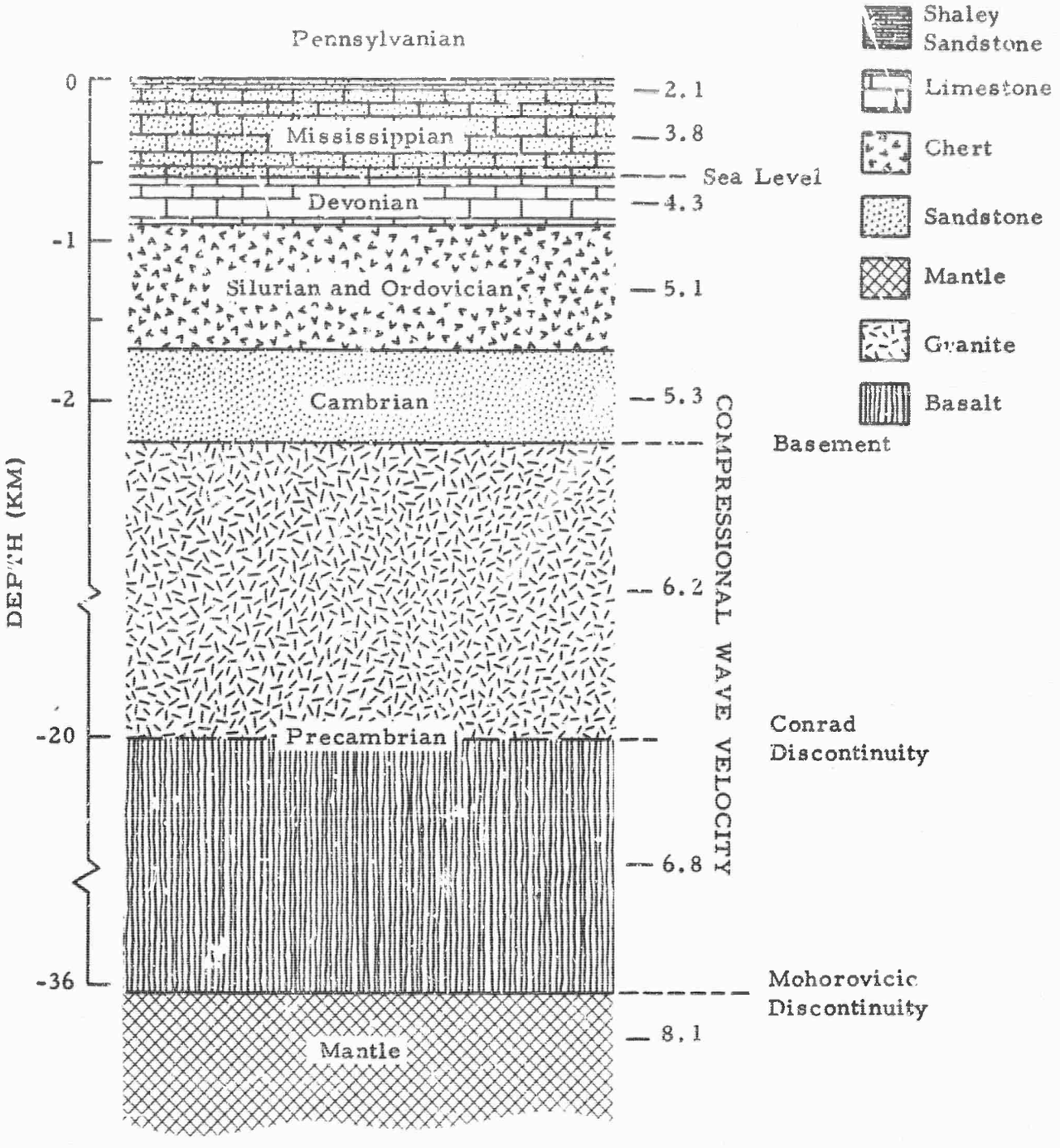

Figure III-9. Model of Crustal Structure Near McMinnille, Tennessee

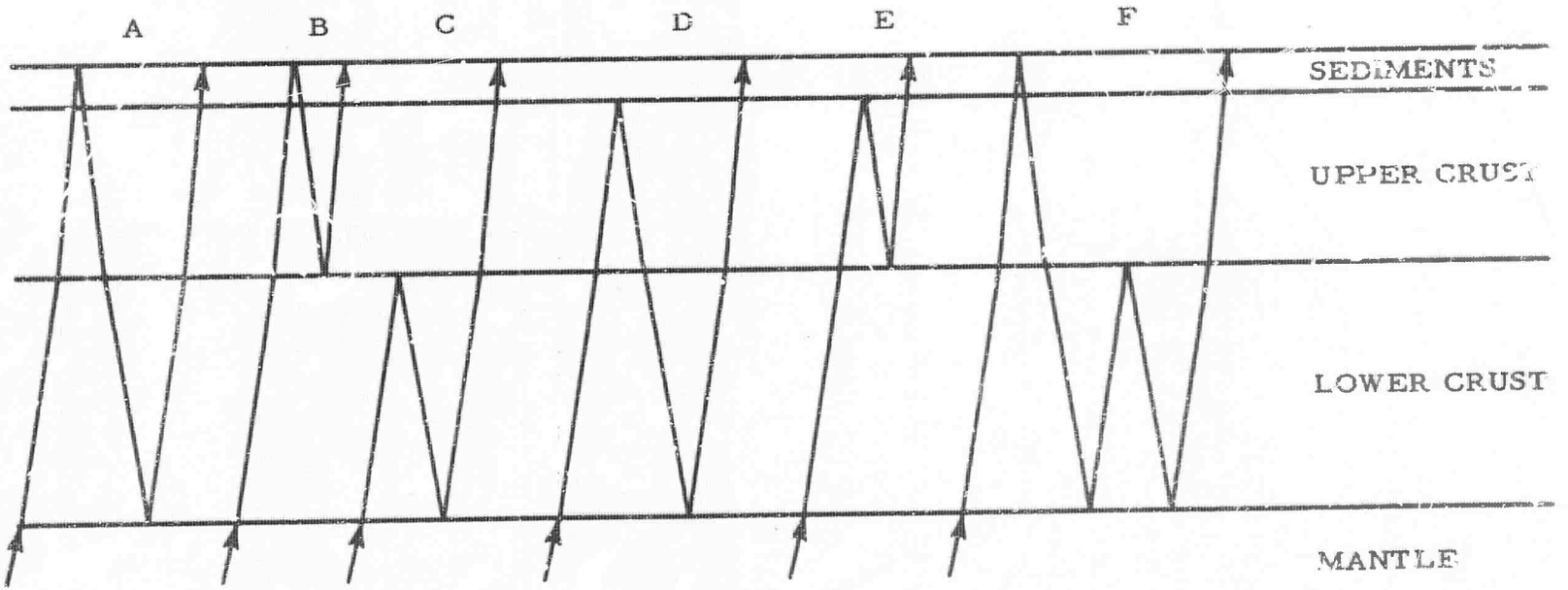

Figure III-10. Travel-Paths of Reflected Arrivals

signal bandwidth implies that optimum resolution is between 1 and 2 sec.

Table III-1

COMPUTED LAG TIMES OF REFLECTED ARRIVALS

Signal Phase Velocity (km/sec)	Arrival A	Arrival B	Lag Time (sec) Arrival C	Arrival D	Arrival E	Arrival F
12.6	10.0	6.0	4.0	9.0	5.0	14.0
22.5	11.0	6.5	4.5	10.9	5.5	15.5
∞	11.5	6.8	4.7	10.4	5.7	16.2

Estimated times for the first two "events" in Figure III-3 are 6.0 sec and 10.5 sec. These probably represent events B and A with 22.5-km/sec phase velocity. If this identification is correct and the lag times have been estimated accurately, then the depths of the Conrad and Mohorovicic discontinuities as given in Figure III-9 are too large by about 2 km. However, the dominant near-surface reflector could be an interface within the sedimentary section or the base of the sediments, in which case the predicted Conrad and Mohorovicic depths might even be too small by about 2 km. The "event" found near 15 sec could be any one of a large set of multiply-reflected arrivals, but event F seems to be the most likely arrival. The ambiguity in interpretation remains, since the apparent error in lag time can be removed either by decreasing the Conrad and Mohorovicic depths or by assuming the dominant near-surface reflector to be the base of the Devonian.

In Figure III-8, "events" have been found at 4.2 and 12.2 sec for a phase velocity of 12.6 km/sec. The major peaks in Figure III-7 occur at intervals of 0.28 cps, implying a reflecting system with a lag time of 3.6 sec. The differences in the lag times found for 22.5 km/sec and 12.6 km/sec are much greater than would be expected, unless different reflecting interfaces predominate in the two cases. It is difficult to conceive of how a model, consistent with Figure III-9, could give rise to only the "events" seen in Figure III-8. Since the four earthquakes contributing to Figure III-8 were so similar, it may be that the observed coincidences can be attributed to source effects.

In summary, the results suggest that the assumed crustal model for CPO is not in error by more than 1 or 2 km, but the results are not of sufficient quality to permit more definite conclusions at this time.

E. INVESTIGATION OF PROPAGATION MECHANISMS

An attempt is being made to use the high-quality teleseism records from the CPO processor to examine such subjects as inelastic absorption in the earth's interior and the dependence of crustal response on source range and azimuth. Therefore, more than 100 different groups of events have been chosen from Ensembles II and III, and autocorrelation functions and power spectra have been computed for each subensemble.

These data have not been studied yet in great detail. A preliminary examination suggests that because of the large number of variables involved (e.g., focal depth, geographical location of source, source-to-receiver distance and azimuth, geological source environment, source spectrum, magnitude, continental or oceanic nature of early part of travel path, source radiation pattern), the number of available recordings is too small to provide useful statistical significance.

SECTION IV

A SUMMARY OF CPO-MCF SYSTEMS

A. INTRODUCTION AND CONCLUSIONS

This is a summary of work which soon will be published as a special report under the title "A Study of Multichannel Filter Systems Incorporating Statistical Gain Fluctuation Designed for Cumberland Plateau Observatory."

MCF systems which were indicated to have had gain inequality problems were redesigned, incorporating statistical gain fluctuation. (Under certain circumstances, gain inequalities can cause multichannel filter systems to separate noise and signal on the basis of these inequalities rather than on true differences in spatial organization. When this happens, a system is said to have gain inequalization problems.) The counterpart systems then were compared in detail. This study also had a bearing on the evaluation of the partial arrays at CPO[3] in that the multichannel filter systems designed on the various partial arrays were thought to have been somewhat affected by gain inequalization problems.

The results of this study indicate that

- The addition of statistical gain fluctuation was a good solution to the gain inequalization problem.
- The addition of statistical gain fluctuation essentially prevents high gains in the frequency response of the filters for individual channels which appear to be necessary for MCF systems to operate on the basis of gain inequalities.
- The conclusions about the effectiveness of the partial arrays at CPO which previously were published [3] appear to be valid.

B. CPO-MCF SYSTEMS WITH GAIN INEQUALIZATION PROBLEMS

When MCF systems are designed in the time domain using equalized signal correlations and measured noise correlations, the systems may misdesign. When the seismometers are gained unequally, the MCF system can use the inequalities in the noise correlations as compared to the equalized signal correlations to separate the noise and the artificial signal. This has been found to most strongly affect the filters at low frequencies where the velocity differences between signal and noise are less significant and the noise is highly coherent. The system so designed

could be far from an optimum system for actual signal-noise separation.

MCF systems IP 13, IP 23 through IP 26 were designed for CPO. These systems showed, in varying degrees, symptoms characteristic of MCF systems which use seismometer gain differences to give artificial signal-to-noise improvement.

CPO IP 13 was designed as a 5-channel system to extract the signal at the center seismometer of the array (Figure IV-1). The 5 channels were the center seismometer, the sum of the 3 seismometers of ring 2, the sum of the 3 seismometers of ring 3, the sum of the 6 seismometers on ring 4, and the sum of the 6 seismometers on ring 5. IP 13 was designed in the time domain using CPO noise sample C^5 and an infinite velocity signal model.

It has been shown that IP 13 was affected adversely by inequalization of the seismometers [2]. In particular, this system rejected seismic noise as recorded through the seismometer-PTA system by as much as 23 db at 0.4 cps, passed perfectly equalized synthetic signals with very little signal distortion and rejected actual signals which were recorded through the seismometer-PTA system. At low frequencies, IP 13 exhibited the characteristics of systems which are designing on the basis of seismometer gain inequalities: high gains in the filters on individual channels, K-space power response of the MCF system not amendable to rejection of the spatial-organized noise. (See Figures IV-2 and IV-11, presented later.)

The MCF systems IP 23, IP 24, IP 25, and IP 26 were designed to test the effectiveness of partial arrays at CPO. These systems have been discussed in detail in a previous publication [3]. They were designed to extract signal at the center seismometer with IP 23 using 5 channels, the center seismometer and each summed ring; IP 24 using 4 channels, the center seismometer and the summed rings 3, 4 and 5; IP 25 using 3 channels, the center seismometer and the summed rings 4 and 5; IP 26 using 2 channels, the center seismometer and the summed ring 5 (Figure IV-1). These systems were designed in the time domain using an infinite velocity signal model.

These systems were thought to have been affected by seismometer gain differences because the systems showed differences in their K-space responses at 0.5 cps. Also, the low-frequency characteristics of the individual channel filters implied seismometer gain differences (p. 5) [3]. The symptoms of gain inequalization problems for these systems were less severe then those of IP 13.

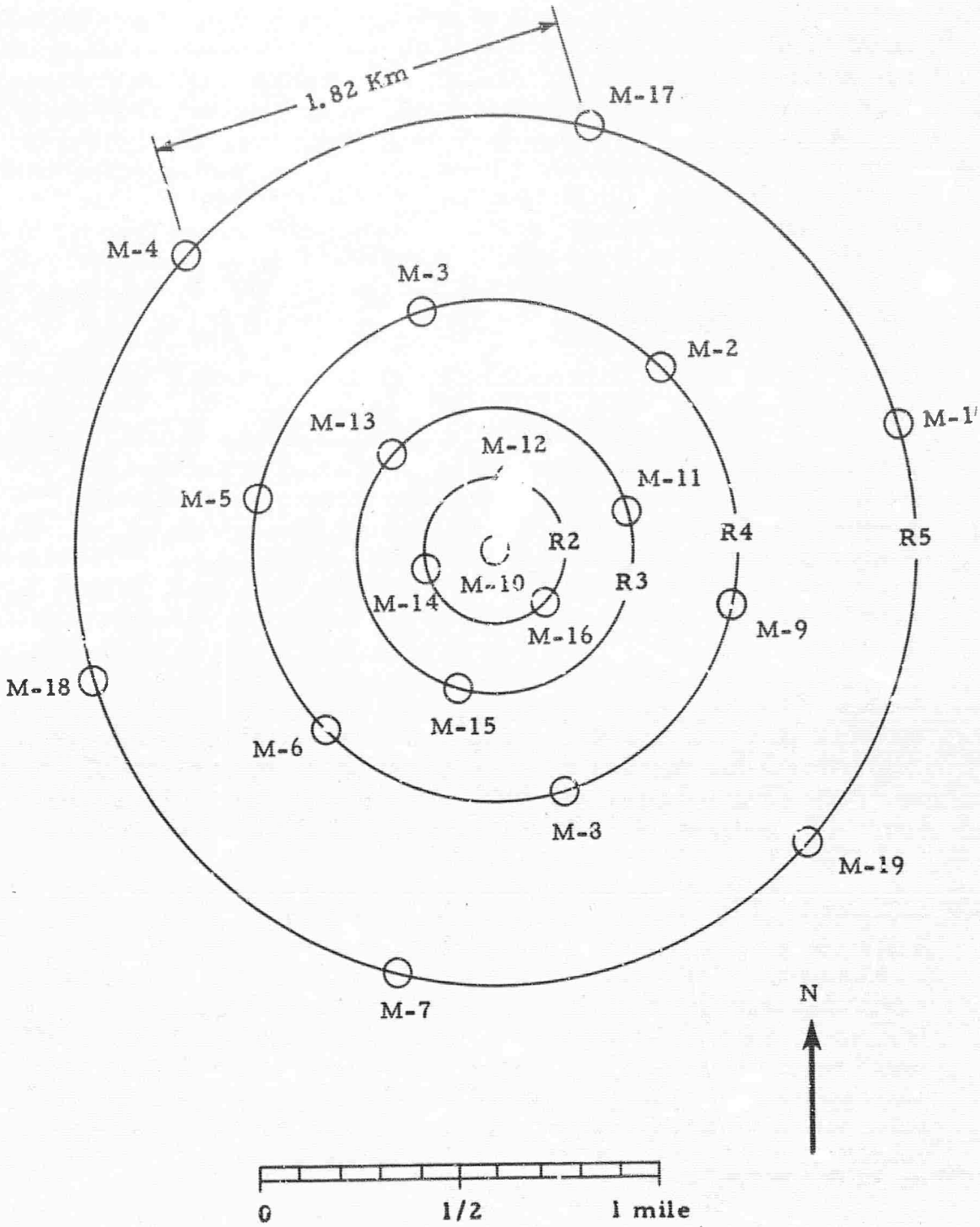

Figure IV-1. Layout of CPO Array

C. DESIGN OF COUNTERPART MCF SYSTEMS WITH GAIN FLUCTUATION

Using the method of incorporating statistical gain fluctuation [2], all of the multichannel filter systems mentioned above were redesigned. The effect of this gain fluctuation was to add spatially random signal to the multichannel filter design problem. IP 13 was redesigned as IP 22; IP 23 through IP 26 were redesigned as IP 33 through IP 36. IP 22 differed from IP 13 in that the method of incorporating statistical gain fluctuation resulted in all signal autocorrelations being scaled up and that the time domain filters were 31 points long for IP 22 as compared with 25 points for IP 13. The MCF systems IP 33 through IP 36 differed from their counterparts IP 23 through IP 26 only in that statistical gain fluctuation was incorporated into the redesigned systems.

D. EFFECTS OF INCORPORATING STATISTICAL GAIN FLUCTUATION

The method of adding statistical gain fluctuation, in effect, adds some spatially uncorrelated signal. The addition of spatially uncorrelated signal makes high gains on any channel unprofitable. If a large gain is applied to one channel, it must be compensated for on another (to maintain signal response). The spatially uncorrelated signal power will be gained up by both channels, with no cancellation occurring, which results in a large contribution to the mean-square-error (MSE). The magnitude of this effect would depend upon signal power at any frequency. High gains on individual channels seem to be necessary [2] for a MCF system which suppresses noise mostly on the basis of inequalized noise discriminated from equalized signal. The method of incorporating gain fluctuation makes these large gains unprofitable, thus, forcing the MCF system to separate signal and noise on the basis of correlation differences which are the result of the spatial organization of the signal and noise.

Spatially uncorrelated signal power tends to force the MCF system to use the center seismometer for signal preservation. Since the system wishes to output an approximation of the signal as seen on the center seismometer, it is obvious that using any other channel to estimate the signal will increase the MSE. To produce a least MSE system at each frequency, the MCF system must weigh the increased signal distortion, which results from using the center seismometer to reject noise (and thus, necessarily other channels to estimate the signal), against the decreased noise power output possible by using the center seismometer to reject noise. This weighing at a particular frequency (in terms of cost in MSE) would be effected by:

- The gains applied to the ring-summed channels

- The signal power

By comparing the frequency responses of the individual channels for the counterpart systems IP 13 with IP 22, IP 23 with IP 33, IP 24 with IP 34, IP 25 with IP 35, IP 26 with IP 36 (Figures IV-2 through IV-10), it is readily seen that the systems with gain fluctuation do not show the high gains at low frequencies and are making heavier use of the center seismometer to pass the signal. The response of channel 1 (center seis) is smoothed for the systems with gain fluctuation. These differences are more pronounced as the number of channels increases. The systems using more channels can better afford (in terms of MSE) to partially give up the center seismometer and still suppress the noise. IP 36, which has only 2 channels, cannot possibly give up one of them to any large degree and still effect noise suppression.

The notably greater dependence of the gain fluctuation systems on the center seismometer to preserve signal at low frequencies is the result of larger gains on the ring-summed channels and more signal power at these low frequencies.

At frequencies where the gain inequalization problem strongly affected the multichannel filter systems, the K-space responses of the counterpart systems with gain fluctuation are notably different. At frequencies which were not affected by gain equalization problems, the K-space responses of the counterpart systems generally are similar.

At frequencies where the multichannel filter systems without gain fluctuation were separating noise and signal strongly on the basis of gain inequalities, the S/N improvement (measured noise and artificial infinite velocity spike signal) was considerably better than the counterpart systems. At frequencies where the systems were operating on the basis of velocity differences and the noise generally was coherent across the array, the S/N improvements of the counterpart systems generally are similar. At certain higher frequencies ($f \geq 2$ cps) the systems with gain fluctuation give notably poorer S/N improvement than the systems without gain fluctuation. The reason for this is not apparent.

Figure IV-11 shows the K-space response of IP 22 and IP 13 at 0.5 cps. IP 13 shows very little noise rejection at 0.5 cps, whereas, IP 22 rejects noise strongly in a velocity band around 3 km/sec. These responses indicate strongly that the system with gain fluctuation (IP 22) was forced to design primarily on the basis of velocity differences in the signal and noise.

Figure IV-12 shows the signal-to-noise improvement for the noise used in the MCF system's design of IP 13 and IP 22. (It should be

Text cont's page IV-18.

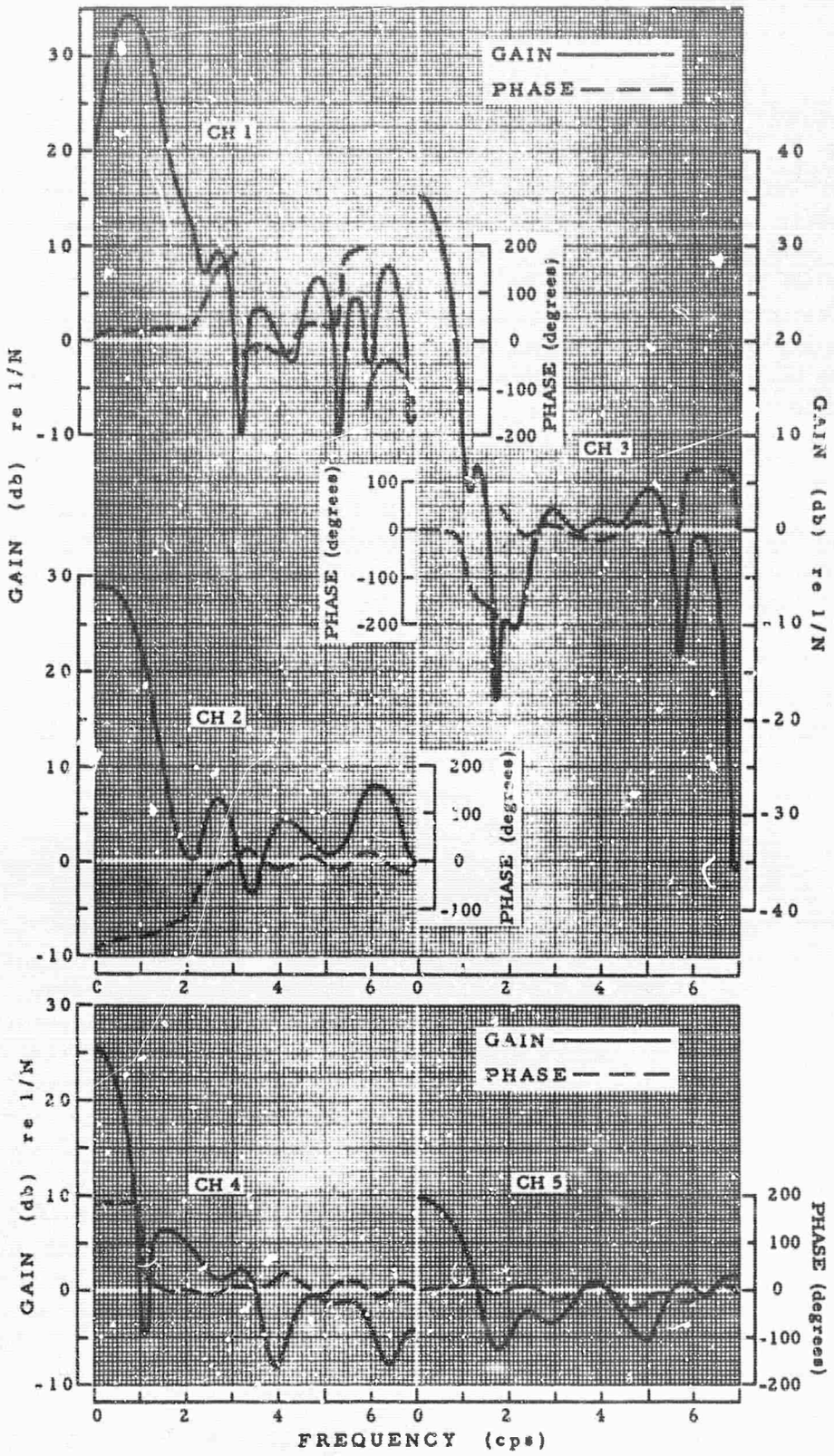

Figure IV-2. Amplitude and Phase Responses of the Filters for CPO IP13

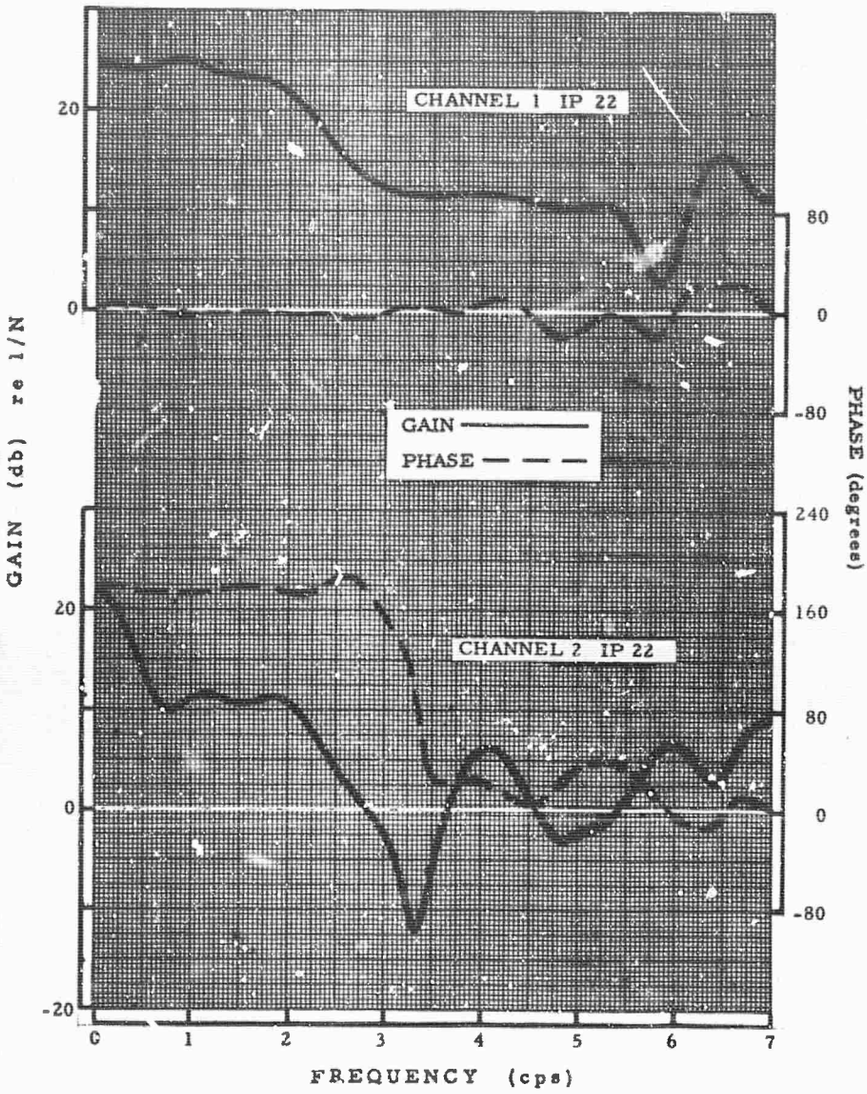
CHANNEL 1 IP 22
CHANNEL 2 IP 22
GAIN
PHASE
GAIN (db) re 1/N
PHASE (degrees)
FREQUENCY (cps)
20
0
-20
80
0
-80
240
160
80
0
-80
0
1
2
3
4
5
6
7

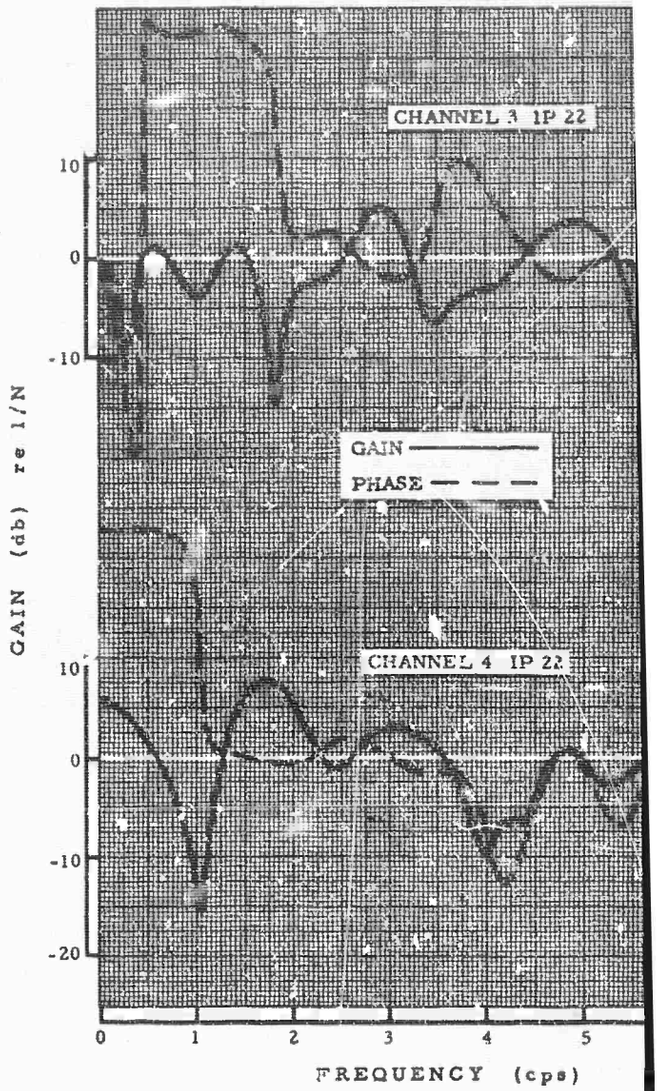
CHANNEL 3 IP 22
CHANNEL 4 IP 22
GAIN
PHASE
GAIN (db) re 1/N
FREQUENCY (cps)
10
0
-10
-20
0
1
2
3
4
5

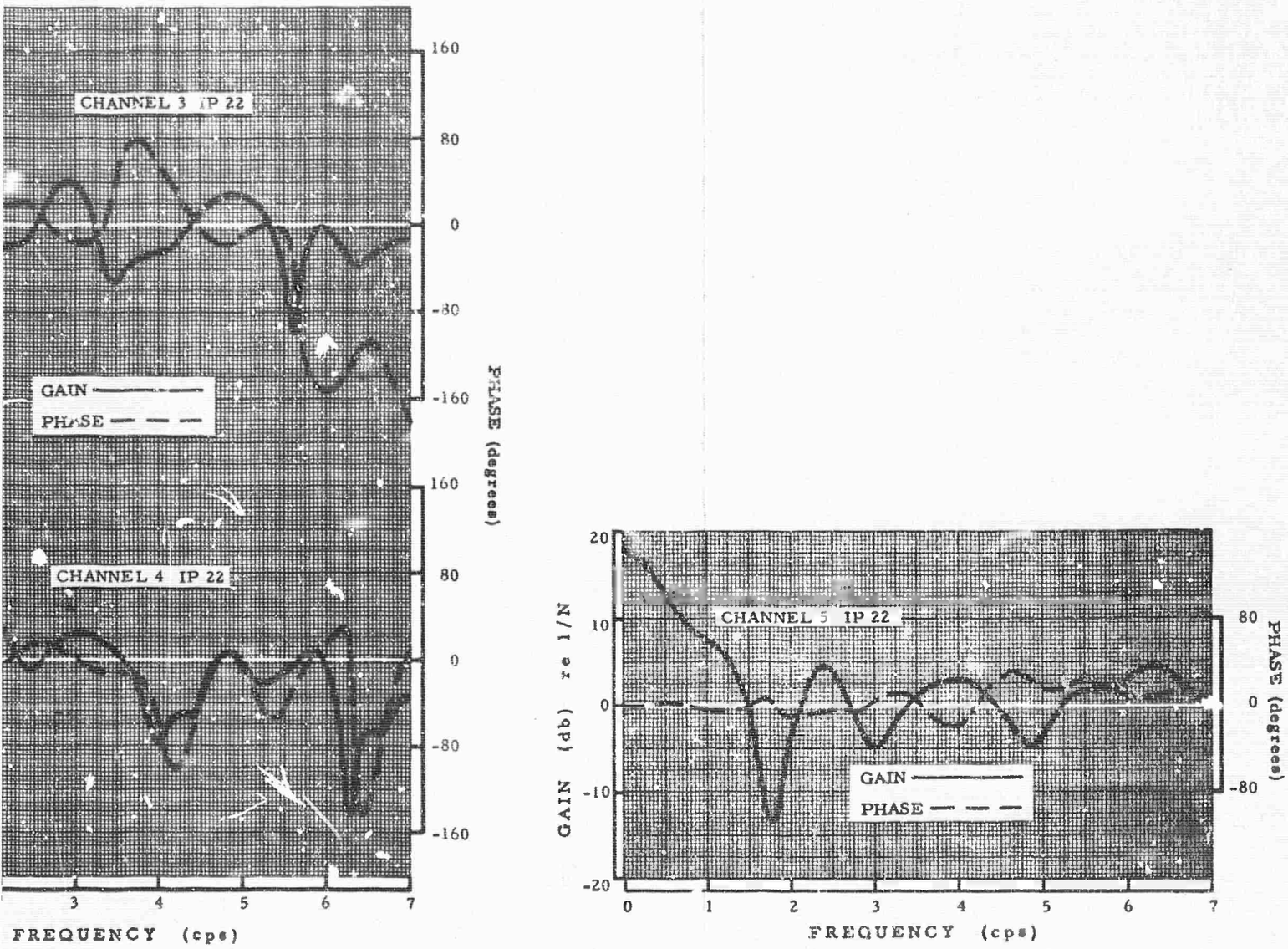

Figure IV-3. Amplitude and Phase Responses of the Filters for CPO IP22

2

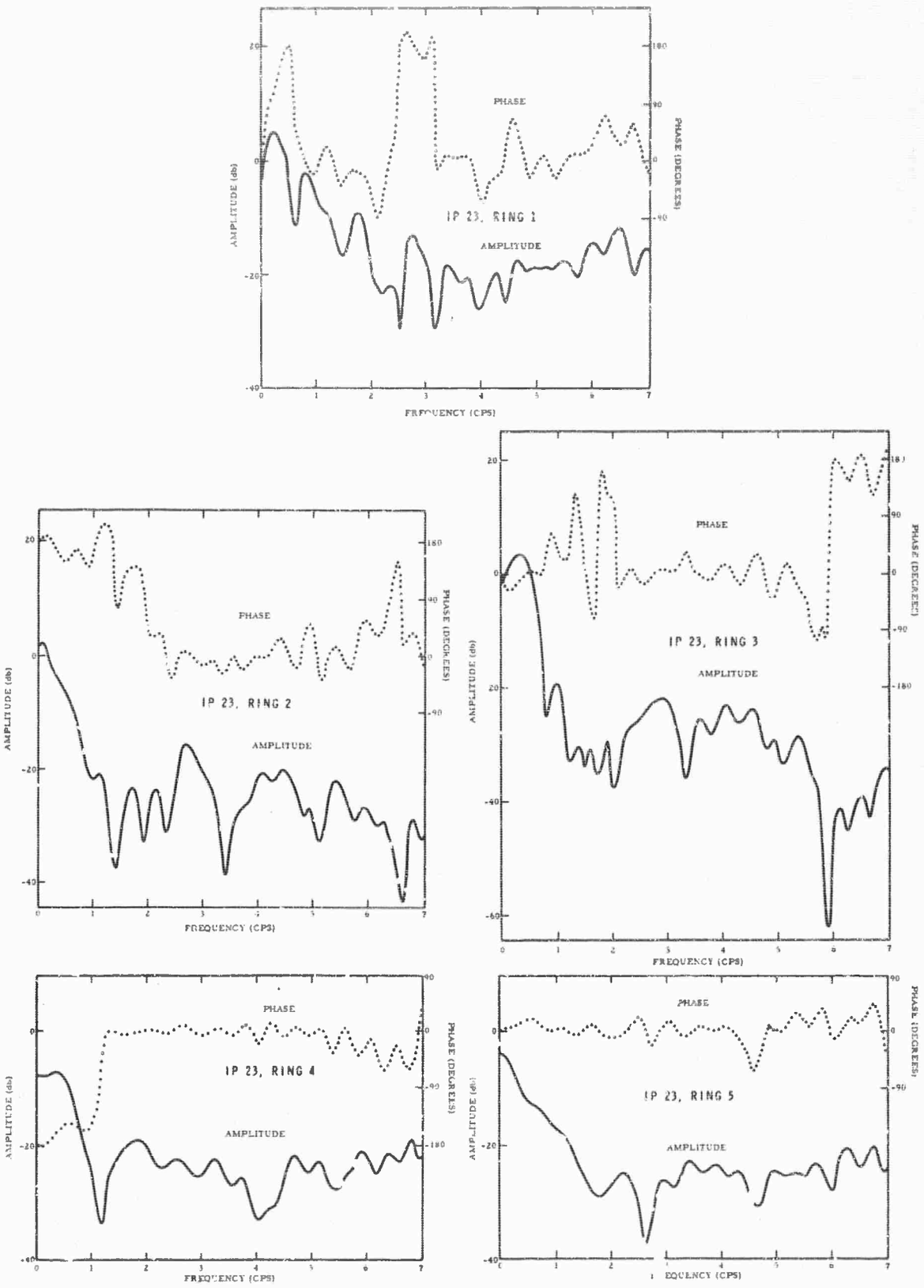

Figure IV-4. Amplitude and Phase Responses of the Filters for CPO IP 23

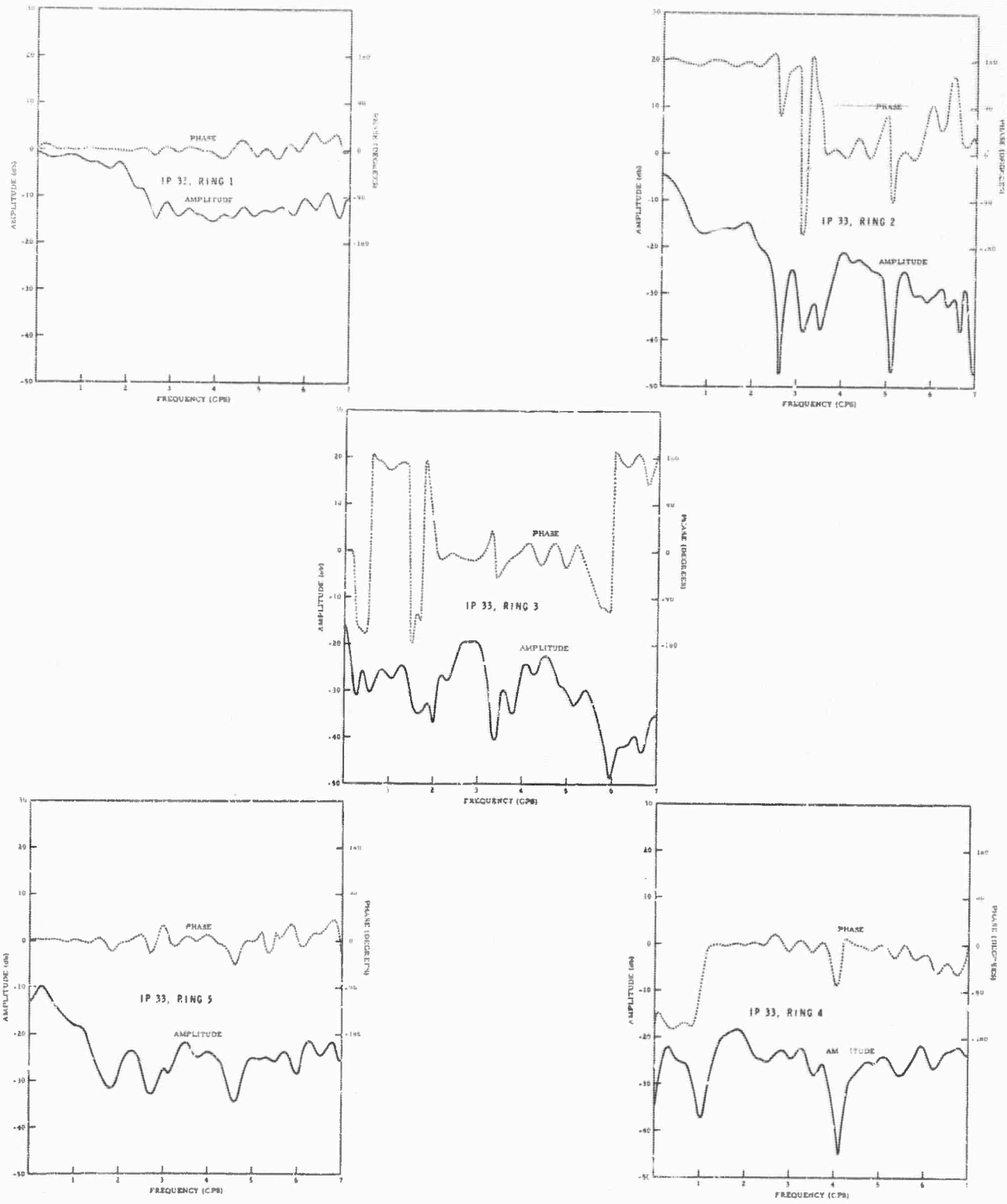

Figure IV-5. Amplitude and Phase Responses of the Filters for CPO IP 33

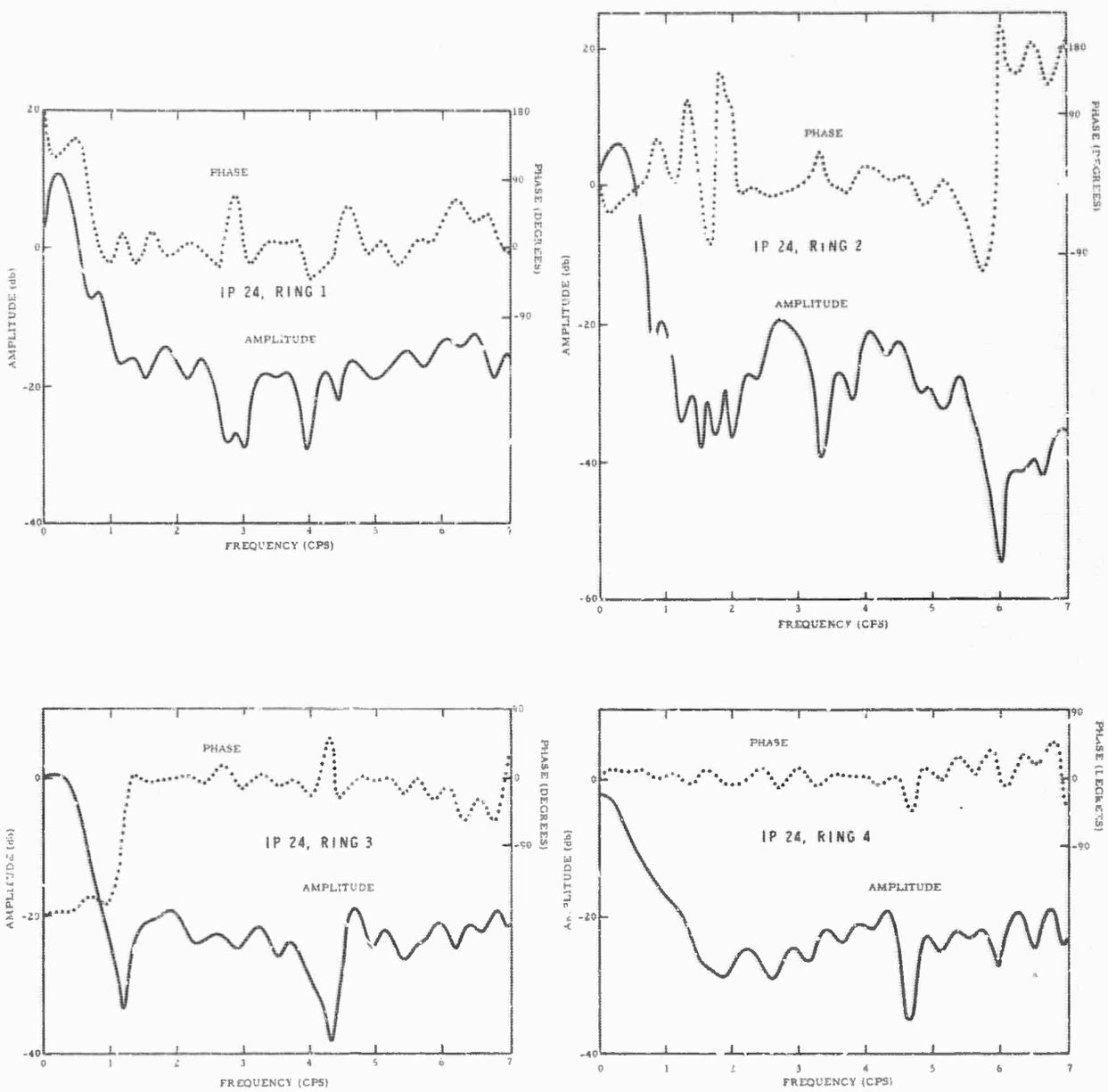

Figure IV-6. Amplitude and Phase Responses of the Filters for CPO IP 24

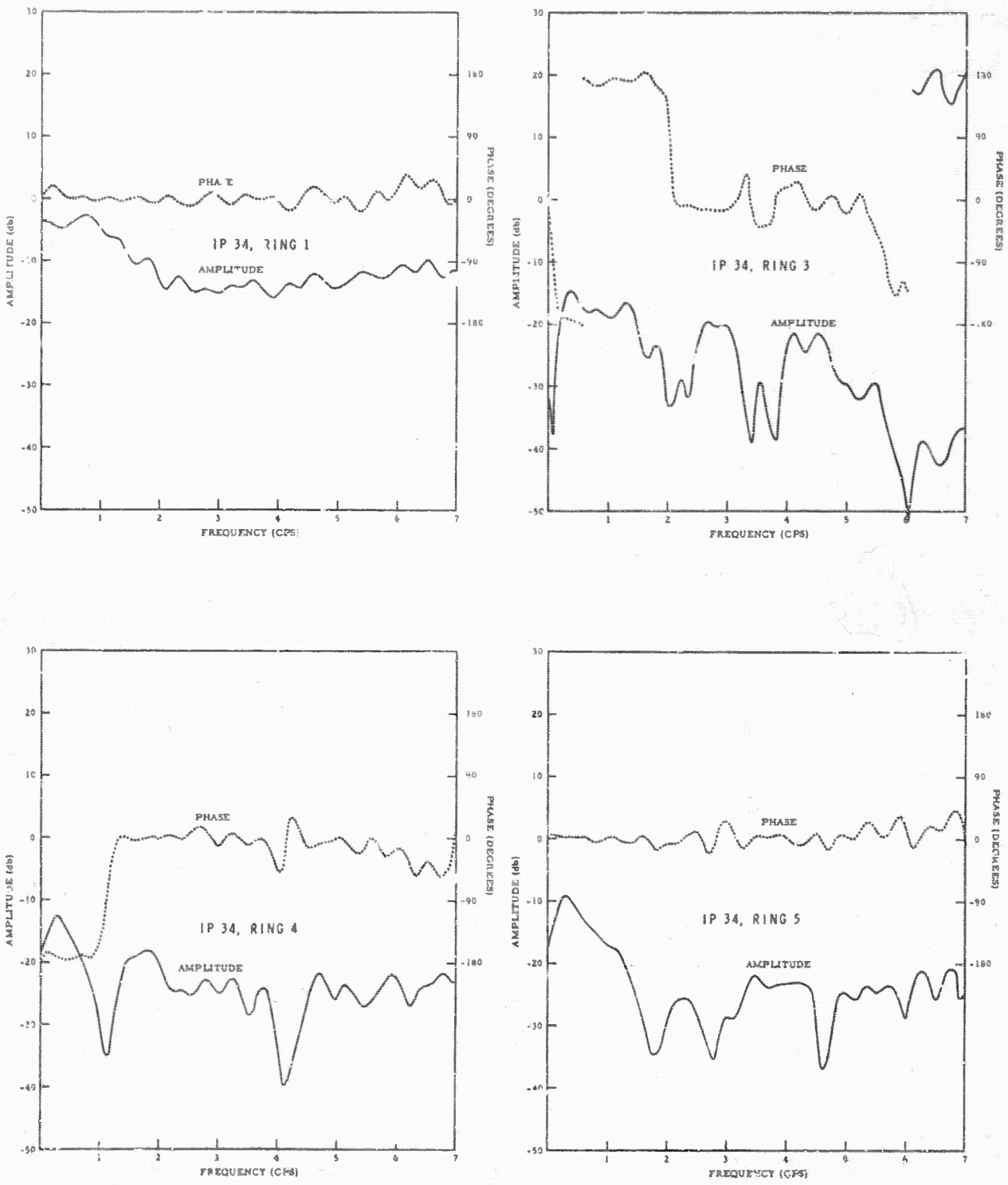

Figure IV-7. Amplitude and Phase Responses of the Filters for CPO IP 34

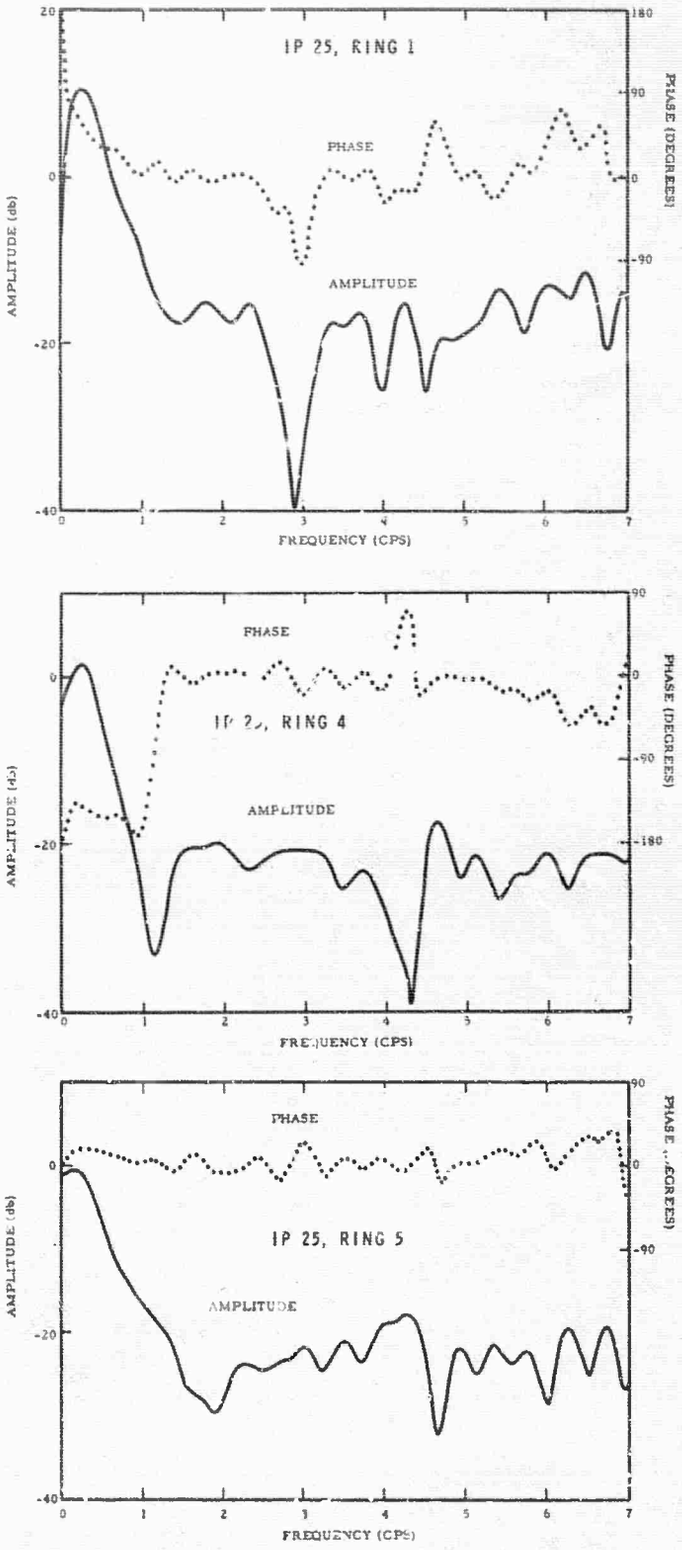

Figure IV-8. Amplitude and Phase Responses of the Filters for CPO IP 25

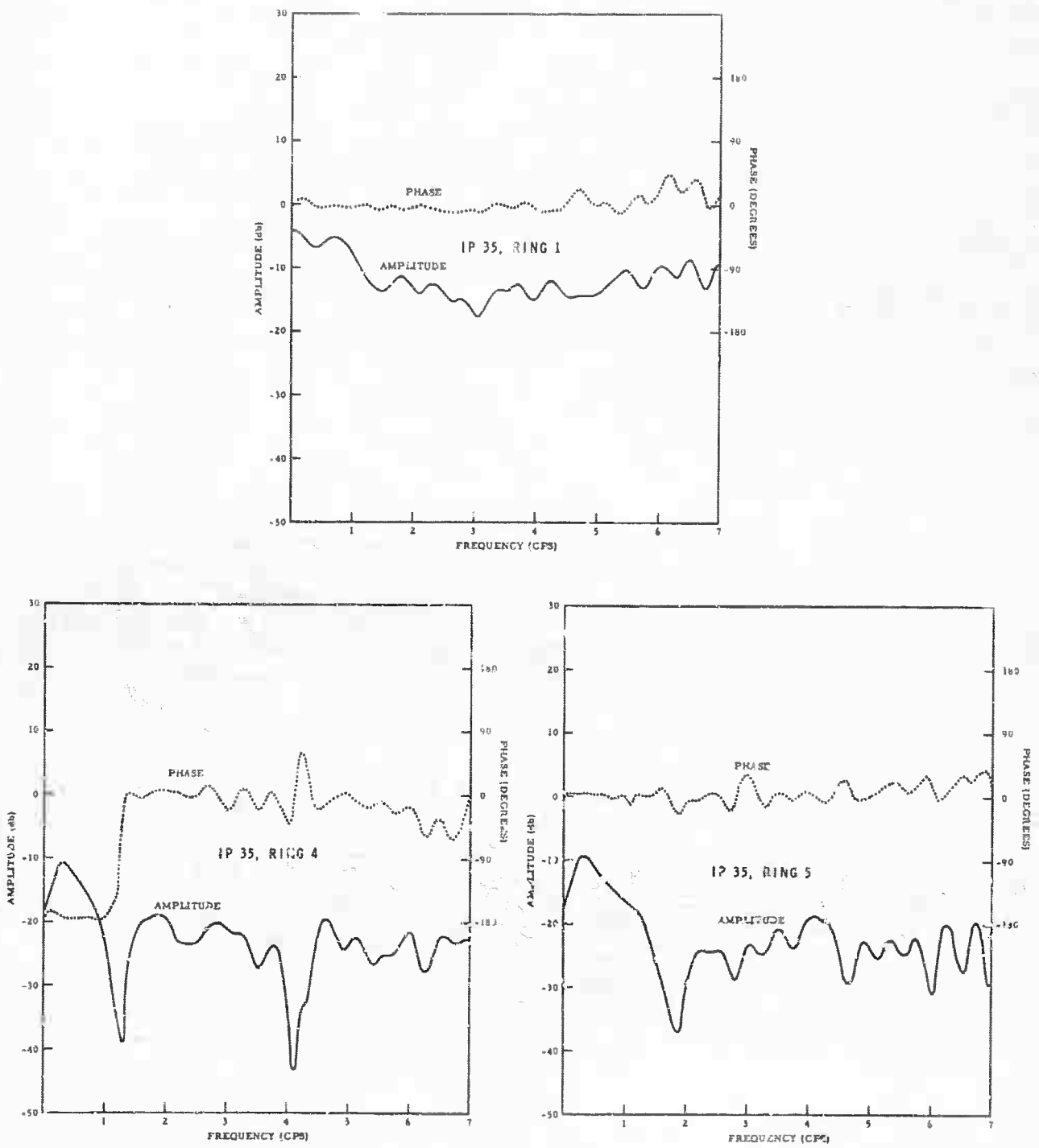

Figure IV-9. Amplitude and Phase Responses of the Filters for CPO IP 35

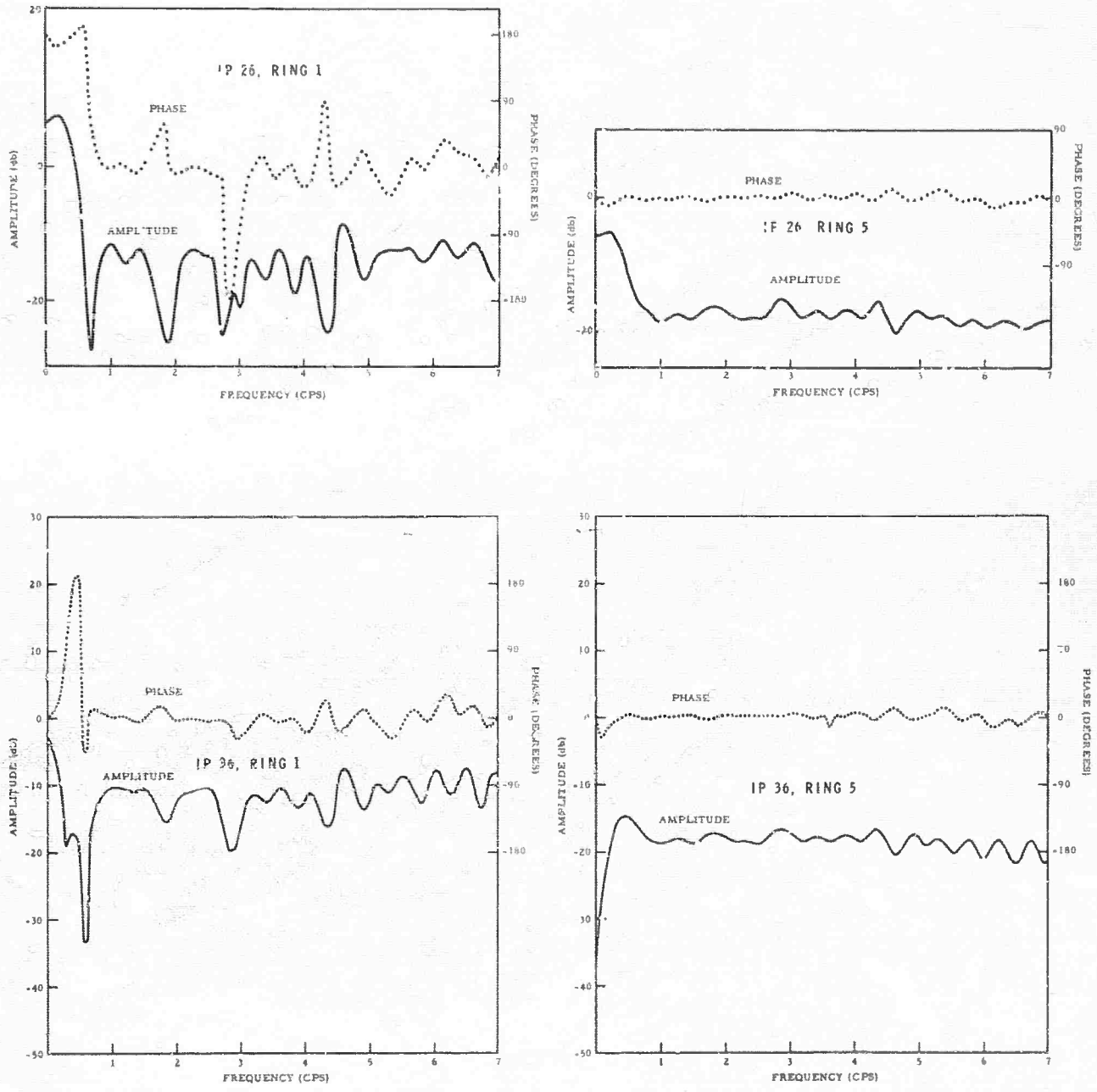

Figure IV-10. Amplitude and Phase Responses of the Filters for CPO IP 26 and 36

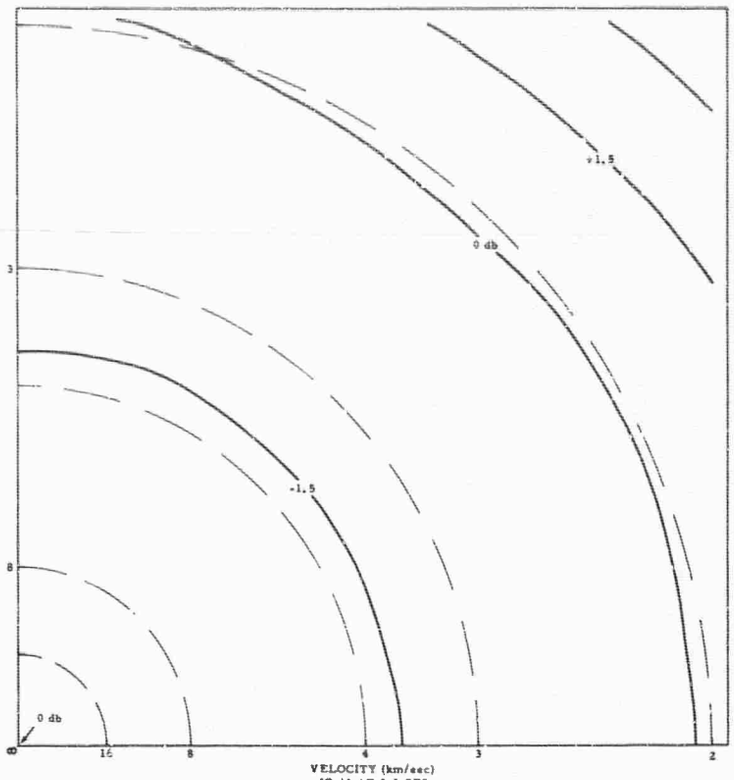

VELOCITY (km/sec)
IP-13 AT 0.5 CPS
CONTOURED IN db

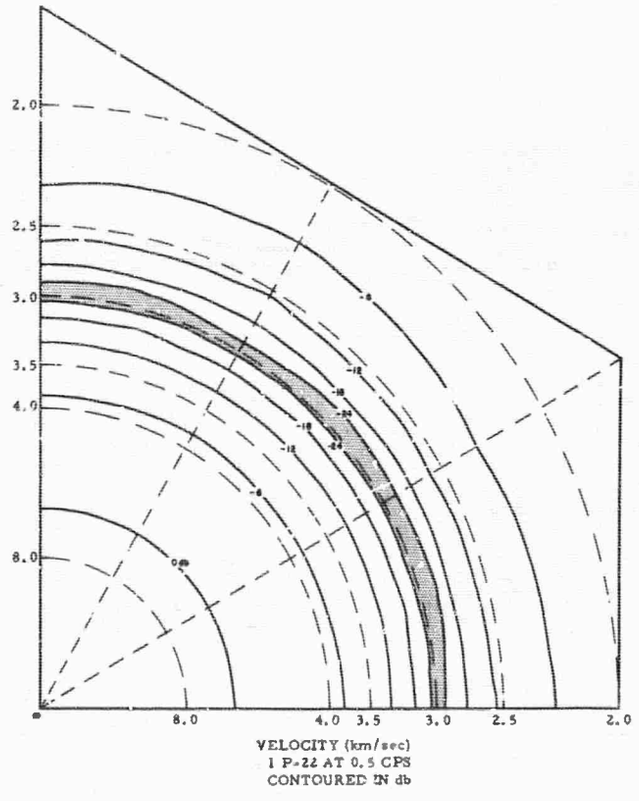

VELOCITY (km/sec)
1 P-22 AT 0.5 CPS
CONTOURED IN db

Figure IV-11. K-Space Responses of CPO IP 13 and 22 at 0.5 CPS

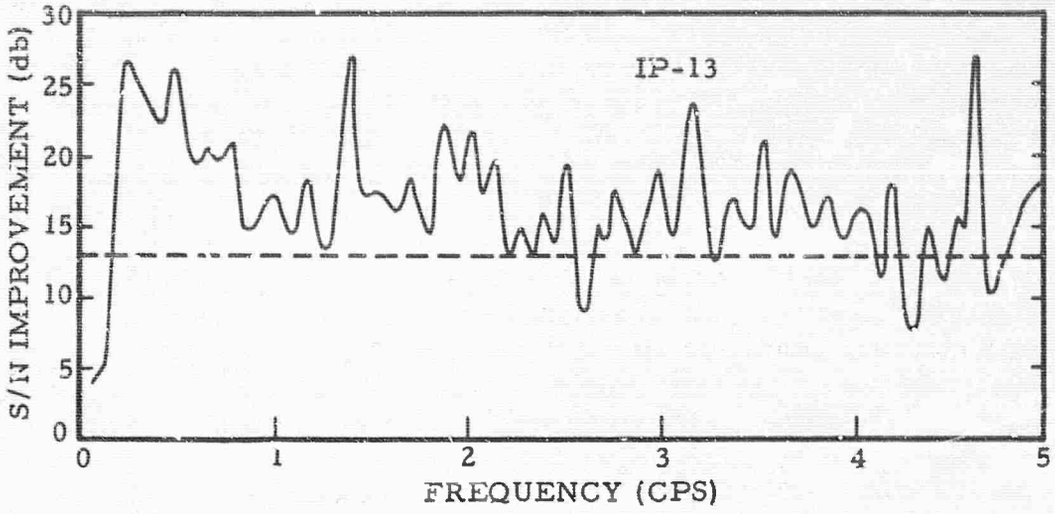

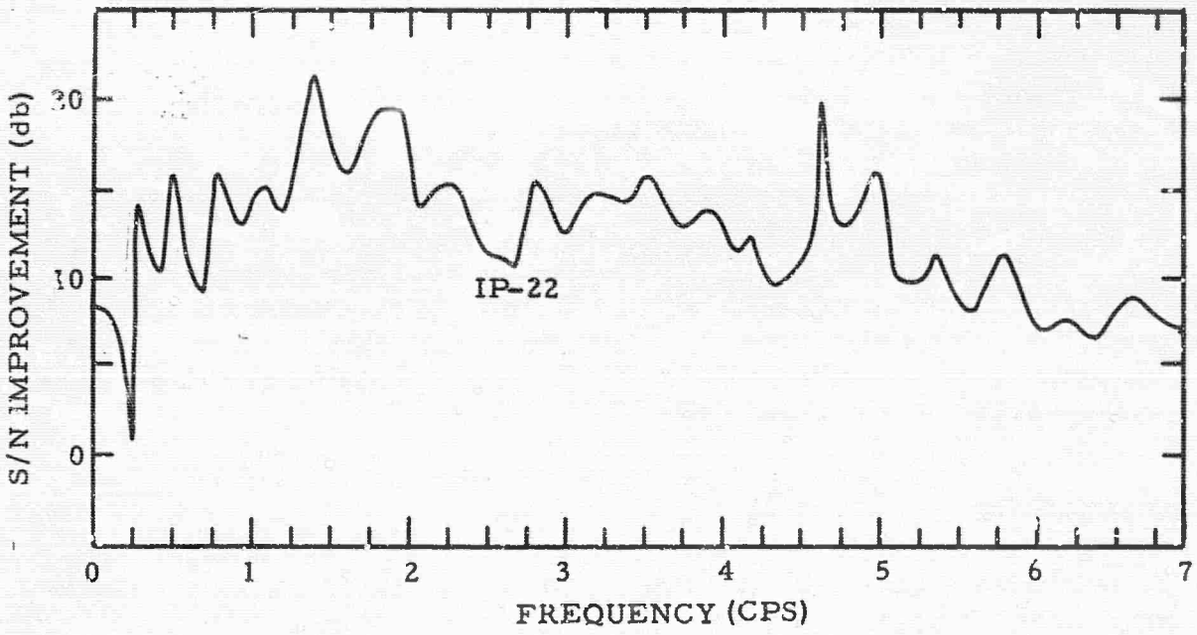

Figure IV-12. S/N Improvement Relative to Single Seismometer for IP 13 and 22

noted that these S/N improvements were obtained from spectral estimates of different resolution.) At low frequencies the S/N improvement obtained from IP 13 is much better (10 db) than that obtained from IP 22. In view of the K-space responses of the two systems at 0.5 cps (Figure IV-11), the S/N improvement obtained from IP 13 is false. To a large extent, IP 13 suppressed the noise on the basis of gain differences. A multichannel filter system which would pass infinite velocity signals as actually recorded could give S/N improvement at low frequencies on the order of that obtained from IP 22.

Figure IV-13 shows the K-space response of IP 13 and IP 22 at 1.0 cps. Both systems show attenuation of plane wave energy centered around 3 km/sec, but the system with gain fluctuation attenuates much more strongly. This indicates that while IP 13 was still affected by gain inequality problems, it was obtaining its noise suppression at 1.0 cps somewhat more on the basis of spatial organization and less on the basis of gain inequalities. This also is indicated by the frequency response of the individual filters (Figures IV-2 and -3). The individual channel gains are considerably lower at 1 cps than at 0.5 cps.

The S/N improvement at 1.0 cps is only slightly better for IP 13 than for IP 22. IP 22 was forced to rely upon velocity differences in the signal and noise and did a better job than IP 13 of suppressing noise on that basis. IP 13, however, was able to use gain differences in addition to the spatial organization of the noise with the net effect being that IP 13 gave a little better (falsely so) S/N improvement.

Figure IV-14 shows the K-space power response of IP 24 and IP 34 at 0.3 cps. IP 34 (system with gain fluctuation) shows a stronger reject band at a bit lower velocity than does IP 24. This strongly suggests that part of the noise rejection obtained from IP 24 resulted from using gain inequalities. This also tends to confirm the observation that high gains on individual channels can mean that the MCF system is using gain differences to separate artificial signal and noise.

The S/N improvements for the MCF systems IP 23 through IP 26 and IP 33 through IP 36 are shown in Figures IV-15 and IV-16. Figure IV-15 shows the S/N improvement relative to a single seismometer obtained from noise sample A^5 that was processed by IP 23 through IP 26 and their counterpart systems IP 33 through IP 36. Figure IV-16 shows the S/N improvement relative to a single seismometer obtained from noise sample I^5 that was processed by IP 23 through IP 26 and IP 33 through IP 36.

The difference in S/N improvement between IP 34 and IP 24 is 8 to 9 db at 0.3 cps for noise-sample I. A portion of this is due to the

Text cont'd page IV- 23

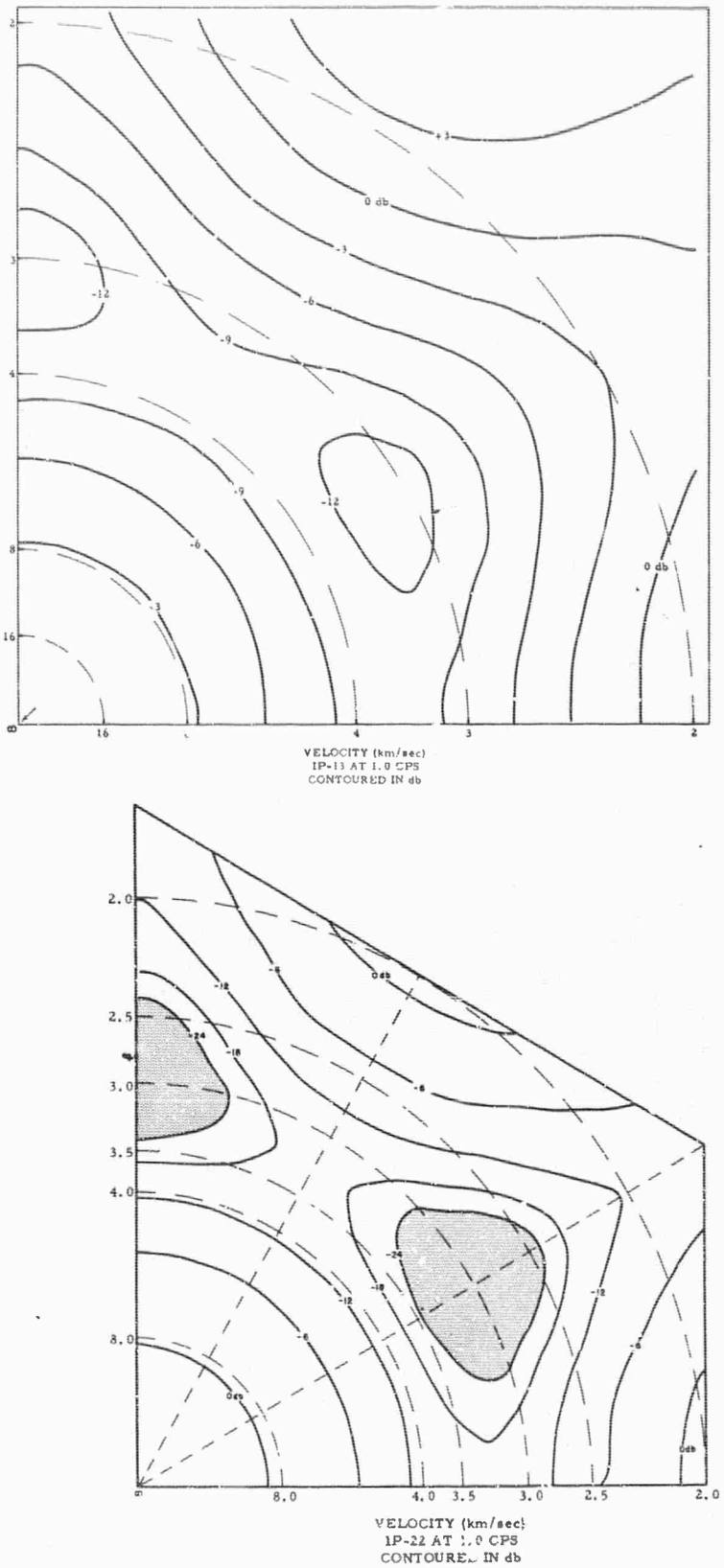

Figure IV-13. K-Plane Responses of IP 13 and 22 at 1.0 CPS

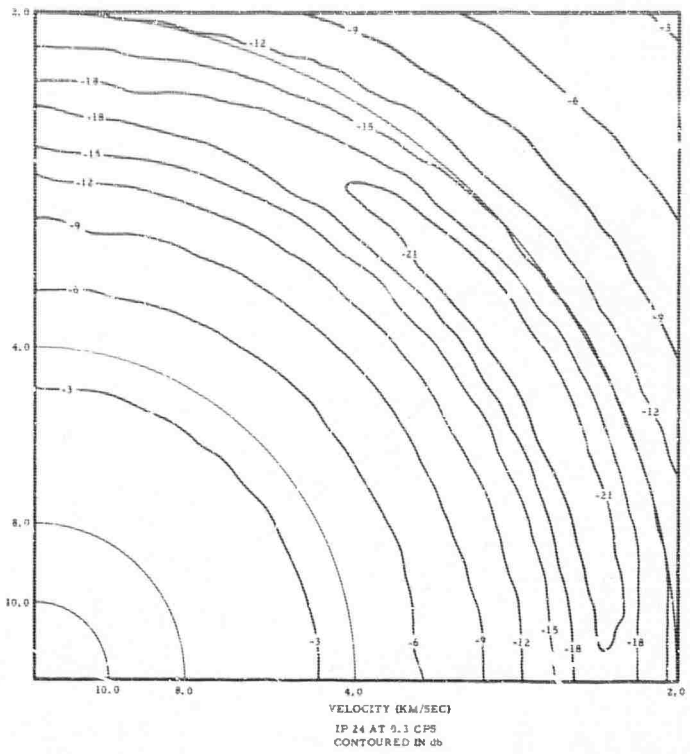

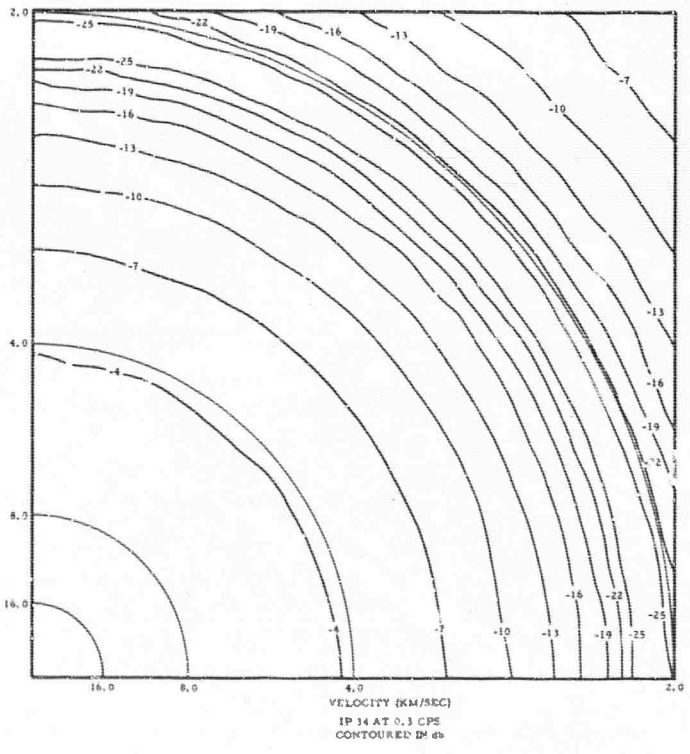

Figure IV-14. K-Plane Responses of IP 24 and 34 at 0.3 CPS

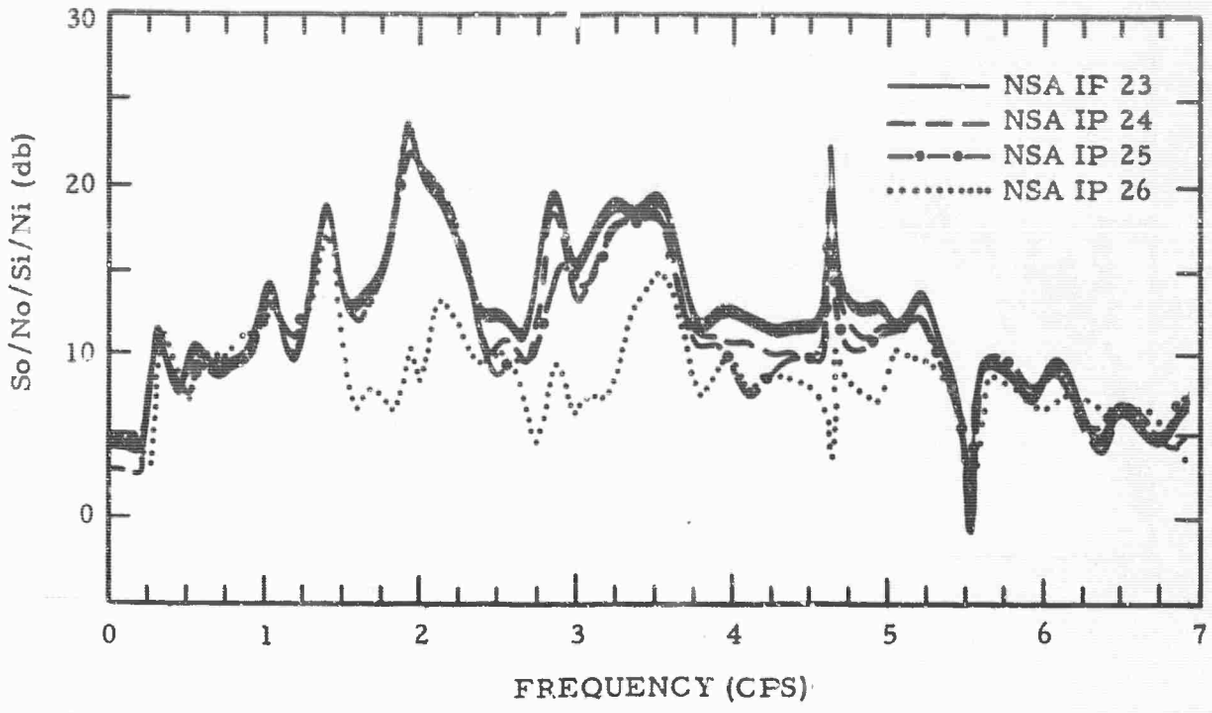

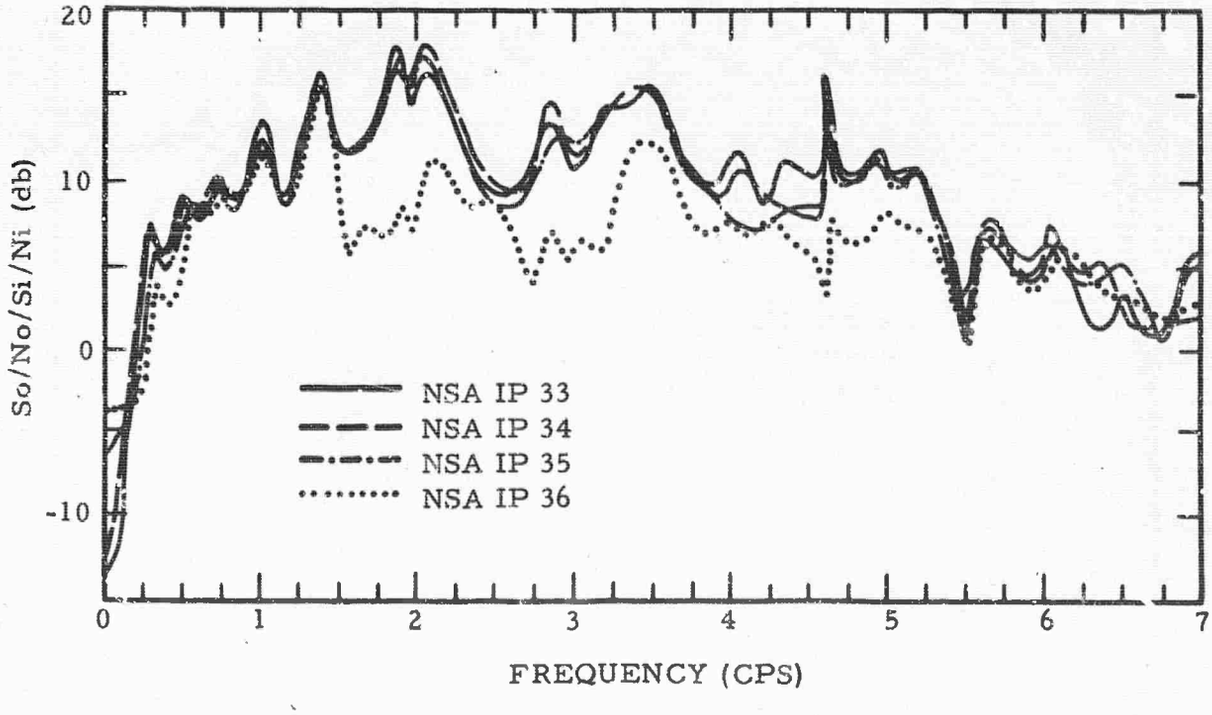

Figure IV-15. S/N Ratio Improvements Obtained Processing NSA and an Infinite Velocity Signal

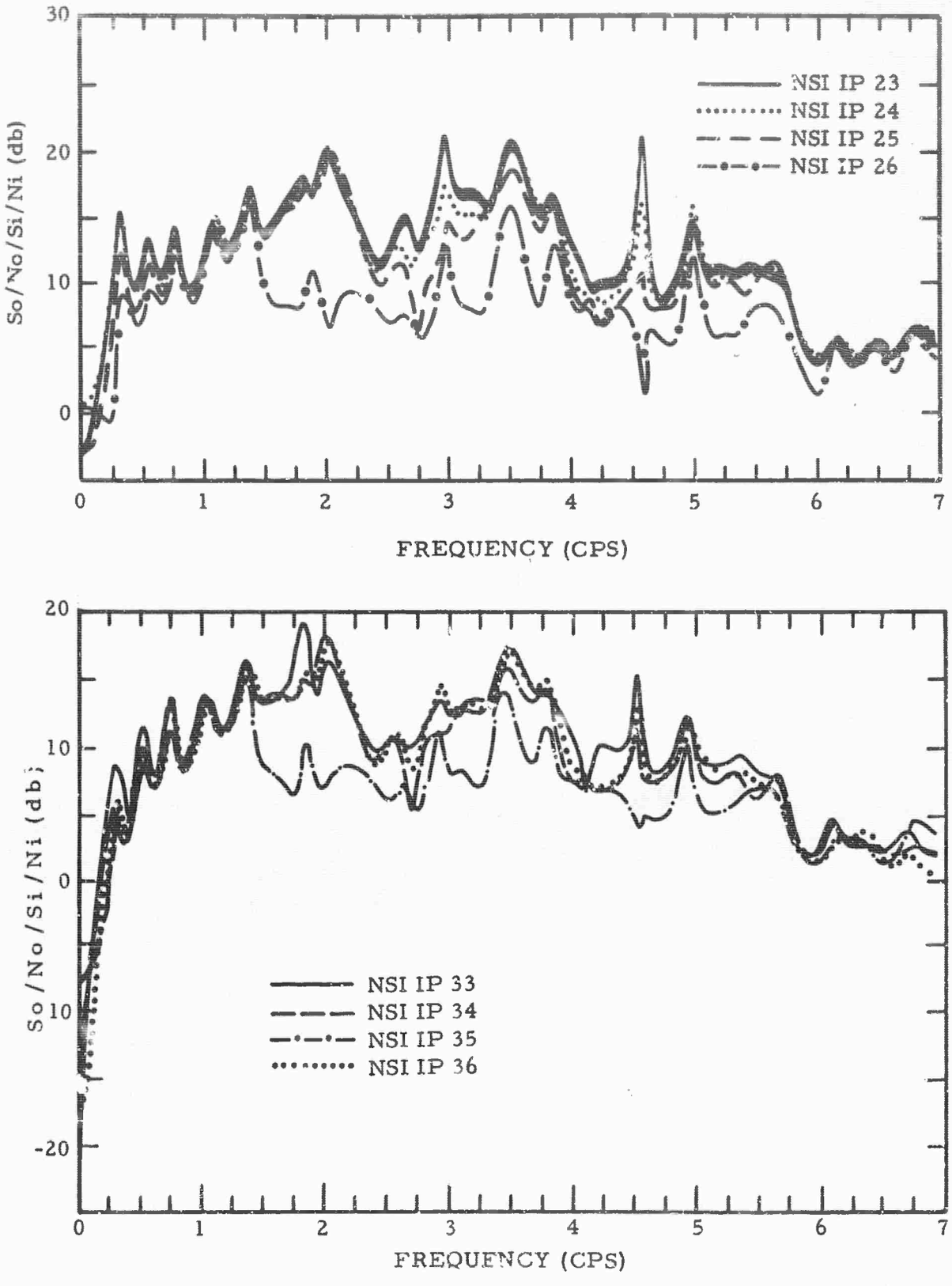

Figure IV-16. S/N Ratio Improvements Obtained Processing NSI and an Infinite Velocity Signal

poorer signal response of IP 34 (the signal responses are not included in this summary). The major reason for this difference, however is that IP 24 was using seismometer output inequalities to suppress the noise.

Figures IV-17 and IV-18 show the wavenumber responses of IP 23 through IP 26 and IP 33 through IP 36 at 1.0 cps. The counterpart systems are seen to have quite similar K-space responses at 1.0 cps. Indeed, all the systems have quite similar K-space responses at 1.0 cps.

At this would indicate, the signal-to-noise improvements are very nearly equal for all MCF systems at 1.0 cps (Figures IV-15 and IV-16).

The effects of multichannel filter systems which have gain inequalization problems on actual signals can be seen from an event from Crete recorded at CPO on March 4, 1963, which is shown in Figures IV-19 and IV-20. Figure IV-19 shows the outputs of IP 23 through IP 26 and Figure IV-20 shows the outputs of IP 33 through IP 36. The figures show the center seismometer output, the multichannel filter system output and the difference of these two. This event occurred at a distance of about 83 degrees from CPO; thus, the signal should have an apparent velocity across the array of about 22 km/sec.

For this event, the energy seems to be concentrated in a frequency range around 0.5 cps. Such a signal should be passed by all the multichannel filter systems with very little attenuation.

The systems without gain fluctuation which were designed using the larger number of seismometers (IP 23, IP 24 and IP 25) show an abnormally low signal amplitude. They are low as compared to their counterparts with gain fluctuation and also as compared to IP 26. While this possibly could be explained on the basis of the proper combination of seismometer gain outputs, it strongly suggests that the design of systems IP 23, IP 24 and IP 25 was affected by gain inequalities. These effects appear to be moderate, but noticeable at about 0.5 cps.

E. COMPARISON OF MCF SYSTEMS WITH A SUMMATION FOR SPECIFIC EVENT

In order to compare the multichannel filter systems with the summation, a straight summation of the 19 seismometer outputs was made for the Crete event. This is shown in Figure IV-21.

The summation does not reject the pre-event noise nearly as well as the multichannel filter systems which use a comparable number of seismometers. The summation is passing a large amount of low-frequency

Text cont'd page IV-29

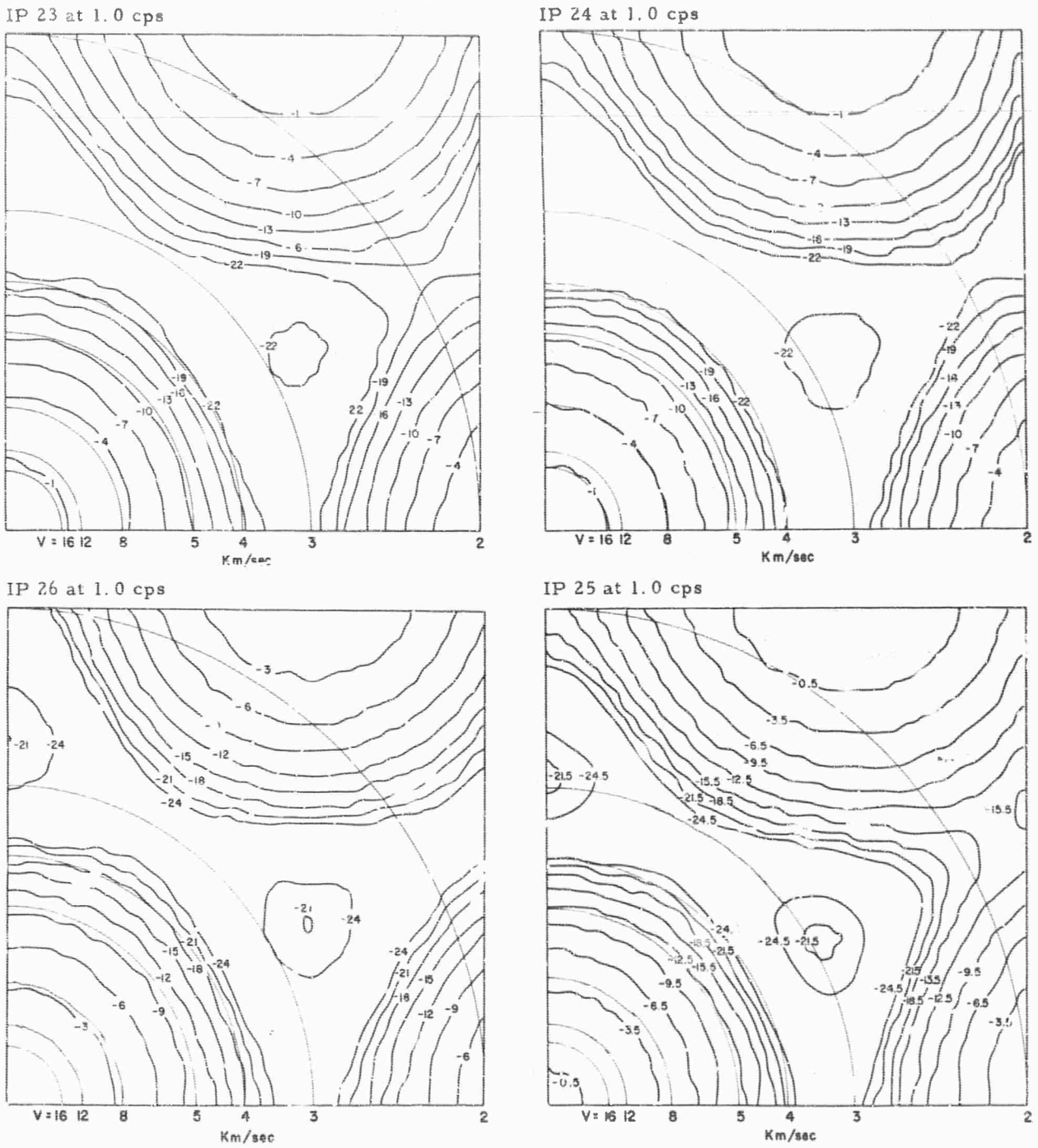

Figure IV-17. K-Plane Responses of IP 23, 24, 25, and 26 at 1.0 CPS (Contoured in db)

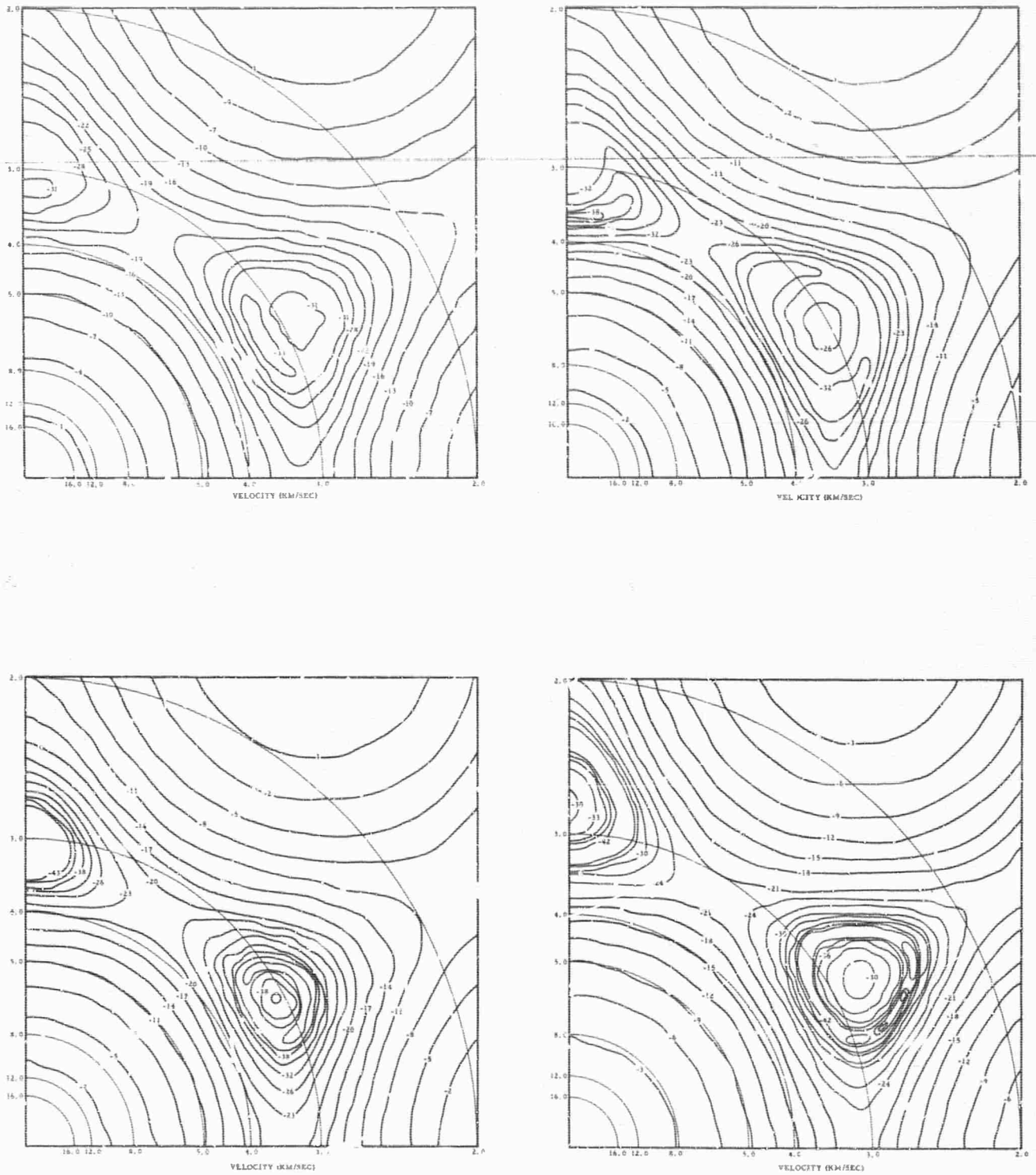

Figure IV-18. K-Plane Responses of IP 33, 34, 35, and 36 at 1.0 CPS (Contoured in db)

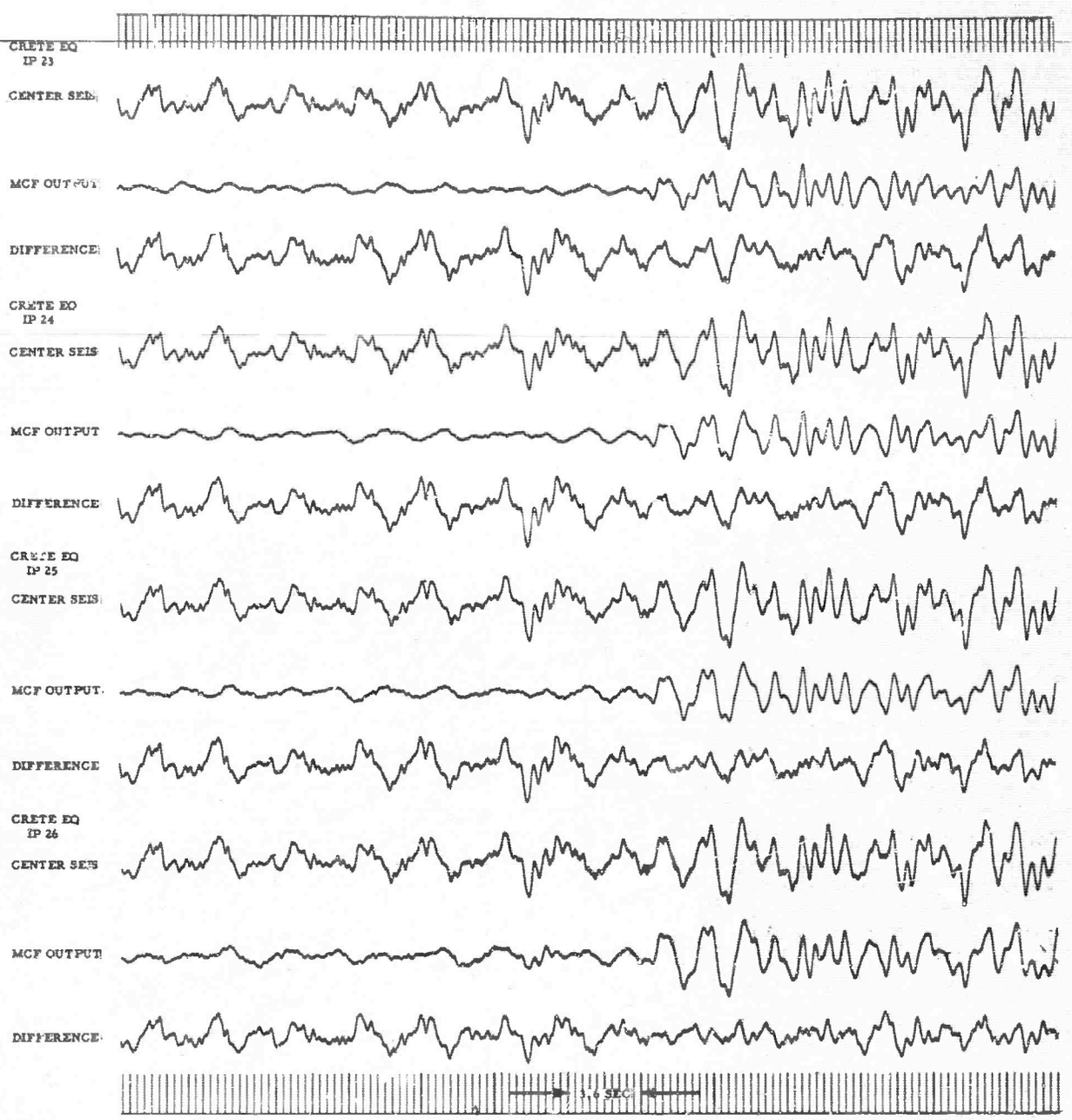

Figure IV-19. Crete Earthquake Signal as Processed by IP 23, 24, 25, and 26

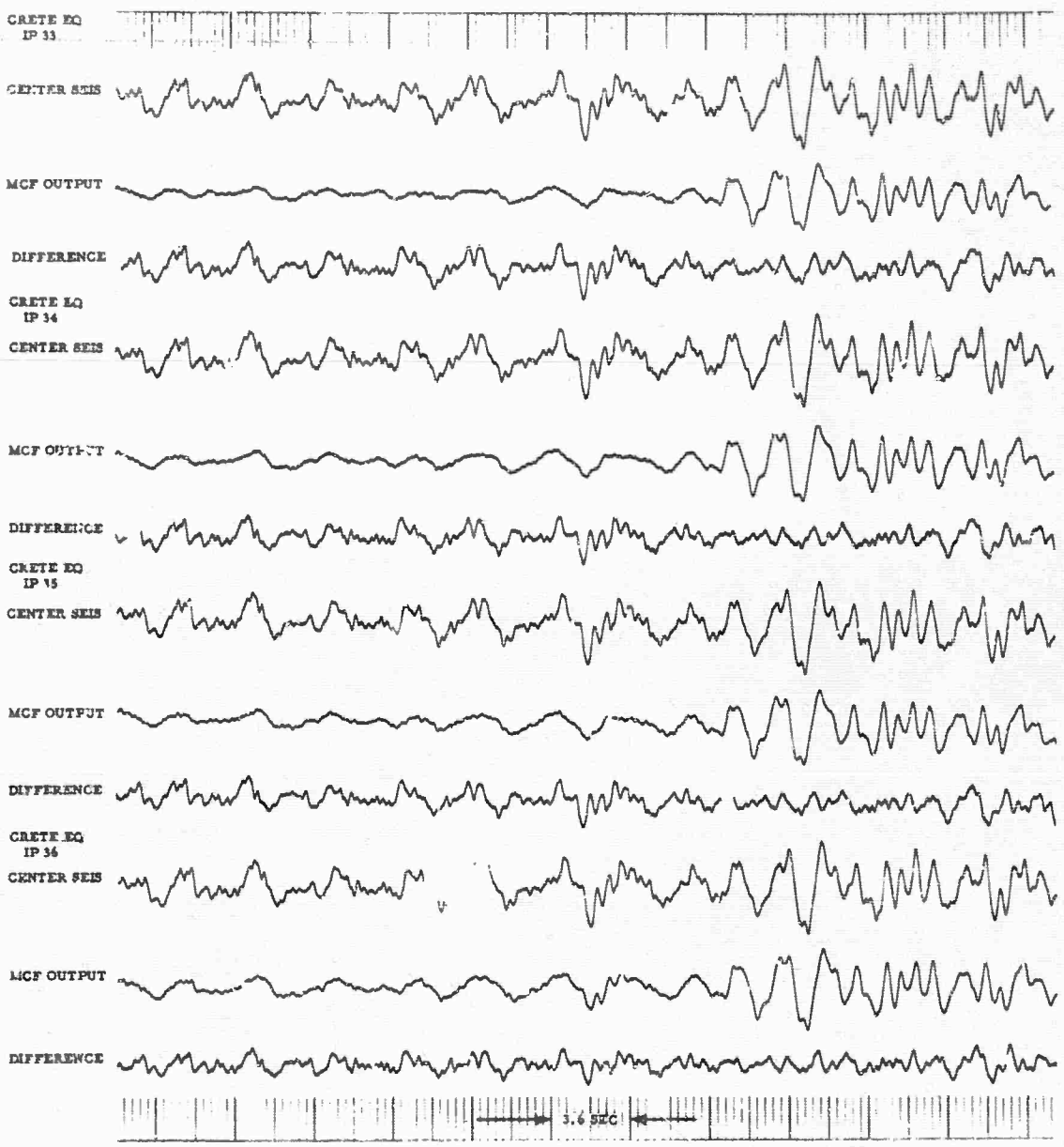

Figure IV-20. Crete Earthquake Signal as Processed by IP 33, 34, 35, and 36

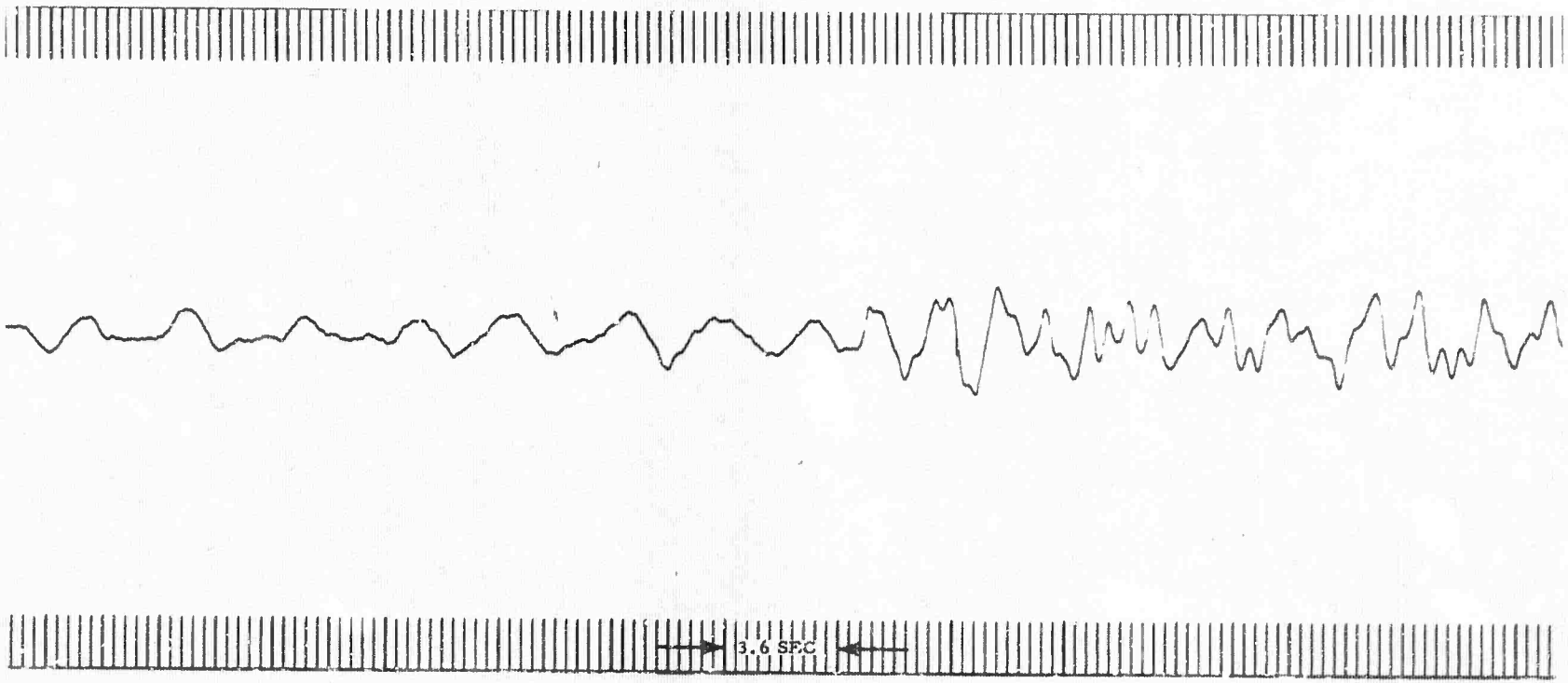

Figure IV-21. Summation of 19-Seismometer Outputs for the Crete Event

($f \approx 1/3$ cps) noise which the MCF systems reject. The superiority of multichannel filter systems for rejecting noise at CPO has been discussed previously (Section V) [5].

F. A COMMENT ON THE EFFECTIVENESS OF PARTIAL ARRAYS AT CPO

The results of this study also lead to some conclusions as to the effectiveness of the partial arrays at CPO. It previously was thought that the MCF systems IP 23, IP 24, IP 25, and IP 26 might have been affected significantly by seismometer gain inequalities below 1.0 cps (p. 35)[3]. This now is indicated to be the case only below about 0.5 cps. Some of the noise rejection below 0.5 cps shown by IP 23, IP 24 and IP 25 undoubtedly is false. Indications are that below 1.5 cps, a properly designed multichannel filter system using only the center seismometer and the outer ring would be about as effective as one designed using the entire array. However, the pre-event noise (Figures IV-19 and IV-20) clearly indicates that suppression of low-frequency ($f < 0.5$ cps) noise is somewhat a function of the number of seismometers used.

REFERENCES

1 Baldwin, R., 1964, Array Research: Semiannual Tech. Rpt. No. 1, Sect. IV; Texas Instruments, 15 May.

2 Baldwin, R., 1964, Array Research, A re-evaluation of S/N improvement for CPO using local noise: Spec. Rpt. No. 5; Texas Instruments, 15 Dec.

3 Binder, F., 1965, Array research: Semiannual Tech. Rpt. No. 3, Sect. IV, Texas Instruments, 3 Jun.

4 Baldwin, R., 1964, Array research, Multichannel filter systems for Tonto Forest Observatory: Spec. Rpt. No. 5, Pt II, Texas Instruments, 21 Sept.

5 Baldwin, R., Burg, Bryan, and Backus, 1963, Synthesis and evaluation of six multichannel filter systems based on measured correlation statistics of ambient noise at Cumberland Plateau Obervatory designed to operate on rings of seismometers: Spec. Rpt., Texas Instruments, 31 Dec.

6 Edwards, J.P., 1965, Multiple Array Processor: Final Rpt., Texas Instruments, 20 Oct.

SECTION V

A MCF SYSTEM DESIGNED FOR THE TFO CROSS ARRAY

This is a summary of work which will be published as a special report under the title "An Evaluation of the Properties of the TFO Cross Array Based on the Evaluation of a Multichannel Filter System Designed Using the Entire Cross Array."

A. DESIGN PROCEDURE AND PURPOSE

A 21-channel multichannel filter system was designed in the time domain using measured noise correlations and an infinite velocity signal model. The channels were the outputs of the 21 vertical seismometers of the cross array (Figure V-1). The signal was to be extracted at the center seismometer (Z-21). The noise correlations used were from the TFO long noise sample.[5] Statistical gain fluctuation was incorporated into the design equations.

The multichannel filter system was designed to determine the possible usefulness of multichannel filtering to enhance distant mantle P-wave signals at TFO. Designing a system which has to preserve only infinite velocity signals and then applying it to the noise used in the design should maximize the MCF system's noise-suppressing abilities.

Noise suppression obtained from the multichannel filter system discussed in this report should represent nearly the maximum noise suppression obtainable using the TFO cross array without going to directional systems. This MCF system, thus, puts a rough bound on noise suppression possible at TFO. This multichannel filter system should not be expected to pass all plane wave energy with velocities ≥ 12 km/sec. It should, however, indicate whether or not multichannel filtering, using the TFO cross array, has a chance of offering advantages.
of

B. EVALUATION OF MCF SYSTEM AND COMPARISON WITH SUMMATION

Figure V-2 shows the signal-to-noise improvement obtained by the MCF system and a summation for an infinite velocity signal input. The signal response of the MCF system is so nearly unity that the S/N improvement essentially is a measure of noise suppression only. It can be seen that the MCF system does a better job of suppressing the noise out to about 1.2 cps; from 1.2 to 2.315 cps, the summation and MCF system show about equal ability to suppress noise. Below 0.9 cps, the MCF system gives S/N improvement generally 3 to 5 db greater than a

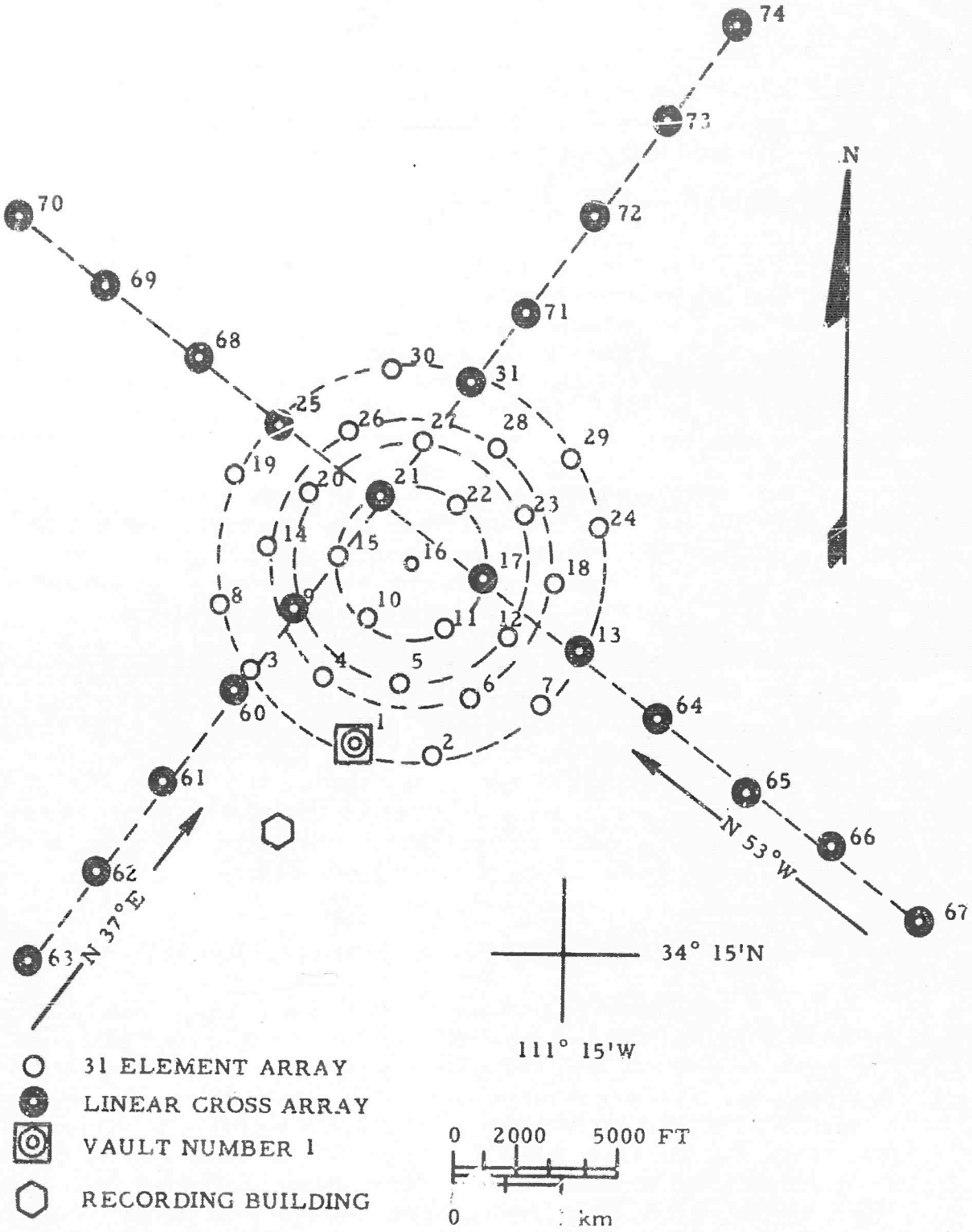

Figure V-1. Arrays at TFO

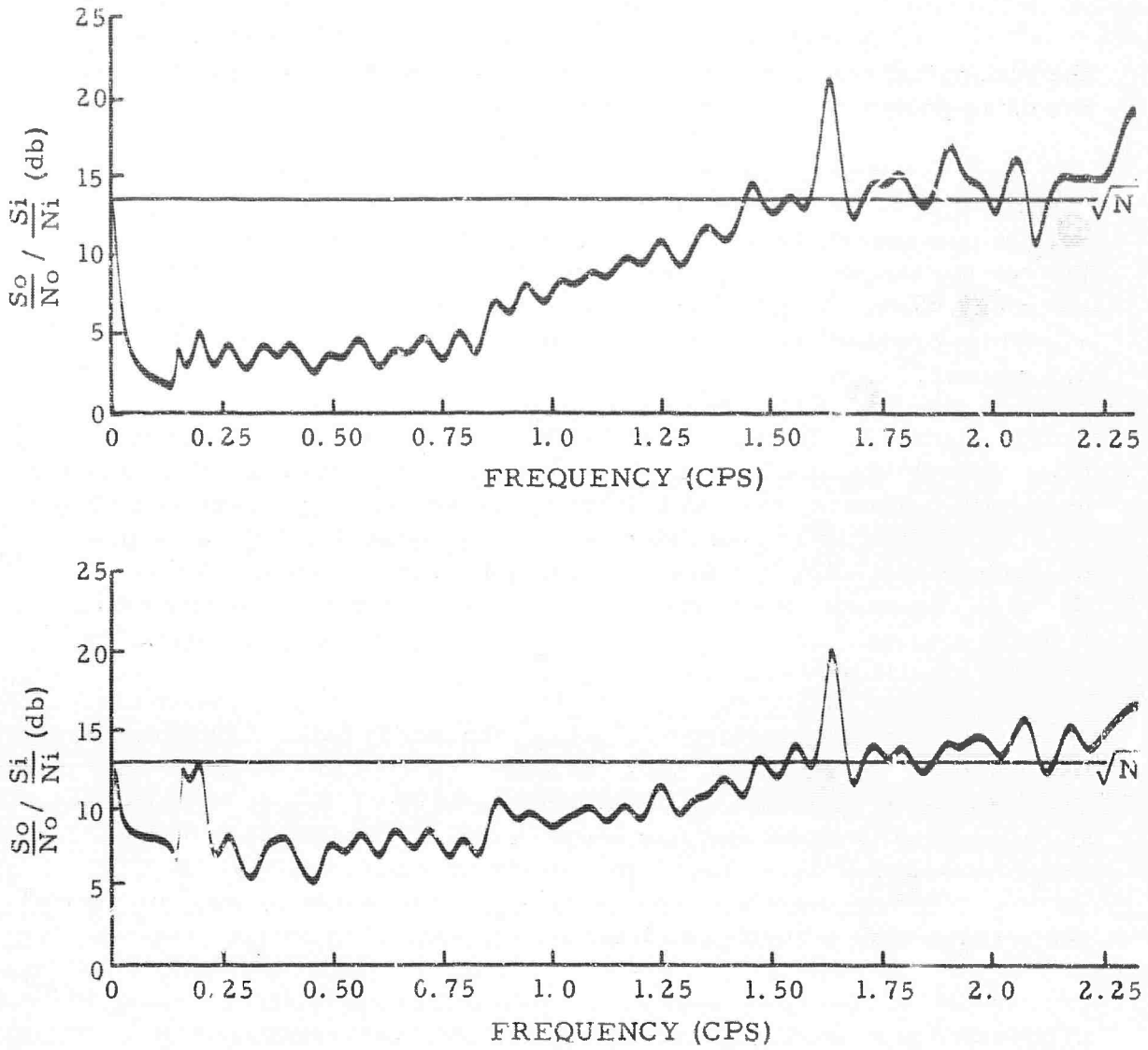

Figure V-2. Summation and Multichannel Processor S/N Improvements Relative to Single Seismometer

summation. At about 0.2 cps, the MCF system shows a signal-to-noise improvement about 8 db superior to the summation.

A study of the K-space responses of the MCF system and the summation taken with what is known about the K-space distribution of the noise power, gives a good insight into the signal-to-noise improvements.

One of the striking features of the S/N improvements (Figure V-2) is the relatively great improvement provided by the MCF system in a narrow band around 0.2 cps. Correlation analysis[5] indicates that for the frequency range of 0 to 0.386, the noise correlations (and, therefore, filter design) were influenced strongly by a Rayleigh-mode wavetrain propagating in a direction about S 60° W with a velocity of about 3.4 km/sec.

The K-space response of the MCF system at 0.25 cps (Figure V-3) indicates that the system designed to "tune out" this Rayleigh wavetrain. A plane wave with velocity 3.4 km/sec and direction S 60°W would be attenuated by more than 20 db. Even though the K-space plot probably is at a slightly higher frequency than the frequency of the Rayleigh wavetrain, the K-space response will vary continuously as a function of frequency; Figure V-3 should be very close to the system's K-space response at 0.2 cps.

The summation K-space response (Figure V-4) indicates that a summation would attenuate the above wavetrain by about 6 db. At 0.25 cps, neither the summation nor the MCF system is attenuating any high velocity ($V \geq 8$ km/sec) plane waves. The MCF system does suppress some of the energy in the velocity range of $4 \text{ km/sec} \leq V \leq 8$ km/sec. The summation, however, passes with only moderate attenuation plane waves with velocities as low as 4 km/sec.

The noise power at these low frequencies is indicated [3, 5] to be made up essentially of the Rayleigh-mode wavetrain and high-velocity noise.

Around 0.25 cps, the major difference between the summation and the MCF system is that the latter suppresses the Rayleigh-mode wavetrain (which was a part of the noise used), much more strongly than does the summation.

Since the same noise was used to design and evaluate the MCF system, it could suppress the noise power of the Rayleigh wave exceptionally well. This gave the substantially greater S/N improvement at 0.2 cps. This MCF system would not be expected to show similar S/N

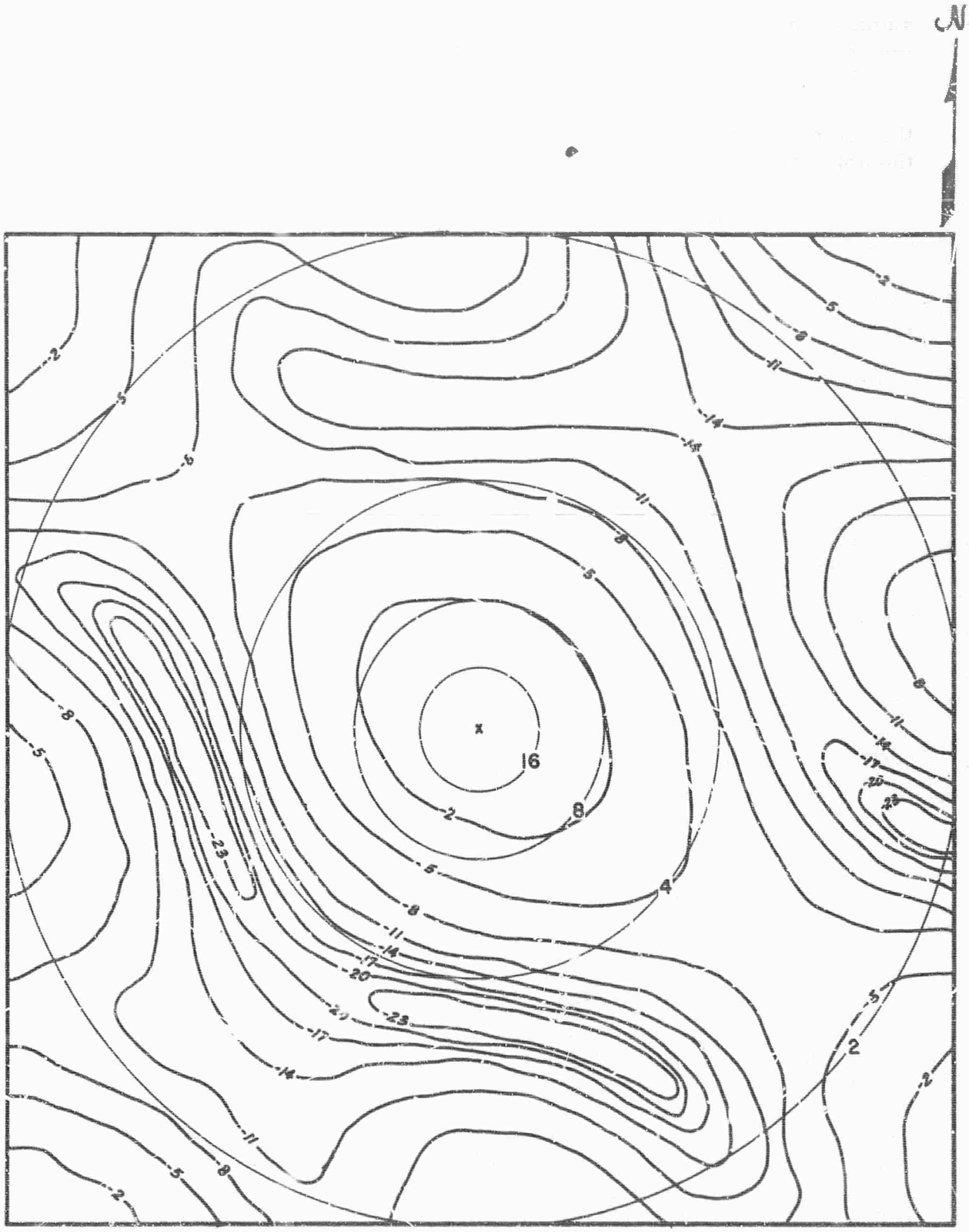

Figure V-3. K-Plane Response of Multichannel Processor at 0.25 CPS

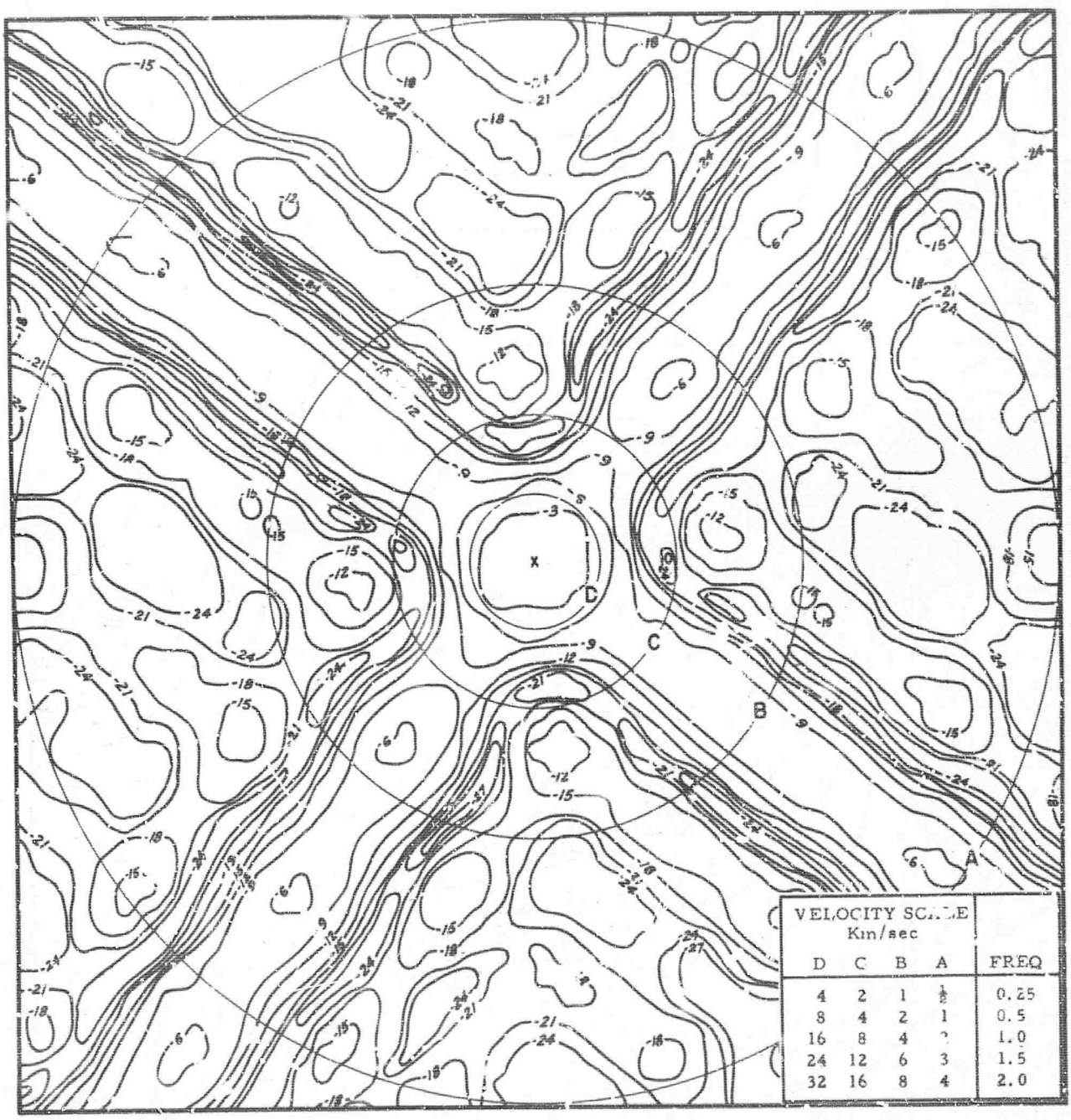

Figure V-4. K-Plane Response of Summation of 21 Seismometers (Contoured in db)

improvement at 0.2 cps on another noise sample which did not include such a directional Rayleigh wavetrain.

At 0.5 cps the MCF system is attenuating a larger portion of the high-velocity energy (Figure V-5). Since the noise at 0.5 cps is indicated to be mostly high velocity [3,5], one would expect the S/N improvement of the MCF system to be noticeably better than the summation at 0.5 cps. Figure V-2 shows that the MCF system gives a S/N improvement about 4 db superior to a summation at 0.5 cps.

The K-space plots of the MCF system and the summation at 1.0 cps (Figures V-6 and V-4) show that the MCF system is suppressing more high-velocity energy at this frequency also. Both the MCF system and the summation are suppressing more of the high-velocity energy than they were at 0.5 cps. The summation is attenuating substantially some of the high-velocity plane wave energy at 1.0 cps; little attenuation was obtained at 0.5 cps.

Previous studies of this TFO noise [3,5] indicate that the noise at 1.0 cps is predominately high velocity ($V \geq 8$ km/sec). Thus, based on the K-space responses, one would expect that the MCF system would give somewhat better S/N improvement than the summation at 1.0 cps. Also, both systems should show better S/N improvement at 1.0 cps than at 0.5 cps.

Figure V-2 shows that the actual difference at 1.0 cps is 1 to 2 db and that both systems do give better S/N improvement at 1.0 cps than at 0.5 cps.

Above 1.2 cps the S/N improvement of the MCF system and the summation are very similar. Noise analysis [5] indicates that this TFO noise sample generally is uncorrelated above 1.2 cps. What correlation there is above 1.2 cps is not space-stationary. Thus, above 1.2 cps, any attempt to explain the signal-to-noise improvement on the basis of the K-space response is not possible.

If the noise were random, the summation should give a signal-to-noise improvement of 13.2 db. However, for the noise sample used in evaluation, the signal-to-noise improvement of the summation and the MCF system (Figure V-2) in the frequency range of 1.5 to 2.3 cps generally is somewhat greater than 13.2 db. At certain frequencies, it is much better. In a narrow band around 1.6 cps, the S/N improvement of both the MCF system and the summation is about 21 db.

Whether or not one generally could expect S/N improvements

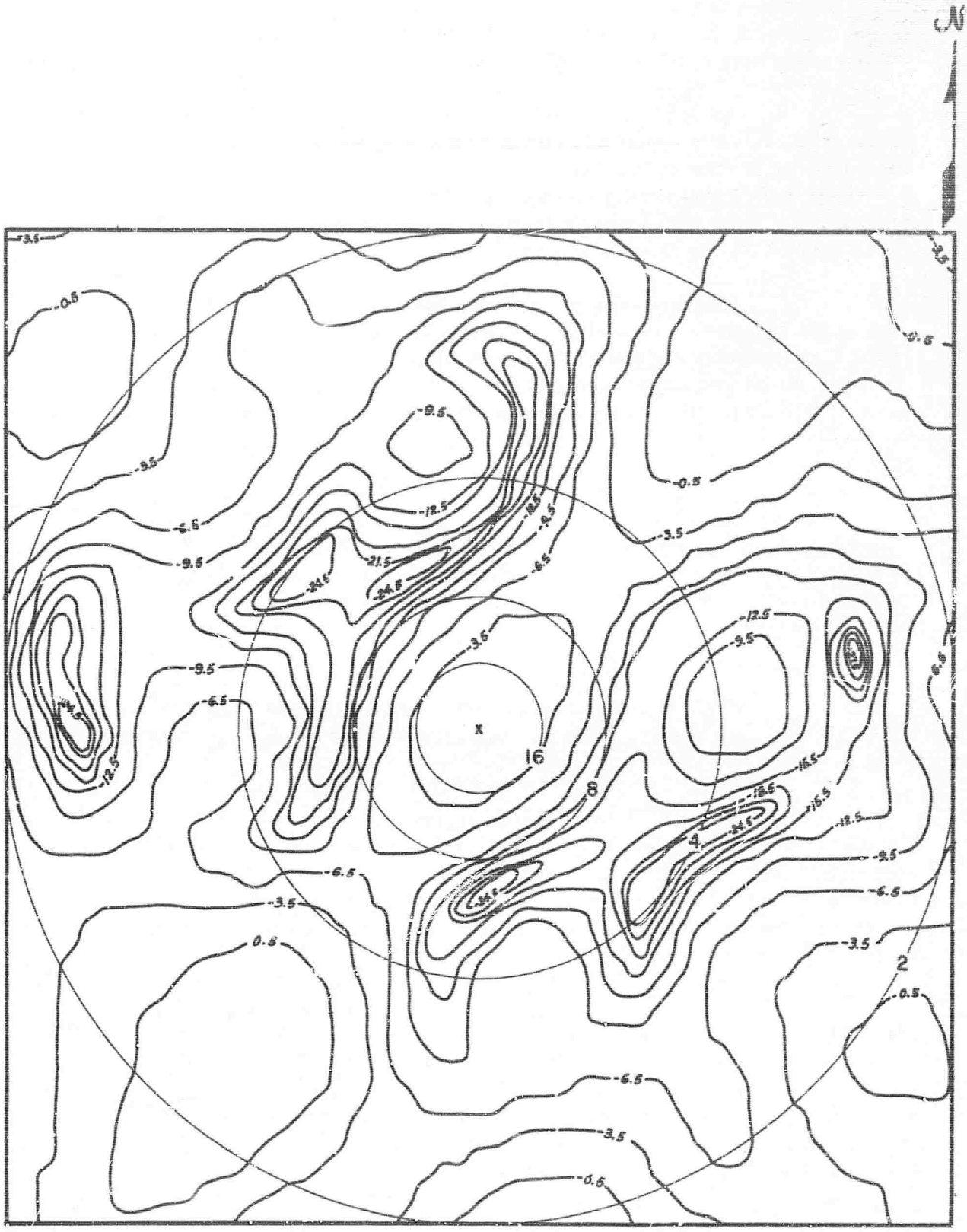

Figure V-5. K-Plane Response of Multichannel Processor at 0.50 CPS (Contoured in db)

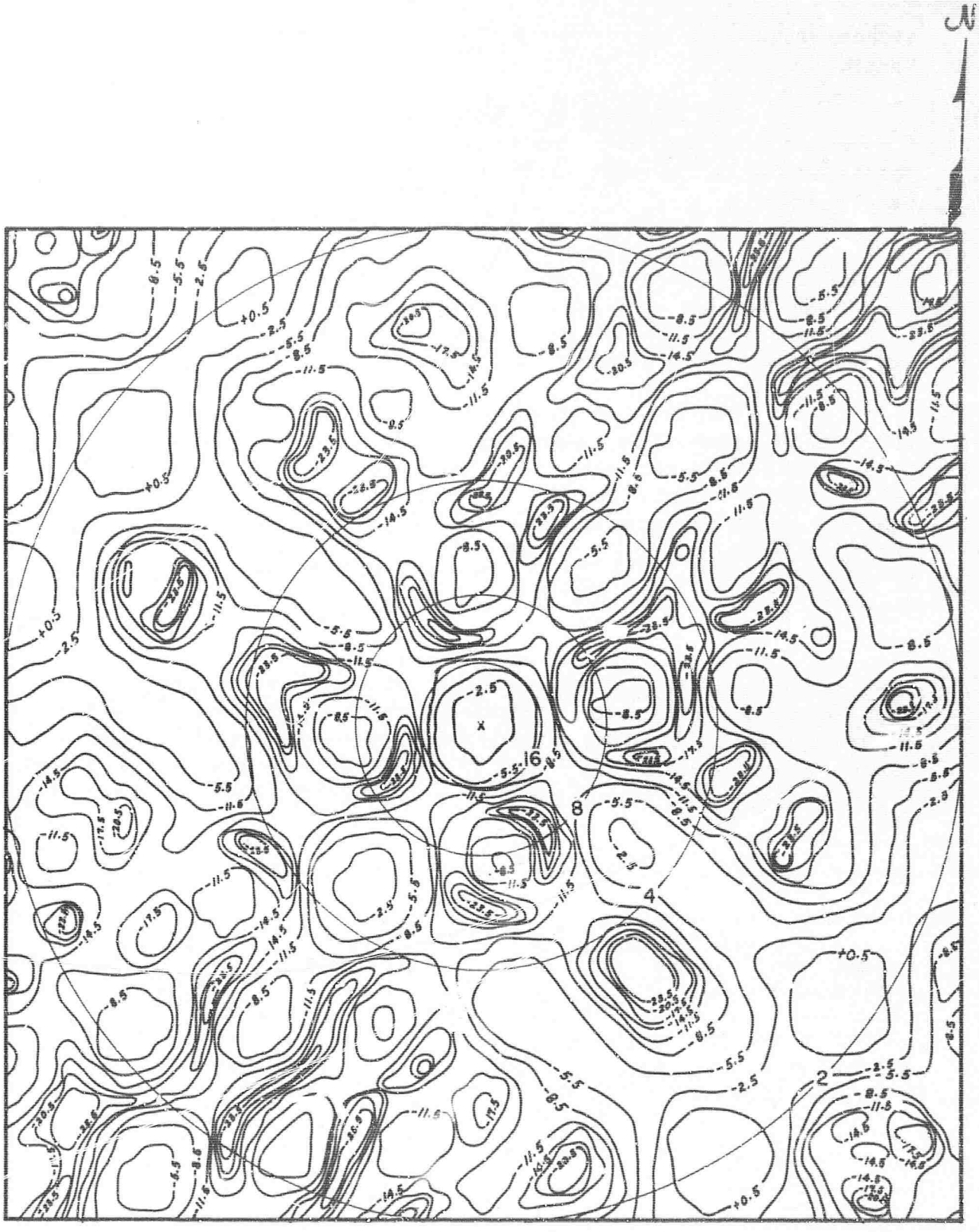

Figure V-6. K-Plane Response of Multichannel Processor at 1.00 CPS (Contoured in db)

at these frequencies in excess of the theoretical for random noise is not known.

The MCF system is better for suppressing noise below 1.2 cps and particularly superior in a band around 0.2 cps. Above 1.2 cps the MCF system and the summation suppress the TFO ambient noise about equally.

The exceptionally good results obtained by the MCF system in a narrow band around 0.2 cps is the result of suppressing some strongly directional Rayleigh-mode energy in this particular noise sample. The MCF system would not show this good S/N improvement at 0.2 cps when applied to noise which contained no such directional low-velocity energy.

The 3 to 5-db increased S/N improvement obtained from the MCF system below 1.0 cps generally is the result of better suppression of high-velocity ($V \geq 8$ km/sec) noise. The MCF system was designed using an infinite velocity signal model and, therefore, tried to eliminate any coherent energy of lower velocity. The MCF system was able to cut more sharply in K-space near $V = \infty$ than was the summation. This effect is significant at low frequencies and resulted in greater S/N improvement for the MCF system as compared with the summation.

In the course of this study, several tests of the stability of the summation and the multichannel filter system to perturbation of seismometer gains were made. These tests indicate that both are quite stable when applied to noise for which the seismometer outputs have been perturbed moderately (25 percent). The details of these results are omitted here, but will be published in the forthcoming special report covering this study.

C. A DISCUSSION OF ISOTROPIC PROCESSING AT TFO

Because of the K-space distribution of the TFO noise (largely high velocity with some surface-wave energy), isotropic processing is not very effective. Any processor which must maintain a good signal pass response for energy propagating with a velocity of 12 to 24 km/sec cannot suppress the high-velocity noise. An isotropic processor could be expected to suppress only the surface-wave energy indicated to be present in at least part of the TFO noise and the random noise.

Except in a narrow band around 0.2 cps, the better low-frequency ($f < 1.0$ cps) S/N improvement obtained from the MCF system, as opposed to the summation, resulted from rejection of high-velocity noise. This was possible because the multichannel filter system was "directional" (i.e., an infinite velocity signal model). Such noise rejection would not be possible with any system which maintained a suitable signal response in the range of $V \geq 12$ km/sec.

Isotropic multichannel filter processing at TFO would be effected little by the array configuration. Any reasonable configuration could be used to suppress the surface-wave energy. The suppression of the random noise is a function of the number of seismometers, not their location.

On the basis of this study and the various TFO noise studies referred to, it is implied that the effectiveness of isotropic multichannel filtering at TFO should not be expected to be affected much by array geometry. Designing isotropic multichannel filter systems for partial arrays at TFO would give little useful information.

D. A DISCUSSION OF DIRECTIONAL MULTICHANNEL FILTERING AT TFO

The multichannel filter system discussed in this report is a "directional" system (i.e., the system was designed to pass an infinite velocity signal only). This "directional" system was superior to the summation at frequencies below about 1.2 cps. At these lower frequencies the multichannel filter system was superior in that it suppressed a portion of the high-velocity noise better than the summation and it did a better job of suppressing some surface-mode energy present in the noise sample processed. Below about 1.0 cps, the MCF system delivers about 3-to 5-db better suppression of the mantle P-wave noise than the summation.

TFO noise analysis [4, 5, 6] indicates that the low-frequency ambient noise is mostly mantle P-wave noise. If this noise can be roughly modeled as a disc of uniform power in K-space with a minimum velocity of about 8 km/sec, one would expect any directional MCF system to suppress the mantle P-wave noise at least as well as a system designed using an infinite velocity signal model. If a multichannel filter system were designed to pass a directional signal not in the center (in K-space) of this high-velocity noise field, it might be considerably more effective than the system designed using an infinite velocity signal model. If the directional signal model were nearer the edge of the noise power disc in K-space, the signal pass region of the processor could lie partially outside the noise field at frequencies of interest. Also, such a directional multichannel filter should develop an asymmetric K-plane response which would further attenuate the high-velocity

noise.

Similarly, a beam-steering would be expected to suppress the mantle P-wave noise as well as or better than the straight summation, but would, of course, maintain a symmetric K-space response around the point of unit response.

Any low-velocity energy could be suppressed effectively by a properly designed directional multichannel filter system. The effectiveness of the time-shifted sum for suppressing surface-mode energy would depend upon the K-space response of the particular beam-steering, but would be expected to be inferior to a MCF system.

Thus, for directional processing using the cross array at TFO, one would expect that

- Below about 1.0 cps, a properly designed multichannel filter system should be at least 3 to 5 db better (in S/N improvement) than a beam-steering.
- When applied to noise containing coherent low-velocity energy (surface-mode energy), the multichannel filter system might give much greater S/N improvement than a beam-steering. A study of directional multichannel filtering using the TFO cross array is now in progress.

REFERENCES

(1) Baldwin, R., 1964, Array research MCF systems for Tonto Forest Observatory: Spec. Rpt. No. 3, Texas Instruments, 21 Sept.

(2) Baldwin, R., 1964, Multichannel filter systems for Tonto Forest Observatory: Spec. Rpt. No. 5, Pt. 1, 2, Texas Instruments, 21 Sept.

(3) Baldwin, R., 1964, Array research: Semiannual Tech. Rpt. No. 2, Sect. II, Texas Instruments, 15 Nov.

(4) Burg, J. and T. Harley, 1964, Computer analysis of Tonto Forest Seismological Observatory noise: Texas Instruments, 10 Feb.

(5) Rodgers, S. and J. Burg, 1965, Array research: Semiannual Tech. Rpt. No. 3, Sect. V, VI, Texas Instruments, 3 Jun.

(6) Wherry, M., 1965, Noise analysis for Tonto Forest Seismological Observatory: Texas Instruments, 16 Aug.

SECTION VI

A SUMMARY OF SIGNAL DETECTION PROCESSING RESULTS

The assumptions, derivations of equations, and an illustration of the method of signal detection by probabilistic processing were presented in Special Report No. 8. The illustration used artificially generated data to satisfy the assumptions. The expected results were determined theoretically and compared favorably with the actual processor output.

The basic assumption is that noise and signal data are independent multivariate normal with zero means and known covariance matrices given by Ω_1 and Ω_2, respectively. The elements of both covariance matrices were generated by an existing program from the following models of signal and noise:

- The 3-dimensional noise spectrum in (f, k_x, k_y) space is assummed to be zero, except for points corresponding to velocities between 3 km/sec and 4 km/sec. The spectrum is uniform for values of f, k_x and k_y in the velocity interval.
- The 3-dimensional signal spectrum is assumed to be zero, except for values of f, k_x and k_y corresponding to velocities greater than 8 km/sec and constant in the high-velocity region. The zero-lag autocorrelation values were set equal and the spectra remained white in frequency for both signal and noise in the previous report.

This section will contain some graphical information related to Special Report No. 8 and some results showing the theoretical effect of varying the signal-to-noise ratio. The results of applying the quadratic processor to three sections of 10-channel CDO data containing teleseismic events will then be discussed.

A. GRAPHS RELATED TO SPECIAL REPORT NO 8

The simple models (4-channel, annular-ring, 3 to 4 km/sec noise and 8-km/sec solid disk signal) were used to generate correlation data and to produce from this data the matrix constants of the quadratic form. The distributions of the quadratic processor, under the two hypotheses of I = noise and II = signal + noise, were shown as

$$P_I(x) \doteq \delta_I \, x^2_{\nu_I}$$

$$P_{II}(x) \doteq \delta_{II} \, x^2_{\nu_{II}} \qquad (6.1)$$

where

$$\delta = \sigma^2/2\mu$$

$$\nu = 2\mu^2/\sigma^2 \qquad (6.2)$$

and the values μ, σ^2 are the mean and variance of the processor output P(x), and x^2_ν is a chi-squared random variable with ν degrees of freedom. Plots of the cummulative distributions of Equation (6.1) are given in Figure VI-1 for 10 and 25 lags. The vertical lines at C(10) = 25.3 and C(25) = 67.5 are the equi-probability critical values.

B. EFFECT OF VARYING SIGNAL-TO-NOISE RATIO

There are actually two questions involving signal-to-noise ratios:

1. How will P(x) designed for S/N = 1 behave for data

   $x \in \Omega_2^* = N + aS$?

2. How does the separation of I and II(a) depend on a;

   here P(x) is dependent on a.

Considering the first problem: since

$$P(x) = y^T(\Lambda - I)y$$

where $x = My$ and $x \in \Omega_2^*(a) = N + aS$, then y has a multivariate normal distribution with mean zero and covariance

$$M^{-1} \Omega_2^* (M^{-1})^T = M^{-1} (a \left[S + N\right] + (1 - a)N) (M^{-1})^T$$

$$= aI + (1 - a) \Lambda^{-1} = F$$

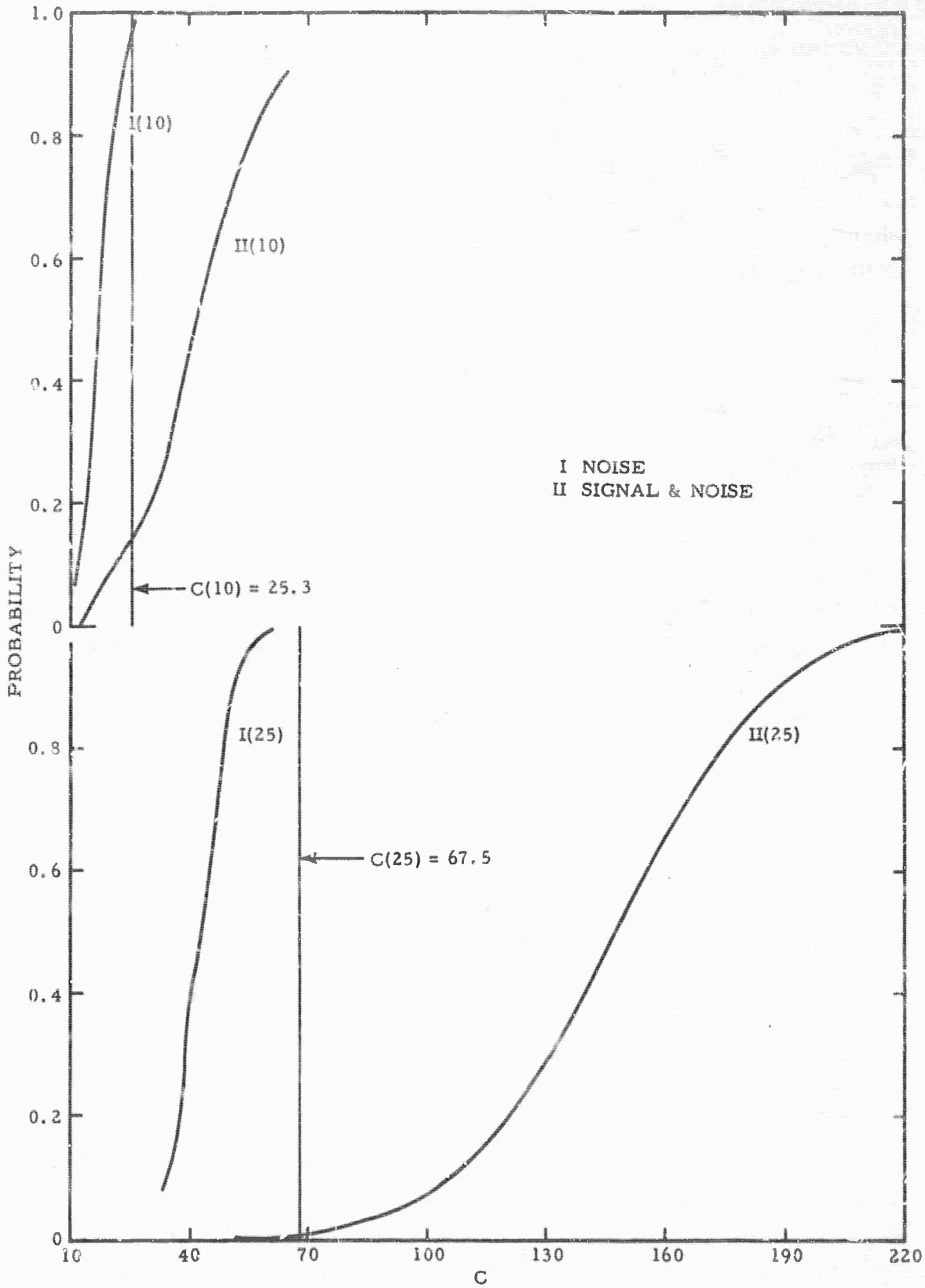

Figure VI-1. Cummulative Distribution Plot of 4-Channel 10 and 25 Lags for Noise (I) and Signal Plus Noise (II)

Now, transform y to z by $y = F^{1/2} z$ so that

$$\Omega_z = E\, z\, z^T = F^{-1/2}\, F\, F^{-1/2} = I$$

and

$$P(y) = z^T (F^{1/2} \Lambda F^{1/2} - F) z$$

Thus, P(y) has the same distribution as

$$\sum_{i=1}^{p} \eta_i x_1^2 (i)$$

with

$$\eta_i = \left[a + (1 - a)\, \lambda_i'\right](\lambda_i - 1)$$

where λ_i is the diagonal elements of Λ and $\lambda_i' = 1/\lambda_i$. Thus, the mean and variance when $x \sim \Omega_2^* = N + aS$ are

$$\mu^* = a\,\mu_{II} + (1 - a)\,\mu_I$$

and

$$\sigma^{2*} = a^2\, \sigma_{II}^2 + (1 - a)\, \sigma_I^2 + 4a(1 - a)\,(\mu_{II} - \mu_I)$$

The behavior of the quadratic processor when applied to data of varying S/N ratio can be described completely in terms of the behavior on noise alone and signal-plus-noise with the ratio 1.

The second question does not have as complete an answer. Suppose we adjust the S/N ratio, thereby obtaining $\Omega_2^* = N + aS$, and consider this a new design problem. It is desirable to determine the behavior of the processor for this new problem in terms of the results of the old problem. Just as before, if λ^* satisfies

$$\left| \Omega_1^{-1} - \lambda^* \Omega_2^{*-1} \right| = 0$$

Then, the behavior of the quadratic processor is specified completely by the quantities

$$\Sigma\ \lambda_i^*,\ \Sigma\ \lambda_i^{*2} \quad \text{when } x \in \text{II}(a)$$

and

$$\Sigma\ \lambda_i^{*-1},\ \Sigma\ \lambda_i^{*-2} \quad \text{when } x \in \text{I}$$

Now, $|\Omega_1^{-1} - \lambda^* \Omega_2^{*-1}| = 0$ is the same equation in λ^* as $|\Omega_2^* - \lambda^* \Omega_1| = 0$ which can be written

$$| N + aS - \lambda^* N | = 0 \quad .$$

$$| SN^{-1} - (\lambda^* - 1) / aI | = 0$$

so that

$$\lambda_i - 1 = (\lambda_i^* - 1)/a$$

and thus

$$\mu^* = a\,\mu_{II}$$

$$\sigma^{2*} = a^2\,\sigma^2_{II}$$

so that the behavior of P(x) as function of a can be described when $x \in$ II(a). The behavior of P(x), when $x \in$ I, has not been solved as a simple function of a.

The curves drawn in Figure VI-2 illustrate the above equations for the lower (25 lags) example of Figure VI-1. The curves in the upper portion of Figure VI-2 show the behavior of P(x) when $x \in aS + N$ for a = 1/4, 1/2, 3/4, and the processor P(x) is designed for a = 1. The lower portion of Figure VI-2 shows the behavior of P(x) for a = 1/4, 1/2, 3/4 when the processor is designed for these values.

C. PROCESSING OF ACTUAL DATA

Three sections of 10-channel CPO data were selected containing weak teleseismic signals with the following descriptions:

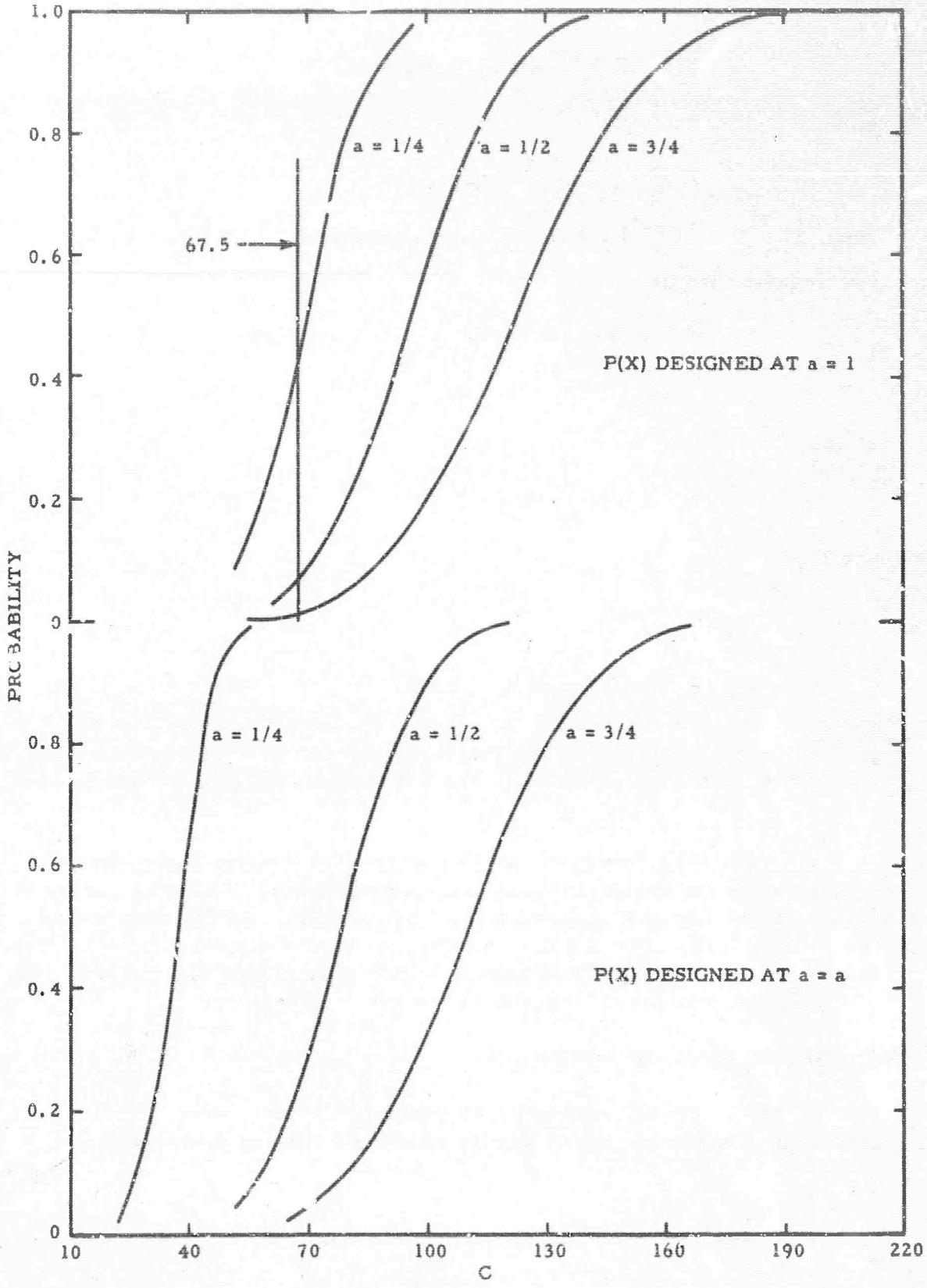

Figure VI-2. Theoretical Behavior of 25-Lag Model at Various S/N Ratios

Figure	Calculated Arrival Time	Origin Time	Latitude	Longitude	Depth (km)	Magnitude	Δ
4	16:48:49.5	16:29:19:0	4.3°N	96.3°E	33	5.7	140°
5	16:42:43.9	16:37:46.9	30.1°N	111.5°W	33	---	22°
6	00:21:56.9	01:14:15.4	76.8°N	94.7°W	33	4.5	41°

Figure VI-3 shows the location of the seismometers for the 10 channels of data used as input to the quadratic processor. The noise model was assumed to be 3 to 4 km/sec annular ring and an 8-km/sec solid disk signal model was used. Ten percent white noise was added to the noise correlation matrix.

The output of the quadratic processor for the three sections of data is presented in Figures VI-4, VI-5 and VI-6. The traces shown are the quadratic process, Wiener square and sum (over 8 points), and the actual seismometer traces. The number of lags used for both the quadratic processor and the Wiener output was 17 with no smoothing for the quadratic processor.

The theoretical critical level is drawn in for the quadratic detection processor on all three sections (Figures VI-4, VI-5 and VI-6). An error apparently was introduced at some stage of the calculation of the critical level for the second section. The other two critical levels are believed to be correct and typical of what might be expected in additional noise samples. Two of the teleseismic events did not produce a detector output significantly greater than the noise output. The third section of data shows a significant detector output for the teleseism. The signals later in this section (Figure VI-6) are the arriving phases of a quarry blast which also produced a significant value of the detector output.

The results for the detection processor show sufficient promise to continue this study using the full 19-channel CPO array with ring data and actual-measured CPO noise correlations.

The theoretical cummulative probability curves for the models of signal and noise used are shown in Figure VI-7. Some cummulative points for the actual data were determined from the first 500 points of the first section and were plotted in Figure VI-7 for comparison.

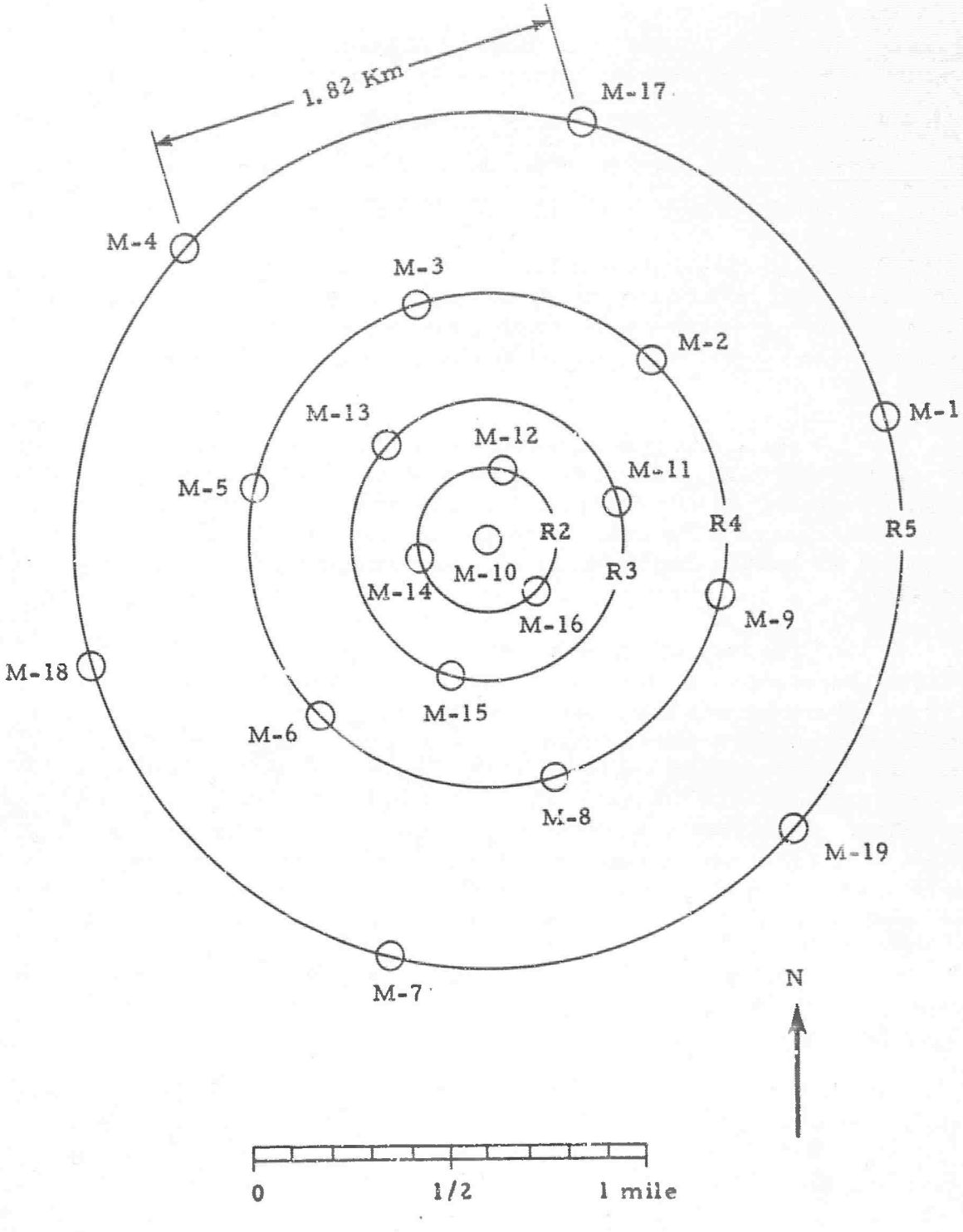

Figure VI-3. CPO 19-Element Array

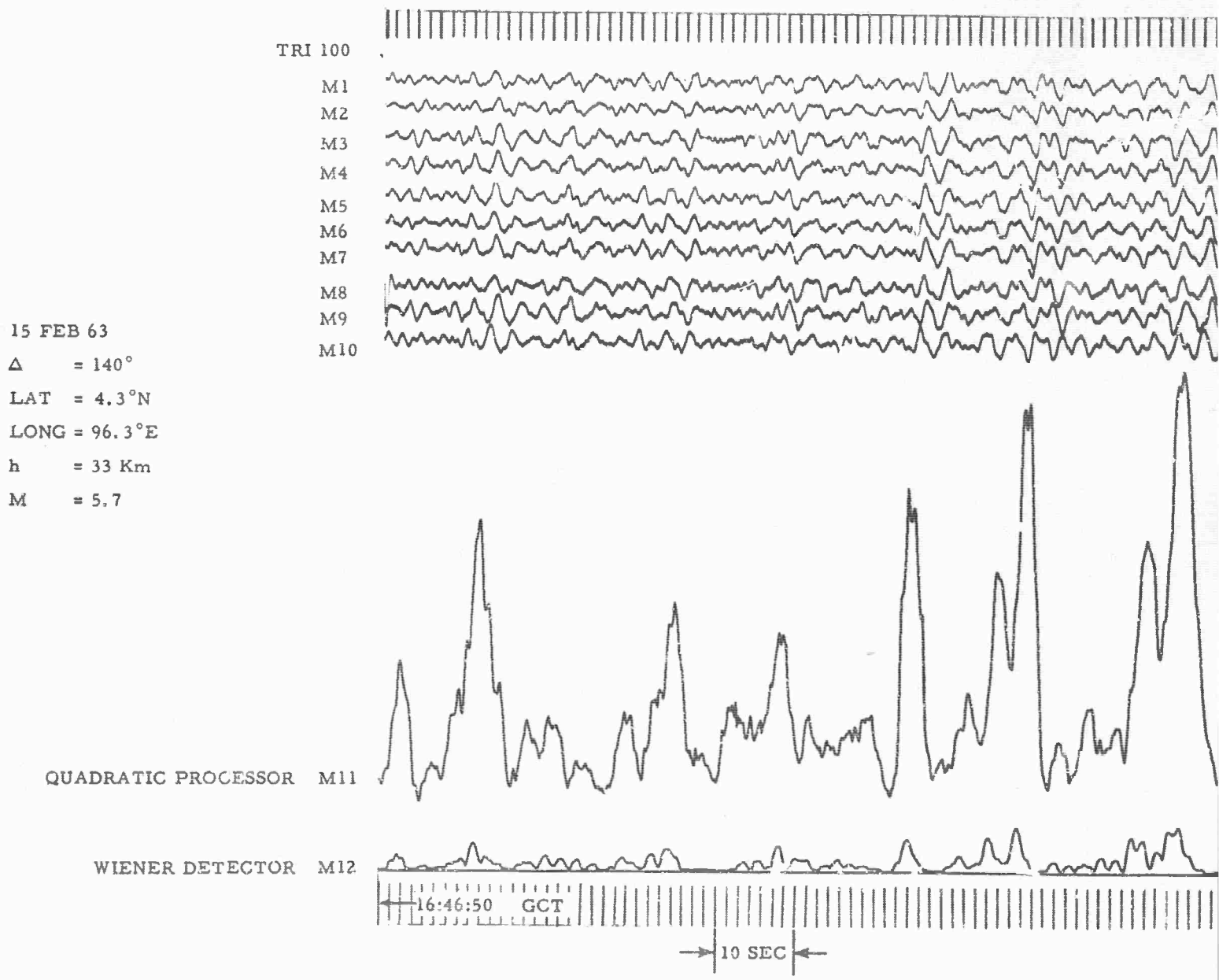
TRI 100
M1
M2
M3
M4
M5
M6
M7
M8
M9
M10
15 FEB 63
Δ = 140°
LAT = 4.3°N
LONG = 96.3°E
h = 33 Km
M = 5.7
QUADRATIC PROCESSOR M11
WIENER DETECTOR M12
16:46:50 GCT
10 SEC

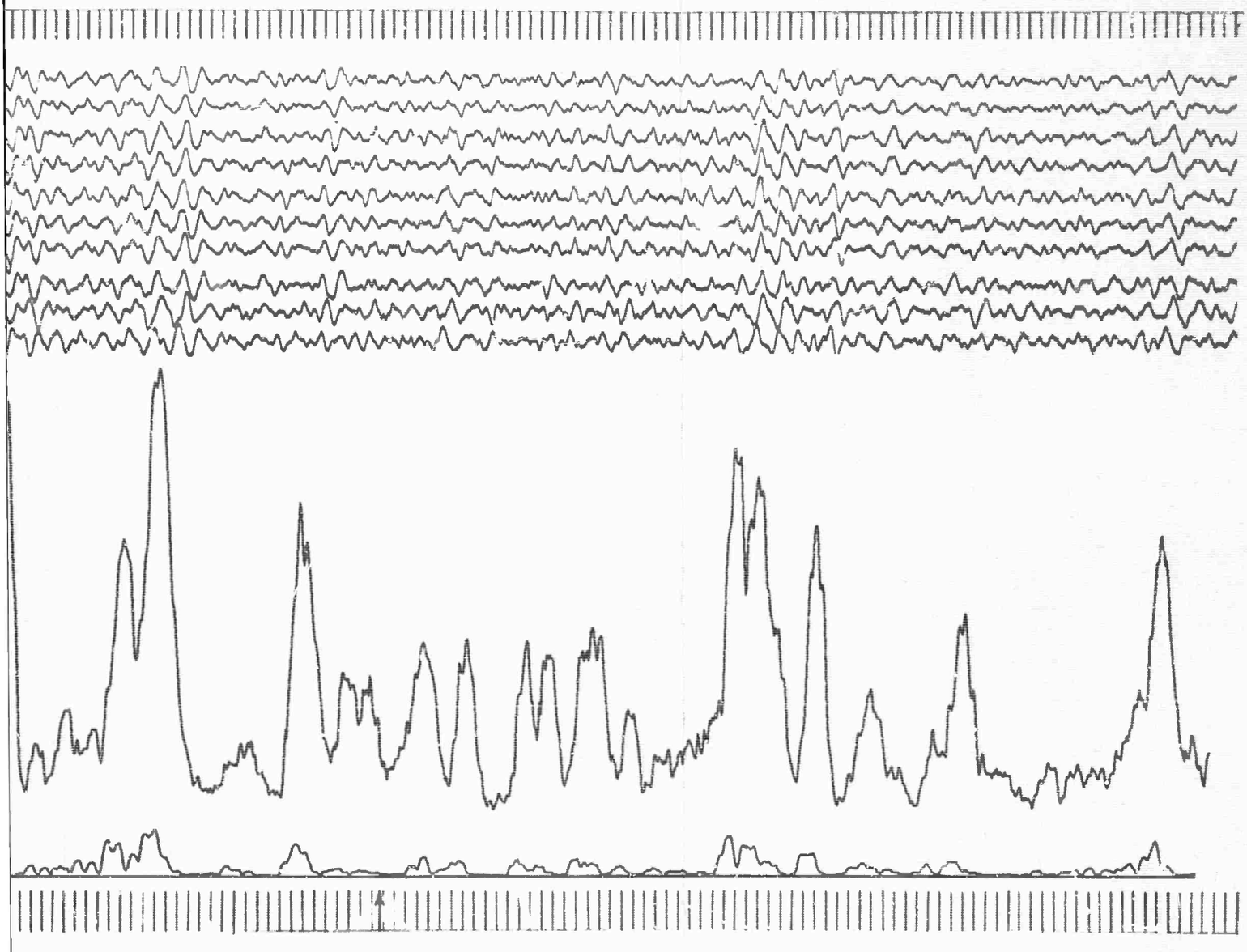

Figure VI-4. Quadratic Processor, Wiener Trace and Raw Data for Section 1 of 10-Channel CPO Data

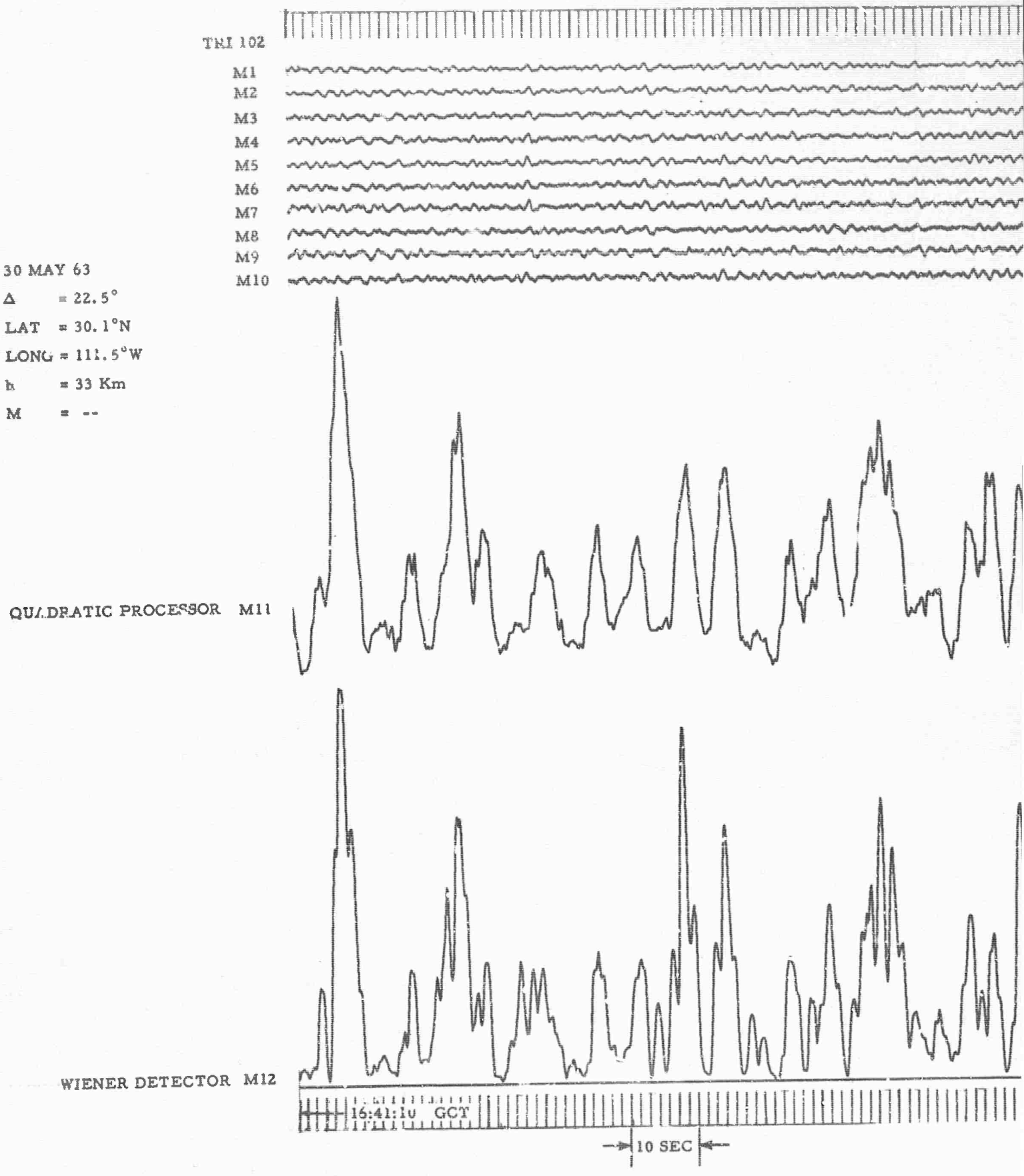
TRI 102
M1
M2
M3
M4
M5
M6
M7
M8
M9
M10
30 MAY 63
Δ = 22.5°
LAT = 30.1°N
LONG = 111.5°W
h = 33 Km
M = --
QUADRATIC PROCESSOR M11
WIENER DETECTOR M12
16:41:10 GCT
10 SEC

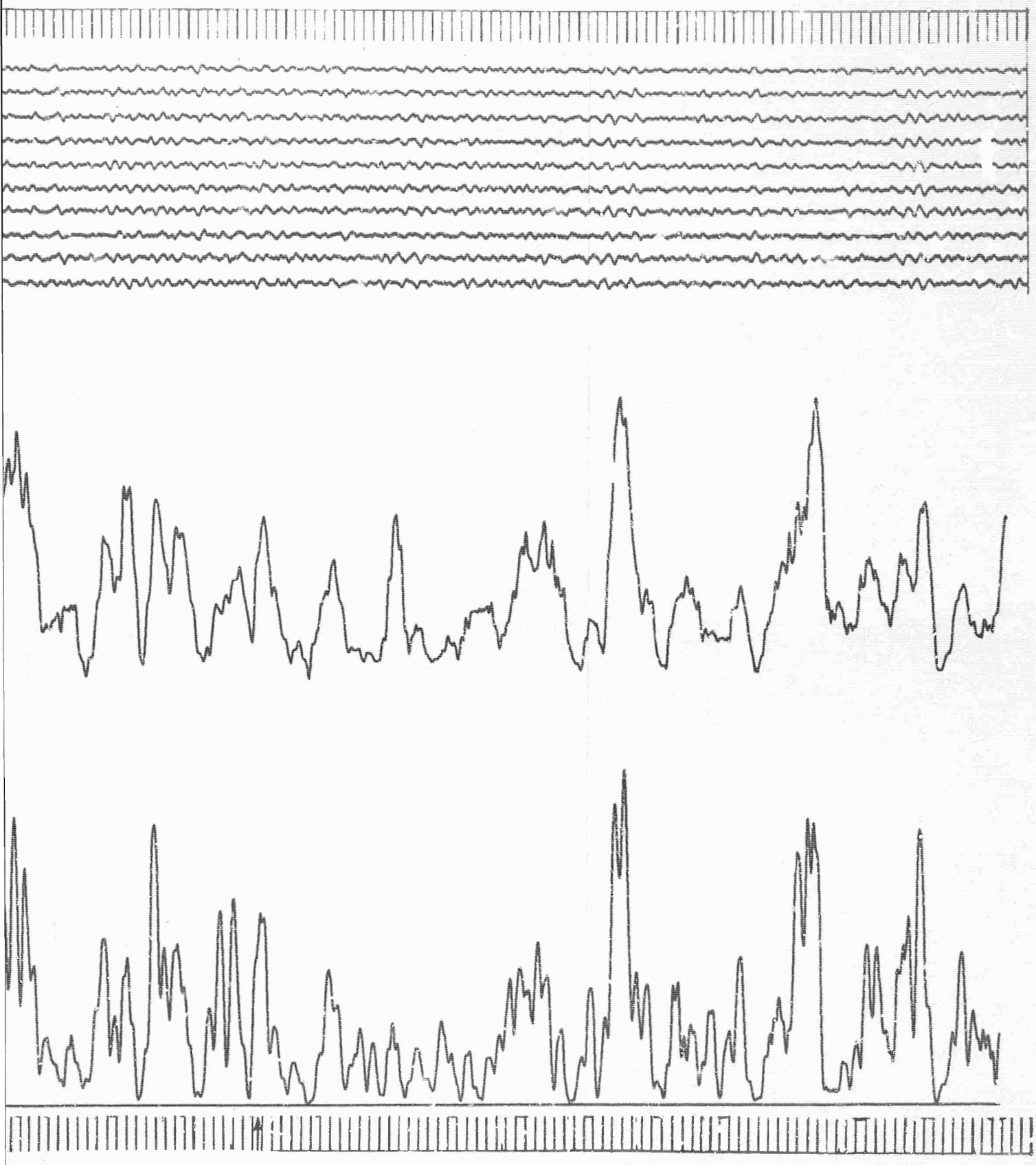

Figure VI-5. Quadratic Processor, Wiener Trace and Raw Data for Section 2 of 10-Channel CPO Data

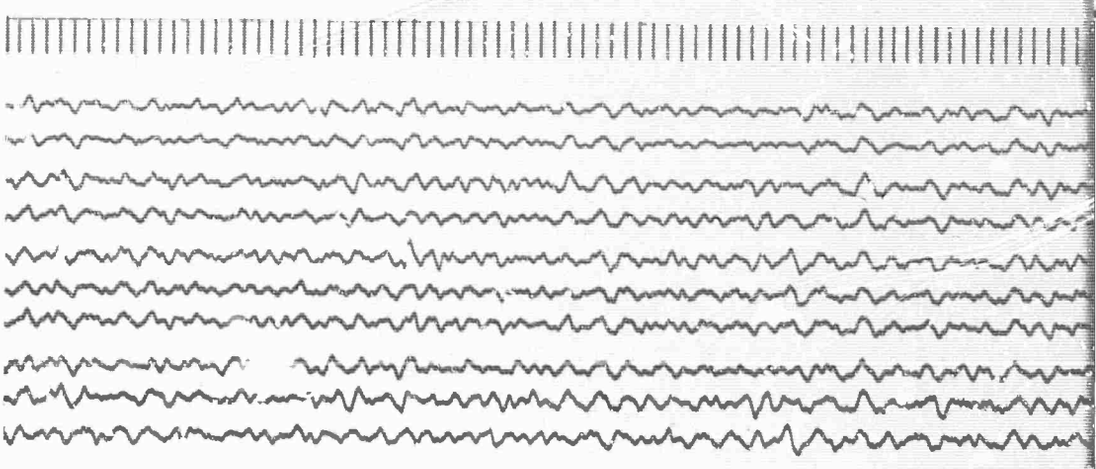

8 MARCH 63

Δ = 41°

LAT = 76.8°N

LONG = 94.7°W

h = 33 Km

M = 4.5

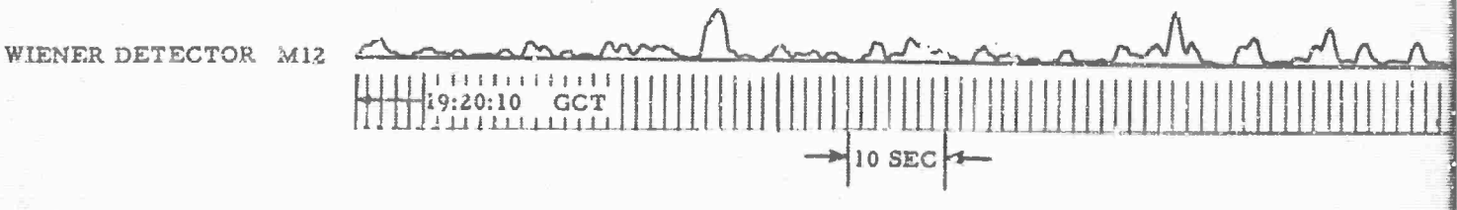

1

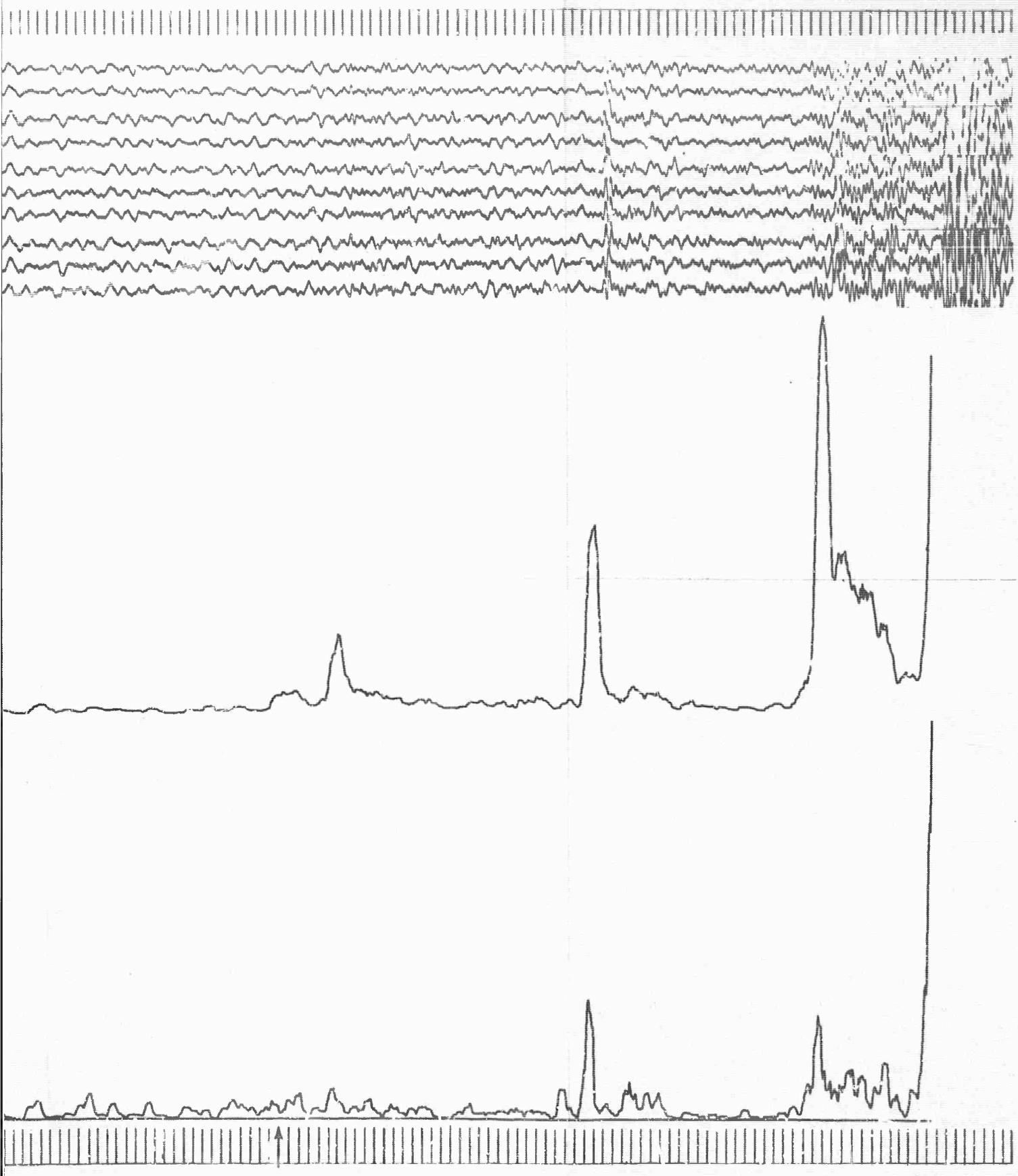

Figure VI-6. Quadratic Processor, Wiener Trace and Raw Data for Section 3 of 10-Channel CPO Data

2

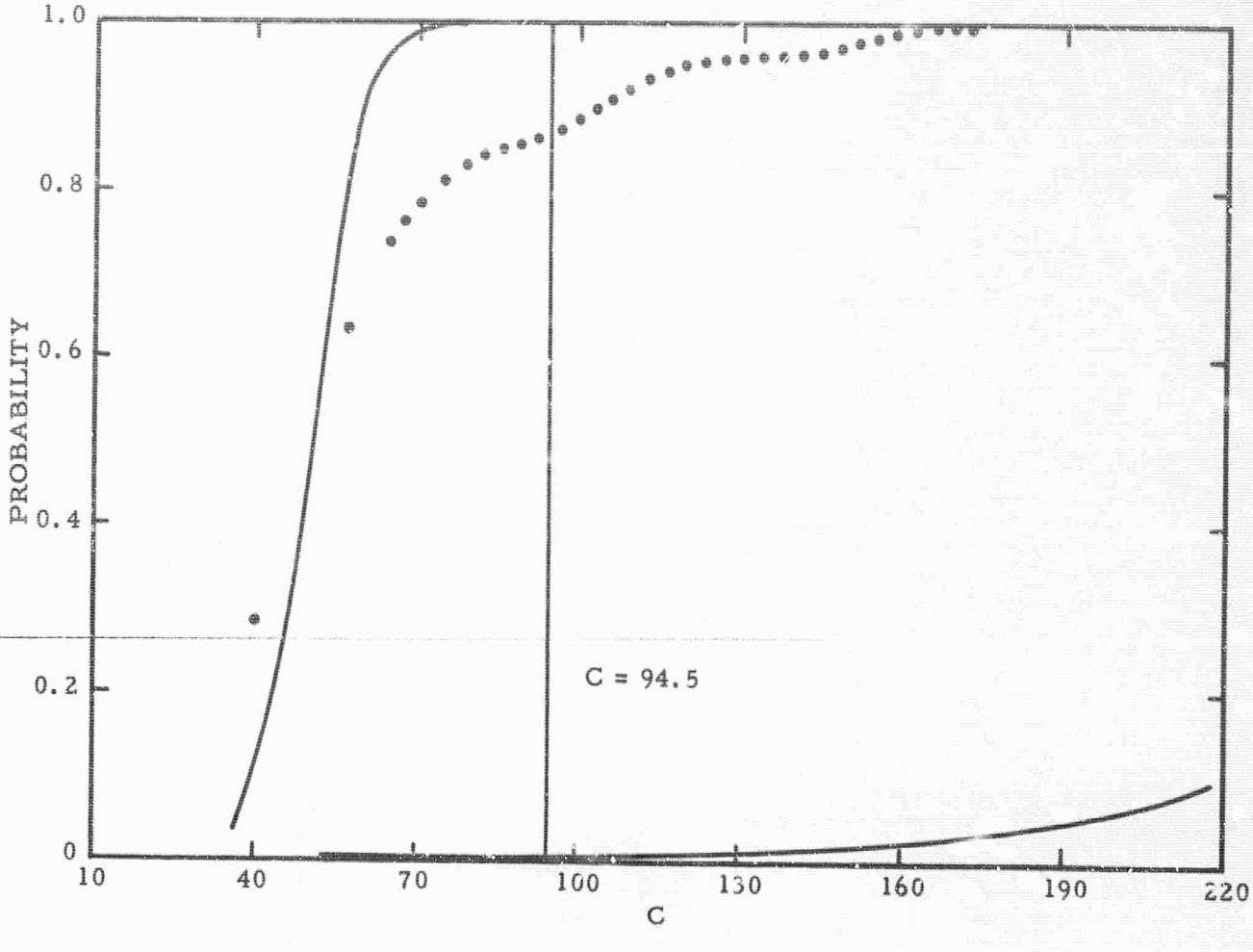

Figure VI-7. Theoretical and Actual Cummulative Probability Curves for the 10-Channel, 17-Lag CPO Data

SECTION VII

LARGE APERTURE SEISMIC ARRAY DETECTION FILTERS

A. SUMMARY

Several sets of multichannel filters were developed in order to investigate the nuclear detection capabilities of the 21-element* Large Aperture Seismic Array (LASA) located in Montana. Each filter was developed to pass a signal from a known or possible nuclear test site and to reject noise events from a known area of earthquake activity. The important factor of this technique of processing the LASA is that the signal area is allowed to be monitored with a single multichannel filter, while many beam steers would be required to monitor the same area.

In developing the LASA multichannel filters, two noise models and three signal models were chosen. The first of the noise models included the portion of world in $\vec{k}$-space within a velocity greater than or equal to 12 km/sec, while the second noise model encompassed the major earthquake regions of the earth. The signal models chosen were Russia, China and Novaya Zemlya. These models encompassed some of the possible or known nuclear test sites. Four of the multichannel filters designed which used various combinations of the signal and noise models are presented in this section.

The results of this study indicated that it is possible to monitor, within a 0- to 6-db passband, a reasonable signal area with a single filter while retaining the ability to reject 3 to 30 db or more known earthquake areas if some trade-off in random noise response is allowed. This implies that any suspected nuclear test area may be monitored with one multichannel filter instead of many beam steers. Such a system designed on this basis not only would simplify considerably the detection problem as related to LASA, but also would result in a significant monetary savings when compared with the beam-steer technique.

Based on the results of this approach to monitoring specific geographic areas, additional research for improved filter performance is warranted. Specific items which should be investigated are the following:

* Each subarray was considered to be represented as a single output channel.

- Use of additional sensors to improve the wide $\vec{k}$-band filter performance. This can be accomplished in one of two ways; first, by considering the subarrays as more than one element (particularly those located close to the center of the array) or, second, by adding additional subarrays to the LASA. This latter approach has been suggested previously on the basis of an array configuration study.*
- Determination of the optimum signal-to-noise ratio and the random (in $\vec{k}$-space) noise level to be used in filter development.
- Development of more refined theoretical coherent noise and signal models which would insure more accurate $\vec{k}$-space area coverage.
- Research to establish a more definite relation between signal area coverage and noise rejection capability. Such information would prove beneficial in setting an upper limit on effective (0- to 3-db) signal area coverage in $\vec{k}$-space while still allowing the filter to possess specified coherent noise response properties.

B. FORMULATION OF NOISE AND SIGNAL MODELS

In order to model accurately the defined noise and signal areas used in this study, the geographic areas of the world, as centered on the LASA, were transformed to f-$\vec{k}$ space to provide the necessary $\vec{k}$-space pattern. Figure VII-1 is this $\vec{k}$-space map. In this figure, the core shadow region is the area from which no direct P-waves can propagate and still arrive at the LASA. The small circles outline the Circum-Pacific belt which is the source area for the majority of all recorded earthquakes and consequently is a prime rejection area for filters to be used in the detection problem. The small triangles represent known underground test sites.

To develop a model to fit the noise and signal areas of interest, several different sized isotropic disks representing coherent noise power spectra were developed using Bessel functions (Table VII-1). The equation for the coherent power spectrum $M_{ij}(f)$ of an annulus area is:

* Texas Instruments, 1965, Large aperture seismic array final specification report: AFTAC, Aug., p. VI-1.

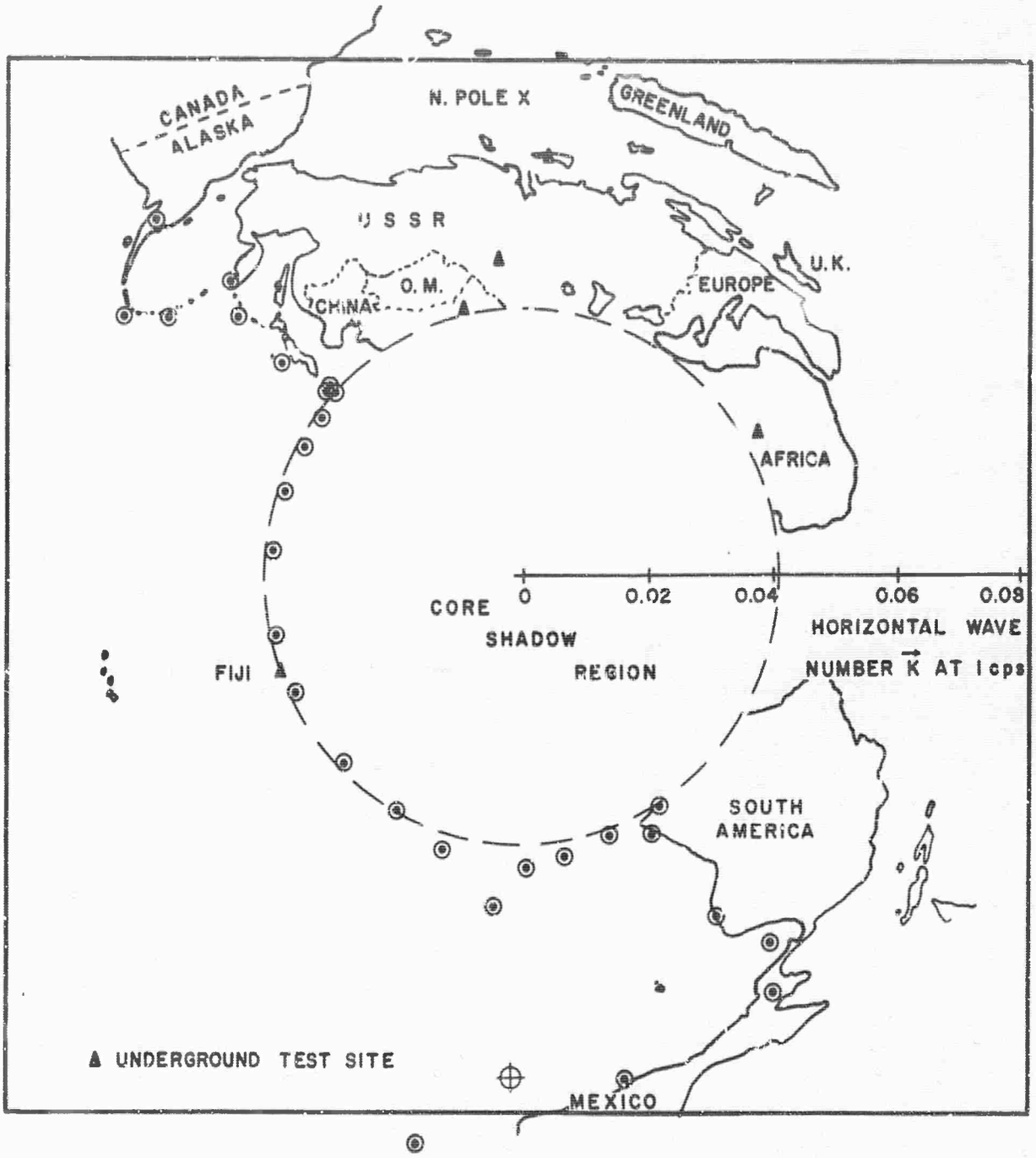

Figure VII-1. K-Space Mapping of the World for P-Wave at 1.0 CPS

$$M_{ij}(f) = \frac{M(f)}{\pi f\left[\frac{1}{V_1^2} - \frac{1}{V_2^2}\right]}\left[\frac{1}{V_1} J_1(2\pi |x_i - \vec{x}_j| \frac{f}{V_1}) - \frac{1}{V_2} J_1(2\pi |\vec{x}_i - \vec{x}_j| \frac{f}{V_2})\right], (x_i \neq x_j)^*$$

where

$M(f)$ = desired spectral weighting

J_1 = first-order Bessel function

$\vec{x}_i$ = sensor coordinate of th i^{th} sensor (subarray)

V_1 = minimum velocity

V_2 = maximum velocity

The coherent power spectrum of a disk region is formed by setting $V_2 = \infty$.

In the cases where the signal or noise areas of interest were not isotropic (i.e., centered about $\vec{k}$=0), the area was approximated by shifting in $\vec{k}$-space the appropriate models in Table VII-1. This shift can be compared to a beam steer or time shift of the coherent noise (or signal) power $M_{ij}(f)$. The resulting shifted coherent noise or signal power $M'_{ij}(f)$ is given by:

$$M'_{ij}(f) = M_{ij}(f) e^{i2\pi \vec{k} \cdot \vec{x}_{ij}}$$

where

$$\vec{x}_{ij} = \vec{x}_i - \vec{x}_j$$

and

$\vec{k}$ = vector wavenumber location of the center of the shifted model.

*Texas Instrument, 1961: Final Rpt., AFTAC Project VT/077, p. 108.

Table VII-1

SIZE OF DISKS FOR ISOTROPIC NOISE AND SIGNAL MODELS

(all R_j = 0 unless otherwise specified)

Model	R in Velocity Values
A	12.00 km/sec
B	163.50 km/sec
C	400.00 km/sec
D	21.92 km/sec R_1 25.72 km/sec R_2

Using this technique, complex signal and noise models may be approximated by shifting many disks of appropriate size to cover the desired area and then stacking these crosspower spectra, term by term, to form a single complex crosspower spectrum matrix, approximately representative of the desired model.

1. Noise Models

The first noise model used, Model I, was chosen as simple as possible to test the merits of the system. This model is composed of one Model A disk (Table VII-1), corresponding to a minimum velocity of 12 km/sec, centered at the origin of the $\vec{k}$-space map and is shown in Figure VII-2.

The second and more complicated noise model, Model II, also is shown in Figure VII-2. This model consists of 14 small disks (Model C), which were shifted from the origin to cover the Aleutian Island chain, and one annulus region (Model D) centered at the origin. This composite model encompasses most of the Circum-Pacific belt and the southern coast of Alaska.

It should be noted that any earthquake from the southern half of the map will not be confused with a nuclear event (assumed to originate from the northern half of the map), since these two events may be distinguished by the direction of propagation of the waves.

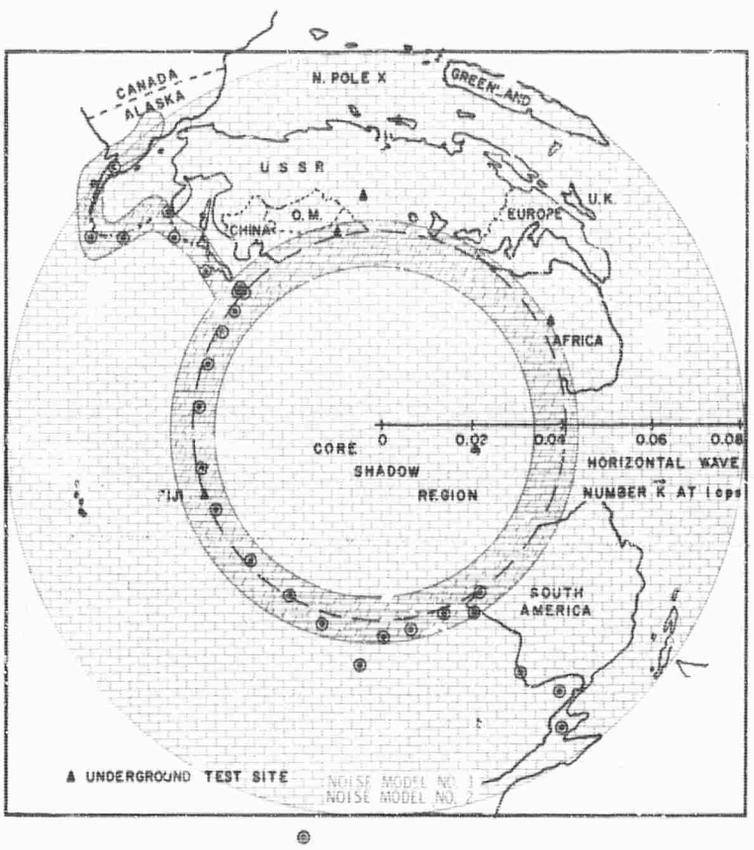

Figure VII-2. Noise Models

2. Signal Models

Signal models were developed to cover three of the known and possible nuclear test sites. These models were developed using the same method and disks which were used to generate the noise models.

The first signal model developed consisted of one Model C that was shifted to encompass the Russian test site on Novaya Zemlya. This model which is shown in Figure VII-3 gave the best results by far, as will be shown in the following parts of this section.

The second signal model was developed to encompass all of Russia. This signal (Figure VII-3) simulates Russia with seven Model B disks and nine Model C disks (Table VII-1).

The third and final signal model (Figure VII-3) uses seven Model C disks (Table VII-1) to simulate China.

C. PRESENTATION OF MULTICHANNEL FILTERS

A total of four multichannel filters were developed using various combinations of the noise and signal models outlined in the previous subsection. The details of these four filters are outlined in Table VII-2. This subsection presents the wavenumber response at frequencies of 0.5, 1.0, 2.0, and 3.0 cps of these four filters and also the response of the filters to random noise. The straight-sum response of the LASA has been included (Figure VII-4) for comparison with the filter results.

Table VII-2

LASA FILTERS

Filter Designation	Noise Model	Signal Model	Signal-to-Noise Ratios	Assumed Random Noise Level
LASA MCF-1	I	Novaya Zemlya	8.0	1%
LASA MCF-2	II	Novaya Zemlya	8.0	5%
LASA MCF-3	II	Russia	8.0	5%
LASA MCF-4	II	China	8.0	5%

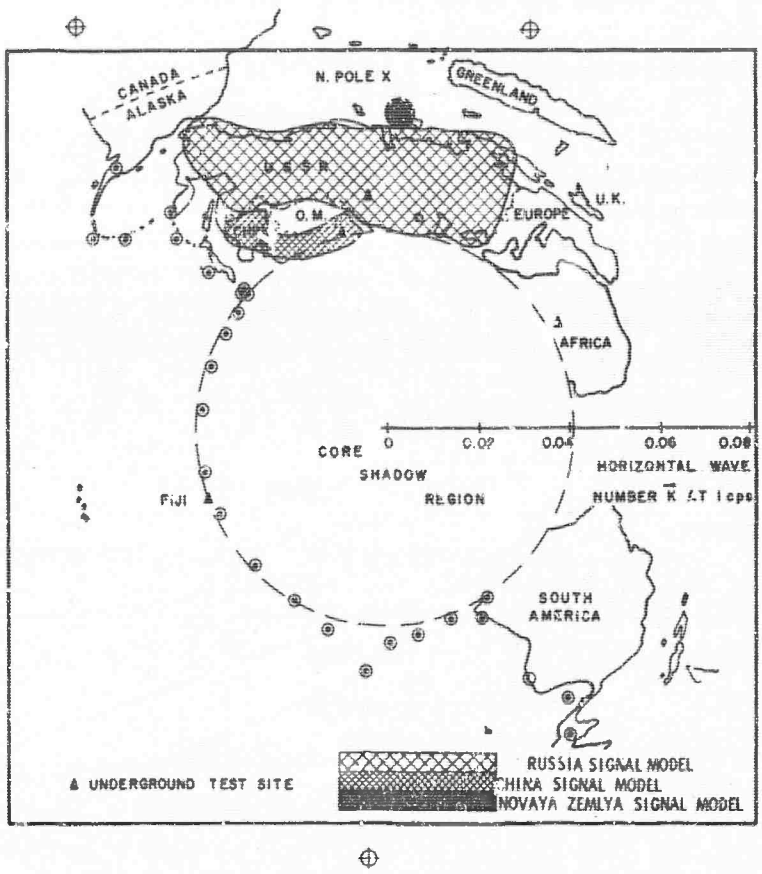

Figure VII-3. Signal Models

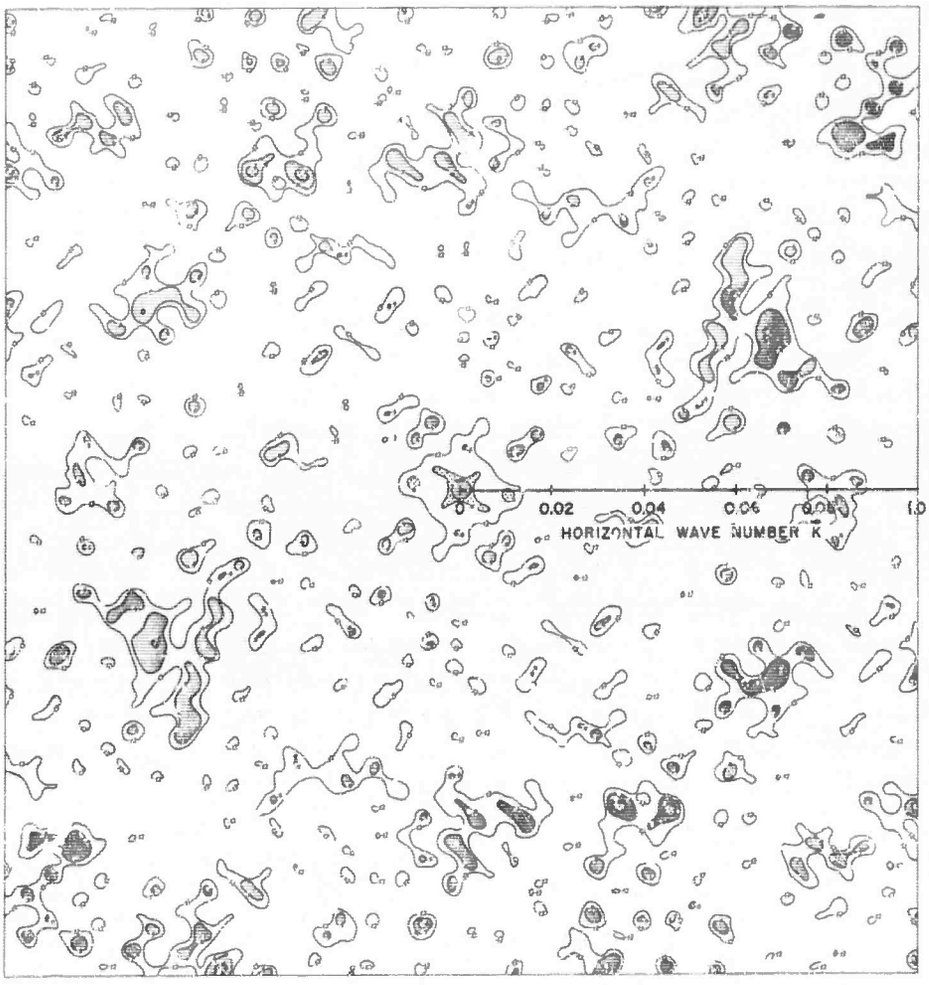

Figure VII-4. LASA Straight-Sum Response

1. Wavenumber Response

LASA MCF-1 was developed using the simplest noise and signal models, Noise Model I and Novaya Zemlya Signal Model, to test the merits of the techniqu, since these particular models were the least complex and easiest models to construct which would adequately encompass a specified signal area and the noise areas. The response of this filter is shown in Figure VII-5 at 0.5, 1.0, 2.0, and 3.0 cps. Because of the model simplicity, the filter is able to strongly reject the noise area. This is best seen at 0.5 cps where the entire noise model is either 12 or 18 db down from the signal. As frequency increases, the noise rejection deteriorates as evidenced by the large number of -6 db levels at 3.0 cps. This property will be discussed in detail in subsection D.

The second set of responses shown in Figure VII-6 are for LASA MCF-2* which was designed using Noise Model II and the Novaya Zemlya Signal Model. The results obtained from this set of responses again are excellent for the lower frequencies of 0.5 and 1.0 cps and indicate the same gradual decrease in effective results as the frequency increases.

The responses of LASA MCF-3 which was designed using Noise Model II and the Russia Signal Model are shown in Figure VII-7. This filter demonstrates results similar to the preceeding two filter responses. The filter performs well at the lower frequencies, but degenerates as frequency increases. Of particular note are the excellent results at 0.5 and 1.0 cps where Russia is at 0 and -3 db and the noise model is at either -12 or -18 db or greater.

The responses of LASA MCF-4 which was designed on Noise Model II and the China Signal Model are shown in Figure VII-8. As in previous cases, the results are very good for the lower frequencies, with the same decrease in results as the frequency increases. It should be noted that the results for China are better than those for Russia, but are not as good as those for Novaya Zemlya.

*The shaded areas show the areas of prime interest in this and the remaining sets of filter responses.

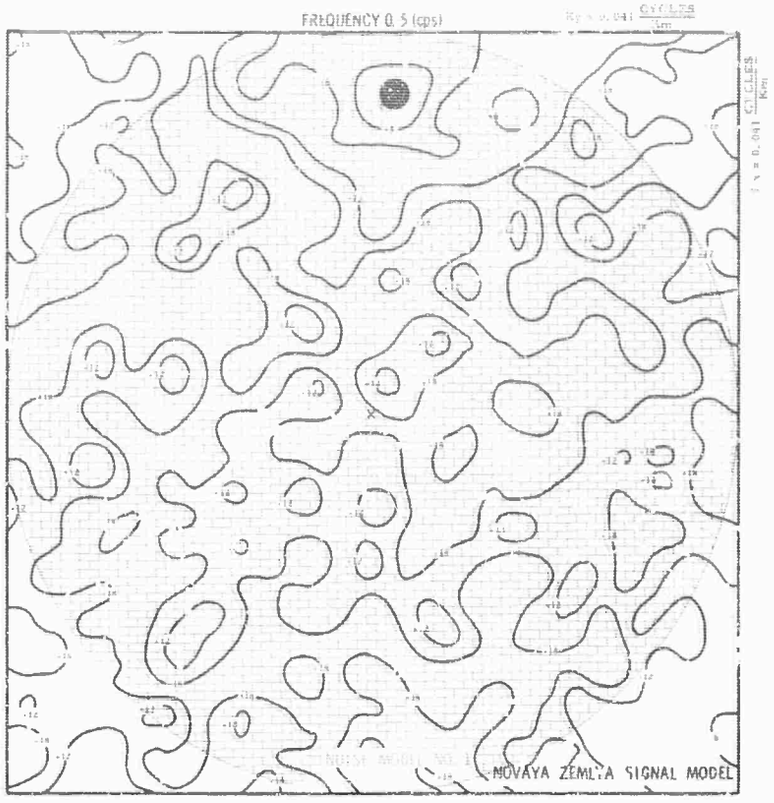
FREQUENCY 0.5 (cps)
NOVAYA ZEMLYA SIGNAL MODEL

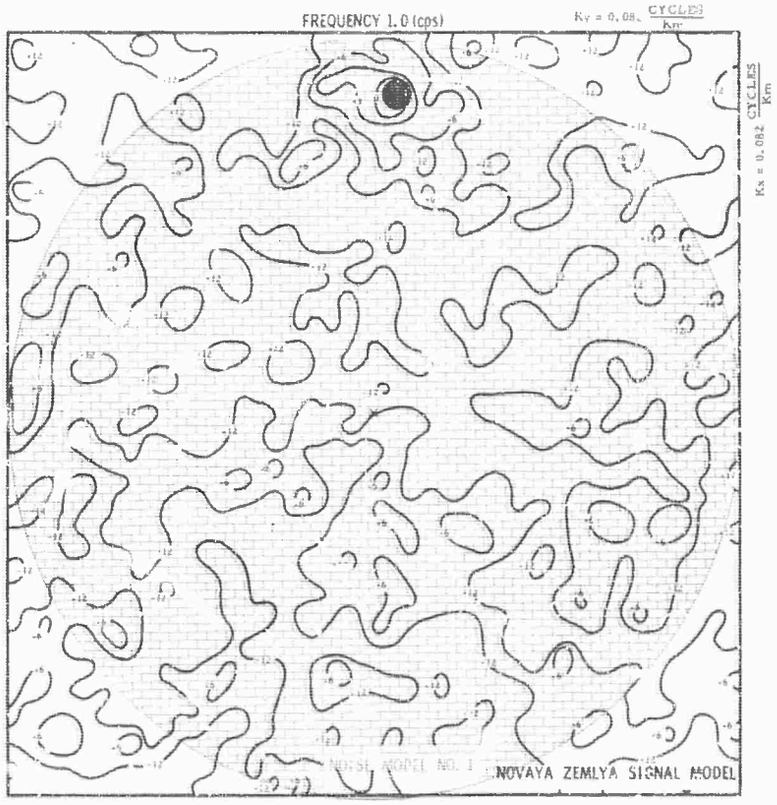
FREQUENCY 1.0 (cps)
NOVAYA ZEMLYA SIGNAL MODEL

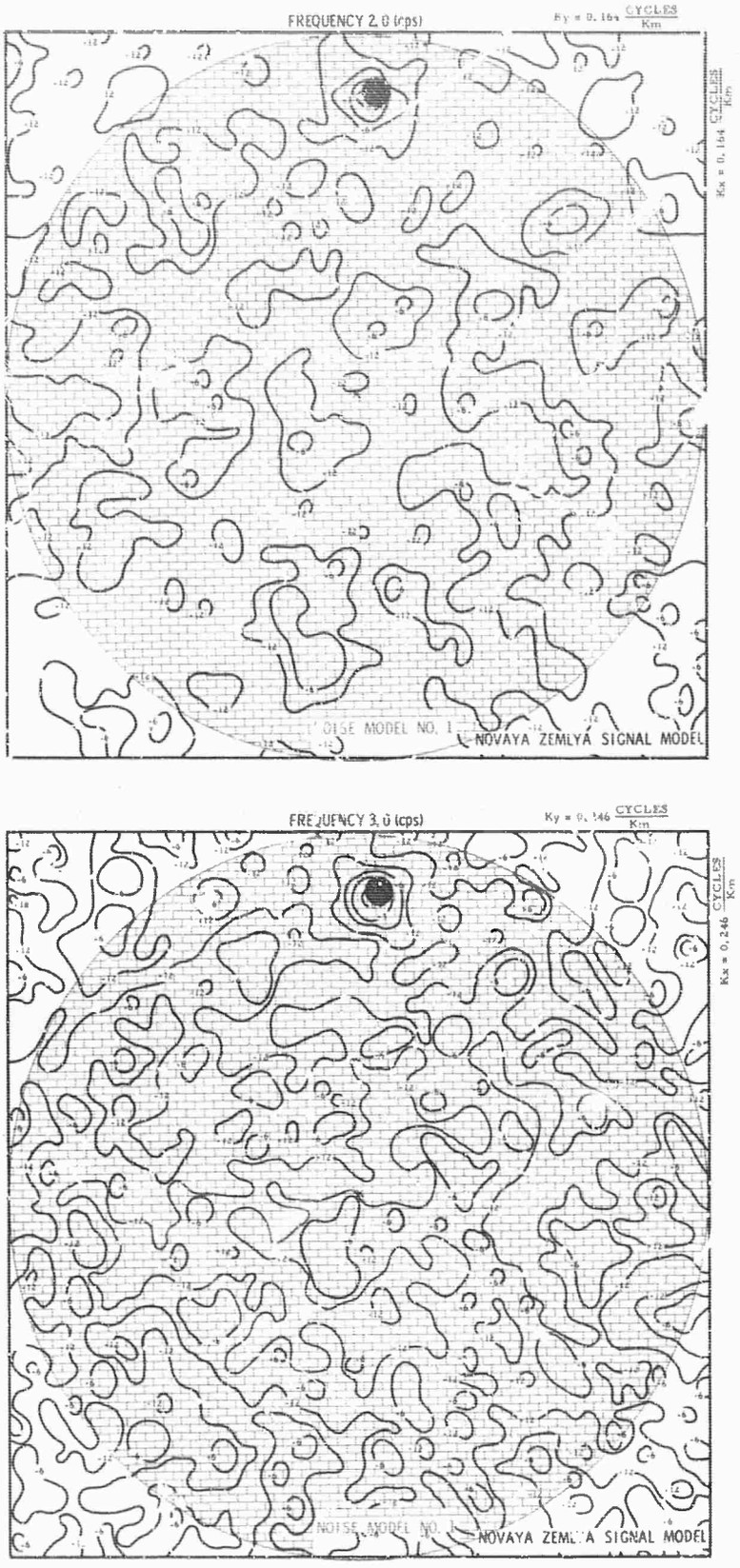

Figure VII-5. 2-Dimensional Wavenumber Response of LASA MCF-1, F = 0.5, 1.0, 2.0, 3.0 CPS (Opposite Page Included)

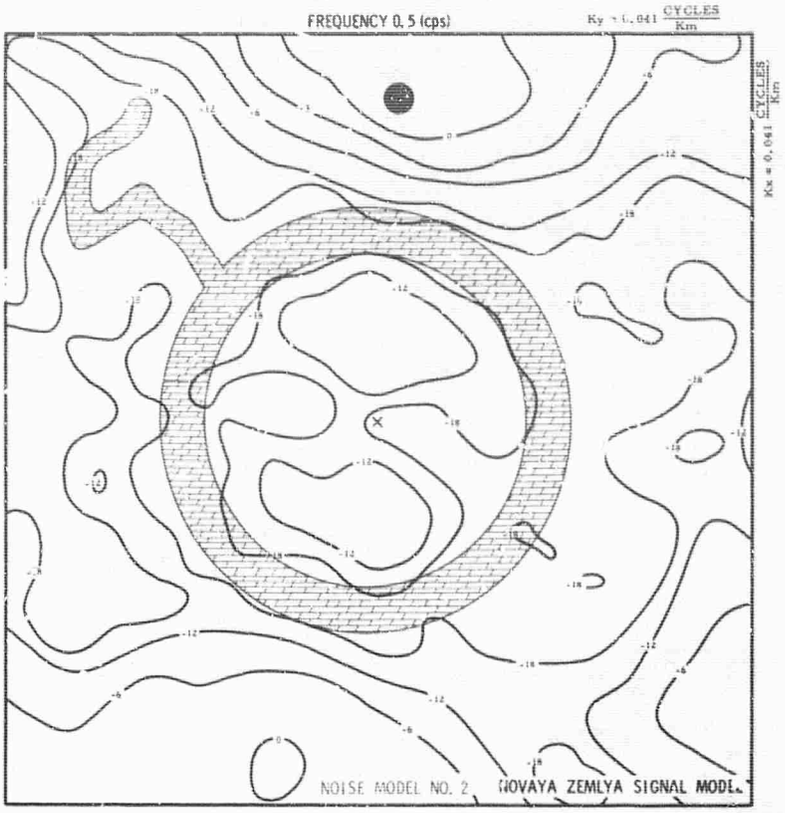
FREQUENCY 0.5 (cps)
Ky = 0.041 CYCLES/Km
Kx = 0.041 CYCLES/Km
NOISE MODEL NO. 2
NOVAYA ZEMLYA SIGNAL MODEL

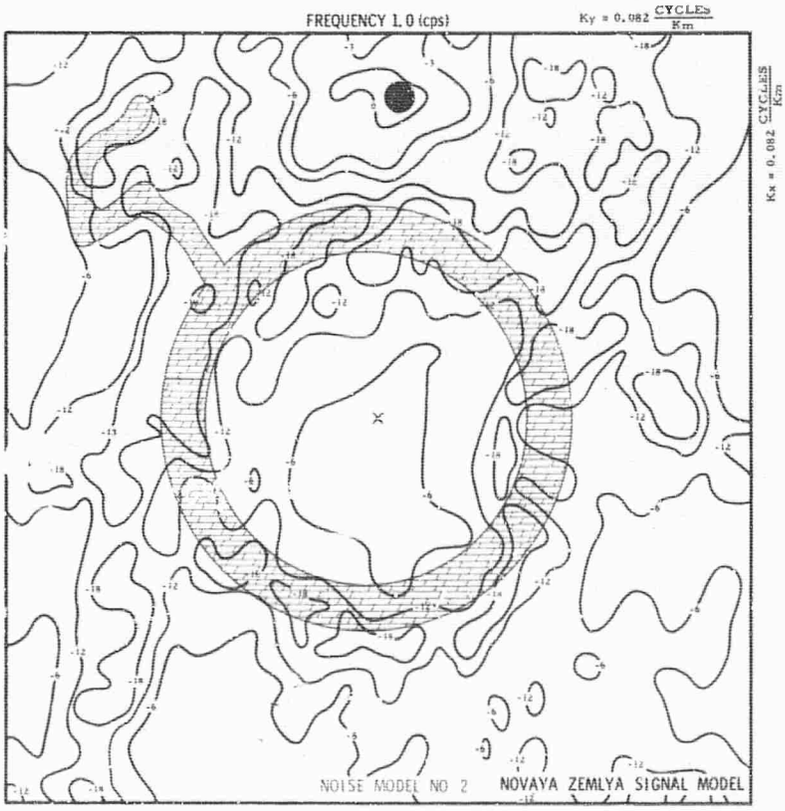
FREQUENCY 1.0 (cps)
Ky = 0.082 CYCLES/Km
Kx = 0.082 CYCLES/Km
NOISE MODEL NO 2
NOVAYA ZEMLYA SIGNAL MODEL

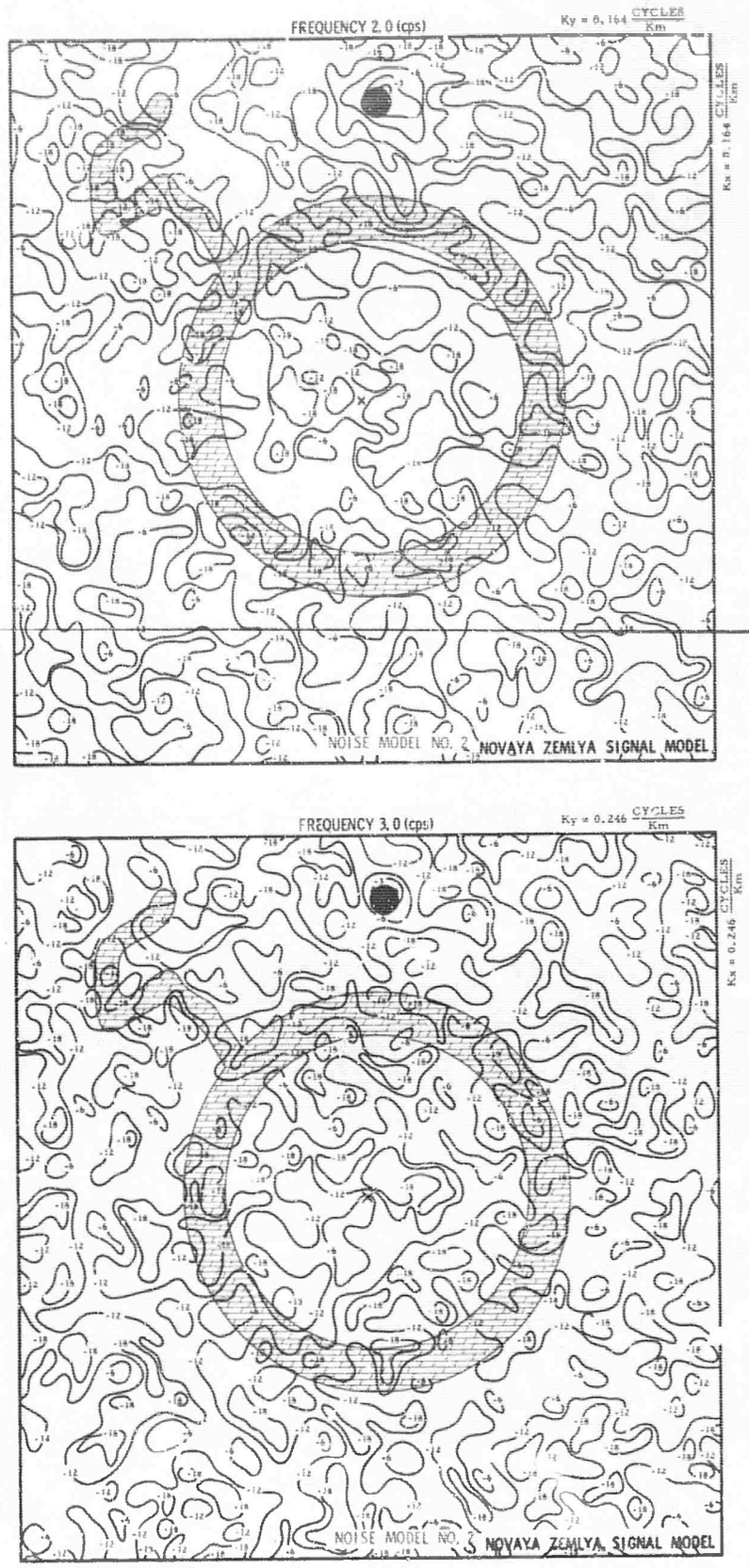

Figure VII-6. 2-Dimensional Wavenumber Response of LASA MCF-2; F = 0.5, 1.0, 2.0, 3.0 CPS (Opposite Page Included)

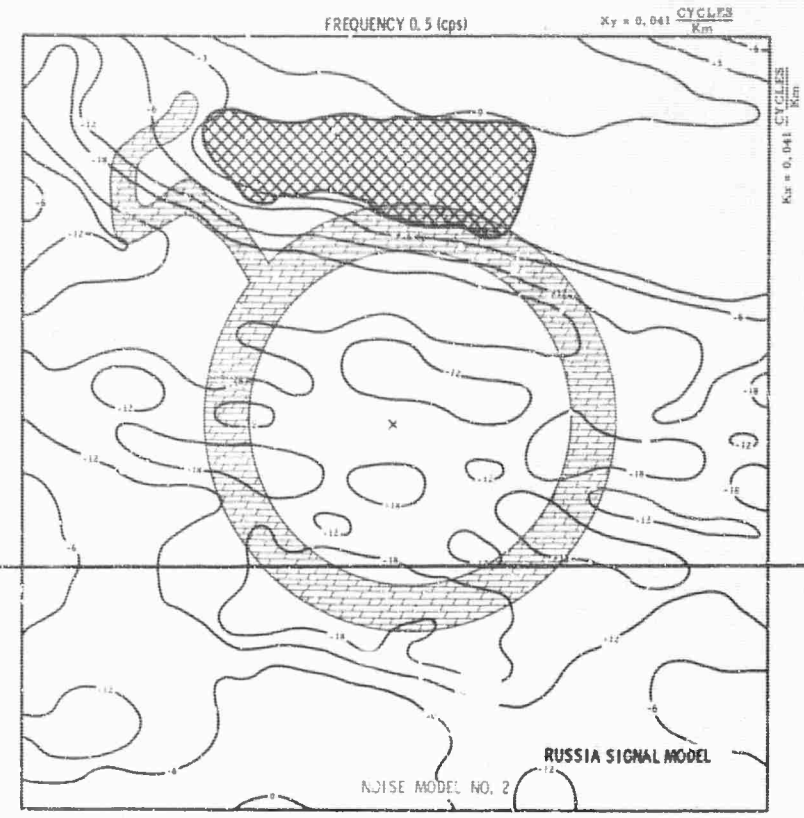
FREQUENCY 0.5 (cps)
Xy = 0.041 CYCLES/Km
Kx = 0.041 CYCLES/Km
RUSSIA SIGNAL MODEL
NOISE MODEL NO. 2

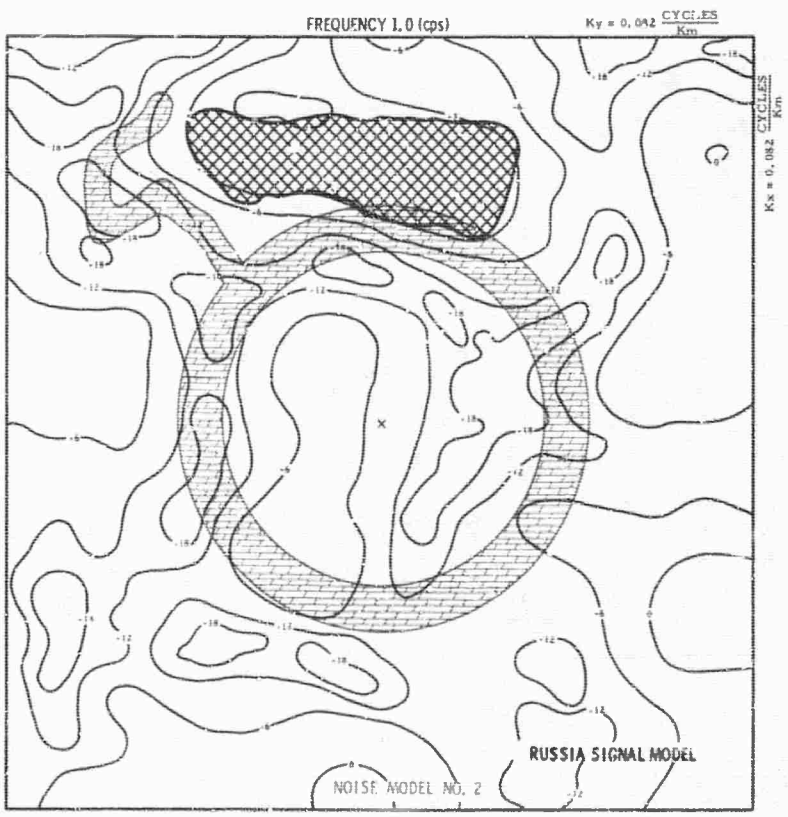
FREQUENCY 1.0 (cps)
Ky = 0.042 CYCLES/Km
Kx = 0.042 CYCLES/Km
RUSSIA SIGNAL MODEL
NOISE MODEL NO. 2

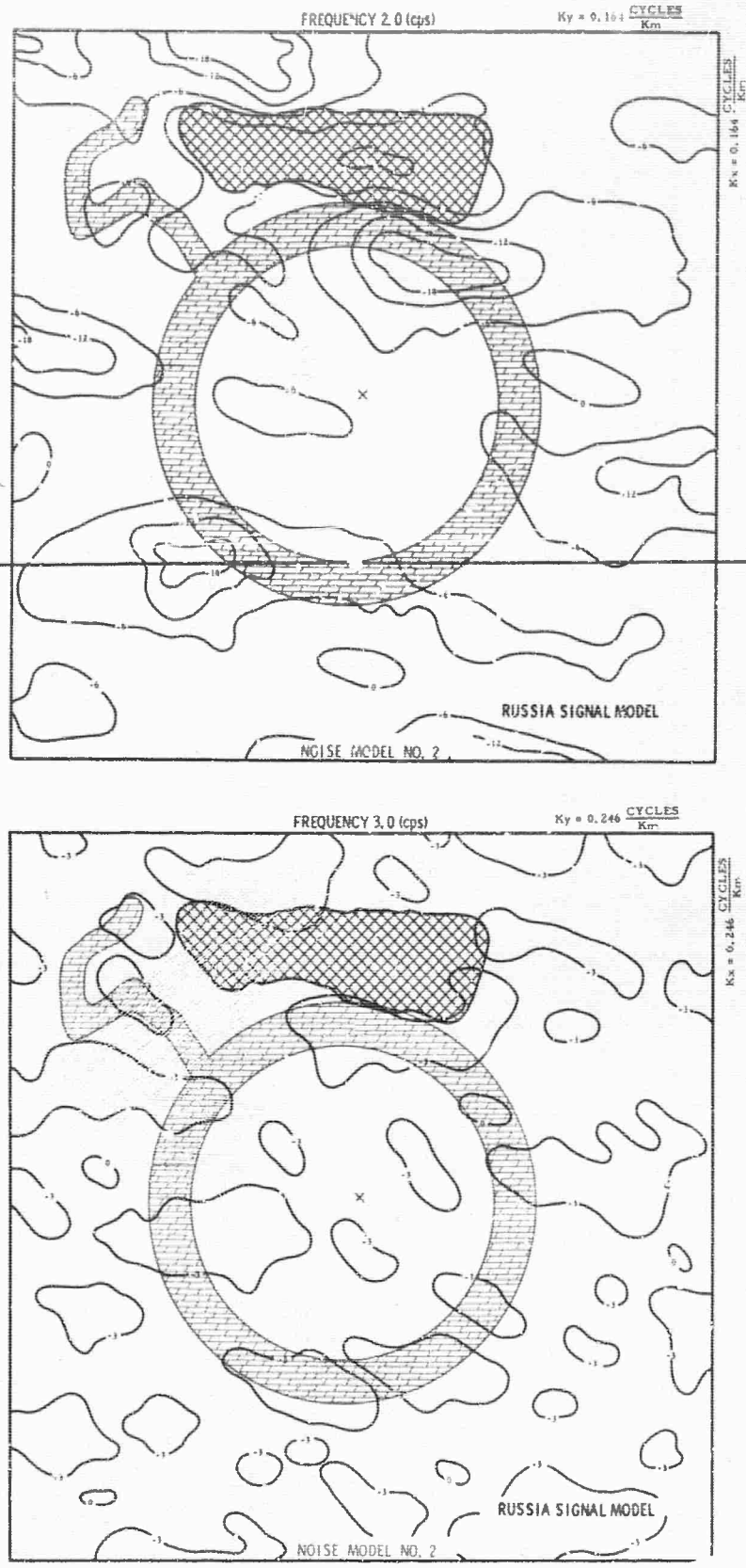

Figure VII-7. 2-Dimensional Wavenumber Response of LASA MCF-3; F = 0.5, 1.0, 2.0, 3.0 CPS (Opposite Page Included)

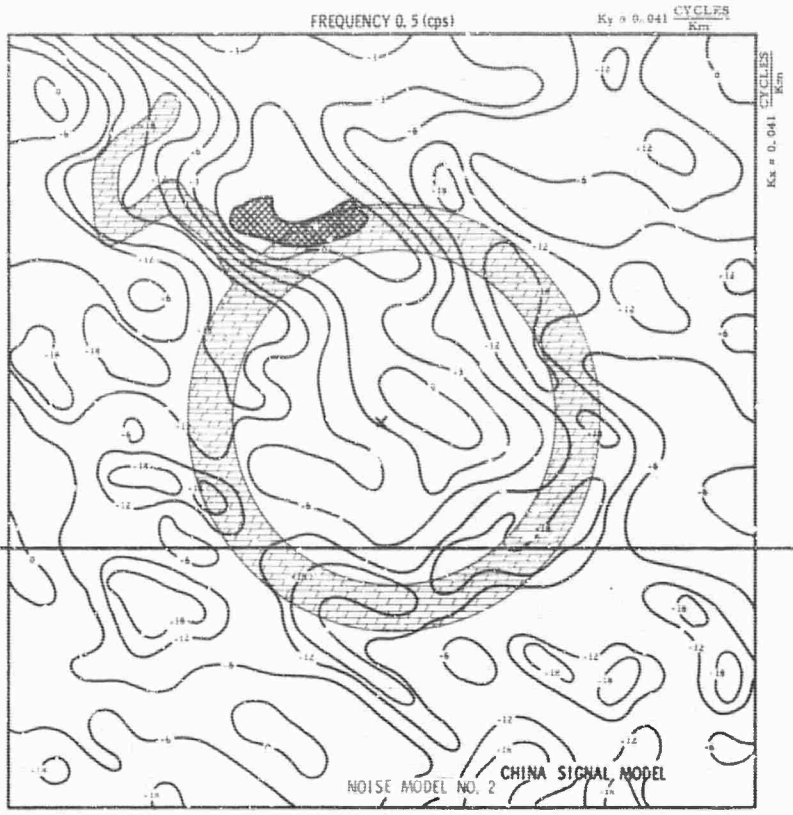
FREQUENCY 0.5 (cps)
Ky = 0.041 CYCLES/Km
Kx = 0.041 CYCLES/Km
NOISE MODEL NO. 2
CHINA SIGNAL MODEL

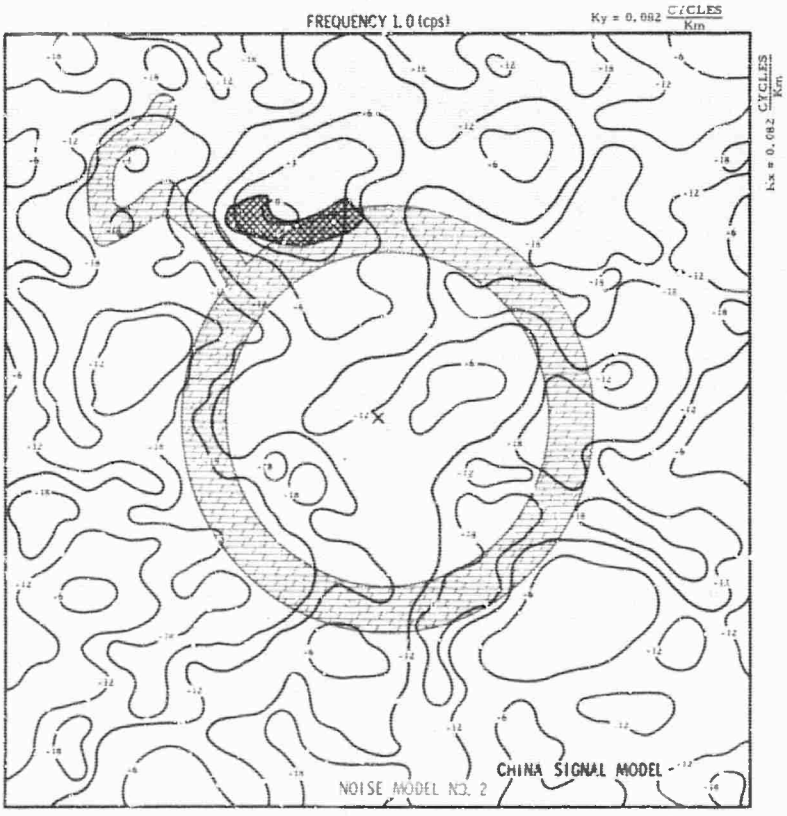
FREQUENCY 1.0 (cps)
Ky = 0.082 CYCLES/Km
Kx = 0.082 CYCLES/Km
NOISE MODEL NO. 2
CHINA SIGNAL MODEL

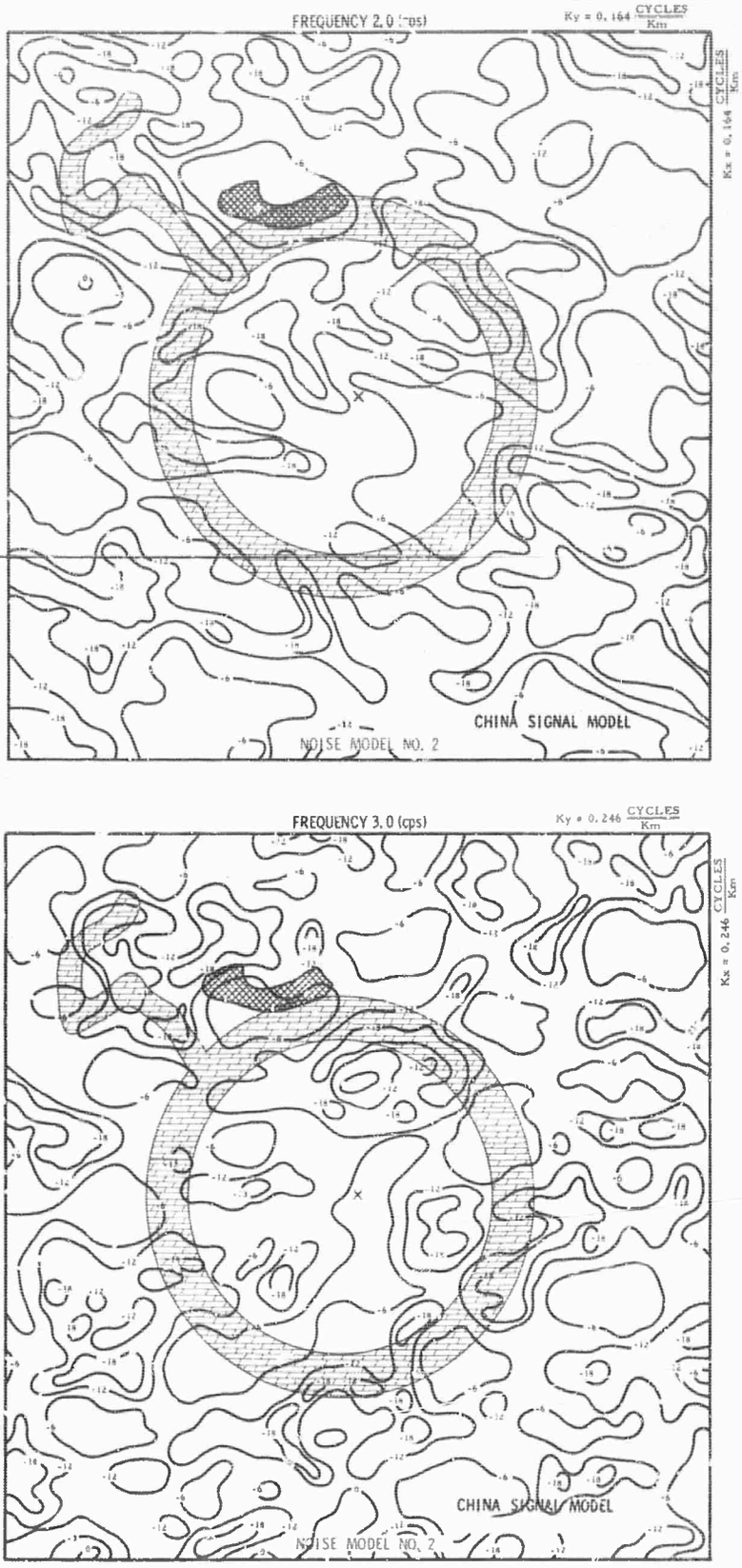

Figure VII-8. 2-Dimensional Wavenumber Response of LASA MCF-4; F = 0.5, 1.0, 2.0, 3.0 CPS (Opposite Page Included)

2. Random Noise Response

The random noise response for LASA MCF-1 through MCF-4 has been computed and is shown in Figure VII-9. Briefly, the random noise response of a multichannel filter is given by:

$$\frac{N_o(f)}{N_i(f)} = \sum_{j=1}^{N} |H_j(f)|^2$$

where

N = number of sensors

$H_j(f)$ = complex transfer function of the j^{th} filter

$N_i(f)$ = input noise power of the reference sensor

$N_c(f)$ = output noise power

Knowledge of the random noise response of a multichannel filter is an important factor for consideration when evaluating a particular filter, since this information is indicative of the filter performance in an actual noise field containing random noise. Comparison of the random noise response should be made in terms of the expected response for straight-summation processing which yields a noise power improvement of N if the noise field is completely random and is the upper limit of improvement obtainable if the processing system has 0-db response for the specified class of signal over the wideband frequency response.

In line with this discussion, it should be noted that LASA MCF-1 indicates noise rejection greater than N (-13.22 db for 21 sensors) at frequencies greater than 1.0 cps. This is due to the filter response to signals from Novaya Zemlya (the specified signal) which, above 1.0 cps, indicates rejection on the order of 3 to 6 db (Figure VII-5). In other words, MCF-1 is actually frequency filtering as well as velocity filtering which causes greater than N rejection. This filter property probably resulted because of the overlapping in $\vec{k}$-space of the signal and noise models and probably can be avoided in future filters by specifying a larger signal-to-noise ratio.

In order to lend physical interpretation to the information presented in Figure VII-9, an estimate was made of the subarray random

2. Random Noise Response

The random noise response for LASA MCF-1 through MCF-4 has been computed and is shown in Figure VII-9. Briefly, the random noise response of a multichannel filter is given by:

$$\frac{N_o(f)}{N_i(f)} = \sum_{j=1}^{N} |H_j(f)|^2$$

where

N = number of sensors

$H_j(f)$ = complex transfer function of the j^{th} filter

$N_i(f)$ = input noise power of the reference sensor

$N_o(f)$ = output noise power

Knowledge of the random noise response of a multichannel filter is an important factor for consideration when evaluating a particular filter, since this information is indicative of the filter performance in an actual noise field containing random noise. Comparison of the random noise response should be made in terms of the expected response for straight-summation processing which yields a noise power improvement of N if the noise field is completely random and is the upper limit of improvement obtainable if the processing system has 0-db response for the specified class of signal over the wideband frequency response.

In line with this discussion, it should be noted that LASA MCF-1 indicates noise rejection greater than N (-13.22 db for 21 sensors) at frequencies greater than 1.0 cps. This is due to the filter response to signals from Novaya Zemlya (the specified signal) which, above 1.0 cps, indicates rejection on the order of 3 to 6 db (Figure VII-5). In other words, MCF-1 is actually frequency filtering as well as velocity filtering which causes greater than N rejection. This filter property probably resulted because of the overlapping in $\vec{k}$-space of the signal and noise models and probably can be avoided in future filters by specifying a larger signal-to-noise ratio.

In order to lend physical interpretation to the information presented in Figure VII-9, an estimate was made of the subarray random

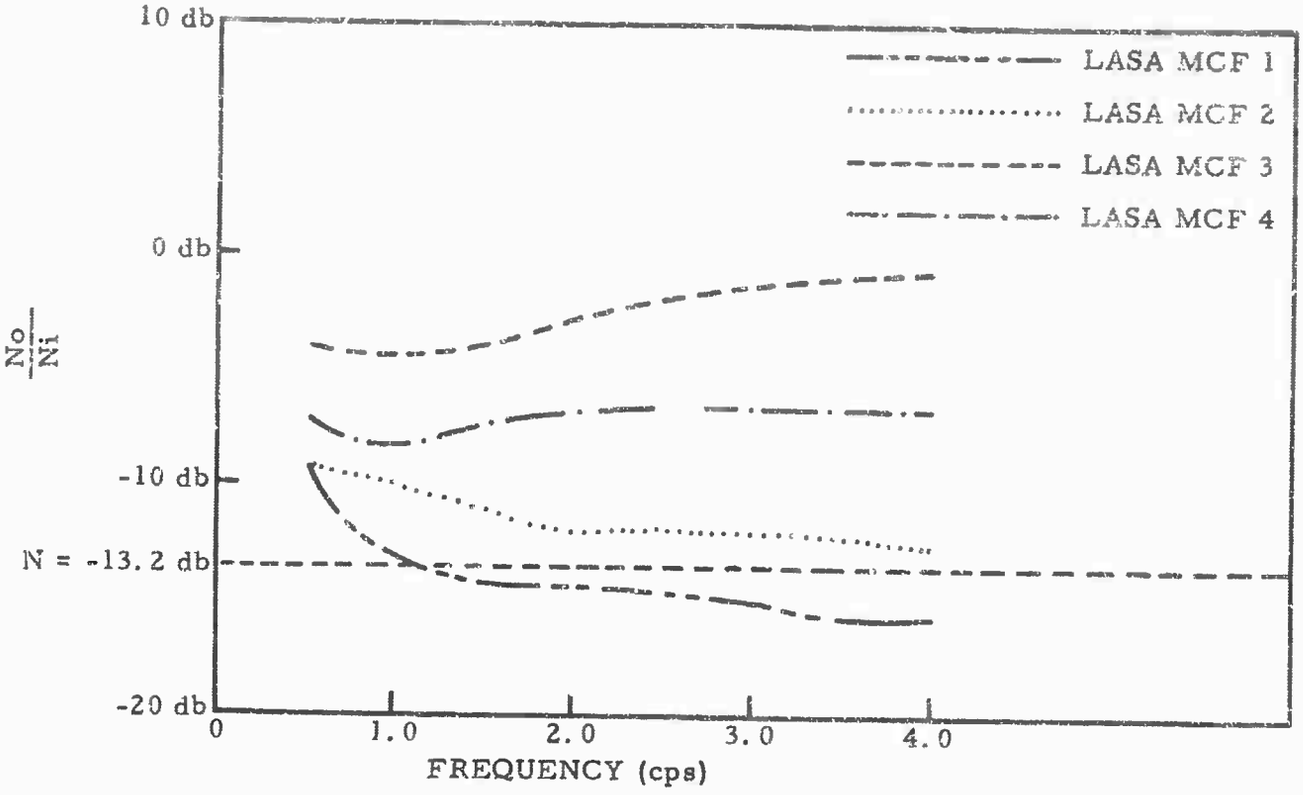

Figure VII-9. MCF Response to Random Noise

noise level and the quantity $\frac{N_o}{N_i}$ computed. This information along with the estimated random noise level is shown in Figure VII-10 and represents the anticipated random noise output for MCF-1 through -4 and for straight summation relative to 1.0 $m\mu^2$ of ground motion/cps at 1.0 cps.

The estimated input random noise level is based upon the straight-summation output for 10 elements of the Angela subarray which was assumed average for each of the 21 subarrays. This level was formed from power-density spectra and prediction filtering results presented in the report "Large Aperture Seismic Array Final Specifications Report." *

D. DISCUSSION OF RESULTS

The wavenumber responses for LASA MCF-1 through -4 indicate that each filter is passing, with 0-to 6-db attenuation, the desired signal area and is attenuating the specified noise regions 3 to 30 db and greater. In analyzing each of the wavenumber responses, the fact that there is a definite trade-off between signal $\bar{K}$-space area coverage and filter noise rejection capability is evident. Analysis of the random noise responses probably gives the best demonstration of this trade-off. (It should be remembered that this approach is limited since it does not show the rejection capability for the specified noise regions but only general filter trends). The Novaya Zemlya filters (LASA MCF-1 and -2), which have the smallest defined signal area of the filters being presented indicate in Figure VII-9 the most desirable random noise responses, when compared with the other filters. As the signal $\bar{K}$-space area coverage increases, the random noise response degenerates, as evidenced by the China filter (LASA MCF-4), which shows results midway between the Russia filter (LASA MCF-3) and the Novaya Zemlya filters.

The trade-off between signal area and filter noise rejection can also be seen within a single filter as frequency increases, since the signal (or noise) area which is normally defined in terms of constant velocity, is proportional to f^2. As an example, LASA MCF-3 (Russia Signal Model, Figure VII-7) shows that at 0.5 cps the noise areas generally are attenuated 12 to 18 db while at 3.0 cps this area is attenuated only about 3 db. The other filters show comparable results, except that the trade-off can appear as signal suppression rather than loss of noise

*Texas Instruments, 1965, Large Aperture Seismic Array Final Specifications Rpt: AFTAC, Aug., p. IV-42 and IV-72.

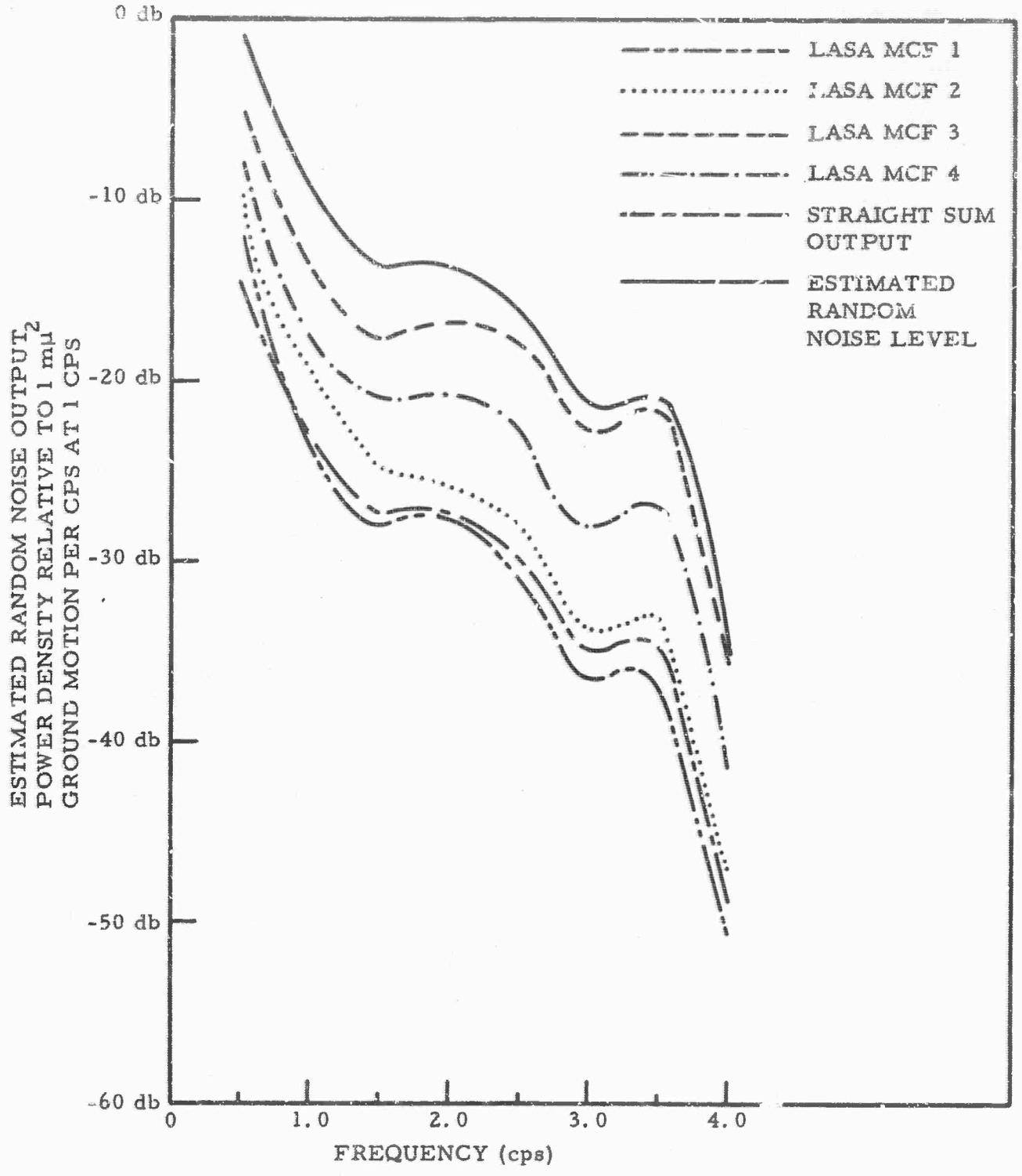

Figure VII-10. Estimated Random Noise Output Level

rejection, as in LASA MCF-4 (Figure VII-8). In this case, China is being attenuated 6 db at 3.0 cps while the defined noise areas are being attenuated 6 to 18 db. This attenuation of signal was observed also in MCF-1, as discussed in paragraph C.2. Apparently, the trade-off under discussion appears in the form of signal attenuation rather than loss of noise rejection capability whenever signal and noise areas overlap in $\vec{k}$-space, which is the case for both MCF-1 and MCF-4. This problem probably can be solved so that signal is attenuated only 0 to 3 db by specifying a signal-to-noise ratio larger than 8.0 during filter synthesis, or by redesigning the noise model to avoid overlapping with the signal area.

Probably the most important consideration in the evaluation of the LASA filters, aside from the signal and noise $\vec{k}$-space response, are the filter random noise responses which were presented in Figure VII-9. These responses indicate that the output random noise power is never greater than the input noise power between 0.5 and 4.0 cps and, for all except MCF-3, input random noise is always attenuated greater than 6 db. The relatively poor random noise response of MCF-3 is reasonable, as explained above, on the basis of the wide $\vec{k}$-space area coverage of the signal model. Since random noise is attenuated approximately 13.98 db at the subarray level (assuming all 25 channels were used in straight-summation or beam-steer processing), even MCF-3 would probably be acceptable for processing actual LASA data. If large areas such as Russia were monitored using two or more multichannel filters, each designed to cover only a portion of the overall area, a random noise response similar to that obtained for MCF-4 could be expected, plus improvement in organized signal and noise response properties would be obtained.

SECTION VIII

CPO NOISE AND SIGNAL ENSEMBLE

A. INTRODUCTION

This section discusses the formulation and processing of a noise and signal ensemble for CPO. The data used in this library was collected on-site, in 1963 in digital format, using a DFS (Digital Field System)*. This library of data is to be used in the following tasks to be performed under this contract:

1) Local MCF Evaluation. Multichannel filters will be synthesized using measured noise and signal for the respective noise and signal matrices. This technique of filter synthesis will be compared with conventional methods which use theoretical signals for P-wave enhancement.

2) Evaluation of Phase Extraction. Multichannel filters will be synthesized using theoretical coherent noise and signal models for extraction of P, S and LR phases of measured signals. The effectiveness of phase extraction will be evaluated by applying the MCFs to quarry blasts.

The events included in this library are 3 teleseisms, 12 quarry blasts, 1 nuclear blast, and 3 noise samples (Table VIII-1).

B. PREPARATION OF ENSEMBLE

The data was prepared for use in the tasks previously mentioned first by decimation and then by whitening. Decimation is accomplished to yield the minimum number of points representative of the desired time-length data in order to reduce computer time. Whitening of the data is advantageous for two reasons. First, whitening permits maximum use of computer accuracy in the wideband frequency sense when computing correlations by reducing the long-period microseismic energy contribution. Second, whitening is necessary when the data is to be used in time-domain multichannel filter development, since the "goodness" of the filter solution as a function of frequency is partially dependent upon the relative spectral weighting. The steps in processing this library are outlined in the following paragraphs.

The original 19-channel data, which is 4 min in length and

---

* Trademark of Texas Instruments

Table VIII-1

CPO EVENT LIBRARY

Event	Location	Date	Occurrence Time	Sample Interval (sec)	Length
		Teleseisms			
AA	Pacific Ocean	9 May '63	164606.0	.144	1667
BB	Crete	4 Mar '63	151619.6	.144	1667
CC	Peru	4 Mar '63	154304.0	.144	1667
		Nuclear			
AA		15 Feb '63		.144	1667
		Quarry Blasts			
AA		9 May '63		.072	3240
BB		19 Apr '63		.072	3333
CC		19 Apr '63		.072	3333
DD		19 Apr '63		.072	3333
EE		19 Apr '63		.072	3333
FF		15 Feb '63		.072	3333
GG		15 Feb '63		.072	3333
HH		10 Apr '63		.072	3333
I I		11 Apr '63		.072	3333
JJ		24 Apr '63		.072	3333
KK		24 Apr '63		.072	3333
LL		24 Apr '63		.072	3333
		Noise Samples			
AA		4 Mar '63		.072	3333
				.144	1667
BB		4 Mar '63		.072	3333
				.144	1667

has a .024-sec sample interval, has been separated into two groups. The first group, decimated by 6 to form 144-msec sample interval data, includes 3 teleseisms, 1 nuclear blast and the 2 noise samples which preceed and overlap two of the teleseisms. The second group, decimated by 3 to form 72-msec data, includes the 12 quarry blasts and the same 2 noise samples.

Before decimation, each group of data was filtered using a minimum-phase 101-point antialiasing filter appropriate to the sample interval. The response of the 144-msec antialiasing filter is given in Figure VIII-1 and that of the 72-msec antialiasing filter is in Figure VIII-2.

After decimation, the overlapping noise-teleseism pairs (noise sample AA-teleseism BB and noise sample BB-teleseism CC) were appended at the appropriate point, forming two records of length 470.16 sec.

The data was next whitened by applying an ensemble whitening (deconvolution) filter to each data set.

These filters were designed on an ensemble basis in order that the relative signal-to-noise ratios would be preserved between noise and signal samples, thus insuring maximum noise and signal information which is necessary in synthesis of local MCFs. Had each record been whitened (deconvolved) using filters designed on single records, the resulting signal-to-noise ratios between signal and noise samples would not have been representative of the original data condition.

The ensemble whitening filters were developed by computing the autocorrelation for the center-seismometer output (Z 10) of each record in both data groups to include signal and noise. The autocorrelations were normalized and stacked (i.e., added point by point) to form two average autocorrelations representative of each ensemble (i.e., the 144-msec ensemble and the 72-msec ensemble). Two whitening filters then were designed on these autocorrelations. Each filter was applied to its respective group of records. The response of these filters is given in Figures VIII-3 and VIII-4. Figure VIII-5 shows noise sample AA before whitening and Figure VIII-6 shows it after whitening. Figures VIII-7 and VIII-8 are before and after whitening samples, respectively, of quarry blast CC. Figures VIII-9 and VIII-10 show absolute power-density spectra of events AA and CC before and after whitening, respectively.

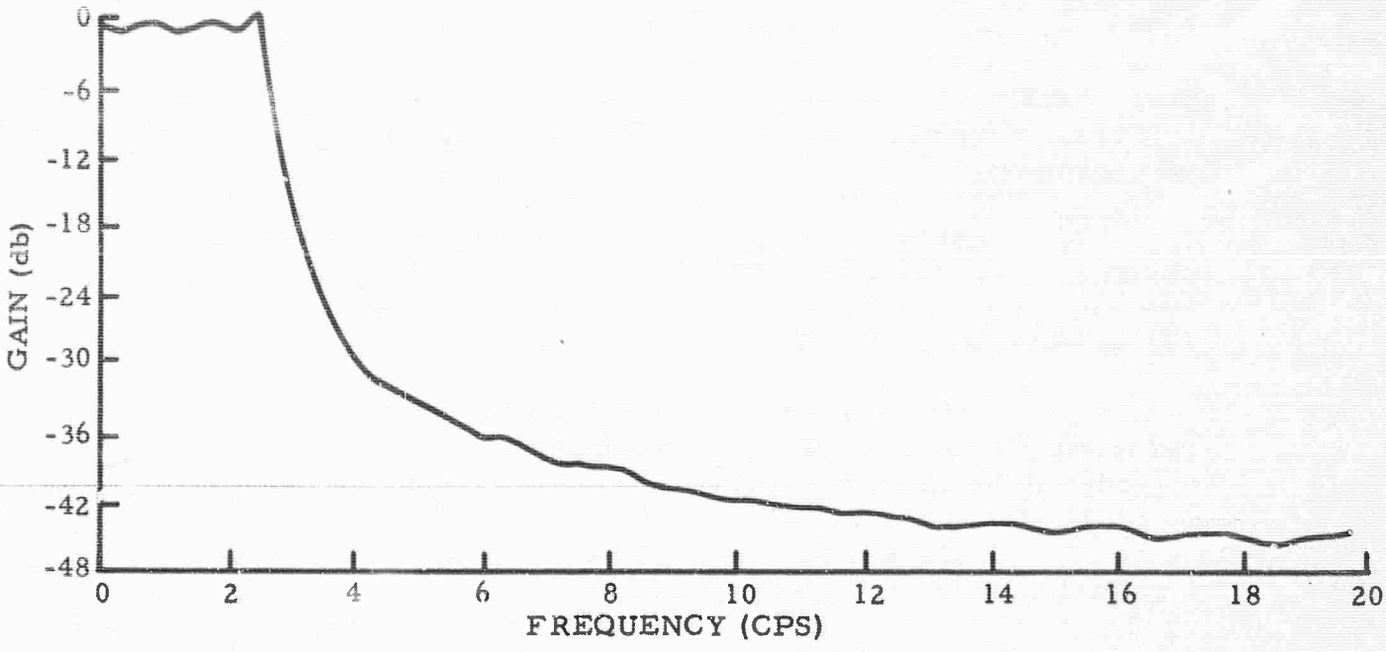

Figure VIII-1. Transfer Function of Minimum Phase Antialiasing Filter for 144-msec Data

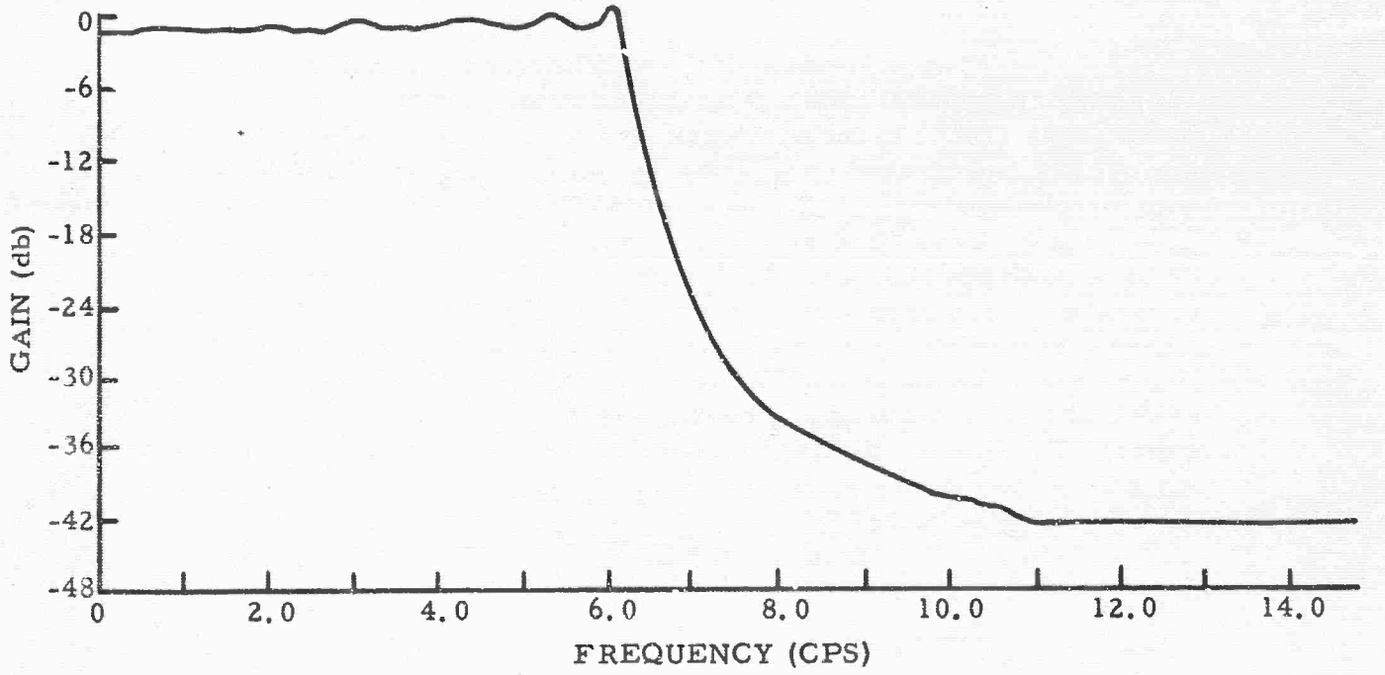

Figure VIII-2. Transfer Function of Minimum Phase Antialiasing Filter for 72-msec Data

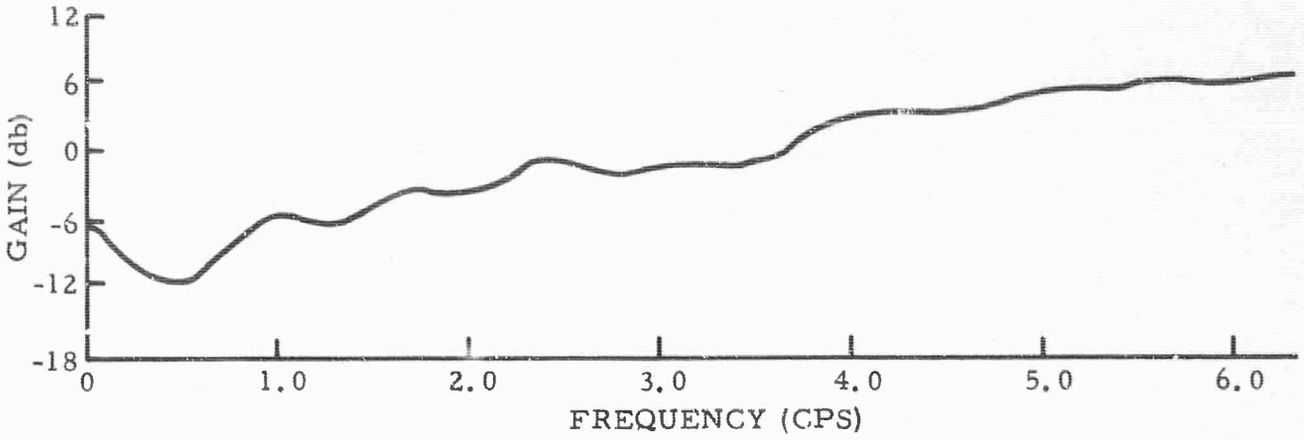

Figure VIII-3. Transfer Function of Whitening (Deconvolution) Filter for 72-msec Data

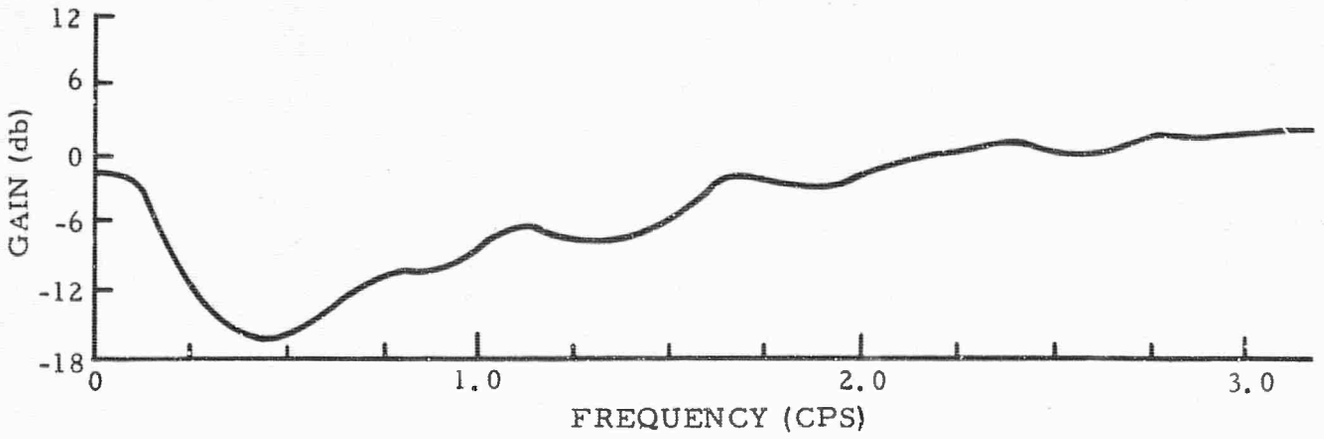

Figure VIII-4. Transfer Function of Whitening (Deconvolution) Filter for 144-msec Data

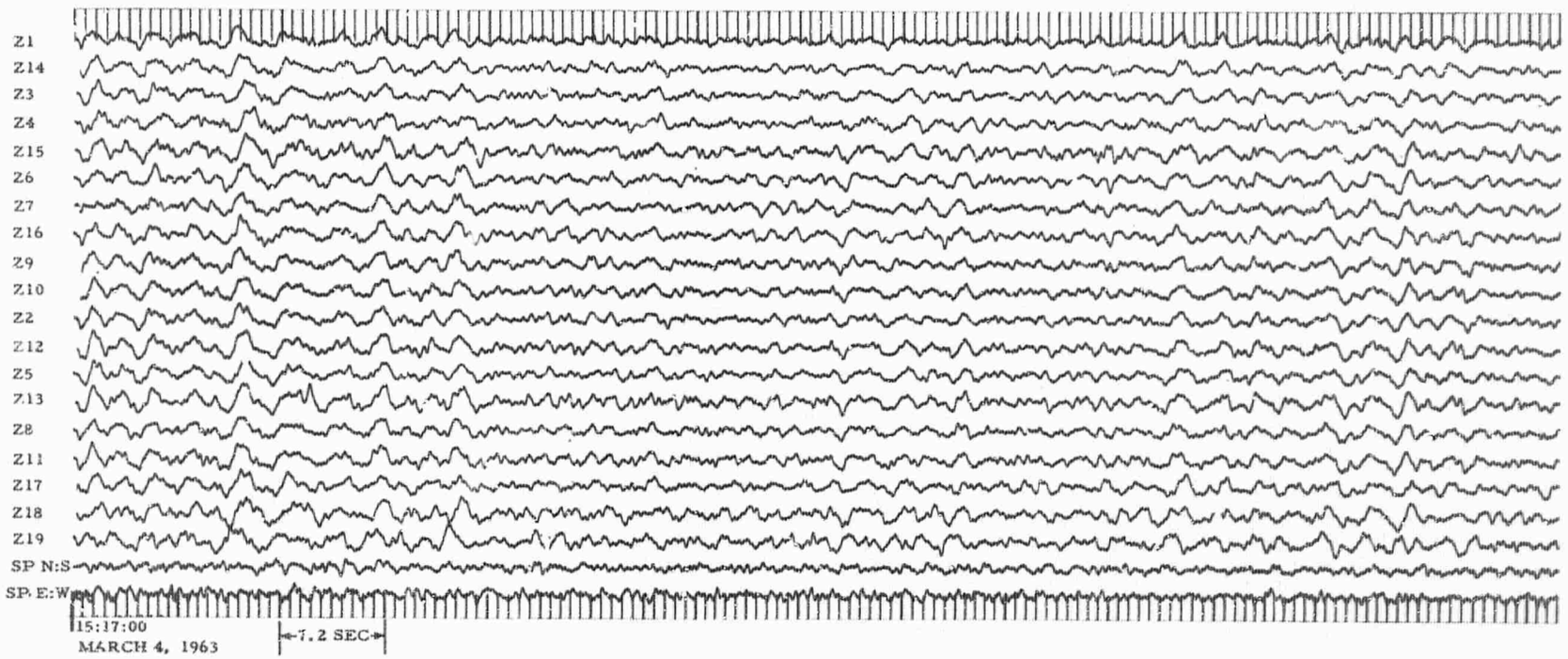

Figure VIII-5. Noise Sample AA Antialias Filtered and Decimated Before Whitening (Deconvolution)

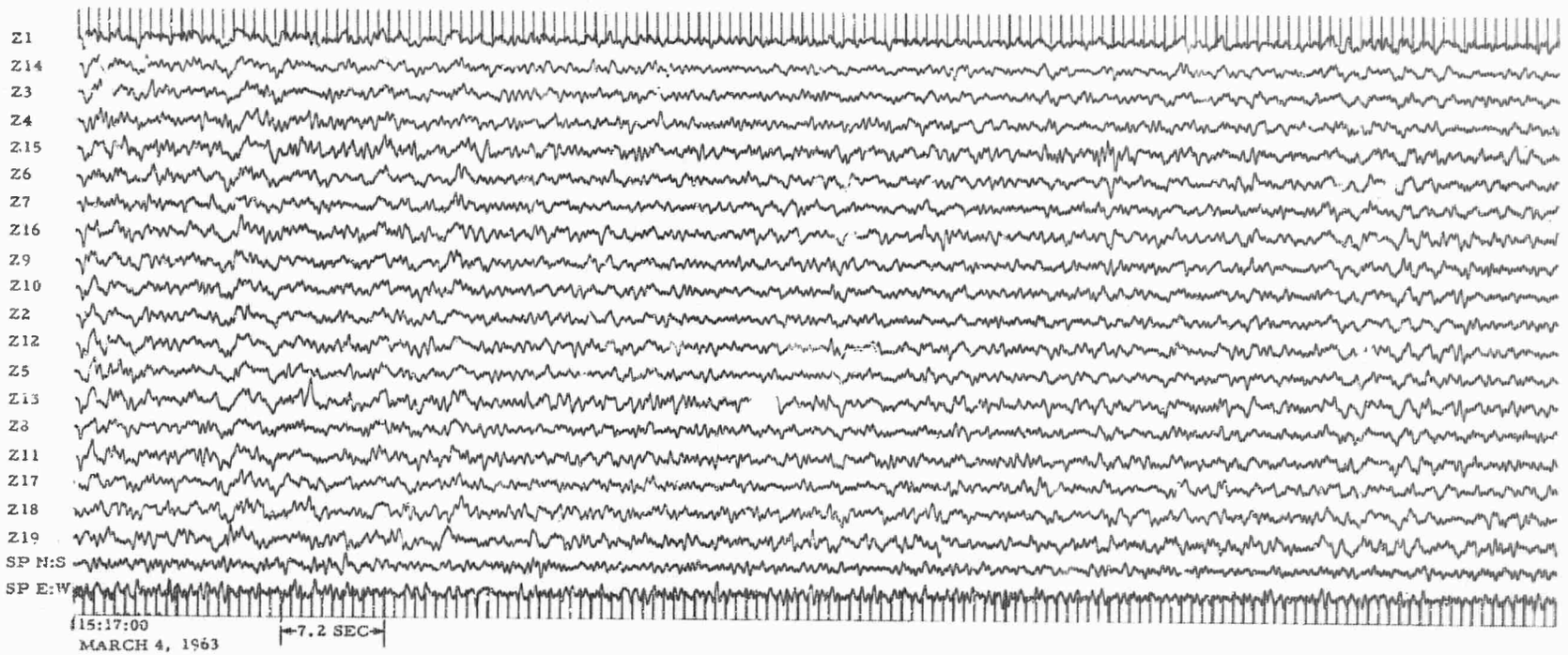

Figure VIII-6. Noise Sample AA Antialias Filtered and Decimated After Whitening (Decorvolution)

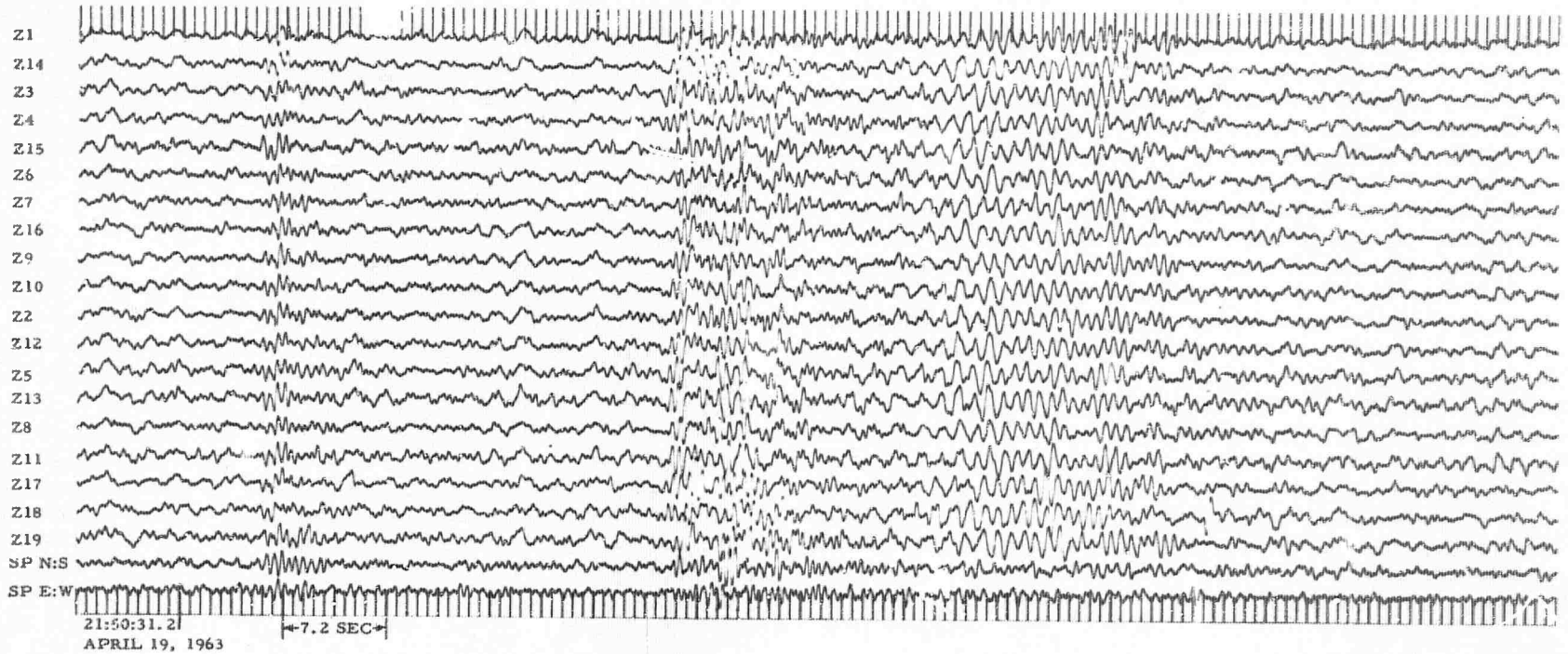

Figure VIII-7. Quarry Blast CC Antialias Filtered and Decimated Before Whitening (Deconvolution)

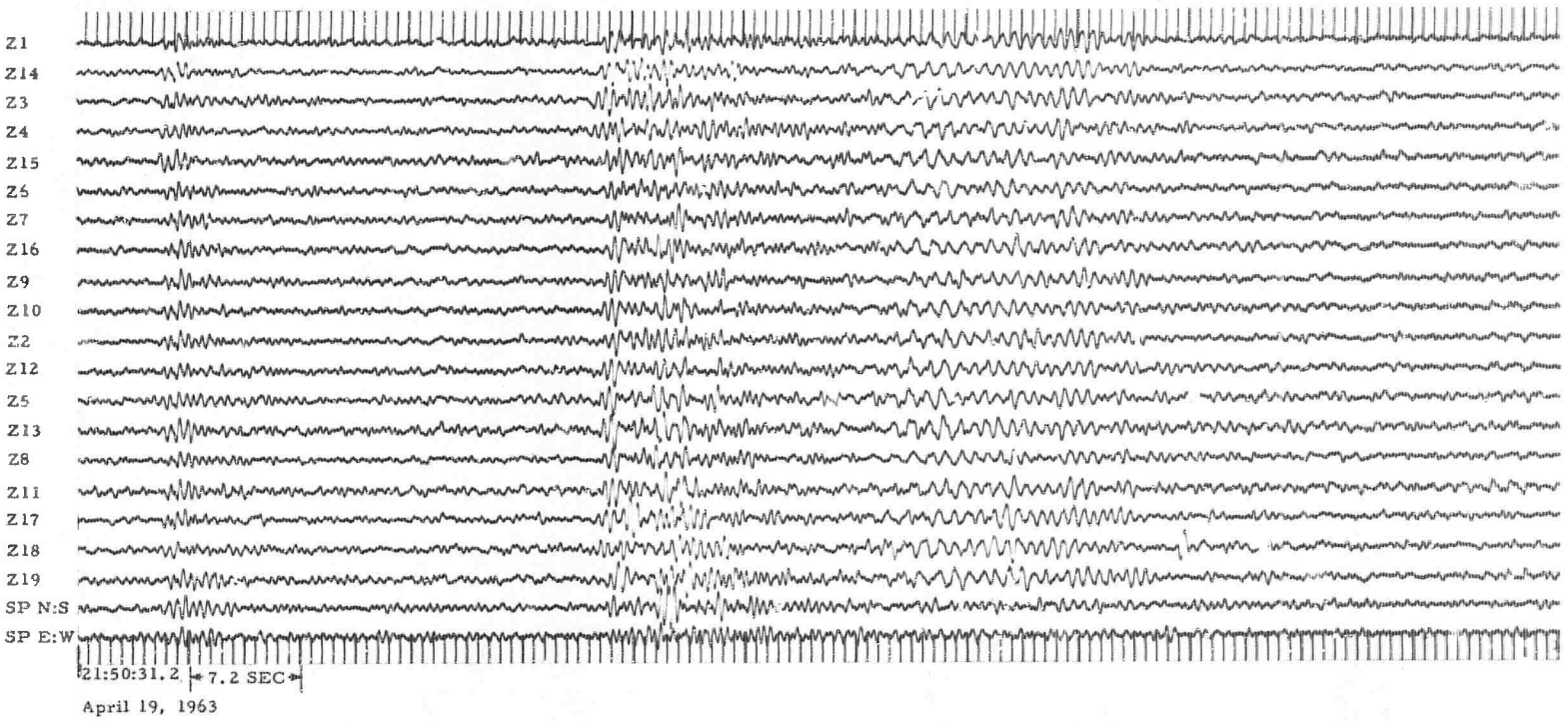

Figure VIII-8. Quarry Blast CC Antialias Filtered and Decimated After Whitening (Deconvolution)

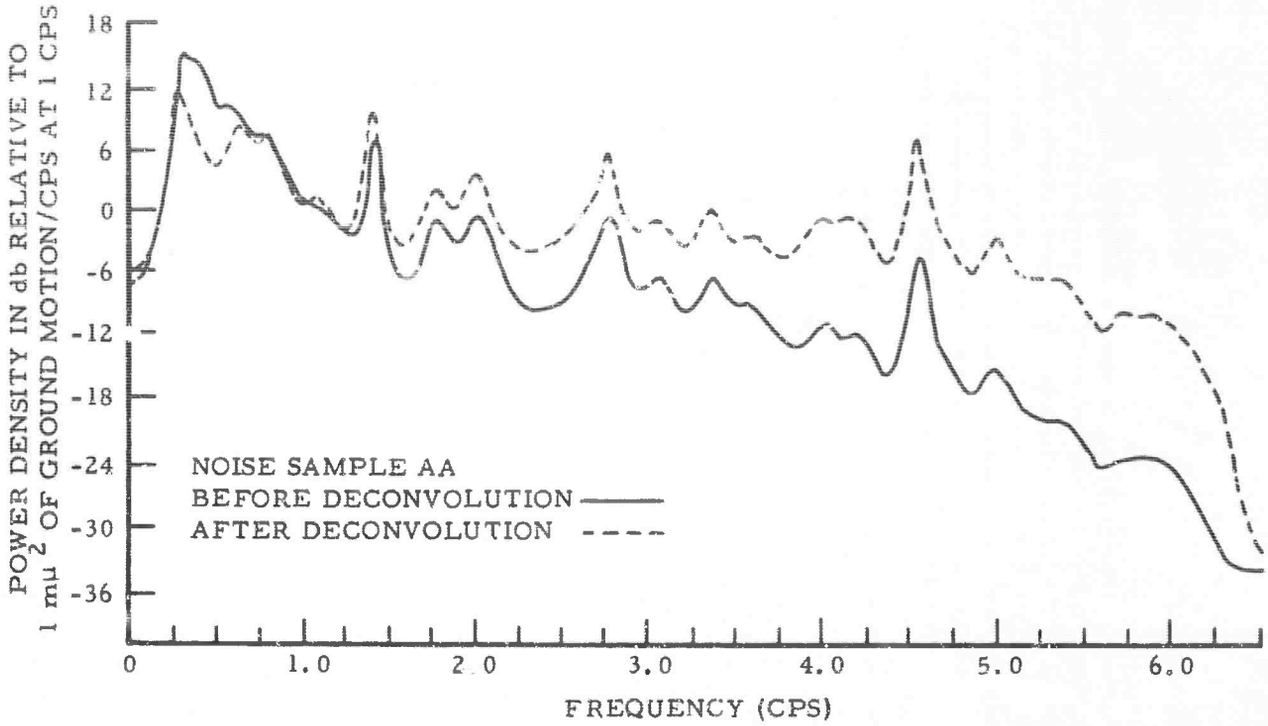

Figure VIII-9. Power Density Spectra of Noise Sample AA Before and After Whitening (Deconvolution)

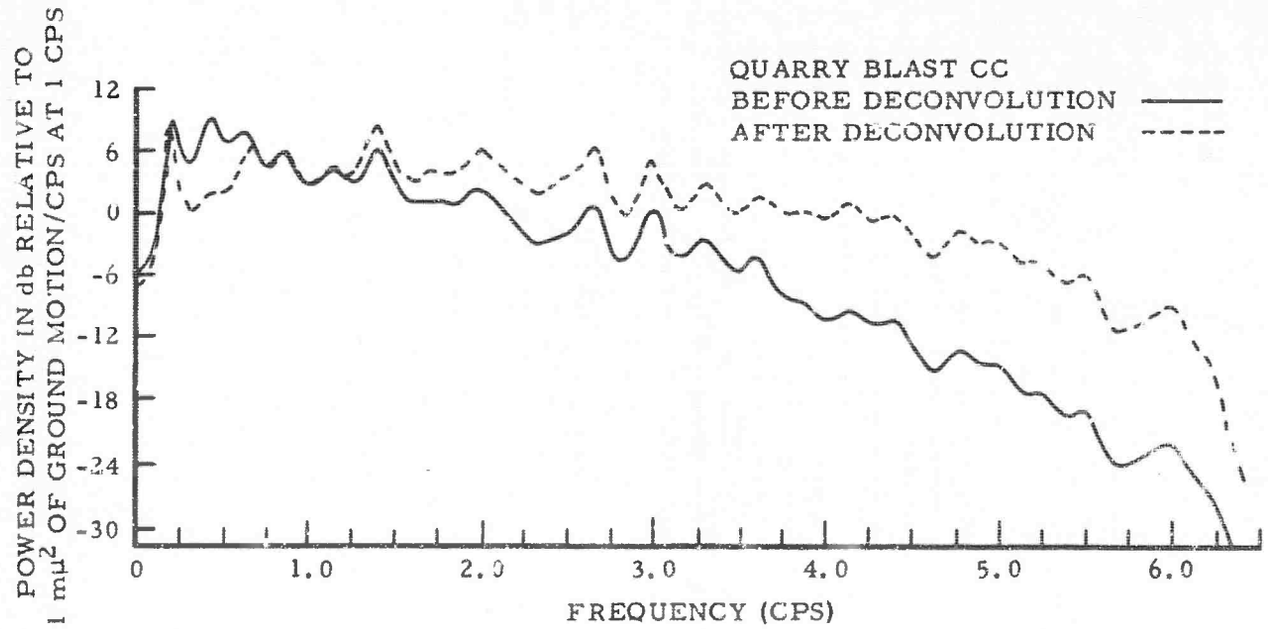

Figure VIII-10. Power Density Spectra of Quarry Blast CC Before and After Whitening (Deconvolution)

SECTION IX

ARRAY RESEARCH DATA COLLECTION

In support of Tasks 1.b. (1), 1.b. (2), 1.b. (3), and 1.d.* data have been acquired from the Tonto Forest Seismological Observatory (TFO), the Wichita Mountains Seismological Observatory (WMO) and the Uinta Basin Seismological Observatory (UBO), respectively. Recordings of events and noise samples from TFO were provided by AFTAC with Texas Instruments assistance. Data from WMO and UBO were recorded digitally on-site by TI.

Details of the data acquisition will be provided in Special Report No. 12.

A. DATA COLLECTION AT TFO

Data from TFO for Tasks 1.b. (1) and 1.b. (2) were provided by AFTAC from recordings made on the Astrodata Digital Data Acquisition System. These recordings were made on 1/2-in. tape in an IBM format and presently are being reformatted and gain-corrected at the Seismic Data Laboratory (SDL) for input to the IBM system associated with the TIAC** (Texas Instruments Automatic Computer). An IBM-to-TIAC conversion will be performed on this data to provide TIAC-format data for subsequent processing.

Responsibility for data collection at TFO was given to Geotech, operator of the station. Texas Instruments provided two people on-site to coordinate the TFO operation and to edit the raw-recorded data for submission to SDL. Coordination and assistance also were provided to the SDL operation.

1. Results

Library data edited at TFO from Astrodata recordings made between 16 August 1965 and 1 October 1965 comprise the following:

- Short-Period Low Gain (16-19, 23-26 and 28-30 August) --35 moderate-to-strong teleseisms and 21 regional events

---

* Tasks (modified) as numbered in contract AF 33(657)-12747.
** Trademark of Texas Instruments

- Short-Period High Gain (27, 30-31 August and 1 September) --24 weak teleseisms, 35 noise samples, 1 regional event and 6 full reels of special noise records (2 night, 1 early morning, 1 morning, 1 evening, and 1 windy)
- Long-Period Low Gain (6, 10, 19, 20, 22, 26, and 29 September and 1 October)-- 8 teleseisms, 12 noise samples, 1 near-regional event, 1 special event and 1 weather frontal passage
- Long-Period High Gain (2, 10, 11, 17, 21, 28, and 29 October)--4 weak teleseisms, 1 regional event, 31 noise samples, 2 windy-rainy samples, and 23 samples associated with the wind and pressure fluctuation of a frontal passage. (Tables I and II summarize these data and related PDE information.

It is reasonable to suspect that not all of this library data will be usable, due to tape errors, dropouts, etc. At this time, only a small portion of the library data have been processed through the Seismic Data Laboratory (SDL), and that has not been evaluated yet.

A standard 8-min edit length was used for all short-period data. Edits from full reels of special noise tapes were made to include a 30-sec overlap, should reconstruction of an entire reel-length sample be desired later. Long-period edits were 40 min. Since field reels could run from 65 to 70 min, it was possible to obtain two 40-min samples from one reel with a 10- to 15-min overlap.

Pertinent daily calibrations were edited for submission to SDL for seismometer channel-gain correction. These calibrations as well as the short- and long-period frequency responses are to be analyzed and the results are to be made available to TI.

Included in the library for the purpose of quality control are records of d-c pulses for long- and short-period channel verification, and records of system-noise tests made with dummy-loaded PTA* and shorted-out Voltage-Controlled Oscillator (VCO) inputs** at the remote vans.

---

* Dummy-loaded PTA testing involved replacing the seismometer by a resistor.

** Shorted-out VCO testing involved removing PTA from telemetering circuit and shorting across the VCO input.

Table IX-1

SUMMARY OF DATA EDITED AT TFO

	Short Period		Long Period	
Event Type	Low Gain	High Gain	Low Gain	High Gain
Teleseism	35 (8 Min)	24 (8 Min)	8 (40 Min)	4 (40 Min)
Regional	21 (8 Min)	1 (8 Min)	---	1 (40 Min)
Near-Regional	---	---	2 (40 Min)	---
Special	---	---	2 (40 Min)	---
Regular-Noise	---	35 (8 Min)	12 (40 Min)	31 (40 Min)
Special-Noise:				
Night	---	17* (8 Min)	---	---
Early Morning	---	9* (8 Min)	---	---
Morning	---	8* (8 Min)	---	---
Evening	---	3* (8 Min)	---	---
Windy	---	9* (8 Min)	---	---
Frontal Passage	---	---	3 (40 Min)	23 (40 Min)
Windy-Rainy	---	---	---	2 (40 Min)

Note: Numbers shown above refer to number of edited samples of the indicated length.

* Samples overlap by 30 sec.

Table IX-2

SUMMARY OF FDE INFORMATION

Short-Period Low Gain							
Date	Origin Time	Lat. Degrees	Long. Degrees	Location	Depth km	Mag. C&GS	Distance in Degrees
16 Aug.	225922.9	17.3 S	167.8 E	New Hebrides Is	33	5.3	91
17 Aug.	103504.1	5.3 N	96.2 E	Sumatra	33 R	5.3	131
17 Aug.	131612.7	52.0 N	175.2 W	Andreanof Is	33 R	4.9	49
17 Aug.	140219*	15.2 N	92.1 W	Mexico-Guatemala Border	121	4.9	27
17 Aug.	161741.5	15.2 S	166.6 E	New Hebrides Is	19	5.8	93
17 Aug.	204532.7	21.1 S	69.1 W	Northern Chile	103	4.8	71
17 Aug.	212552.6	5.2 N	77.5 W	Off Coast of Columbia	54	4.5	44
17 Aug.	221852.5	20.4 S	168.8 E	Loyalty Is	33	5.2	95
18 Aug.	100148.1	37.9 S	73.6 W	Off Coast of Cent Chile	33 R	4.7	80
18 Aug.	141428.6	23.3 S	175.3 W	Tonga Is Region	20 R	5.0	82
18 Aug.	142520.2	23.3 S	175.3 W	Tonga Is Region	20 R	4.9	82
18 Aug.	143829.5	23.7 S	175.3 W	Tonga Is Region	20 R	4.8	82
18 Aug.	145129.3	16.0 S	167.0 E	New Hebrides Is	5	5.7	93
18 Aug.	152529*	81.3 N	5.6 W	North of Svalbard	33 R	4.3	60
29 Aug.	023254*	13.9 N	90.6 W	Guatemala	80	4.3	28
29 Aug.	023501.7	19.2 S	167.7 E	New Hebrides Is	33 R	5.0	93
29 Aug.	172525*	19.5 S	176.2 W	Fiji Is	316	4.6	82.5
29 Aug.	183125*	15.7 S	167.6 E	New Hebrides Is	18	5.1	91
30 Aug.	004313*	37.4 N	113.2 W	Utah	49	---	4
30 Aug.	005605.3	16.9 S	167.2 E	New Hebrides Is	8	5.0	93
30 Aug.	033202.2	16.9 S	167.4 E	New Hebrides Is	15	5.5	93

Table IX-2 (contd)

Short-Period High Gain							
Date	Origin Time	Lat. Degrees	Long. Degrees	Location	Depth km	Mag C&GS	Distance in Degrees
27 Aug.	063337*	15.9 S	174.2 W	Tonga Is	128	3.8	78.5
27 Aug.	071057*	27.8 N	142.6 E	Bonin Is	33	4.4	86
27 Aug.	075128*	14.7 N	93.2 W	Cost of Chiapas, Mexico	72	4.1	25
27 Aug.	083505*	16.0 N	96.0 W	Coast of Oaxaca, Mexico	33 R	4.1	23
27 Aug.	084244*	15.4 N	92.8 W	Mexico-Gautemala Border	72	4.0	25
31 Aug.	010921	50.5 N	129.5 W	West of Vancouver Is	33 R	3.9	21
31 Aug.	023108*	39.8 N	138.5 E	Eastern Sea of Japan	30	4.6	81
31 Aug.	072947.4	39.3 N	40.9 E	Turkey	22	5.1	101
31 Aug.	074857.3	43.5 N	144.2 E	Hokkaido Is, Japan	33 R	4.9	76
31 Aug.	095128*	12.4 N	144.3 E	South of Mariana Is	38	4.6	94
31 Aug.	194314.5	17.0 N	145.2 E	Mariana Is	339	5.3	90
1 Sept.	063836.2	14.5 S	167.4 E	New Hebrides Is	189	5.6	91
1 Sept.	070220.9	34.2 N	138.9 E	Off Coast of Honshu, Japan	48	4.8	84
1 Sept.	073337*	18.5 S	172.9 W	Tonga Is	119	4.6	79
6 Sept.	211330.5	6.6 N	84.4 W	Off Coast of Cent America	21	5.1	38
19 Sept.	012652.5	22.1 S	174.9 W	Tonga Is	33 R	5.4	83

Table IX-2 (contd)

Long-Period Low Gain							
Date	Origin Time	Lat Degrees	Long. Degrees	Location	Depth km	Mag. C&GS	Distance in Degrees
20 Sept.	113143.6	15.4 N	94.6 W	Off Coast of Oaxaca, Mexico	58	4.3	23.5
22 Sept.	143610*	18.7 N	107.3 W	Near Jalisco Mexico	60	3.9	16
22 Sept.	220801.1	36.4 N	141.3 E	East Coast of Honshu, Japan	44 R	5.6	83
26 Sept.	070000.9	34.7 N	116.5 W	Southern California	16 R	4.6	5
1 Oct.	085205.8	50.1 N	178.3 E	Rat Is	32	6.3	50
1 Oct.	132228.5	20.0 S	174.4 E	New Hebrides Is	553 R	6.2	89

Long-Period High Gain							
10 Sept.	225744.0	18.6 N	100.6 W	Guerrero, Mexico	92	4.2	18
17 Sept.	011345*	54.2 N	162.7 W	Alaskan Peninsula	50 R	4.6	40
21 Sept.	070231.3	22.0 S	174.5 W	Tonga Is	33 R	4.6	83

The desired quantities of various types of data were not obtained always. The effective recording period was shorter than anticipated. Few long-period events that had a P, S and L signal-to-noise ratio greater than 1 which did not over-modulate the recording system, were recorded. No regional events with known epicenter were observed, since station personnel had not determined areas of mining activity greater than near-regional distances. There was no frontal passage during short-period recording, nor was there any rain not accompanied by lightning and spiking.

B. DATA COLLECTION AT WMO

Data collection in support of Task 1, b. (3) was begun at the Wichita Mountains Seismological Observatory (WMO) on 16 November 1965. Data were recorded from 3-component strain instrumentation, 3-component inertial instrumentation and the 13-channel surface areal array.

It should be noted that the cutoff date of this report precluded inclusion of the details of WMO data collection, however, the task was completed at the time this report was published.

A later report will detail the results of the data recording and will present a conventional seismological analysis of recorded events. Noise samples, events and special tests selected by the analyst for inclusion in the library will be transcribed on IBM-format tape and will be supplied to the Vela Seismic Center.

It was planned to record for a total of nine days during the period ending 30 November. In general, normal station-working hours were to be followed especially in view of the remote location of the station and the accompanying military activities.

It was planned to record the following data:

- Twenty 30-min ambient noise samples
- 10 strong teleseisms
- 20-30 quarry blasts and/or near-regionals (with well-developed surface wavetrains)
- Calibrations (including all daily and special calibrations)
- System-noise tests (at start and finish of data collection)

All data were to be field-edited. The data on each reel were to be preceded by a brief DFS calibration and 5-min recording (truck-noise test made with the operational-amplifier inputs grounded). Skew

tests were to be performed at least once per day.

The following DFS channelization was to be used:

Channel	Contents
1	Vertical Strain--SZS--High Gain
2	Horizontal Strain--SNS--High Gain
3	Horizontal Strain--SES--High Gain
4	Vertical Inertial--SPZ--High Gain
5	Horizontal Inertial--SPN--High Gain
6	Horizontal Inertial--SPE--High Gain
7	Vertical Strain--SZS--Low Gain
8	Horizontal Strain--SNS--Low Gain
9	Horizontal Strain--SES--Low Gain
10	Vertical Inertial--SPZ--Low Gain
11	Horizontal Inertial--SPN--Low Gain
12	Horizontal Inertial--SPE--Low Gain
13-25	13-Element Surface Array---Low Gain
26	SPN at Z6 Location
27	SPE at Z6 Location
28	Summation, 13 Surface Verticals
29	Spare
30	WWV
31	Station Time

Channels 1-6 were to be recorded at such gain settings that would cause typical noise peaks to come within 10 db of DFS clipping. Each channel was to be adjusted individually in order to make maximum use of dynamic range. Channels 7-12 were to have gains in the same proportion as channels 1-6, but approximately 20 db lower. The amount of decreased gain was to be determined by whatever was required to record reasonably large teleseisms without digital clipping. Channels 13-25 were to be operated with a gain sufficiently low that average teleseisms could be recorded without clipping.

Station develocorder film and all logs were to be obtained from the station manager and sent to Dallas for copying. Film and logs from the strain-instrumentation group were to be obtained from Garland.

The station manager and the strain-instrumentation group leader were to be kept informed of TI on-site activities. Efforts were to be made to minimize departures from station routine.

C. DATA COLLECTION AT UBO

1. Program

Task 1.d. of the program requires that a Seismic Data Library be created from on-site digitally recorded data collected at the Uinta Basin Seismological Observatory (UBO). These field data are to be edited, gain-corrected and made available to AFTAC on IBM tapes, together with a report of a conventional seismological analysis.

2. History

The AFTAC Digital Recording System was dispatched from Dallas to UBO on 13 September 1965, but accidentally was overturned at Moab, Utah, on 16 September. This truck eventually was repaired enough to be driven back to Dallas. Because the program at UBO involved collecting data which would not be available at a later date, Texas Instruments made ready and dispatched its own Digital Recording System to UBO to accomplish the data collection. This second truck departed Dallas on 20 September and arrived at UBO on 22 September. All data sources being recorded were cabled into the Digital Recording System, and internal tests and calibrations were performed. The first recordings with all input systems properly calibrated and operating were made on 3 October 1965.

Several data sources had to be operational simultaneously for the ultimate schedule of instrument evaluation, array evaluation and eventual library formation to be successful. Sources required were the two short-period areal arrays, both multichannel filters, and the 6-element vertical array. The latter array was a temporary installation whose operation required that all other schedules be keyed to its availability. Consequently, all time and equipment schedules were carefully coordinated among Texas Instruments, AFTAC and Geotech.

Recording continued from 3 October on a routine schedule until the 6-element vertical array malfunctioned on 8 October. Investigation showed extensive and time-consuming repairs would be necessary before usable data would be available again. This time lag, other commitments of

the Texas Instruments Digital Recording System, and the accumulation of a satisfactory amount of usable recorded data from UBO prompted the decision to return the system to Dallas on 14 October.

3. Data Sources

Data sources and their channelization in the Digital Recording System are given in Table I. Outputs from the multichannel filters were taken parallel to the Develocorder input terminals. Outputs from all UBO instruments were obtained at the PTA outputs; outputs from the 6-element vertical array were taken from the Signal Conditioner and Filter package located in the auxilliary instrument van. During all sine-wave calibrations, a signal was obtained directly from the driving function generator and recorded in channel 30.

4. Recorded Data

The recordings at UBO were made on 17 field tapes distributed as shown in the following list:

- High-gain noise 6 reels
- Normal-gain events 8 reels
- Calibrations 2 reels
- Tests 1 reel

The six high-gain tapes contain a total of 11 hr 40 min of noise data recorded in 12 separate sessions. The eight event tapes contain, on the basis of a preliminary analysis, 15 records of either quarry blasts or near-regional earthquakes, and 25 teleseisms.

Calibration and test reels contain daily calibrations and special frequency-response calibrations and system-noise tests.

5. Utilization of Data

Approximately half of the data recorded at UBO have been edited and transcribed into TIAC records. This edit was necessary to provide data for an early evaluation of the vertical array. Details of this program are given elsewhere in this report.

The remaining data are being edited currently and will be transcribed into TIAC records. An analysis of array calibration data will yield the proper multiplication factors to normalize each data channel to some uniform equivalent transducer gain. This gain-corrected TIAC

ensemble will be transcribed next into an IBM-tape library which will be made available to AFTAC. A listing of library contents, along with a conventional seismological analysis, will be presented in a special report.

SECTION X

DISCUSSION OF LASA PROCESSING REQUIREMENTS

A. INTRODUCTION

At the invitation of the Advanced Research Projects Agency in September, Texas Instruments personnel prepared and delivered several presentations at the LASA Conference in Washington, D.C. One of these presentations dealt with the problems associated with processing LASA data. A brief summary is given here.

The full text of this paper will be published as Special Report No. 13.

B. GENERAL CONCEPT AND PROCESSING FUNCTIONS

1. On-Line Detection and Approximate Location

The total processing of data from a LASA and the nature and quantity of data permanently stored on magnetic tape are determined by the status of the seismic-wave field at the time. For example, when ambient noise is present with no teleseismic events above a given magnitude threshold and the absence of such events is known, no further processing is required and only a limited amount of data need be stored. In the presence of a teleseismic event above the threshold, additional on-line processing dependent on the approximate location of the event would be carried out. A greater amount of data would be stored in the presence of a teleseismic signal with certain characteristics. In the presence of an abnormally high noise field, a large amount of the data (possibly up to the 525 channels) would be stored so that maximum processing capability might be exploited. Therefore, the major on-line function of the processor must be determination of the status of the seismic-wave field. The processor must detect teleseisms above a specified magnitude threshold, but need determine their location only to sufficient precision to permit additional on-line processing for extracting more detailed information about the event.

2. Data Storage

An on-line temporary buffer storage for the full 525 channels is contemplated. The buffer storage must save the raw data from the 525

channels long enough for appropriate action to be taken for detected events. This period is probably on the order of 1-1/2 min.

Magnetic tape units are provided for permanent storage. Worldwide P-wave outputs from the 21 subarrays would be stored for all data. On the basis of the detection logic, a number of other storage operations up to and including storage of the full 525 channels would be provided.

3. Postdetection Processing

Postdetection processing would include immediate on-line processing of the buffered data to develop the best steered beam for each of the 21 subarrays based on the approximate location of the event. Additional processing of this data would include improved location and measurement of arrival time and would accomplish signal extraction for subsequent measurement of classification parameters. In the case of larger teleseisms, special redetection processing would be provided for locating possible smaller events which might be buried in a larger teleseismic arrival.

4. Built-in Learning Function

It is anticipated that determining the necessary corrections (particularly between subarrays) to provide maximum enhancement in the beam-forming function will require a long period of time and the use of data from a large number of teleseisms. Large-detected events, therefore, would undergo processing for upgrading of the beam-former corrections.

5. Off-Line Network Processing

Finally, the function of combining information from a number of LASA stations must be performed to accomplish source classification.

6. General Implementation

A generalized picture of this processing concept is shown in Figure X-1. The 525 channels from the subarrays are delivered to a special-purpose processor which provides signal detection and preliminary location. In addition, the special-purpose processor provides 21 processed broadband subarray outputs for permanent magnetic-tape storage. The

SECTION XI

AUTOMATED MAPPING SYSTEM

A. INTRODUCTION

A series of five programs has been written for the IBM-7044 Computer and the Calcomp Plotter to aid in the evaluation of potential array sites and in the interpretation of data recorded at an array site. These programs utilize sets of worldwide geographic coordinates and array-site coordinates, and provide maps of various types including stereographic projections centered on the array site and a map of the world in $\vec{k}$-space centered on the site.

Descriptions of these five programs and information required to run each program will be published, together with a listing of Fortran statements, as Special Report No. 11. Source decks for these programs and for the Calcomp Plotter subroutines have been supplied to the Project Monitor at the Vela Seismic Center.

To obtain coordinate sets of the major land masses, seismic areas and other points of interest, a Polar Stereographic Projection map, published by the Aeronautical Chart and Information Service, U.S. Air Force, having a scale of approximately $1:25X10^6$ was used.

Approximately 2900 points were used to outline continental and political boundaries and major islands. An additional 460 points were required to show major seismic areas; 266 points were used to show 15° increments of latitude and longitude. About 3600 points are contained in the present library.

Cards and listings containing these points have been supplied to the Project Monitor.

B. APPLICATION OF MAPPING SYSTEM

This mapping system provides an economical, graphical solution to the following problem: from a specified site, what is the appearance of the world in $\vec{k}$-space (for a specified frequency and propagation phase) and in geographic space? In general, the programs will plot sets of coordinates as any definable function of distance from any one site. By plotting major earthquake epicenter areas, it can be determined if a site is likely to record a large number of earthquakes or if, perhaps, it lies in a shadow zone for many seismic areas. By plotting possible areas of nuclear activity, it can be determined if a site will likely record events from a majority of them. By plotting coordinates of the reported earthquakes of the last few years, one can determine if there is an "earthquake

screen" between the site and a possible area of interest.

For use in evaluation or interpretation of several sites, a graphical solution may be obtained by plotting the same data centered on each site and comparing individual results simultanously. Plans are being formulated now for representing data from several sites on the same chart. This capability will be valuable for multiple-site evaluation and interpretation.

1. Examples

Figures XI-1 through XI-3 show the finished output from the series of programs. Data were taken from the Calcomp Plotter and the maps were drawn by a draftsman using the plotted points.

Figures XI-1, XI-2 and XI-3 serve a 3 fold purpose. Figures XI-1 contains the following information:

- It is a stereographic projection of the areas of the world 90° or less from Tonto Forest Seismological Observatory (TFO), near Payson, Arizona. True distance and azimuth may be measured from TFO to any point on the map.
- It presents 15° latitude and longitude lines (shown as screened light grey lines) as they appear on the sterographic projection
- It shows the earth's major seismic areas (black triangles) as seen on the stereographic projection from TFO.

Figure XI-2 shows the following information:

- It is a stereographic projection centered on the antipode of TFO or that point diametrically opposite TFO; this encompasses all points greater than 90° from TFO. True distance from TFO to any point on this map may be computed by finding the distance from the antipode of TFO to the point and subtracting it from 180°. Azimuth from TFO to any point on this map can be figured by finding the azimuth from the antipode and subtracting it from 360°.
- It presents 15° latitude and longitude lines (shown as screened light grey lines) as seen on the stereographic projection centered on TFO's antipode.

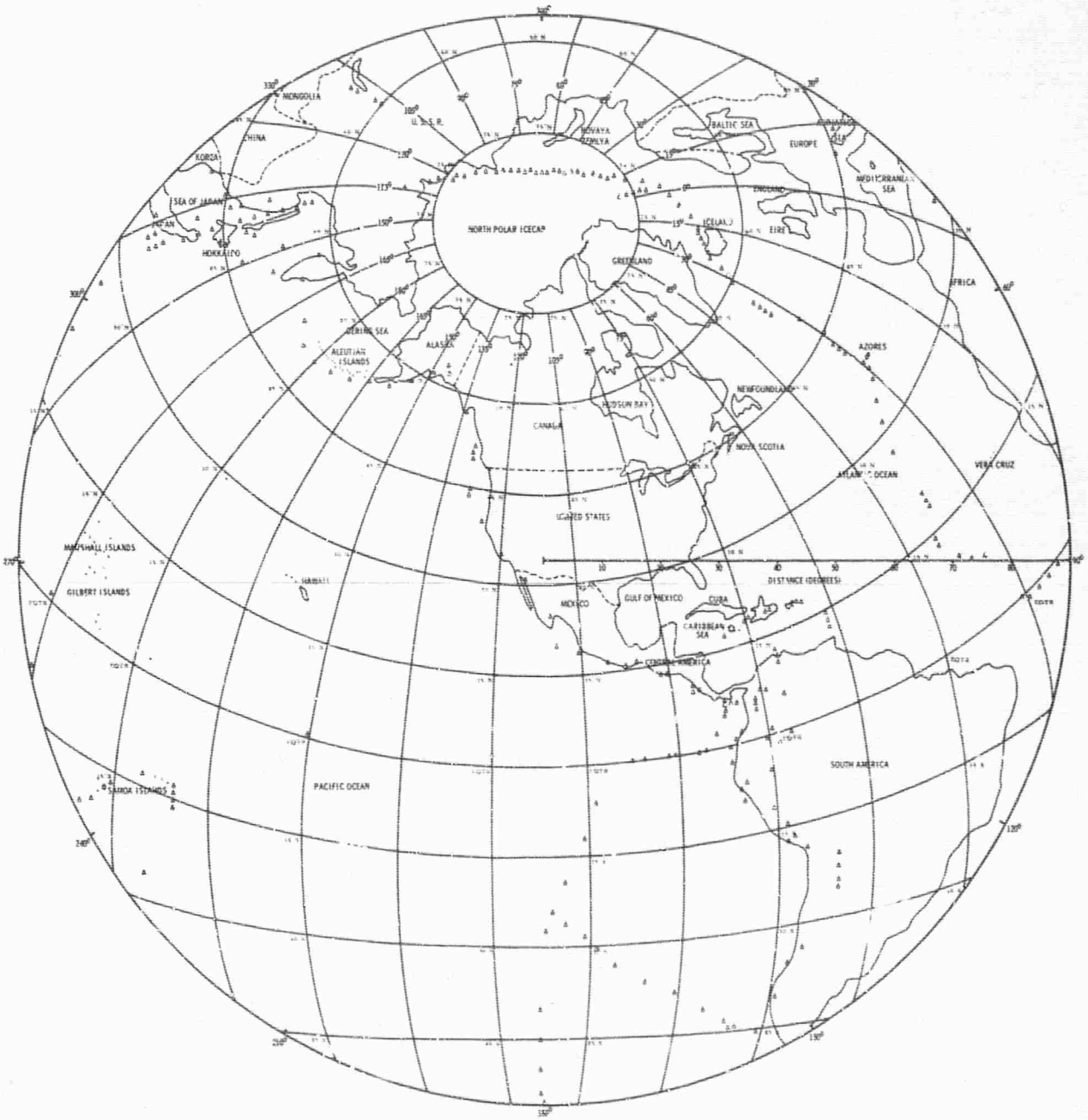

Figure XI-1. Stereographic Projection Map Showing Lat. and Long. Lines, and Earth's Major Seismic Areas

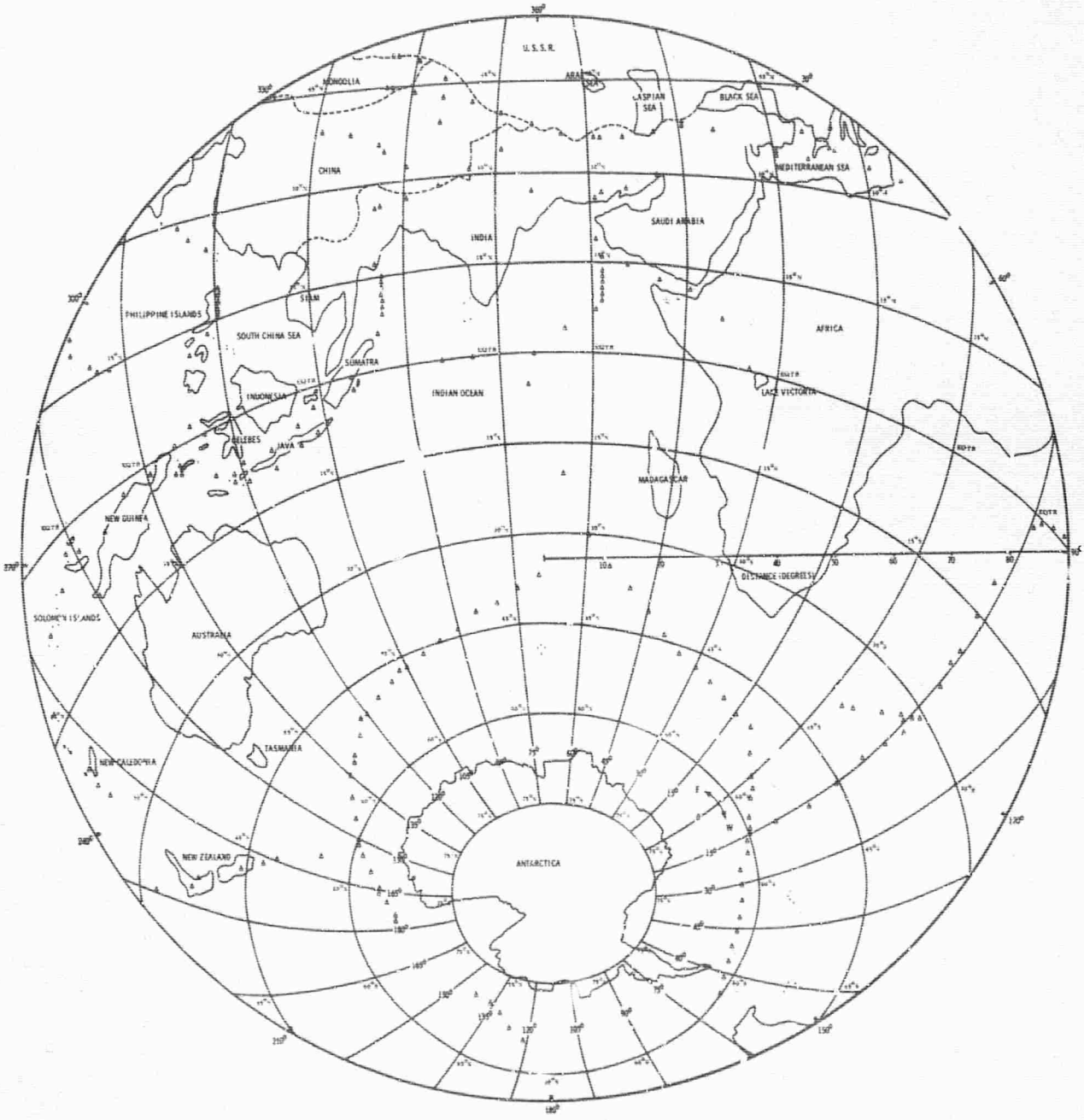

Figure XI-2. Stereographic Projection Map Centered on Antipode of TFO showing Lat. and Long. Lines and Earth's Major Seismic Areas >90° from TFO

- It shows the earth's major seismic areas (black triangles) greater than 90° from TFO, as seen on the stereographic projection.

Figure XI-3 presents the following information:

- It is a map of the world as a function of wavenumber seen from TFO for a 1-cps P-wave. The points plotted lie on true azimuths from TFO. The shadow zone contains all points greater than 104° from the station, that being the approximate distance beyond which initial P-waves are not recorded. Points actually located near TFO are greatly distorted on the projection because of their large $\vec{k}$-number; thus, the map shows only points of $\vec{k}$ = .09 or less.
- It presents 15° latitude and longitude lines (shown as screened light grey lines) as seen on the $\vec{k}$-projection from TFO.
- It shows the earth's major seismic areas (black triangles) in $\vec{k}$- space.

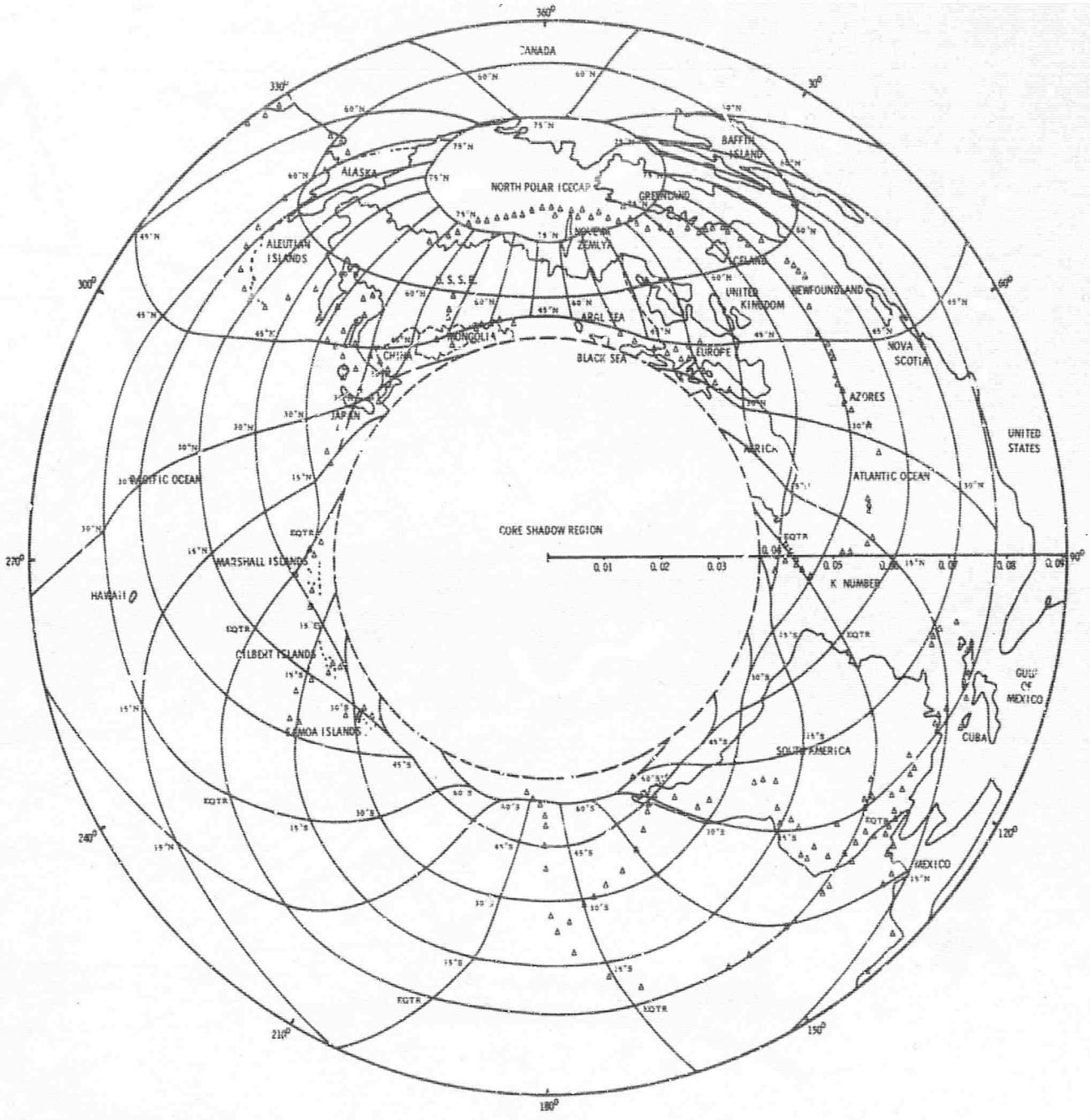

Figure XI-3. World Map Seen from TFO for a 1.0 CPS P-Wave Showing K-Projection Lat. and Long. Lines, and Earth's Major Seismic Areas in K-Space